Ontwikkeling en studie van verschillende numerieke plasmastraalmodellen en experimentele studie van plasmavergassing van afval

Development and Study of Different Numerical Plasma Jet Models and Experimental Study of Plasma Gasification of Waste

Nicholas Agon

Promotoren: prof. dr. ir. J. Vierendeels, ereprof. dr. ir. G. Van Oost, prof. dr. M. Hrabovský
Proefschrift ingediend tot het behalen van de graad van
Doctor in de Ingenieurswetenschappen

Vakgroep Mechanica van Stroming, Warmte en Verbranding
Voorzitter: prof. dr. ir. J. Vierendeels
Faculteit Ingenieurswetenschappen en Architectuur
Academiejaar 2014 - 2015

UNIVERSITEIT GENT

ISBN 978-90-8578-831-7
NUR 928, 952
Wettelijk depot: D/2015/10.500/75

Supervisors:

Prof. dr. ir. Jan Vierendeels
Prof. dr. ir. Guido Van Oost
Prof. dr. Milan Hrabovský

Research lab:

Department of Flow, Heat and Combustion Mechanics (FloHeaCom)
Ghent University
Sint-Pietersnieuwstraat 41
B–9000 Gent
Belgium

Members of the exam committee:

Chairman:	
Prof. dr. ir. Luc Taerwe	Faculty of Engineering and Architecture, UGent
Secretary:	
Prof. dr. ir. Christophe Leys	Faculty of Engineering and Architecture, UGent
Reading committee:	
Dr. ir. Jiří Jeništa	Institute of Plasma Physics, Academy of Sciences of Czech Republic
Prof. dr. ir. Jan Pieters	Faculty of Bioscience Engineering, UGent
Prof. dr. ir. Lieve Helsen	Faculty of Engineering, KU Leuven
Other members:	
Prof. dr. Milan Hrabovský	Institute of Plasma Physics, Academy of Sciences of Czech Republic
Prof. dr. ir. Guido Van Oost	Faculty of Engineering and Architecture, UGent
Prof. dr. ir. Jan Vierendeels	Faculty of Engineering and Architecture, UGent

This research was funded by the Agency for Innovation by Science and Technology in Flanders (IWT).

Acknowledgements

During my Master in Bioscience Engineering, I remember answering the question about my future outlook with: “The last thing I want do is start a PhD!”...
This was before I got passionate about plasma gasification via my master thesis. Since I owe the introduction to this subject to Greet Van Eetvelde, who I admire for her inexhaustible drive and enthusiasm, she is (un)willingly responsible for changing my life course.
Thanks to the encouragement and guidance of Prof. Jan Pieters and Prof. Guido Van Oost, I could continue in the dynamic and interesting field of plasma gasification after graduation by committing to a PhD. This 4 year and a half long challenge could not have been brought to a successful conclusion if it wasn't for all the people around me who contributed in their own way to this achievement.

First of all, I would like to acknowledge my supervisors.
Prof. Jan Vierendeels has been instrumental in guiding me through the maze of computational fluid dynamics, in which I frequently got lost. I am very grateful for his patience, willingness and perseverance in sharing his knowledge with me. Thank you for encouraging my critical thinking and for allowing me to grow as a research scientist. My sincere gratitude is also due to Prof. Guido Van Oost, who has been coaching me from the sideline since the very beginning of this journey. He is one of the few people with whom I can share my interest for plasma gasification. I enjoyed our interesting discussions on the topic, which from now on will probably have to take place in a tearoom in De Haan. Furthermore, he acted as an excellent liaison for the collaboration with the Institute of Plasma Physics (IPP) in Prague (Czech Republic).
During the many visits to the IPP, Prof. Milan Hrabovský was always very accommodating. Thanks to him, I got the opportunity to participate in experiments and gain expertise in the field of plasma gasification.

Next, I would especially like to thank my girlfriend Maxine Frimpong. Her love and reassuring support, particularly in the final stretch, have helped me bring this manuscript to completion. I dearly appreciate you for being by my side during both the smooth and the rough periods of the PhD. Thank you for riding out this roller-coaster with me!
Many thanks to my mother for her empathy and motivation which helped me find the strength to tackle the challenges along the way, and to my father for his advice and admonitions. I also want to thank my brothers, Michael and Thomas and my cousins, Tim, Ben and Rob, for the nice lunch breaks together, and their understanding: I still owe you a snowboard trip!

I had the pleasure of being surrounded by great colleagues, both in Ghent as in Prague, to whom I would like to express my gratitude. In the first years of the PhD, I was fortunate to share an office with Dieter Fauconnier who was always prepared to assist me with any problem presented. Later on, I could call on Joris Degroote with my questions, who might be the most intelligent and most friendly 'helpdesk' in the world.
Many thanks to my other colleagues, office roomie Akil Osman and especially Alireza Rasekh, who I rather consider as a good friend than a colleague. Thank you for the great times over the course of my PhD, both at work as well as outside of work. Furthermore, I wish to acknowledge the help from Tanya Kavka, Oleksiy Chumak, Jiří Jeništa, Michal Hlina, Alan Mašláni and the late Miloš Konrád at the IPP. Big thanks to Anouk Bosmans for the pleasant collaboration and Rudi Smet for the occasional English proofreading.
Finally, I want to thank all my friends for allowing our friendship to survive beyond the PhD years!

Nicholas Agon
Gent, September 2015

Summary
Samenvatting

Samenvatting

Thermische plasmas worden reeds uitgebreid toegepast in een waaier van veeleisende industriële toepassingen. De omzetting van organische materie tot een hoogwaardig gas met behulp van plasma wordt plasmavergassing genoemd. Oorspronkelijk was het doel van deze verwerking door plasmatoortsen uitsluitend om vaste stoffen zoals assen en metalen onschadelijk of vloeibaar te maken. De laatste jaren ligt de nadruk in de afvalsector op een circulaire economie, hetgeen geavanceerde verwerkingmethodes vereist met de mogelijkheid om secundaire grondstoffen te bekomen uit afvalstromen. Dit was een drijfveer voor de recente ontwikkeling van de plasmavergassingstechnologie voor afvalverwerking.

Twee onderdelen met betrekking tot plasmavergassing worden in dit onderzoek bestudeerd, namelijk het modelleren van een plasma jet en de plasmavergassing van een afvalstroom met een hoge anorganische fractie (bv. 'refuse-derived fuel' of RDF). In het luik rond plasma modelleren worden eerst de karakteristieken van plasma en de uitdagingen in verband met het correct weergeven van de complexe fysische fenomenen in een stromingsmodel (CFD) beschreven. In een dergelijk model dienen onder andere de thermodynamische en transporteigenschappen van het gasmengsel van plasma en andere gassen correct toegewezen worden. Het correct berekenen van deze eigenschappen voor een uitgebreid gasmengsel is niet voor de hand liggend en daarom worden vaak mengwetten toegepast. Hoewel de accuraatheid van deze mengwetten reeds werd onderzocht, blijkt uit de literatuurstudie dat de invloed van de afwijkende waarden, bekomen door gebruik van mengwetten, op de berekende stromingspatronen nog niet werd bestudeerd.

Met dit doel wordt een model van de plasma jet uit een gelijkstroom (DC) plasmatoorts in stikstof atmosfeer ontwikkeld. Dankzij de karakteristieken van de geselecteerde toorts, volgend uit de typerende combinatie van zowel water- als gas (argon) stabilisatie van de vlamboog, is deze toorts uitermate geschikt voor plasmavergassingsdoeleinden. Met deze modelopstelling worden drie CFD simulaties uitgevoerd die verschillen in de mate waarin mengwetten gebruikt

worden voor de berekening van de thermofysische eigenschappen van het driedelig gasmengsel ($Ar/H_2O/N_2$).
Het eerste 'mengmodel' (model 1) past mengwetten toe tussen alle gassen. Model 2 berekent de eigenschappen van het tweedelig plasma gasmengsel (Ar/H_2O) afzonderlijk zonder mengwetten en combineert deze met de eigenschappen van stikstof aan de hand van mengwetten om de eigenschappen van het driedelige gasmengsel te bekomen. Het derde 'mengmodel' (model 3) berekent de thermofysische eigenschappen van het gasmengsel rechtstreeks en maakt geen gebruik van mengwetten. Het laatste model wordt ook wel het 'full multicomponent' model genoemd. Aan de hand van een vergelijking van deze drie simulaties op basis van de berekende snelheids-, temperatuurs- en concentratievelden, kan de invloed van de mengwetten kwantitatief onderzocht worden. De resultaten tonen aan dat de geschatte thermofysische eigenschappen aan de hand van mengwetten een grote invloed kunnen uitoefenen op de processen aan de rand van de jet (zoals de ontwikkeling van turbulente structuren en inmenging van andere gassen). De aanname, die vaak in de literatuur wordt gebruikt, dat de afwijkende waarden voor de transporteigenschappen berekend door mengwetten met beperkte accuraatheid (zoals die van Wilke, en Mason en Saxena) een verwaarloosbare bijdrage zouden leveren ten opzichte van de turbulente transporteigenschappen wordt weerlegd. De turbulentie in de hete zone van de plasma jet, dicht tegen de toortsuitlaat, is immers vaak beperkt. Daaruit volgt dat het samenspel tussen de thermodynamische en moleculaire transporteigenschappen bepalend is voor de ontwikkeling van de plasma jet.

Het tweede luik van het doctoraatsonderzoek betreft de plasmavergassing van afval. Plasmavergassing wordt eerst gesitueerd ten opzichte van andere conventionele thermochemische verwerkingsmethodes. Daarna worden de voor- en nadelen van het proces en de mogelijke eindtoepassingen van de vergassingsproducten besproken. Een uitgebreide oplijsting van alle huidige plasmavergassingsinstallaties is toegevoegd en in detail gedocumenteerd. Eén van de weinige academische plasmavergassingssystemen bevindt zich op het Institute of Plasma Physics (IPP) in Praag (Tsjechië). De experimenten met deze reactor hebben reeds een belangrijke bijdrage geleverd in dit onderzoeksgebied. De details van de opstelling en de diagnostiek van deze reactor worden in detail besproken.
De eigenschappen van het materiaal (RDF) dat geselecteerd werd om de haalbaarheid van de plasma behandeling van een afvalstroom met een hoge anorganische fractie aan te tonen, worden besproken. Dit afvalmengsel werd bekomen na scheiding en voorbehandeling van huishoudelijk en industrieel afval afkomstig

uit een stortplaats. Verschillende combinaties van vergassingsmedia (CO_2, O_2 en H_2O) werden toegevoegd aan het proces tijdens het experiment voor verschillende debieten van het materiaal (21.3 en 28.9 kg/u). De resultaten van negen verschillende casussen bestaan uit de samenstelling van het syngas, de energieverliezen in de toorts en via de reactorwanden en temperatuursmetingen langs de reactorwand. Aan de hand van deze variabelen wordt aangetoond dat het plasmavergassingsproces een syngas van hoge kwaliteit en met lage concentraties aan teer (132-543 mg/Nm^3) kan produceren uit RDF.

Uit de vergelijking tussen de gemeten samenstelling van het syngas en de theoretisch berekende samenstelling wordt de afwijking van thermodynamisch evenwicht nagegaan. De effecten van 'equivalence ratio' (ER), materiaaldebiet en type vergassingsmedium worden vervolgens onderzocht via vergelijkende analyses van de prestatiecriteria (zoals 'carbon conversion efficiency' (CCE), 'CO yield' en 'H_2 yield') en energie-efficiënties van de verschillende casussen. De CCE voor plasmavergassing van RDF aan een debiet van 28.9 kg/u varieert voornamelijk tussen 82 en 87 %. De hoogste energie-efficiënties worden verkregen via plasmavergassing met water als vergassingsmedium, terwijl de O_2-H_2O casus de hoogste prestatiecriteria weergeeft. Verder wordt er aangetoond dat CO_2 en H_2O als vergassingsmedia kunnen uitgewisseld worden zonder weerslag op de performantie van het process, op voorwaarde dat de ER constant gehouden wordt.

Een vergelijking tussen de experimenten met RDF en vorige experimenten met biomassa wordt getoond waaruit voortkomt dat de grovere verdeling van de deeltjes, het hogere vochtgehalte en de hogere asfractie van het RDF een negatief effect op de efficiëntie van het proces hebben. Een tweede vergelijking wordt gemaakt tussen de huidige resultaten van de eentraps plasmavergasser met die van een tweetrapssysteem. Beide systemen vertonen een goede afbraak van teercomponenten en houden er elk een specifiek voordeel ten opzichte van elkaar op na. Enerzijds bezit het syngas bekomen via het eentrapsproces gunstigere karakteristieken (hogere CO en H_2 concentraties en een hogere CO/CO_2 verhouding), anderzijds slaagt het eentrapsproces er niet in om de anorganische fractie te verwerken tot een inerte verglaasde materie. Dit laatste werd wel succesvol gedemonstreerd door het tweetraps-plasmavergassingsproces.

Plasmavergassing kan beschouwd worden als een veelbelovende verwerkingsmethode voor RDF dankzij de goede controle van de syngas samenstelling, de hoge kwaliteit van het syngas en de algemene flexibiliteit van het systeem.

Summary

Thermal plasmas have been widely used in a large number of high-technological industrial applications. The conversion of organic matter to a high-quality syngas by using plasma torches is called plasma gasification. The original goal for this plasma treatment was to either melt or immobilize solid materials such as ash and metals, making them safe for disposal. The recent emphasis in the waste industry on a circular economy requires more advanced conversion technologies which yield improved resource recovery. This has triggered the recent development of the plasma gasification technology for waste treatment.

In this work, two subjects associated with plasma gasification have been studied, i.e. plasma jet modelling and plasma gasification of refuse-derived fuel (RDF). The first part of the research related to plasma jet modelling is situated by outlining the details of thermal plasma systems and the challenges of modeling the complex physical phenomena involved. An important issue arising from the mixing of high-temperature plasma gas(es) with surrounding gas(es) is the correct estimation of thermodynamic and transport properties of the resulting gas mixture. The use of mixing rules for the calculation of thermophysical properties of a gas mixture is common practice. However, it was recognized that the influence of these approximations on the accuracy of the simulated flow field has not yet been quantitatively investigated.

A model of the plasma jet from a direct current (DC) hybrid water/gas-stabilized torch, particularly suited for plasma gasification, issuing in nitrogen atmosphere has been developed. With this model case, three computational fluid dynamics (CFD) simulations were performed, which differ in the extent to which mixing rules are used for the calculation of the thermophysical properties of the ternary ($Ar/H_2O/N_2$) gas mixture. The first model approach (model 1) estimates the properties of the gas mixture by using mixing rules with the temperature-dependent properties of each individual gas. The second model approach (model 2) calculates the properties of the plasma gas (Ar/H_2O) rigorously and combines them with those of nitrogen by using mixing rules to estimate the properties of

the ternary gas mixture. Model 3 represents the full multicomponent approach in which no mixing rules are used and the thermophysical properties of the gas mixture are calculated rigorously.
The effect of the mixing rules for the calculation of gas mixture properties is evaluated through comparison of calculated temperature, velocity and gas concentration fields of the plasma jet flow.
The results revealed that the use of approximate mixing rules can greatly influence the calculated flow of a plasma jet. It was demonstrated that the effect caused by deviations from the exact molecular transport properties by using low-accuracy mixing rules such as the one of Mason and Saxena for thermal conductivity is non-negligible. It is proven that the assumption of a negligible contribution of the laminar transport properties in relation to their turbulent counterparts (frequently postulated in literature), is not self-evident. In plasma jet modelling, the level of turbulence in the high-temperature region close to the torch exit is often low and the interaction of the thermophysical properties at the boundary of the jet in this quasi-laminar region determines to a great extent the onset of turbulence and hence the entrainment of surrounding gas.

The second subject studied in the PhD work is the plasma gasification of waste. The thermal plasma application in solid waste treatment is first put in relation to conventional thermochemical waste conversion methods. The advantages and challenges of plasma gasification are explained and the different possibilities for end-use of the products (syngas and slag) are listed. The state of the art of plasma gasification is illustrated by summarizing all the plasma gasification facilities currently operating in the world. The plasma gasification system at the Institute of Plasma Physics (IPP) in Prague (Czech Republic) is one of only a limited number of academic installations and has delivered significant contributions to this field of research. The configuration of this reactor system and details of its extensive diagnostics system are described.
Refuse-derived fuel (RDF), a processed mixture of excavated municipal and industrial solid waste was selected as the feedstock to evaluate the performance of the in-flight plasma gasification process for materials with a high inorganic content. During the experimental run, different combinations of gasifying agents (CO_2, O_2 and H_2O) were added to the reactor volume and the material was supplied at different mass flow rates (i.e. 21.3 and 28.9 $\mathrm{kg\,h^{-1}}$). The sets of experimental data consist of syngas composition and flow rate, energy losses from the torch and the reactor walls, and temperature distribution in the reactor volume. Nine experimental cases with different operating parameters were identified during steady

state operation. The production of high-quality syngas with low levels of tar (132-543 mg/Nm^3) was demonstrated for all cases. The measured syngas composition was in good accordance with the calculated syngas composition in thermodynamic equilibrium. The effects of equivalence ratio, material feed rate and type of gasifying agent were investigated by comparing the performance criteria (carbon conversion efficiency, CO yield and H_2 yield) and energy efficiencies of the different cases. The carbon conversion efficiency of plasma gasification with a RDF feeding rate of $28.9\,kg\,h^{-1}$ ranges between 82 and 87 %. The highest registered cold gas efficiency and mechanical gasification efficiency are 57 % and 97 %, respectively. It was found that the oxy-steam plasma gasification showed the highest material conversion efficiency. Furthermore, it was found that for the same equivalence ratio, the H_2/CO ratio in the syngas can be inverted by interchanging CO_2 with H_2O as gasifying agent without affecting the performance of the process.
The lower performance of the RDF experiments compared to biomass experiments on the same plasma gasification system were attributed to the coarser particle size, higher moisture content and higher ash fraction of RDF. The comparative analysis between this single-stage plasma gasification experiment and two-stage plasma gasification of a similar waste material revealed advantageous characteristics (higher CO and H_2 content and higher CO/CO_2 ratio) for the syngas produced by the former system. The tar destruction efficiency is considered similar for both systems. The inorganic content is collected as a vitrified slag in the two-stage plasma gasification system, whereas a large portion of the residual material in the single-stage in-flight gasification system was recovered as particulates and only a small fraction of the inorganic fraction was vitrified in the wake of the plasma jet. It was concluded that the good control of the characteristics of the high-quality syngas and the overall flexibility of the system make plasma gasification a promising technology for the treatment of refuse-derived fuel.

Contents

Abbreviations and Symbols

Abbreviations

AC	Alternating Current
AER	Absorption Enhanced Reforming
APP	Advanced Plasma Power
ASCR	Academy of Sciences of the Czech Republic
ASR	Automobile Shredder Residue
BFB	Bubbling Fluidized Bed
BM	Biomass
BTEX	Benzene, Toluene, Ethylbenzene and Xylene
BTX	Benzene, Toluene and Xylene
CCE	Carbon Conversion Efficiency
CEN	European Committee for Standardization
CFB	Circulating Fluidized Bed
CFC	Chlorinated Fluorocarbons
CFD	Computational Fluid Dynamics
CGE	Cold Gas Efficiency
CHP	Combined Heat and Power
DC	Direct Current
DCM	Dichloromethane
DME	Dimethyl Ether
DNS	Direct Numerical Simulation
DOM	Discrete Ordinates Method
ELFM	Enhanced Landfill Mining
ER	Equivalence Ratio
FTS	Fischer-Tropsch synthesis
GC	Gas Chromatography
GC-FID	Gas Chromatography with Flame Ionization Detector
GFC	Gas Flow Controller

GHV	Gross Heating Value
HTFT	High Temperature Fischer-Tropsch
IGCC	Integrated Gasification Combined Cycle
IGFC	Integrated Gasification Fuel Cell
IPP	Institute of Plasma Physics
IW	Industrial Waste
LCE	Local Chemical Equilibrium
LES	Large Eddy Simulation
LHV	Lower Heating Value
LILRW	Low and Intermediate-Level Radioactive Waste
LTE	Local Thermodynamic Equilibrium
LTFT	Low Temperature Fischer-Tropsch
MAS	Mixed Alcohol Synthesis
MGE	Mechanical Gas Efficiency
MPTS	Mobile Plasma Treatment System
MS	Mass Spectrometry
MSW	Municipal Solid Waste
MTBE	Methyl Tetra Butyl Ether
NCV	Net Calorific Value
NEC	Net Emission Coefficient
NLTE	Non Local Thermodynamic Equilibrium
ODS	Ozone Depleting Substances
PAHWTS	Plasma Arc Hazardous Waste Treatment System
PAWDS	Plasma Arc Waste Destruction System
PCB	Polychlorinated Biphenyl
PCDD	Polychlorinated Dibenzo-p-dioxins
PCDF	Polychlorinated Dibenzofurans
PDMR	Plasma Direct Melting Reactor
PEM	Plasma Enhanced Melter
PEPS	Plasma Energy Pyrolysis System
PODS	Plasma Ordnance Demilitarization System
POP	Persistent Organic Pollutant
PRRS	Plasma Resource Recovery System
PTDR	Plasma Thermal Destruction & Recovery
RANS	Reynolds-Averaged Navier Stokes
RDF	Refuse-Derived Fuel
RMS	Root-Mean-Square
RF	Radio Frequency

RTE	Radiative Transfer Equation
S	Soret effect
SI	Spark Ignition
SMR	Steam Methane Reforming
SPA	Solid Phase Adsorption
SPE	Solid Phase Extraction
SOFC	Solid Oxide Fuel Cell
SRF	Solid Refuse Fuel
SSW	Sewage Sludge Waste
TF	Thermo-field
UDF	User-Defined Function
UV	Ultraviolet
VITO	Flemish Institute for Technology Research
VOC	Volatile Organic Compound
VUV	Vacuum Ultraviolet
WPC	Westinghouse Plasma Corporation
WtE	Waste-to-Energy
WtM	Waste-to-Material
YSZ	Yttria-Stabilized Zirconia

Symbols

a	Subscript to an element in the chemical formula of reactant	-
A	Substitute chemical notation for ash	-
A	Surface of the plasma column cross section	m^2
$\boldsymbol{B}$	Magnetic field	T
CFL	Courant-Friedrichs-Lewy number	-
c	Speed of sound	$\mathrm{m\,s^{-1}}$
C_p	Specific heat at constant pressure	$\mathrm{J\,kg^{-1}\,K^{-1}}$
D_{ij}	Binary diffusion coefficient	$\mathrm{m^2\,s^{-1}}$
D_i^T	Thermal diffusion coefficient of species i	$\mathrm{g\,m^{-1}s^{-1}}$
$\overline{D_{ij}^T}$	Combined temperature diffusion coefficient	$\mathrm{g\,m^{-1}s^{-1}}$
$\overline{D_{ij}^x}$	Combined ordinary diffusion coefficient	$\mathrm{m^2\,s^{-1}}$
e	Electron	-
e	Electronic charge	C
E	Specific total energy	$\mathrm{J\,kg^{-1}}$

E_f	Energy content from enthalpy of formation	$\mathrm{kJ/kg_{RDF}}$
E_{gas}	Energy required for complete gasification of RDF	$\mathrm{kJ/kg_{RDF}}$
E_q	Energy content from sensible heat	$\mathrm{kJ/kg_{RDF}}$
ϵ	Dissipation rate of turbulent kinetic energy	$\mathrm{m^2\,s^{-3}}$
ϵ_N	Net emission coefficient	$\mathrm{W\,m^{-3}\,sr^{-1}}$
η	Thermal torch efficiency	%
F	Flow rate	$\mathrm{slm\ or\ ml\,min^{-1}}$
g	Gravity	$\mathrm{m\,s^{-2}}$
G	Conductance	S
h	Enthalpy	$\mathrm{J\,kg^{-1}}$
$H_f{}^\circ$	Standard enthalpy of formation	$\mathrm{kJ\,mol^{-1}}$
I	Current	A
$\boldsymbol{j}$	Current density	$\mathrm{A\,m^{-2}}$
$\boldsymbol{J}_i$	Mass flux of species i	$\mathrm{kg\,m^{-2}\,s^{-1}}$
k	Thermal conductivity	$\mathrm{W\,m^{-1}\,K^{-1}}$
k	Turbulent kinetic energy	$\mathrm{J\,kg^{-1}}$
k_B	Boltzmann Constant	$\mathrm{J\,K^{-1}}$
l	Length	m
m	Mass	kg
$\dot{m}$	Mass flow rate	$\mathrm{g\,min^{-1}\ or\ kg\,h^{-1}}$
M	Molecular weight	g/mol
$\overline{m_i}$	Average molar mass of the heavy species of gas i	g/mol
μ	Dynamic viscosity	$\mathrm{kg\,m^{-1}\,s^{-1}}$
μ_0	Permeability of free space	$\mathrm{H\,m^{-1}}$
μ_t	Turbulent viscosity	$\mathrm{kg\,m^{-1}\,s^{-1}}$
n	Molar amount	mol
N	Total number density	$\mathrm{m^{-3}}$
n_{ash}	Number of ash components	-
n_e	Electron number density	$\mathrm{m^{-3}}$
n_i	Number density of gas i	$\mathrm{m^{-3}}$
n_{prod}	Number of products in the full oxidation reaction of RDF	-
n_{RDF}	Number of elements in the generic formula for RDF	-
n_{SG}	Number of syngas components	-
p	Pressure	Pa
P	Power	kW
P_{static}	Static or gauge pressure	Pa
q	Coefficient to the products of a chemical reaction	$\mathrm{mol/mol_{RDF}}$

r	Radial position	m
r	Molar ratio of gasifying agents	-
R	Net energy loss by radiation	$\mathrm{W\,m^{-3}}$
R	Torch radius	m
r_i	Net rate of production of species i	$\mathrm{kg\,m^{-3}\,s^{-1}}$
R_p	Absorption radius in the NEC method	m
ρ	Density	$\mathrm{kg\,m^{-3}}$
Sc_t	Turbulent Schmidt number	-
σ	Electrical conductivity	$\mathrm{S\,m^{-1}}$
t	Time	s
T	Temperature	K
T_H	Temperature of the heavy species	K
$\boldsymbol{\tau}$	Stress tensor	-
U	Potential difference	V
v	Velocity	$\mathrm{m\,s^{-1}}$
V_m	Molar volume at standard conditions	$\mathrm{l\,mol^{-1}}$
w_{H_2O}	Moisture content	dry wt%
$w_{i,ash}$	Normalized weight fraction of ash component i excluding P_2O_5 and SO_3	-
x	Molar fraction	-
y	Mass fraction	-
Y	Mass fraction	-
z	Coefficient to oxygen in a chemical reaction	$\mathrm{mol/mol_{RDF}}$

Units

A	Ampere
C	Coulomb
J	Joule
kt	Kilotonne
Pa	Pascal
S	Siemens
slm	Standard litres per minute
T	Tesla
tpd	Tonnes per day
tpy	Tonnes per year
tph	Tonnes per hour

vol%	Volumetric percent
W	Watt
wt%	Weight percent

Subscripts

0	Centreline
C	Carbon
e	Electron
(g)	Gas
H	Hydrogen
i	Species i
in	Inlet
j	Species j
JH	Joule heating
(l)	Liquid
mix	Gas mixture
req	Required
SG	Syngas
t	Turbulent
w	Wall

Superscripts

$^\circ$	Standard conditions
(2)	Binary gas mixture
(3)	Ternary gas mixture

Introduction

Problem statement

The intense research and development efforts in plasma research since the 1960s are allowing plasma to continuously find its way into new fields of applications. Besides the well-established plasma spraying, plasma cutting and plasma welding techniques, thermal plasma materials processing applications also include the melting of metals and the vitrification of incinerator ashes. The recent focus on resource recovery in the waste industry (i.e. material recuperation and/or energy valorization) has triggered the search for more advanced waste treatment technologies, in which thermal plasma treatment has been recognised as a promising technology. Thermal plasma technology has several advantages over conventional waste elimination technologies (incineration in particular) which can allow viable resource recovery from non-conventional sources like municipal solid waste (MSW) and industrial waste (IW) through the production of synthetic gas (syngas). Hence, the thermochemical conversion of a wide variety of waste materials by plasma pyrolysis (in absence of oxygen) and by plasma gasification (i.e. by adding controlled amounts of oxygen) has been studied with ever-growing interest over the last 15 years.
Within the scope of these evolutions, the Hybrid Plasma Thermal Gasification & Vitrification research- and development project was erected at the Department of Thermal Plasma of the Institute of Plasma Physics (IPP) of the Czech Academy of Sciences in Prague (Czech Republic) under impulse and in close collaboration with the Faculty of Engineering of Ghent University in 2004. A picture of the pilot-scale plasma gasification reactor which was built is shown in Figure I.1. This system is equipped with the IPP's signature DC hybrid plasma torch, ideally suited for materials treatment thanks to its high-temperature, high enthalpy flow at low mass flow rates.

Through a great number of experiments, the research on this system has significantly contributed in showing a proof of concept for the performant and

Figure I.1: Picture of the plasma gasification reactor at the IPP during operation

environmentally-sound treatment of waste by the innovative plasma gasification technology. Most of the materials treated (e.g. pure plastics or biomass) contain almost exclusively organic components. Considering the distinct advantages of plasma treatment, such a system is more likely to be employed for the conversion of more difficult waste streams. Therefore, it is necessary to validate the performance of the system for waste streams with a significant inorganic content.

Generally, the main challenges in further development and optimization of the process are identifying the effects of process parameters and operating conditions and demonstrating reproducibility of the results. These complications can only be removed by trial and error methods through repeated black-box experimentation. Unfortunately, plasma-based experiments are time consuming and costly (mainly because of the large amount of electricity used). Ruj and Ghosh [164] are among many researchers who therefore put forward that modelling of plasma gasification systems is much required. Babu [9] also

concluded that the capability of describing the process by kinetic modelling and simulation would be useful to predict the product gas concentration for various operating conditions and for a variety of feed mixtures. The overall purpose of the numerical modelling of a plasma gasification system is to improve the efficiency of the process through enhanced process control and to optimize the design.

A lot of the attempts at modelling the plasma gasification process found in literature are limited to a thermodynamic analysis by an equilibrium model. Mountouris et al. [130] developed the GasifEq model which aims at predicting the performance of the plasma gasification process through detailed energy and exergy analysis. In the validation of the equilibrium model with results from experiments, non-negligible deviations from the experimental values can be observed. The indication by Montouris et al. [130] that this is caused by the fact that equilibrium might not be attained in the experiments, illustrates the need for a more comprehensive fluid dynamic modelling approach. The incorporation of the effect of the flow field on the simulation results was also suggested as a next step from equilibrium modelling by Wang et al. [198].
The starting point in the computational fluid dynamic (CFD) modelling of plasma gasification is the accurate calculation of the plasma flow. The correct prediction of the velocity, temperature and concentration fields of the plasma jet exiting the torch is important since it directly influences any physical process taking place downstream. Nevertheless, the effect of the description of a plasma gas mixture and the connected thermophysical properties calculation have not yet been the subject of a quantitative study.

Research objectives

In this work, the goal is first to develop a CFD model of the plasma jet of the above-mentioned hybrid-stabilized plasma torch. This plasma model can then serve as the basis for a universal in-depth analysis of the effect of the estimation of thermophysical properties of a ternary plasma gas mixture on the three-dimensional (3D) simulated flow field. The second objective is to analyse the feasibility of treating waste materials with a high inorganic content in the plasma gasification system at the IPP.

Thesis outline

The first four chapters of the manuscript, grouped in Part I, present a literature study on the most important aspects related to the research. **Chapter 1** first provides background information about plasma. After explaining the general features, the focus is put on thermal plasmas and the characteristics of thermal plasma torches. Conventional gasification is the topic of **Chapter 2**, in which the technique is first situated among other thermochemical conversion methods. Next, the chemistry of the gasification process is summarized and an overview of the different elements of conventional gasification technology is given.
Chapter 3 is the culmination of the subjects of the two previous chapters, discussing plasma gasification. The added value of plasma to the gasification process and the consequent distinct features and (dis)advantages are presented. The possible end-uses of the products from a plasma gasification system, with the emphasis on syngas are also elaborated upon. Finally, a comprehensive list is given of all currently operating plasma gasification facilities in the world. Details of the plasma gasification technology providers, the treated material and the output of these plants are discussed and summarized. The last chapter of the literature study, **Chapter 4**, explains the different aspects of numerical modelling of plasma (jets). Special emphasis is put on the calculation of thermodynamic and transport properties and the use of mixing rules for multicomponent plasma gas mixtures.

Part II encompasses **Chapter 5**, which deals with the research related to plasma jet modelling. The modelling approach to the DC hybrid water/gas-stabilized plasma torch serving as the model case for the CFD simulations is explained. Then, the set-up of three plasma jet models which differ in the method for calculating thermophysical properties by the extent to which mixing rules are used, is presented. Through comparative analysis of the features of the calculated flow fields, the influence of the use of mixing rules on the accuracy of the simulation results is determined.

Chapter 6 in Part III presents the contribution to the performance evaluation of the plasma gasification unit located at the IPP. The experimental set-up of the system is first described in detail. Next, the experimental parameters and procedures used in the experiments on the plasma gasification reactor with refuse-derived fuel (RDF) using different combinations of oxidizing media are

given. The results from these experiments are evaluated by mass- and energy balances and compared with plasma gasification experiments with other materials, with other plasma gasification set-ups and with conventional gasification of RDF.

Finally, overall conclusions of the research work and some thoughts about future perspectives for plasma gasification and plasma modelling are given.

One

Literature Study

CHAPTER 1

Plasma

1.1 Definition and General Features

Plasma as a phenomenon was first described in 1879 by the English physicist Sir William Crookes, but it was only until 1929 that it was given the name plasma by Dr. Irving Langmuir [190]. Although natural plasmas on Earth are very exceptional (e.g. lightning and northern light), it is by far the most common state of matter, estimated to make up 99 % of the visible universe both by mass and by volume.

Plasma is described as the fourth state of matter, next to the solid, liquid and gas states. In forming a plasma, the molecules of a gas get sufficient energy and dissociate. If the thermal motion is strong enough, more and more atoms will be split into electrons and ions until the gas becomes ionized and is transformed into a plasma. In contrast to other phase transitions, ionization does not occur at a precise temperature, but happens gradually over a large temperature interval.

Plasma is defined as a quasi-neutral ensemble of positively and negatively charged particles and neutral particles, featuring collective behaviour, because local charge separation and electrical currents create additional electric and magnetic fields which, together with externally imposed fields, determine the equations of motion of the individual particles [190].

In other words, plasma resembles a high temperature gas with freely moving charged particles (positive and negative ions), neutral particles in ground and

exited states, high-mobility electrons and photons. In spite of the presence of positive and negative particles it remains an electrically neutral medium. This property is known as quasi-neutrality.
In contrast to a normal gas with electrically neutral particles, the charged particles make the plasma electrically conducting. Plasma is a source of concentrated energy, positive and negative ions, highly active radicals and intense radiation, which leads to complicated physical phenomena.

1.2 Classification of Plasma

Density and temperature are the two most important parameters characterizing a plasma.
The temperature (or kinetic temperature) of a plasma is defined by the average kinetic energy of a particle (molecule, atom, ion or electron), i.e.

$$\frac{1}{2}m\bar{v^2} = \frac{3}{2}k_B T \tag{1.1}$$

where m is the mass of the particles, $\bar{v^2}$ is defined by $(\bar{v^2})^{\frac{1}{2}}$, which is the root mean square speed of the particle, k_B is the Boltzmann constant and T represents the absolute temperature (K).
It is clear from this equation that the temperature is dependent on a mean speed. In a plasma, the speed of the particles at equilibrium is not unique but follows a Maxwell-Boltzmann distribution.
Plasmas can be classified into different categories in terms of electron temperatures and electron densities (see Figure 1.1). Extreme conditions in terms of electron density and temperature exist in thermonuclear fusion plasmas with temperatures above 10^6 K and as high as 10^8 K [18]. These plasmas, also called 'high-temperature plasmas', imply that all species (electrons, ions and neutral species) are in a thermal equilibrium state. Besides thermonuclear fusion plasmas, a distinction is made between thermal and non-thermal plasmas. Consistent with the previously mentioned terminology, these two categories can also be referred to as 'low-temperature plasmas' or gas discharges.
Thermal plasmas (hot plasmas) are characterized by their high-energy densities and the equality between the temperatures of the heavy particles T_H and those of the electrons T_e. The thermodynamic state of the plasma approaches local thermodynamic equilibrium (LTE) and these plasmas are therefore also called quasi-equilibrium plasmas. Non-thermal plasmas (cold plasmas) on the other hand are characterized by their lower energy densities and by the large difference between the electron and heavy particle temperatures ($T_H \ll T_e$) and are also

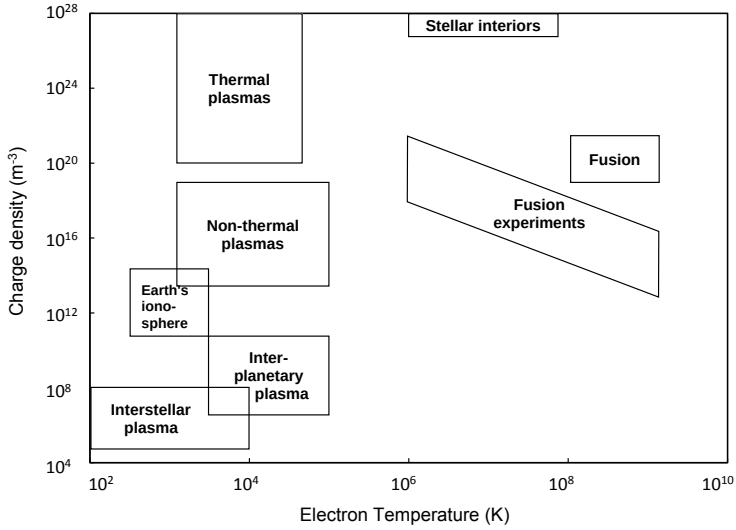

Figure 1.1: Classification of plasmas. Reproduced from [142]

called non-equilibrium plasmas [17].
It will be described in Paragraph 1.3 that a plasma is maintained throughout collisions between the different particles. The state of equilibrium of a plasma will depend on the collision frequency and the energy exchange during a collision. These two parameters strongly depend on pressure, as can be seen from Figure 1.2. A high gas pressure implies many collisions in the plasma (i.e. a short collision mean free path, compared to the discharge length), leading to an efficient energy exchange between the plasma species, and hence, equal temperatures. A low gas pressure, on the other hand, results in only a few collisions in the plasma (i.e. a long collision mean free path compared to the discharge length), and consequently, different temperatures of the plasma species due to inefficient energy transfer [15].

1.2.1 Non-Thermal Plasma

Cold plasmas refer to low-pressure plasmas where most of the coupled electrical energy is primarily channelled to the electron component of the plasma. Energetic electrons are thereby produced with a high temperature (T_e) instead of heating the entire gas stream. The plasma ions and neutral components remain at or near room temperature (T_H) and their thermal motion can be ignored. Non-thermal

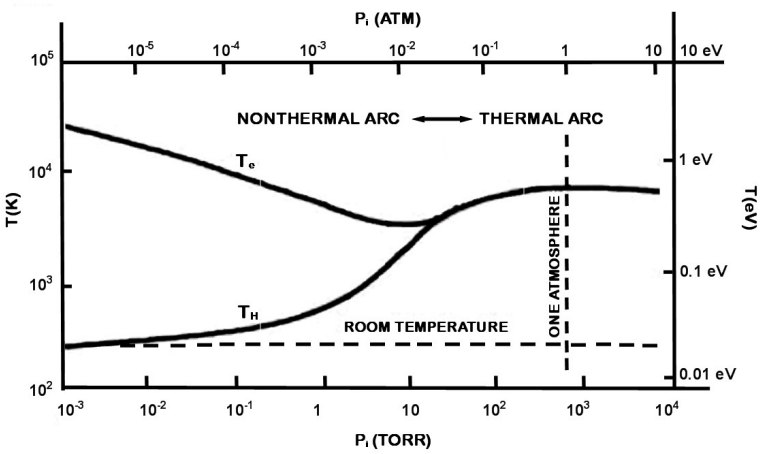

Figure 1.2: The electron temperature (T_e) and heavy particles temperature (T_H) as a function of pressure. Reproduced from [108].

plasmas are thus characterized by non-equilibrium (i.e. the non-thermal arc region in Figure 1.2). Examples of these plasmas are different types of glow discharges, low-pressure radio frequency (RF) discharges and corona discharges.
Because the temperature of ions and neutrals remains relatively low, this characteristic provides the possibility of using cold plasmas for low temperature plasma chemistry and for the treatment of heat sensitive materials including polymers and biological tissues [143]. A detailed review comprising various types of non-thermal plasmas with the mechanisms of their generation and with their applications is published by Bogaerts et al. [15].

1.2.2 Thermal Plasma

Thermal plasmas are typically at atmospheric pressure or higher and are characterized by an equilibrium or near equality between electrons, ions and neutrals ($T_e = T_H$). These plasmas are in a local thermal equilibrium (LTE) state, because it is assumed that the collisions dominate other physical processes in the plasma. In that case, the local velocity and energy distribution of particles is given by the Maxwell distribution and Boltzmann distribution respectively, and consequently a temperature can be defined. Thermal plasmas are characterized by high enthalpy contents and high temperatures, typically 2000 up to 20 000 °C [194].
Other properties of thermal plasmas include:

- A high energy density and a high energy transfer rate

- Short reaction times for chemical reactions in the plasma
- Wide choice of plasma media; at high temperatures any material can be plasma

These characteristics make plasma suitable for a diversity of industrial applications and interesting for many research possibilities. Next to lightning as a natural phenomenon, well established industrial applications of thermal plasmas are cutting, welding, spraying, analysis by inductively coupled plasma, furnaces for metallurgy with DC arcs and graphite electrodes, tundish heating, metal melting and purification, and environmentally friendly treatment of waste streams with plasma torches, etc.
The research presented in this work deals with thermal plasma and the content of the next chapters will concern only this type.

1.3 Plasma Forming Mechanisms

Plasmas are formed by supplying energy to a neutral gas causing the formation of charge carriers. When man-made plasmas are considered, this can be achieved by either subjecting the gas to electromagnetic radiation (e.g. microwaves for non-thermal plasmas and lasers for thermal plasmas), or by driving an electric current through the gas. Other possibilities include supplying thermal energy, for example in flames, where exothermic chemical reactions of the molecules are used as the prime energy source, or applying adiabatic compression to the gas which can heat it up to the point of plasma generation.
The most common way for transferring energy to the working gas and generating plasma is by means of an electric field. The mechanism of formation of a thermal plasma is further illustrated through the process of electrical breakdown of a direct current (DC) gas discharge.

At room temperature, gases consist of neutral species and are good insulators (i.e. non-conductive). The collisions that occur between molecules are elastic so they only change in speed and direction. To generate enough charge carriers to make the gas electrically conducting, a sufficiently high potential difference is applied between two electrodes placed in a gas. In a normal gas, the negatively charged electrons form an electrically neutral system around the positive charge in the nucleus. However, it is supposed that a few electrons are always present in

the gap between the electrodes, either by emission from the electrodes, by cosmic radiation or as a consequence of field emission from asperities on the surface, close to which electric fields are strongly enhanced [20]. These electrons are accelerated by the action of the electric field and collide with the gas molecules. If these collisions are inelastic, new electrons and ions are produced in the gas phase by different ionization processes (incl. direct or stepwise electron-impact ionization or photo-ionization) [59].

$$\begin{aligned} e^-_{fast} + A &\rightarrow e^-_{slower} + A^* \\ &\rightarrow e^-_{slower} + A^+ + e^- \end{aligned} \tag{1.2}$$

Due to the externally supplied electric field, the ejected electrons accelerate and gain kinetic energy and more inelastic collisions occur. This process leads to an avalanche of charged particles in an intense quasi-neutral cloud of free electrons, ions and neutrals in constant agitation [36]. This creates a conductive path for an electric arc to form between the cathode and anode. This event is called electrical breakdown. Because of the electrical resistivity across the system, significant heat is generated by the arc (in general by the Joule effect), which is first captured by the electrons because of their high mobility and which strips them away from the gas molecules. The electrons transfer part of this absorbed energy to the heavy particles by elastic collisions. Due to the high electron number density, n_e, in thermal plasmas, elastic collision frequencies are very high, so energy transfer is important and leads to an equal distribution of the energy. The electrons are also mainly responsible for inelastic collisions, such as ionization, recombination, excitation, de-excitation, attachment, and detachment. To summarize, in a discharge, the plasma is generated by a current flowing in a partially or fully ionized gas, dissipating sufficient energy to keep the gas ionized and conducting. This process continues in a self-sustaining manner, provided a steady source of energy is continually applied. The arc discharges provide a high density, high temperature region between the electrodes. With the aid of a sufficiently high gas flow, introduced in the electrode gap, the plasma extends beyond one of the electrodes, thereby transporting the plasma energy to the reaction region [68]. This part of the plasma is called the plasma jet.

A plasma torch, also known as plasmatron, is the device that generates a directed flow of thermal plasma from its nozzle. Plasma torches vary in the primary electricity source used, which can be direct current (DC), alternating current at mains frequency (50Hz) (AC) or alternating current at radio frequency (RF). Other

aspects which distinguish a specific plasma torch are the arc stabilization mechanism, the plasma gas, the type of flow, electrode geometry and electrode cooling. These elements will be presented with the main emphasis on the characteristics of a DC plasma torch, which is of interest in this research.

1.4 Thermal Plasma Torch Characteristics

Plasma can be generated by various methods of discharges. In Bogaerts et al. [15], the different types forming non-LTE plasmas, their working principles and their applications are elaborated upon. The two main types of discharges used for the generation of thermal plasmas are the electric arc (DC or AC) and the high frequency (HF) or radio frequency (RF) induction discharge. For the arc discharge generator, further classification can be made, first according to the energy transfer mechanism, namely as non-transferred arc or transferred arc plasma torch if the material to be treated serves as one of the electrodes and secondly according to the cathode emission mechanism [74]. Some hybrid plasma torches have also been developed by the superposition of more than one plasma-generating device. Examples are a combination of DC and RF plasma torches and the combination of two RF plasma torches in tandem operating at two different frequencies. Although these can be advantageous in specific applications, it is unlikely because of their complexity that their use will grow to replace alternate simpler plasma systems [17].

1.4.1 Type of Plasma Discharge

1.4.1.1 Alternating Current (AC)

AC thermal plasma torches are particularly applied as high-power plasma generators, but are not widely used. In this type of generator, the gas is heated by the energy of an alternating current of industrial frequency. The physical processes of the burning of the arc at direct and alternating current are basically identical [217]. The application of alternating current is associated with difficulties caused by the variability with time of the electrical parameters of the power source. On the other hand, the technological complexity of the power supplies of the DC torches involves a costly price, mainly due to the rectifier part of the electrical signal which can involve an increase of 30 percent of the price of the power supply. AC power supplies could be an alternative for reducing costs [53].

1.4.1.2 Radio Frequency (RF)

Almost all RF torches are inductively coupled discharges, in which the discharge is sustained by the coupling of energy to the plasma through the electromagnetic field of the induction coil. The plasma gas does not come in contact with the electrodes, thus eliminating possible sources of contamination and allowing for the operation of such plasma torches with a wide range of gases, including inert, reducing, oxidizing and other corrosive atmospheres. The excitation frequency is typically between 200 kHz and 40 MHz. Laboratory units run at power levels of the order of 30-50 kW, while large-scale industrial units have been tested at power levels up to 1 MW.

1.4.1.3 Direct Current (DC)

Among the most commonly used plasma-generating devices in material processing are DC plasma torches [17]. DC arc generated plasmas involve the use of DC electric currents as high as 10^5 A, across two electrodes which create a potential difference in the input gas. The gas is forced to pass through the confined space between the two electrodes which provides the energy required, beginning the electrical breakdown that leads to plasma generation. The plasma extends beyond the anode in the form of a high enthalpy, high-temperature plasma jet. The majority of plasma arc generators used in materials processing use DC rather than AC because there is less flicker generation and noise, a more stable operation, better control, a minimum of two electrodes, lower electrode consumption, slightly lower refractory wear and lower power consumption [68]. Ruj and Ghosh [164] describe one major drawback with DC thermal plasma arc generators, a phenomenon called sputtering where the discharged ions and atoms from the plasma gas collide with the cathode surface causing the release of some atoms from the cathode. These can be deposited along the circular anode surface or pass through the opening along with the arc and contaminate the reactants. This reduces the life-span of the electrodes and extensive cooling of the electrodes is necessary for stable arc operation. More than 50 percent of electrical energy fed into thermal plasma can be wasted through cooling water resulting in a poor energy efficiency of the thermal plasma torch. Power dissipated in the arc column is divided between Joule heating effect (heat generation) and the heat losses by conduction, convection and radiation. The essential components, which determine the functional design of the plasma torch and consequently the plasma properties, are the arc electrode design and the choice of plasma forming gas.

1.4.2 Torch Operating Mode

The design of DC plasma arc generators differs greatly depending on whether they are transferred or non-transferred. The plasma jet can be operated in a transferred/non-transferred mode depending on whether the arc is electrically transferred to the work piece or not. With transferred arcs (Figure 1.3a), the

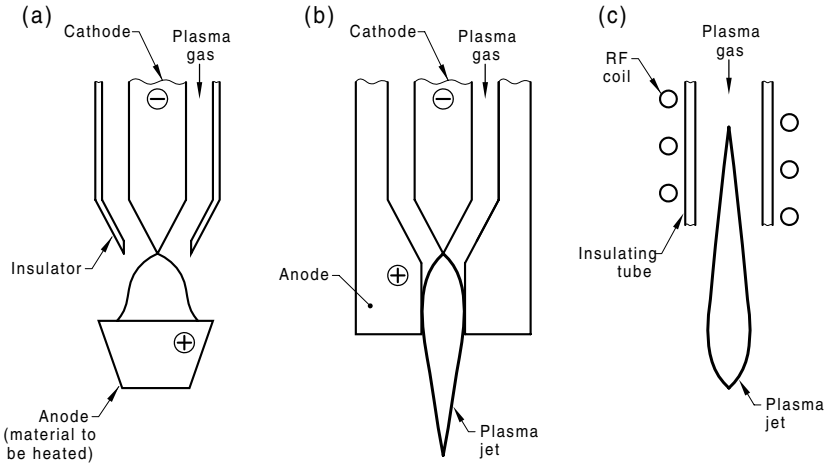

Figure 1.3: Operating modes of thermal plasmas. (a) DC transferred arc; (b) DC non-transferred arc; (c) RF inductively-coupled plasma torch [136].

treated material forms one of the electrodes, whereas with non-transferred arcs (Figure 1.3b), both electrodes are incorporated in the generator and differ from the substance being treated. The electrodes in the latter configuration have the sole function of generating the plasma. The transferred arc mode torches operate with low gas flows and high torch voltages. The torches in non-transferred arc mode need high operating currents and have comparatively lower efficiencies [194]. Non-transferred DC arc torches are used popularly for their high temperature plasma arcs and better mixing of the plasma with reactants. In transferred arc generators, one of the electrodes, usually the anode has a large separation with respect to the cathode. Transferred arc reactors can utilise multiple rod electrodes to generate a plasma arc.

1.4.3 Type of Electrodes

To achieve reliable and reproducible processes, the erosion of the torch electrodes has to be understood and controlled. The concept of DC torches is simple: they

comprise of a cathode, a plasma forming gas injector and an anode nozzle. An additional classification of the arc discharge generator can be made by the cathode emission mechanism which characterizes the arc operation. The cathode is the source of electrons for maintaining the arc discharge. There are two basic mechanisms by which a surface can provide these electrons. The first mechanism involves thermionic emission from the cathode surface heated by the arc to a temperature allowing the escape of sufficiently large numbers of electrons [194]. In most cases (98 %), they are made of tungsten doped with 1-2 wt% of ThO_2 (thoriated tungsten) [57]. The role of the dopant is to lower the tungsten work function and thus the operating temperature. Thoriated tungsten cathodes cannot be used with oxidizing gases since they would damage the tungsten cathode. Consumable graphite electrodes are used instead. For industrial applications various types of DC plasma torches are used with either stick- or button-type 'hot cathodes'. The stick-type cathodes are cylindrical (diameter-length ratio $< 2/20$) with a conical tip and operate at power levels in a range between 10 and 150 kW, with arc currents generally below 1000 A.
The second method is field emission of electrons due to high electric fields in front of the surface. This emission mechanism rarely provides a sufficient number of electrons for arc plasmas, but combinations of field emission with either thermionic emission (thermo-field (TF) emission) or an emission mechanism where microscopic evaporation sites provide a partially ionized metal vapor, are the dominant providers of electrons with "cold cathodes" [74]. These water-cooled cathodes are of the well-type. Typical materials are copper or zirconium/zirconia [194]. It is also good to mention that the design of the gas injector, close to the cathode tip, plays a key role not only in the operating conditions of the torch, but in the cathode erosion as well. Because the cathode spot is molten over a given current, the cold gas flow close to the cathode tip has to be well controlled to avoid the blowing of the molten pool.
The anode can have different configurations with respect to the jet axis. The two orientations are orthogonal to the jet axis (in transferred arcs) and parallel to the jet axis. In the latter case, with a superimposed flow to the arc, the anode attachment is unsteady. The connection column between the arc column and the anode surface crosses the cold gas boundary layer and is pushed downstream by the flow.

1.4.4 Arc Stabilization Mechanisms

Venkatramani et al. [194] describe the need for arc stabilization well by stating that the plasma arc is a highly unstable, turbulent discharge phenomenon

and that disturbances from equilibrium are undesirable, as they will tend to extinguish the arc. The instabilities inherent to thermal plasmas (e.g. electrical, thermal and magneto-hydrodynamic instabilities) are described in detail by Heberlein [74]. Under these circumstances, the stabilizing mechanism should come into play. The word 'stabilize' means to create and maintain boundary conditions, which will enable the arc to remain in a steady state. A plasma torch is a device which provides arc stabilization and enables the arc to remain in a steady state. It constricts the arc, cools the outer layers efficiently and defines the path for a steady passage of the electric current. Besides natural convection in free burning arcs, the two main types of stabilization are gas and water flows [194]. Other types of external stabilizing mechanisms are the cold surface of the arc torch chamber in wall-stabilization and an axial magnetic field preventing the expansion of the arc column, increasing the temperature and stabilizing the arc. The principle physical mechanisms that control arc and plasma properties in both gas- or water-stabilized arcs are axial heat transfer by convection and radial heat transfer by heat conduction and radiation [81].

1.4.4.1 Gas Flow Stabilization

Gas flow stabilization is the simplest and most common technique. A flowing external cold layer of gas surrounds the arc column and constricts it. Additionally, it serves as a protection for the torch walls from overheating. The flow can be vortex or axial, depending on the mode of injection. The vortex-stabilization is extremely effective in constricting the arc, increasing the energy density and the temperature, resulting in a short and intensive arc. The vortex flow creates centrifugal forces, which drive the cold gas towards the walls of the chamber and the axial component of the flow replenishes the cold gas flow.
The axial flow-stabilized arcs on the other hand have a laminar flow and the cold gas tends to surround the hot core and forms longer arcs. Illustrations of an axial flow-stabilized torch and a vortex flow-stabilized torch are shown in Figure 1.4.

Plasma torches used for cutting or spraying applications are normally vortex-stabilized, while axial flow-stabilized torches are used for metal processing applications. The most commonly used gases in the generation of plasma in gas-stabilized torches are argon, helium, nitrogen, air and hydrogen, or a mixture of these [194]. The choice of the plasma gas is based on gas enthalpy, reactivity and cost. Argon gas is used in some plasma torches as a heat transfer medium and for forming an inert atmosphere. This helps to prevent undesirable reactions, thus ensuring the purity of the operation and the product.

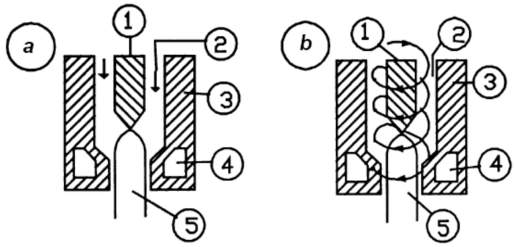

Figure 1.4: Plasma torch gas-stabilization schemes: (a) Axial flow-stabilized; (b) Vortex flow-stabilized. 1, Cathode; 2, Gas flow; 3, Anode nozzle; 4, Cooling channel; 5, Plasma jet [194].

Performance characteristics of a gas-stabilized torch in a specific application are determined by plasma jet characteristics which can be adjusted by torch design, choice of plasma gas and by arc current. In general the plasma created by this type of torch has a temperature between 8000 K and 15 000 K and a mean enthalpy that is usually not higher than 10 MJ kg^{-1} [81]. Gas plasma torches using steam as plasma gas only achieve mean temperatures below 4000 K [192].

1.4.4.2 Water-Stabilized Torches

Substantially different plasma jet parameters can be achieved in plasma torches with water flow stabilization. The arc is ignited in the centre of a water vortex, which is created in a cylindrical arc chamber by tangential injection of water. In water-stabilized torches (see Figure 1.5), the arc column is confined inside a vortex of liquid and it is stabilized by its interaction with the inner wall of that vortex.

Plasma is created by heating and ionization of steam that is produced by evaporation of water from the inner surface of the vortex. The steam that flows into the arc column is heated by absorption of radially transferred heat.
Water torches are characterized by very low mass flow rates of plasma, but high velocities of the plasma flow. For the same arc power the plasma enthalpy is several times higher (150-300 MJ kg^{-1}) than enthalpies achieved in common gas torches [95]. Water torches have typical low-density and high enthalpy, high temperature plasmas. These high reaction temperatures reduce the time constants of the decomposition of chemical substances and high process throughputs can be achieved.

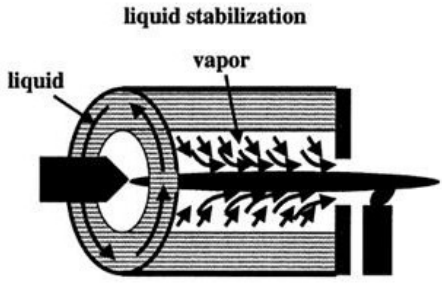

Figure 1.5: Water-stabilized torch [95]

1.4.4.3 Hybrid Water/Gas-Stabilized Torches

The substantial difference between gas- and water-stabilized arcs lies in the torch aspects that determine the flow rate of the plasma mass. In gas torches, the plasma mass flow rate is controlled independently by a flow rate of supplied gas. In water-stabilized torches, the flow rate of plasma is controlled by a balance of heat transfer in the arc column and cannot be adjusted independently like in gas-stabilized torches [81].

There are some limits in the range of adjustable plasma jet characteristics that are given by the principle of arc-stabilization. Physical limits of both gas- and water-stabilized arcs do not allow to cover a wide gap in plasma parameters between high enthalpy, low-density plasmas generated in liquid-stabilized torches, and lower enthalpy plasmas generated in gas-stabilized torches [191]. The different ranges of both types of torches as a function of these parameters is shown in Figure 1.6.

For better control of plasma jet characteristics, a new type of DC hybrid plasma torch (Figure 1.7) has been designed at the Institute of Plasma Physics (IPP) that utilizes combined gas-liquid stabilization. The hybrid torch unites both principles of water- and gas-stabilization of the arc.

Gas, such as argon, is supplied along the cathode with a vortex component to assure proper stabilization of the arc at the cathode nozzle. The gas which flows in this cathode part of the torch protects the cathode tip and hence the consumable carbon cathode used in water-stabilized torches can be replaced by a fixed tungsten cathode [191].

Subsequently, the plasma enters the second chamber which is surrounded by a water vortex, formed by a tangential injection of water. Interaction of the arc column with the water vortex causes evaporation from the inner surface of the vortex. The steam mixes with the gas flowing from the cathode section, and forms

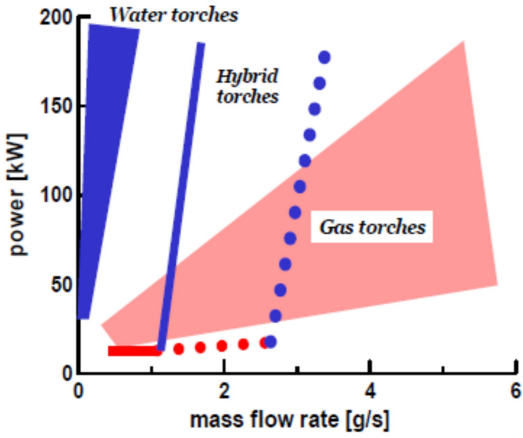

Figure 1.6: Operation regimes of plasma gas- and water-stabilized torches. Plasma mass flow rate (g/s) as a function of power (kW) [81].

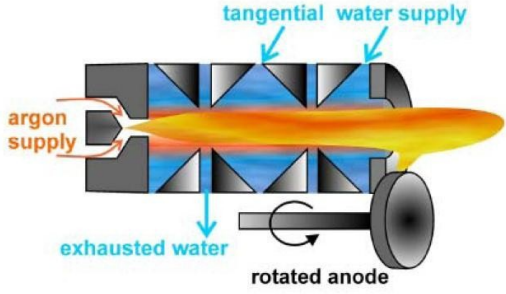

Figure 1.7: DC hybrid water/gas-stabilized plasma torch [95]

a plasma that consists of a mixture of steam and gas (e.g. argon). The overpressure which is produced in the arc chamber due to the evaporation, accelerates the plasma towards the exit nozzle. The anode of the torch is created by a rotating copper disk, which is positioned outside the arc chamber downstream of the torch exit nozzle (see Figure 1.7). Due to the principle of arc stabilization by a water vortex the flow rate of plasma gas is very low, plasma enthalpy is more than $200\,\mathrm{MJ\,kg^{-1}}$ and mean plasma temperature is more than $15\,000\,\mathrm{K}$ [88]. If argon is used as stabilizing gas, the hybrid torch keeps the same thermal characteristics as a water-stabilized torch with high enthalpy and high temperature but plasma density, velocity and momentum flux can be increased significantly (Figure 1.8).

These increases are due to the substantial difference between the plasma proper-

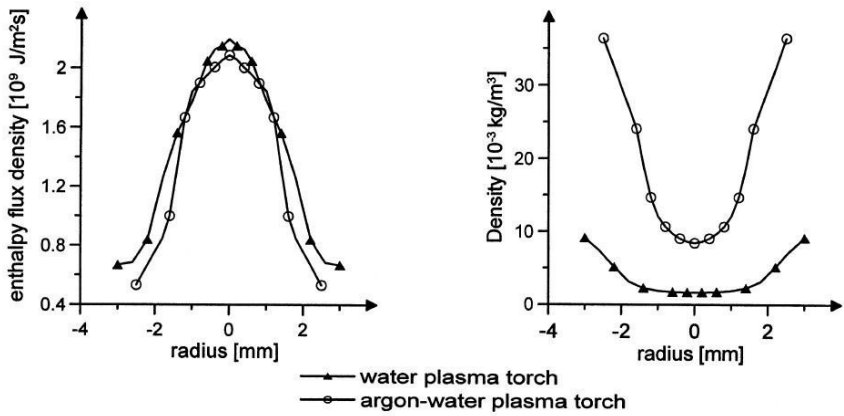

Figure 1.8: Radial profiles of enthalpy flux density and plasma density at the nozzle exit of water-stabilized and hybrid-stabilized torch at an arc current of 400 A [81].

ties of argon and steam plasmas. Enthalpy, heat conductivity, radiation intensity and absorption coefficients of argon plasma are much smaller than in the case of steam plasma. Therefore, the properties of plasma that are controlled by heat transfer change only slightly. The change of properties related to mass balance, on the contrary, is more substantial. By changing the argon flow rate, the hybrid torch provides the possibility of controlling the plasma jet characteristics and plasma composition in a wide range from high enthalpy, low density plasmas typical of water stabilized torches to lower enthalpy, higher density plasmas generated in gas stabilized torches [81] (see Figure 1.6). The other characteristic feature of this hybrid torch is the very low mass flow rate of plasma.

Experimental measurements of the plasma temperature showed that the energy balance in the arc column is almost independent of argon flow rate [22]. The inflow of argon plasma with very low enthalpy does not noticeably influence the radial transfer of energy to the wall, so the arc has electrical characteristics and power balances that are very close to the ones of water-stabilized torches. On the other hand, mass flow rate and momentum flux are strongly influenced by the argon flow and can be thus controlled almost independently of the power balance. Plasma velocity, enthalpy and other thermodynamic and transport properties can be varied in a wide range by changing argon flow rate [99].

The wide range of operating parameters of the hybrid-stabilized torch has distinct advantages in certain plasma applications.

- In plasma spraying, desired plasma characteristics according to the application can be selected by adjusting the torch parameters. This allows the same torch to be used for extremely high spraying rates and plasma temperatures, as well as for a reduction of spraying rate with an increase of particle velocities.
- Materials treatment such as plasma gasification could benefit from the specific characteristics of this torch. As a low amount of plasma carries high energy, the power needed for heating of plasma to reaction temperature is relatively low, and the efficiency of utilizing plasma power for decomposition is high. The large amount of energy at a low mass flow rate also decreases the contamination of plasma components in the product gas produced from decomposition of organic matter and provides high heat transfer rates from the plasma gas to the material.

The hybrid stabilization of the plasma arc also has an effect on the entrainment of surrounding atmosphere in the plasma jet [99]. The strong interaction between plasma and the ambient gas is brought about by the strong velocity and density gradients at the jet fringes and becomes apparent in reducing plasma temperature and velocity. The control of this effect is crucial for efficient plasma processing since it determines the conditions of the plasma flow field at the point of entry of material interacting with the plasma. That is why study of the entrainment process in the jets generated under different conditions is a question of great importance.

Many of the features of the hybrid stabilized plasma jet discussed above have been elaborately investigated by experimental measurements. A CFD model of the plasma jet from this hybrid plasma torch, however, has not yet been developed. Such a model would accelerate the efforts of visualizing the temperature and velocity field across the wide range of operating parameters. Additionally, the dynamic interaction between the plasma flow and the surrounding gas could be studied in detail. This could provide an understanding of the plasma properties controlling the entrainment processes. A model of the plasma jet would also allow optimization of the application of this torch for plasma spraying and plasma gasification. Based on a correct simulation of the plasma flow field, the point of entry of powder in plasma spraying or the position and configuration of plasma torches in a plasma gasification reactor can be determined.

CHAPTER 2

Plasma Gasification

2.1 Background

The fewer reserves of fossil fuels and a greater environmental awareness have prioritized sustainability in waste management practices. Simultaneously, the energy industry is experiencing a transition to renewable energy systems, in which among solar, wind and water, also waste (incl. biomass) is considered as a sustainable (potentially CO_2-neutral) energy source. The focus on improved resource recovery and the interest in energy valorization from waste have been triggering the development of more advanced methods and concepts for the conversion of waste to useful end-products.

One of the most current concepts is a circular economy, in which waste is managed as a resource, material loops need to be closed by direct recycling of pre-consumer manufacturing scrap/residues (e.g. steel slags), by urban mining of post-consumer End-of-Life products (e.g. recovery rare earth metals from electronic waste), and by landfill mining of historic (and future) urban waste streams [96]. In the context of the third approach, the concept of Enhanced Landfill Mining (ELFM) has been introduced by the Flemish ELFM Consortium in 2008. Currently, ELFM is defined as "the safe conditioning, excavation and integrated valorization of (historic and/or future) landfilled waste streams as both materials (Waste-to-Material, WtM) and energy (Waste-to-Energy, WtE), using innovative transformation technologies and respecting the most stringent social and ecological criteria" [96].

On the one hand, this definition incorporates the temporary storage concept and on the other hand, more relevant to the subject of the presented research, the need for innovative separation and transformation technologies. The development of advanced waste treatment technologies starts with understanding the conventional conversion methods and identifying their shortcomings.
The different conventional conversion pathways that have been commercially proven in a full-scale plant are shown in Figure 2.1, adapted from Helsen and Bosmans [75]. Depending on the type and characteristics (e.g. composition, moisture content, etc.) of the waste, the most suitable treatment option can be selected. The waste after pre-treatment, storage and/or transport can be treated

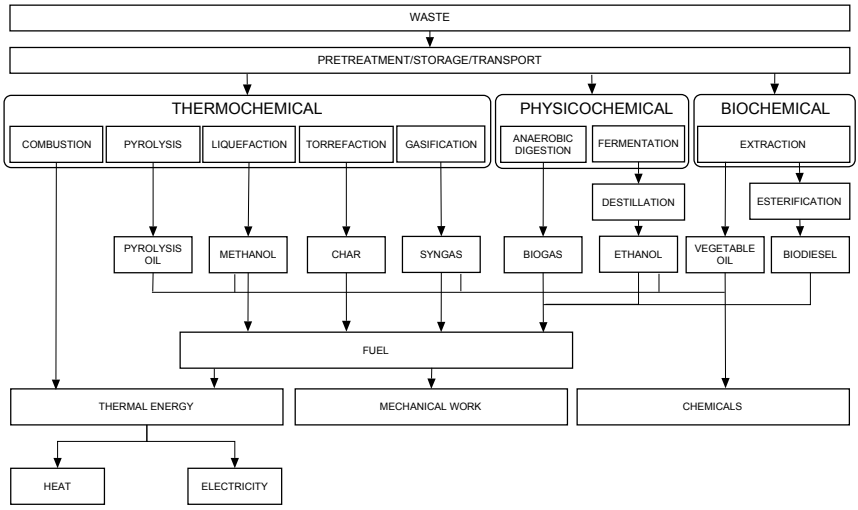

Figure 2.1: Different conversion pathways for waste

with a range of conversion technologies. The main products obtained from these processes (potentially after an intermediate physical or chemical step) can have different end-uses. The most frequently used approach for energy valorization from waste is combustion, from which the retrieved thermal energy can supply heat and/or generate electricity. The secondary energy carriers in the other pathways can be directly applied as chemical raw materials or utilised as alternative fuel sources. If these are not burned to provide heat and/or electricity, their energy content can be transformed to mechanical work (e.g. to drive a car or fuel a plane).
The waste-to-resource technologies can be divided into three categories, being thermochemical, physicochemical and biochemical conversion methods. Besides

combustion (or incineration), the other two main thermochemical conversion methods are pyrolysis and gasification. Since plasma gasification is a variation on conventional gasification, the specifics of this technology are briefly presented and its performance compared to the other thermochemical conversion methods. These will not be described in detail, but a comprehensive review of the available technologies for thermochemical treatment of waste streams was published by Bosmans et al. [16].

2.1.1 Incineration

Incineration is the exothermic oxidation of the combustible organic content in waste. During combustion, the majority of the fuel energy is contained as heat in the reaction products (mainly CO_2, H_2O and O_2), also called flue gases. If air is used as the oxidizer, the flue gas also contains nitrogen. For effective oxidative combustion, a sufficient oxygen supply is essential and the ratio of the amount of supplied air to the stoichiometric required amount for full oxidation usually ranges from 1.2 to 2.5. The incineration process has undergone rapid technological developments over the last 10 to 15 years which have been mainly directed towards reducing emissions. However, because of the oxidizing environment and relatively low operating temperatures between 500 and 1000 °C, not all harmful components (CO, hydrogen halides, nitrous oxides, sulphur oxides, heavy metal compounds and tar (e.g. dioxins (PCDD), furans (PCDF) and other volatile organic compounds (VOCs)) can be broken down and extensive gas cleaning is needed for save flue gas exhaust.
The inorganic content and unreacted carbon (soot) are recovered as fly ash (dust in the flue gas) and bottom ash (i.e. the heavier solid ash). Additional treatment can improve bottom characteristics and would allow its use in congregate aggregates. Fly ash immobilisation is required in order to make it environmentally safe for landfill disposal [16].

2.1.2 Pyrolysis

Pyrolysis is the thermal decomposition of organic material at elevated temperatures with limited amounts or in the absence of oxygen. The typical temperature range is from 400 to 900 °C, but usually lower than 700 °C. The pyrolysis process is endothermic, so heat needs to be provided to the material. This can be done by partial combustion of the waste material, by direct heat transfer from either the recycled product gas or circulating solids, and by indirect heat transfer from exchange surfaces. Three products are obtained depending on the modes of pyrolysis (slow, fast or flash): pyrolysis gas, pyrolysis oil and solid coke (charcoal).

The usefulness of pyrolysis for secondary fuel production or substance recovery from waste depends on the presence of potential pollutants, which could make the pyrolysis products (very) difficult to use [75].

2.1.3 Conventional Gasification

Gasification is the thermochemical conversion of solid, liquid, or gaseous carbonaceous material at increased temperatures (usually in the range of 700-1800°C) by means of sub-stoichiometric amounts of free oxygen or bound in the form of, for example, steam [72]. This means equivalence ratios, which are lower than 1, typically around 0.4-0.5. The carbon-rich material is converted by addition of controlled amounts of oxygen to a low-or medium-value syngas, which contains varying amounts of carbon monoxide, hydrogen, methane and possibly other gases.

The history of gasification dates back to the seventeenth century when the process was discovered in 1699 by Dean Clayton, who obtained coal gas from pyrolytic experiments. It was not until 1788 that the first patent with regard to gasification was issued to Robert Gardner [169]. Gasification was further developed during the nineteenth century in factories to produce town gas from coal and peat for lighting and cooking purposes, prior to the introduction of electricity and natural gas. Due to the shortage of petroleum during World War II, the gasification process for the production of fuel and chemicals was re-implemented and improved. The end of the war and the availability of cheap fossil fuel reduced the usefulness of this process but with new contemporary global challenges, gasification of waste is re-emerging, becoming one of the most advanced waste conversion methods.

2.1.3.1 Gasification Process

To understand the influence of the gasification agents and conditions, it is convenient to consider the thermodynamics of the gasification process. In the gasifier, the treated material successively undergoes three major stages: heating and drying, de-volatilization, and char reaction [185]. The latter two steps cover several different processes and reactions (with the standard enthalpy change at 298 K included).

- The pyrolysis or de-volatilization process occurs as the carbonaceous particle heats up. Volatiles are released and char is produced, resulting in up to 70 % weight loss during coal gasification. The process is dependent on the properties of the carbonaceous material, which also determine the structure

and composition of the char. The volatiles consist of tar, water vapour and light gases (CO, CO_2, H_2, CH_4,...).

- The combustion process occurs as the volatile products and some of the char reacts with oxygen to form carbon dioxide and carbon monoxide, which provides heat for the subsequent gasification reactions. Letting C represent a carbon-containing organic compound, the important reactions are partial oxidation (2.1) and the combustion reaction (2.2) [72].

$$C + \frac{1}{2}O_2 \rightarrow CO \quad \text{(-110.5 kJ/mol)} \tag{2.1}$$

$$C + O_2 \rightarrow CO_2 \quad \text{(-393.5 kJ/mol)} \tag{2.2}$$

- Other gasification reactions that occur on the carbon of the char are with steam to produce carbon monoxide or carbon dioxide and hydrogen, via the water-gas reaction (2.3) and the carbon-steam reaction (2.4). Two other important heterogeneous gasification reactions are the Boudouard reaction (2.5) and the hydrogasification reaction (2.6).

$$C + H_2O \rightleftharpoons CO + H_2 \quad \text{(+131.3 kJ/mol)} \tag{2.3}$$

$$C + 2H_2O \rightleftharpoons CO_2 + 2H_2 \quad \text{(+90.2 kJ/mol)} \tag{2.4}$$

$$C + CO_2 \rightleftharpoons 2CO \quad \text{(+172.4 kJ/mol)} \tag{2.5}$$

$$C + 2H_2 \rightleftharpoons CH_4 \quad \text{(-75 kJ/mol)} \tag{2.6}$$

- The most important homogeneous volatile reactions that can be identified during the gasification process are the gas phase water-gas shift reaction (2.7), the methanation reaction (2.8) and carbon monoxide, hydrogen and methane oxidation (2.9, 2.10, 2.11).

$$CO + H_2O \rightleftharpoons CO_2 + H_2 \quad \text{(-41.1 kJ/mol)} \tag{2.7}$$

$$CO + 3H_2 \rightleftharpoons CH_4 + H_2O \quad \text{(-206.1 kJ/mol)} \tag{2.8}$$

$$CO + \frac{1}{2}O_2 \rightarrow CO_2 \quad \text{(-283 kJ/mol)} \tag{2.9}$$

$$H_2 + \frac{1}{2}O_2 \rightarrow H_2O \quad \text{(-242 kJ/mol)} \tag{2.10}$$

$$CH_4 + \frac{1}{2}O_2 \rightarrow CO + 2H_2 \quad \text{(-38 kJ/mol)} \tag{2.11}$$

- The high-temperature environment also promotes the decomposition of tar to smaller, desirable gas components. In the listed tar reactions, which are - in order of appearance - partial oxidation, dry reforming, steam reforming

and thermal cracking, tar is represented by C_mH_n.

$$C_mH_n + \frac{m}{2}O_2 \rightarrow \frac{n}{2}H_2 + mCO \quad (2.12)$$

$$C_mH_n + mCO_2 \rightarrow \frac{n}{2}H_2 + 2mCO \quad (2.13)$$

$$C_mH_n + mH_2O \rightarrow (m + \frac{n}{2})H_2 + mCO \quad (2.14)$$

$$(m-p)C_mH_n \rightarrow mC_{m-p}H_{n-q} + \frac{mq-pn}{2}H_2 \quad (2.15)$$

The balances of these reactions, depending on the gasifying medium and temperature, determine the share of carbon monoxide, carbon dioxide, hydrogen and methane in the syngas composition.

Besides the operating parameters of the gasifier (such as temperature, catalysts, material flow rates, etc.), a gasification system is defined by the design of the gasifier. The design depends on the choice of oxidizing agent and on the type of gasifier configuration.

2.1.3.2 Oxidizing Medium

The process can be carried out by partial oxidation with air, oxygen-enriched air, pure oxygen or as steam gasification. Air-blown gasification is the simplest way to convert biomass into a low-calorific value syngas. The calorific value of the producer gas ranges between 4 and 7 MJ/Nm^3 [7]. The low energy content of the produced syngas is caused by the inherent dilution with nitrogen (up to 60 %) [100].

For enhanced chemical conversion to a medium-calorific value syngas (characterized by a heating value in the range of 10-20 MJ/Nm^3), nitrogen must be removed from the process. Some processes are operated with oxygen-enriched air, i.e. a mixture of nitrogen and oxygen with an oxygen content up to 50 %. This produces a higher heating value gas without the consumption of expensive pure oxygen. The investment of an air separation unit (ASU) to achieve partial oxidation with pure oxygen appears only justified for large scale units (larger than 100 kilotonnes per year). The characteristics of oxygen-enriched air gasification are a higher syngas heating value, reduced volumetric flow rate, low tar content and vitreous ash production [7].

Steam gasification can also provide an attractive alternative for the production of medium-calorific value syngas, free of atmospheric nitrogen. This process is especially attractive when increased hydrogen content in the syngas is desired.

No exothermic reactions are involved, so an external source of energy for the endothermic gasification reactions is needed. This is called allothermal gasification in contrast to autothermal gasification, which relies on the partial and complete oxidation of some of the material to generate the heat for the gasification reactions (diluting the syngas with CO_2).
The MILENA gasification process is an example of allothermal gasification where the gasification of biomass material is separated from the combustion of the remaining char. The energy for heating the biomass is transported by the circulating bed material from the combustion chamber. Although this type of indirect gasifier is only in the development stage of the technology, a higher fuel conversion and lower ash load is reported compared to direct gasifiers [188]. In other allothermal gasification systems, electric heaters are also used to supply the external heat to the system [200].
More recently, CO_2 is also investigated as an oxidizing medium, either exclusively or in combination with oxygen or steam. Analogous to these combinations of gasifying agents, oxy-steam (O_2+H_2O) gasification is also a technology which is being developed [165].

2.1.3.3 Type of Configuration

Gasifiers can be categorized based on the type of bed and type of flow [106]. The different configurations include fixed-bed, fluidized-bed and entrained-flow type gasification. The fixed bed gasifiers can be further differentiated in the way the reagents and the gasifying agent come into contact with one another. In an updraft or counter-current reactor, the waste feeding system is at the top of the gasifier and the oxidant intake is at the bottom. In this configurations, the product gas moves upwards. In downdraft or co-current reactors, the material is fed in from the top and drops downwards, while the gasifying agent is injected from the side and mingles with the products of the pyrolysis. The solids and product gas then move downward in parallel streams. The syngas exits from the bottom at higher temperature (around 800 °C in stead of around 500 °C), with lower tar level compared to an updraft configuration.
In the category of fluidized bed-type gasifier, bubbling or circulating fluidization is possible. In a bubbling fluidized bed (BFB), the flow of gaseous oxidant is blown upwards through a distributor plate and permeates a bed of inert material (typically silica sand or olivine) located at the gasifier bottom, which contains the waste to be treated [7]. The resulting fluid-like state achieves an intense mixing between gas and solids allowing very high heat and mass transfers. Circulating fluidized beds (CFB) have higher flow rates which carry most of the bed partic-

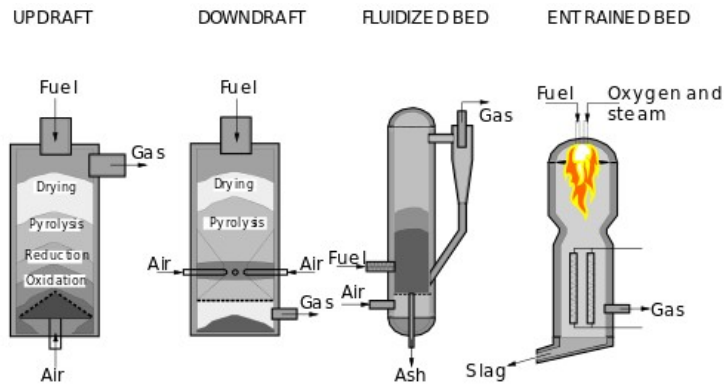

Figure 2.2: Different types of gasifiers

ulates and ungasified material to an attached cyclone separator, from which the solids are re-circulated to the gasifier bed. This is one of the preferred technologies for large-scale biomass gasification plants [163]. A complete overview of the differences between fixed bed and fluidized bed gasifiers and the (dis)advantages of each type have been summarized by Warnecke [199].

The last type of the most commonly used gasifier types is the entrained flow reactor. These reactors are operated at high pressures (about 25 bar). Very fine particles (smaller than 1 mm) are mixed with water to form a slurry which is entrained by the pressurized gasifying medium upon entering the reactor. The rapidly occurring combustion at the top of the reactor raises the temperature to high temperatures which melts the ash onto the gasifier walls. The molten slag can then be further discharged [7].

2.2 Definition and General Features

The application of the previously mentioned thermochemical conversion technologies in waste management faces fundamental problems and does not meet the stringent requirements of sustainable development. Sustainable development is defined as the development that meets the needs of the present without comprising the ability of future generations to meet their own needs. Recuperation of by-products or thermal energy from waste streams is not only motivated by cost saving, but also by resource saving considerations for future generations. The bottom line idea advocated here is to develop and to implement technology

using waste as a source for 'green energy' or 'green chemicals', in other words, not detrimental to the environment.
An advanced technology for the environmentally friendly treatment of all types of waste streams is needed. Plasma gasification is a promising alternative for conventional thermochemical conversion technologies as it offers a substantially higher resource recovery potential and much better tar removal capabilities.

Plasma torches have been used in materials processing as long ago as the 1960s [24]. Several applications which have been developed since its first use for testing heat shields for spacecraft were previously mentioned in Paragraph 1.2.2. These processes rely on the high temperature, high intensity, non-ionizing radiation and high-energy density characteristics of plasma torches. Heberlein [74] describes why the heat transfer by thermal plasma to a material occurs more effectively than by normal gas convection. Since in a thermal plasma the molecular components are mostly dissociated and atomic species are partially ionized, the energy transport occurs not only by transfer of kinetic energy as in ordinary gases, but includes transfer of the heat of dissociation and of ionization. This transport of reaction energy in addition to the fact that electrons transport heat more efficiently results in thermal conductivity values for thermal plasmas which are considerably higher than those of gases. The heat source is also directional with sharp interfaces and steep thermal gradients that can be controlled independently of chemistry.

The specific properties of plasma have triggered the interest for applying plasma torches in gasification. Thermal plasmas can be combined with gasification in two ways. The first possibility is to use the plasma as a downstream processing step after the gasification process, where it cleans the syngas by destroying most of the unwanted contaminants and melts the inorganic components (ash and metals) into a vitrified slag. In the second way, the thermal plasma torch is directly incorporated in the gasification reactor, where it serves as the energy source for the allothermal gasification process. The latter interpretation of plasma gasification is the subject of the further explanation of the technology.
Plasma allows a better process control than other energy carriers in the allothermal gasification process. Whereas an upper temperature limit of 2000 °C can be achieved by burning fossil fuels, electrically generated thermal plasmas can reach temperatures of 20 000 °C or more [68]. This high-temperature, reactive environment accelerates the kinetics and improves the thermal decomposition

of hazardous organic compounds (such as tar) into desirable gas species. As energy for the process is supplied by the plasma power, chemical reactions with the treated material and its devolatilization products are not the primary source of energy, allowing the adjustment of the injected energy independently of the heating value of the treated material. Additionally, the enthalpy provided by the plasma can easily be adjusted by the tuning of the electrical power supplied to the system, making the process independent of O/C ratio and the nature of the plasma medium (neutral, oxidizing or reducing atmosphere) [53].
At the elevated temperatures in the reactor volume, the inorganic constituents of the treated material can reach their melting point and can be reduced to a nonhazardous melt with a very low unburnt organic residue content.

2.3 Advantages

The advantages of plasma gasification which follow from the plasma features and their effects on the gasification process are [24, 53, 57, 68, 74, 82, 164]:

- Better control of process temperature by adjusting the plasma power in relation to the material feed rate.
- The produced syngas is of higher quality and contains a reduced amount of unwanted contaminants. These include soot, char, higher hydrocarbons, tars and other complex molecules, toxic gases such as oxides of sulphur or nitrogen and pathogens.
- A better overall control of the composition of the syngas because of several elements; first, the decoupling of the process chemistry from the heat source. Because the plasma can carry sufficient energy to the process at substantially lower flow rates, the composition of produced syngas is not much influenced by plasma gas composition. Secondly, a uniform composition can be attained by high-temperatures and a homogeneous temperature distribution inside the reactor. Additionally, the steep thermal gradient for the gas exiting the reactor leads to high quench rates, which allows to obtain non-equilibrium compositions or metastable states and non-equilibrium compositions, thereby minimising the reformation of persistent organic pollutants (POPs), such as polychlorinated biphenyls (PCB) or dioxins [68].
- Reduced off-gas treatment. The amount of gases added is much smaller since they only serve as oxidant to generate syngas and not for producing the process heat source. A lower amount of gases are therefore diluting the

produced syngas, i.e. lower off-gas flow rates and consequently lower gas cleaning costs.

- A low thermal inertia makes it possible to control and to provide feedback to the process in a fast and easy way.
- The fast reaction times and higher process rates correspond to shorter residence times and larger material throughputs. This means that the footprint of the reactor installation can be smaller for a given waste throughput.
- The possibility of producing saleable co-products from the inorganic residues. This eliminates the need for extensive ash-handling and/or disposal.
- Rapid start-up and shutdown times can be achieved without compromising refractory performance thanks to the high heat flux densities at the reactor boundaries and fast attainment of steady-state.
- A wide range of materials can be treated with plasma gasification. The treated materials can be in gaseous (e.g. poisonous gases), liquid (such as sludge or urine) or solid state. A higher level of heterogeneity can also be handled, which requires less pre-sorting. Besides ashes and metals, the various waste streams which have been known to be treated by plasma gasification can be divided in three categories for which a non-exhaustive list of materials is given.
  A first group of raw materials are residues from agricultural activities and other natural resources which are of insufficient quality to be accepted by conventional combustion processes.
  - Woody biomass
  - Biological waste, e.g waste from slaughterhouses
  - Tar sands
  - Peat
  - High-sulfur brown coal (lignite coal) and bituminous coal
  - Oil shale

  A second group consists of materials from consumer's and industrial activities:
  - Municipal solid waste
  - Sewage sludge waste (SSW) and other sludge wastes, with a range of organic contaminants, and high moisture content
  - Waste aboard ships (cruise ships, large warships)

- Unrecoverable plastic waste
- Used automobile tyres and rubber waste
- Auto-shredder residue (or car fluff)
- Residues from chemical industry: paint, ink, textile products
- Waste from leather manufacturing

A third group is hazardous wastes:

- Pathological clinical waste from hospitals and outdated pharmaceuticals
- Contaminated soils, usually with hazardous organic materials
- Hazardous liquids and gases, including PCB-containing oils, chlorinated fluorocarbons (CFC's) and various widely used solvents
- Asbestos cement waste
- Low level radioactive waste ranging from contaminated structural materials to clothing
- Military waste

The better process characteristics of the treatment of these waste streams by plasma lead to environmental benefits by the offset of greenhouse gases and prevents undesired pollution in the by-products (a possibly non-leachable vitrified lava) and end product (a clean syngas of high caloric value).

2.4 Disadvantages

The main disadvantage associated with the plasma process is the use of electrical power as an energy source, which is expensive. Another disadvantage is the short lifetime of the electrodes of the plasma torch, which implies additional high maintenance costs. Consequently, economic considerations provide the strongest barrier for the development of plasma gasification projects [73].
Plasma gasification offers the technology for waste disposal, combined with power generation. The feasibility of this treatment however, depends greatly on the energetic and economical balance of the process.

2.5 Product Applications

Waste is considered a very promising renewable resource which is wide-spread and abundantly available on a global level. The produced syngas from waste plasma

gasification can be the feedstock for a broad range of energy- and material end-purposes. As such, it can substitute fossil fuels as raw materials. The general added value of the syngas produced by plasma gasification compared to that from conventional gasification is its high quality. A first reason for this is the syngas composition, which contains higher levels of carbon monoxide and hydrogen and much lower concentrations of carbon dioxide. After all, the energy for the gasification reactions does not originate from the full oxidation reaction of the treated material (which produces CO_2 amounting up to 35 volumetric percent of the syngas), but rather from the plasma energy. The more desirable composition also translates into a higher calorific value of the syngas. For example, the lower heating value of syngas from air-blown conventional gasification typically ranges between 5 and 7 MJ/Nm^3 [7], while the syngas heating value from plasma gasification with air as the oxidizing medium can reach 10 MJ/Nm^3 [21]. In terms of unwanted contaminants, the lower concentrations in the syngas from plasma gasification reduces the extent of gas cleaning prior to its use as fuel or as feedstock.

2.5.1 Syngas

2.5.1.1 Thermal Valorization

Syngas can be used to generate electricity by means of different technologies. The syngas can be burned in a boiler to produce high-pressure steam which drives a **steam turbine**. More efficient electricity production systems are gas engines and gas turbines.

Gas engines running on syngas are mostly spark-ignition (SI) reciprocating engines. The normal energy source in a gaseous-fueled engine is methane. A number of the components of syngas cause challenges which must be countered by a number of technical modifications. Gas contaminants in syngas, most notably tar and humidity, are a key technical challenge to the utilisation of synthetic gases. The concentration of tar allowed in the syngas for downstream use in gas engines is limited to 50 mg/Nm^3. The high hydrogen levels in the syngas can also cause problems. Hydrogen is much quicker to burn than methane and faster combustion in the engine cylinders would lead to the potential of pre-ignition, knocking and engine backfiring. These elements reduce the output of the engine to between 50 % to 70 % of its typically natural gas output.

With emphasis on clean engine operation, burning of syngas in SI engines proved to be viable due to significantly lower exhaust gas emissions, equal heat release

characteristics and larger usable operating range when compared to methane. Due to the low energy content of syngas, it is necessary to use much higher amounts of syngas to obtain similar performance output values [175].
The net electrical efficiency of gas engines related to the energy content of the syngas is reported around 35 percent (e.g. efficiencies of 37 % and over can be achieved with Jenbacher gas engines) [77]. Gas engines (and steam turbines) can also be operated in combined heat and power mode (also called co-generation). The sensible heat of the off gases is then recuperated by use of an exhaust gas heat exchanger to generate pressurised hot water or steam, which can be used for district heating or for heating a process.

Gas turbines are a type of internal combustion engines, consisting of a compressor unit, a combustion chamber and a turbine. Fresh atmospheric air flows through the compressor which brings it to higher pressure. Energy is then added by spraying fuel into the air and igniting it so the combustion generates a high-temperature flow. This high-temperature, high-pressure gas enters a turbine, where it expands down to the exhaust pressure. The turbine shaft work is used to drive the compressor and the electric generator. Some key issues that need to be considered when using syngas rather than natural gas to fire a gas turbine are: flame stability issues, the level of water vapour, the lower calorific value and the higher corrosion potential [64].
Syngas-fueled gas turbines are almost exclusively used in a combined cycle power block (consisting of one or more gas turbines and a steam turbine). Clean syngas (with tar levels lower than 5 mg/Nm^3 is combusted in highly efficient gas turbines to produce electricity. The excess heat from the gas turbines and from the gasification reaction is then captured, converted into steam, and sent to a steam turbine to produce additional electricity.
Moreover, the system is referred to as **integrated gasification combined cycle (IGCC)** (Figure 2.3) when material and gas flows are internally linked between the gasification process and the heat- and electricity generating unit. An important aspect, among others, is the conversion of the heat captured from the hot syngas to steam and consequently additional electricity through the steam turbine. In an IGCC, where power generation is the focus, electricity is generated with very low emissions and high electrical efficiencies up to 60 % (higher heating value of the feed gas).

Analogous to an IGCC power plant, the **integrated gasification fuel cell (IGFC)** cycle links a high-temperature type fuel cell (such as the solid oxide

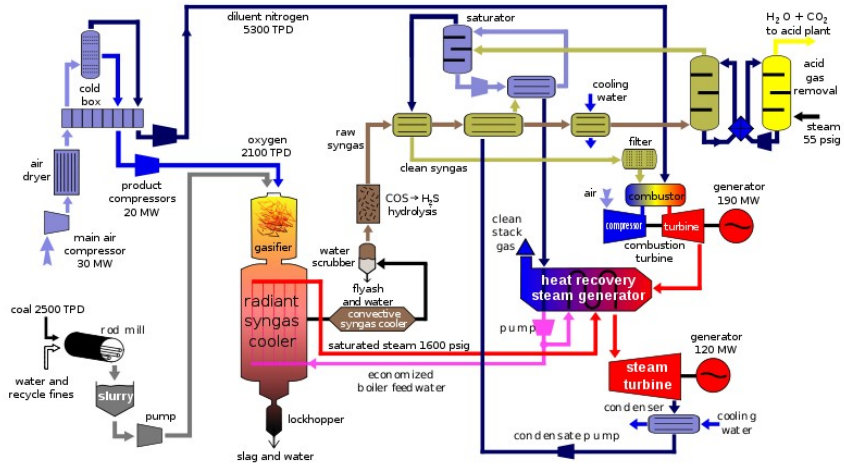

Figure 2.3: Schematic of an IGCC system [145]

fuel cell (SOFC)) power generation unit to the gasification process instead of a gas turbine (Figure 2.4). A SOFC operates at higher temperatures than

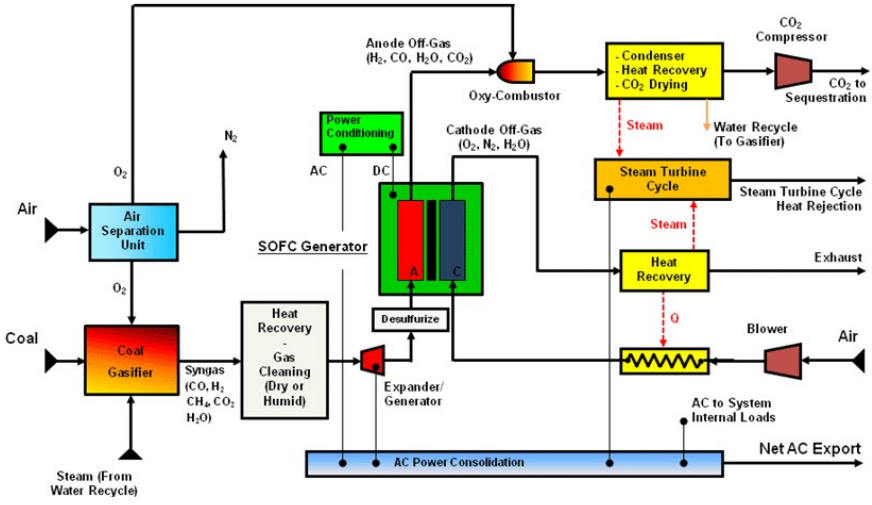

Figure 2.4: Schematic of an IGFC system [144]

lower-temperature fuel cell types such as proton exchange membrane fuel cells or alkaline fuel cells. The latter fuel cell types require pure hydrogen as fuel, whereas the SOFCs are not poisoned by carbon monoxide and carbon dioxide, and can accept hydrogen, carbon monoxide, carbon dioxide, steam, and methane mixtures

as fuel directly, because of their internal shift and reforming capabilities [65].
Fuel cells offer the ability to convert chemical energy directly into electrical energy with a very low environmental impact. A diagram of the SOFC and its principle of operation are shown in Figure 2.5. The key to the operation is a thin,

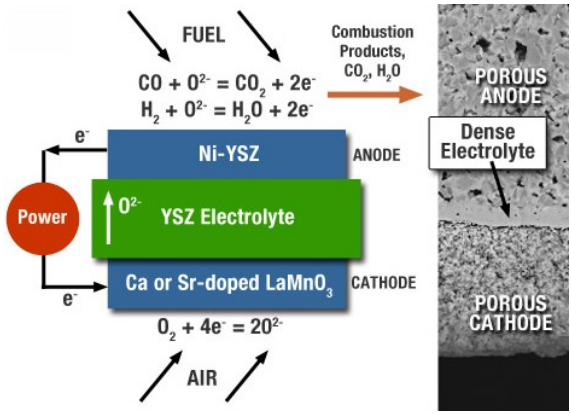

Figure 2.5: Diagram of a solid oxide fuel cell [141]

dense layer of ceramic material, called yttria-stabilized zirconia (YSZ), which separates the air-side (with cathode) from the fuel-side (with anode) of the cell, and performs as the electrolyte.
At high temperature (800–1000 °C), the hydrogen and/or other fuel gas at the porous anode layer, can flow towards the electrolyte. An oxidation reaction on the catalyst sites strips the hydrogen atoms from their electron. The electrons cannot go through the electrolyte and flow around the membrane through an external circuit. At the cathode, or air electrode, which is a thin porous layer on the electrolyte, oxygen reduction takes place. The Y–doped zirconia allows the negatively charged oxygen ions to pass through to the anode, where the oxygen ions and the hydrogen combine to produce heat and water. The external flow of electrons in the process creates the electrical current. A single fuel cell produces less than 1.16 volts, so to increase the amount of electricity generated, hundreds of individual fuel cells can be combined in a fuel cell stack.
The waste heat from SOFC systems may be captured and reused, increasing the theoretical fuel utilization ratio to as high as 80 % to 85 % [141].
Recent developments allow an accessible incorporation of carbon capture & storage technology with IGCC and IGFC plants, which reduces the flow of CO_2 emitted to the atmosphere. Such IGCC-CCS and IGFC-CCS also have reduced energy efficiencies, because of the energy requirements for the carbon capture &

storage, with maximum reported values for system efficiencies of 60 % [171].
The syngas can contain tars and trace species such as particulates, chlorides (HCl), sulphur (H_2S) and alkali compounds among others, which could be detrimental to SOFCs if they are contained within the feeding syngas stream. Therefore the syngas must be pre-treated in order to reduce these trace species to a level that SOFCs are able to tolerate [115]. In terms of tar concentrations in the syngas, the limit for a fuel cell is 1 mg/Nm^3.

The higher calorific value of syngas from plasma gasification due to less dilution by CO_2 compared to conventional gasification increases the efficiency of the power generation mechanisms. It is important to note that the net produced electricity from syngas from plasma gasification can only be considered renewable if the power demand of the torch was supplied by the generated electricity of the system or by another renewable energy system (e.g. solar panels).

2.5.1.2 Chemical Valorization

Hydrogen is of special importance, because it is pollution-free and usable in many power and propulsion systems and as a chemical building block for different chemicals. Because of its cleaner burning characteristics (only H_2O is produced) as well as a high-energy density on mass basis, it is being considered as a possible replacement for fossil fuels.
The global market for hydrogen is already greater than $40 billion per year [103] including hydrogen used in ammonia production (49 %), petroleum refining (37 %), methanol production (8 %), and miscellaneous smaller-volume uses (6 %) (e.g. as a fuel gas, or for electric power generation with fuel cells). Hydrogen might be pollution free, but nevertheless, it is only as clean as its method of generation. Today, most of the hydrogen is produced from natural gas by steam reforming. Presently, 77 % of the worldwide hydrogen production comes from petrochemicals, 18 % from coal, 4 % from water electrolysis and 1 % from other sources [10]. Hydrogen production using steam methane reforming (SMR) is the most economical method among the current commercial processes. The popularity of SMR is due to its low cost; however, the volatile price of methane can elevate the SMR-based hydrogen cost and in addition, this method of hydrogen production results in the release of carbon dioxide, which is of great concern, since CO_2 is a main component of greenhouse gases.
Waste can offer an economical and environmental-friendly feedstock for renewable hydrogen production through plasma gasification. Similar to the SMR process,

this alternative for production of hydrogen also encompasses a water-gas shift reaction with catalysts such as copper-zinc and a CO_2 adsorption step using an adsorbent such as CaO, but the need for extensive pre-treatment and steam reforming is eliminated. A preliminary assessment reported by Lau et al. [107] suggests that hydrogen can be produced economically from biomass, but large-scale infrastructure is needed to be competitive with the cost of hydrogen produced from natural gas. However, the process is definitely more advantageous than fossil fuel reforming in consideration of environmental benefits, which can be even higher for plasma gasification of waste instead of biomass.
In the future, the costs of renewable hydrogen production are expected to be lower than the costs for production from natural gas, which will allow thermochemical biomass conversion to become one of the most economical large-scale renewable hydrogen technologies [146]. There are still challenges that must be overcome, but as technology improves, natural gas prices increase, and government incentive programs evolve, syngas produced from plasma gasification will present an economical way to produce hydrogen.

As stated in the previous section, the largest end-use of hydrogen is for the production of **ammonia**. If the air-blown gasification of biomass and waste is considered, one might speculate that ammonia could be directly synthesized from the produced hydrogen-rich syngas, since it already contains the two reacting compounds (N_2 and H_2) for ammonia production. However, the catalysts in the process have high requirements, i.e. there cannot be any H_2O, CO, CO_2, O2 and other poisons present in the gas. Therefore, the syngas is first purified to hydrogen and then recombined with nitrogen to form ammonia.

Methanol produced from biomass and/or waste is a promising carbon neutral fuel, well suited as a transportation fuel and as a chemical building block. From a thermodynamic point of view, utilisation of methanol in internal combustion engines could bring some advantages such as an increase in power (due to the increase of the engine's compression rate) and in energy efficiency, besides reducing the emission of pollutants. Because of its specific properties and high hydrogen to carbon ratio, it is also considered an ideal hydrogen carrier for fuel cell vehicles. Methanol is further used as a precursor in the synthesis of chemicals such as acetic acid, methyl tetra butyl ether (MTBE), dimethyl ether (DME) and olefins (such as polypropylene acrylonitrile). According to Galindo-Cifre and Badr [62], more than 75 % of methanol is currently produced from natural gas.

An interesting alternative way for the production of methanol is via synthesis of syngas from waste plasma gasification. The technological process of producing biomethanol includes gasification, gas reforming and catalytic synthesis [212]. One concept, discussed in a study published in [6] incorporates an innovative Absorption Enhanced Reforming (AER) gasification process, which enables an efficient conversion of a carbonaceous waste source into a hydrogen-rich gas and then, uses the Mitsubishi methanol converter (superconverter) for methanol synthesis. Analyses in this study show that the unit cost of methanol production mostly depends on the capital investments. The researchers give a positive outlook for the commercially competitive production of methanol from syngas.

The Fischer-Tropsch synthesis (FTS) is a well established process for the production of long-chain hydrocarbons from a CO and H_2 gas mixture (usually after steam reforming of natural gas or gas from coal gasification). FTS yields a complex mixture of saturated or unsaturated hydrocarbons (C_1-C_{40+}) and C_1-C_{16+} oxygenates, as well as water and CO_2 [46]. The product distribution depends on the polymerization at the surface of the catalyst (iron, cobalt, ruthenium and potassium).
In the FTS, one mole of CO reacts with two moles of H_2 in the presence of a cobalt (Co) based catalyst to afford a hydrocarbon chain extension (-CH_2-). The reaction of this synthesis is exothermic [167].

$$CO + 2H_2 \rightarrow \text{-}CH_2\text{-} + H_2O \quad (\Delta H_r = \text{-}206 \text{ kJ/mol}) \tag{2.16}$$

The -CH_2- is a building stone for longer hydrocarbons. The FTS can be operated at low temperatures (LTFT) to produce a syncrude with a large fraction of heavy, waxy hydrocarbons (>C_{20}). This can be refined to waxes or converted by hydrocracking and/or isomerization to excellent diesel, base stock for lube oils and a naphtha which is an ideal feedstock for cracking to light olefins. The FTS can also be operated at higher temperatures (HTFT) to produce a light syncrude and olefins. These primary products can also be refined to environmentally friendly gasoline and diesel, solvents and olefins.
Biomass has been used as a feedstock for producing synthesis gas, which was consequently converted to FT liquids. This production of synfuels from biomass and waste will lower the energy cost, improve the waste management and reduce harmful emissions [46]. The syngas, originating from plasma gasification, provides an environmentally sound substitute for the natural gas as feedstock for the production of FT liquids.

The catalytic process of **mixed alcohol synthesis (MAS)** from syngas is one of the challenging and attractive subjects in the field of chemistry. The resultant mixed alcohols obtained from this process can be used as fuels, fuel additives for octane or cetane enhancement, and intermediates for value-added chemicals such as pharmaceuticals, cosmetics and polyester. When this conversion of syngas is developed to an efficient pathway for the production of chemicals, then the mixed alcohol technology is expected to become one of the attractive routes for lowering the petroleum dependency. In this process, the major reaction is the alcohol formation (Reaction 2.17), while hydrocarbon formation and water-gas-shift reaction are side-reactions.

$$\mathrm{nCO} + 2\mathrm{nH_2} \rightarrow \mathrm{C}_n\mathrm{H}_{2n+1}\mathrm{OH} + (\mathrm{n\text{-}1})\mathrm{H_2O} \tag{2.17}$$

MAS is similar to methanol synthesis, Fischer-Tropsch synthesis and ammonia synthesis, but the difference is the catalyst. The above MAS reaction takes place over the catalysts with the function of hydrogenation, C-O bond breaking and CO insertion [54].

2.5.2 Slag

In some configurations, the plasma gasification of waste material can yield a vitrified slag from the inorganic components (ash and metals). The melting of bottom ash residues from gasifiers and incinerators is commonly subject to heavy metal leaching, therefore dedicated plasma vitrification facilities are already commercially operational to offset this potential liability. Generally, the results of compliance leaching and chemical testing of the vitreous slag from a plasma gasification process indicate that it is non-leaching and can be assumed as readily and completely recyclable [121]. The resulting by-product can be used as supplementary asphalt or road paving material and as ballast for railways, roads and airports tracks. Alternatively, it can replace granulates in special concrete applications (e.g. oil well cement).
In addition to the use as an aggregate material, it also has potential for use in other applications where technological specifications require some combination of strength and/or particle size, such as pipe bedding and fill materials. Furthermore, it can be a raw material source for more technically demanding applications, such as insulation wool manufacture where the molten state of the slag at point of generation could be spun on high speed spinning wheels generating a mass of fine, intertwined fire resistant fibres.
Other applications such as alumino-silicate geopolymers would utilize the alkali-rich activated alumino-silicate content of the slag. Geopolymer binder technology

based on the by-product of a plasma gasification system can offer a 'green' replacement to Portland cement [180].

2.6 State of the Art

It is clear that prudent use of plasmas through controlled gasification processes can offer distinct advantages in waste treatment and for future use of the syngas. Utilization of thermal plasmas for destruction of waste materials has been in the focus of interest of scientists as well as industrial companies in the recent decades. There exists only a couple of industrial-scale plasma waste treatment installations which have been in operation for some years and the number of plasma gasification developments is further increasing all over the world. A limited number of the plasma gasification facilities are for research and/or demonstration purposes. The configuration of these installations differs in the type of gasifier, the type of thermal plasma used (AC or DC, transferred or non-transferred and water-stabilized or gas-stabilized torches), in the position and purpose of the plasma unit (single- or two-stage systems), the material treated and the oxidizing medium.

2.6.1 Industry

The published information about industrial-scale commercial plasma gasification facilities is often very scarce. Therefore, most of the available data about these plants are based on their reported design criteria, keeping in mind that the actual operational results can possibly deviate somewhat from these numbers. The listed facilities are sorted according to the technology provider and do not include any ash vitrification or metal melting plants. An overview of the current existing industry-oriented plasma gasification facilities can be found in Table 2.1

Westinghouse Plasma Corporation (WPC) is a company which has a long track record in the plasma industry. As a wholly owned subsidiary of Alter NRG, they progressed from their know-how of plasma torches to the development of plasma gasification systems. The different generations of their gasification system are displayed in Figure 2.6. Their gasifiers are equipped with non-transferred plasma torches to provide part of the heat. The rest of the required energy for the waste processing is obtained from the chemical energy of the waste and typically by addition of coke (about 4 % of the total load) [202].

The Waltz Mill plasma gasification pilot plant of Westinghouse Plasma Corporation which has tested a wide variety of material feedstock is located in Madison (USA). This reactor was built in 1984 with a design capacity of 48 tonnes per day (tpd) and serves as a testing unit prior to new project developments [204]. In addition to this pilot facility, Alter NRG's WPC has a number of commercially operating reference sites with plasma assisted gasifiers using the WPC plasma torch technology [47, 158, 189, 202–206]:

- One of the first installations was the pilot-scale plasma gasification plant located in Yoshii (Japan) and operated by Hitachi Metals Ltd. It was commissioned in 1999 and could treat 24 tonnes per day (tpd) of unprocessed municipal solid waste (MSW). The plasma energy supplied to this Plasma Direct Melting Reactor (PDMR) was 100 kWh/ton of MSW, which is reportedly about 5 % of the MSW heating value. After it was demonstrated to the Japanese government that the Yoshii Waste-to-Energy facility was capable of using plasma energy to reliably and economically gasify waste materials for energy production, it was decommissioned in 2004. The lessons learned from this unit were applied to other full-scale facilities of Hitachi Metals in collaboration with Westinghouse Plasma Corporation in Japan.
- The one in Utashinai uses two 83 tpd trains of primarily automobile shredder residue (ASR) as fuel but has been designed to run with a 50 % mixture of MSW. Each train can also process approximately 110 tpd of 100 % MSW. Each reactor has four WPC Marc 3a plasma torches (which can operate between 80 and 300 kW) arranged at 90° intervals around the circumference of the cylindrical reactor. When operating at capacity, the facility exports 1.5 MW of electricity to the grid [210].
- The other facility, which is located between the two cities of Mihama and Mikata, processes 17.2 tpd of MSW and 4.8 tpd of sewage sludge and became operational in December of 2002. The MSW is shredded on-site and the sewage sludge is partially dried to 50 % moisture content by the heat released from combustion of the produced syngas. Because of its smaller capacity, the reactor has only two plasma torches arranged opposite of each other. The produced slag (at 1.5 tpd) is locally used in road construction [97].
- In Ranjangaon, Pune (India) Westinghouse Plasma Corporation has teamed up with SMS Envocare LTD (a group company of SMS Infrastructure Ltd.) to build the Maharashtra Enviro Power Ltd. (MEPL) plant, which has been in operation since 2009. The plant can process up to 72 tpd of hazardous

wastes (with a calorific value of 3000 MJ m^{-3}), generating 1.6 MW of net electricity. The gasifier consists of two stages, with a coke bed reactor (at 1500 °C) as a first step and a second chamber for oxidation reactions at 1100 °C. Four plasma torches of 300 kW are installed of which two are in continuous operation and the other two operate one hour before lancing (molten slag removal), which is carried out two times in an eight hour shift. A similar 72 tpd of hazardous waste to energy facility (called Vidharbha Enviro Protection Limited) is also constructed in Mandwa, Nagpur (India), but no further information about this plant has been made public.

- The WPC technology is also applied in an integrated biorefinery, operated by Coskata in Madison (USA). In this system, the plasma gasifier converts biomass and waste to syngas on the front end and Coskata's syngas-to-biofuels conversion process on the back end produces bio-ethanol [23].
- In Hubei (China), the Chinese company Wuhan Kaidi converts the produced syngas from plasma gasification with biomass waste as feedstock to liquid fuels via their patented Fischer-Tropsch process. This demonstration facility has a WPC gasifier with a capacity of 150 tpd and was commissioned in 2013.
- The latest project of Westinghouse Plasma Corporation is at Tees Valley, Teesside (UK). The development of this site by Air Products includes two plasma gasification units treating non-recyclable residual waste at 950 tpd. The first stage of this project is currently in commissioning. The output per unit is expected to be about 50 MW of electricity, generated from 65 000 Nm^3 per hour of syngas by a combined power cycle. This plasma gasifier is the largest one in the world and is equipped with a number of Westinghouse Marc 4.5 plasma torches (550 kW per torch) [25].

Europlasma is another company that provides industrial plasma-based solutions for waste recycling. Through its subsidiary company, Inertam, it has been operating a plasma vitrification facility for the conditioning of asbestos-containing material in Morcenx (France) since 2001 with a capacity of 8000 tonnes per year (tpy). In June 2014, a new plasma gasification facility next to this one was commissioned by CHO Power. It is designed to convert 37 000 tpy of local ordinary industrial waste and 15 000 tpy of wood chips in the patented gasification technology Turboplasma. The produced syngas is generating a gross 12 MW of electricity and 18 MW of hot water which is valorized on site in the wood dryer. The gasifier includes two plasma torches, a first one to refine the raw synthesis gas produced during gasification, and a second one to vitrify metals and minerals.

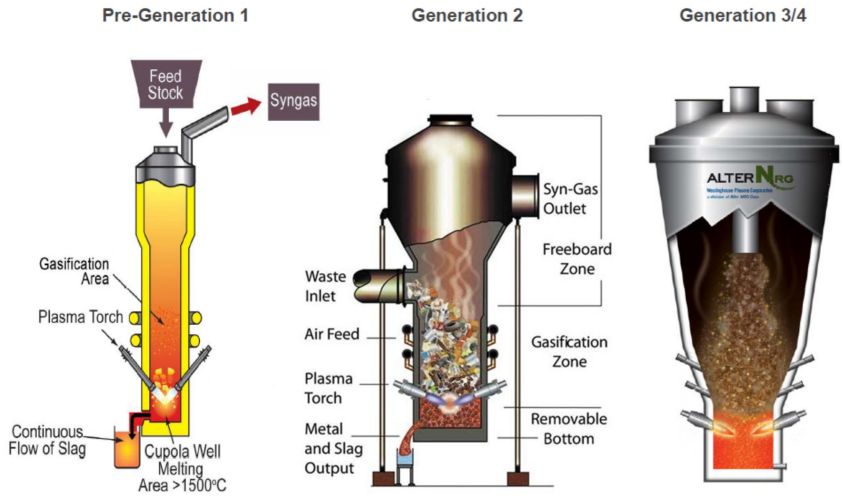

Figure 2.6: Gasifier evolution of Westinghouse Plasma Corporation [205]

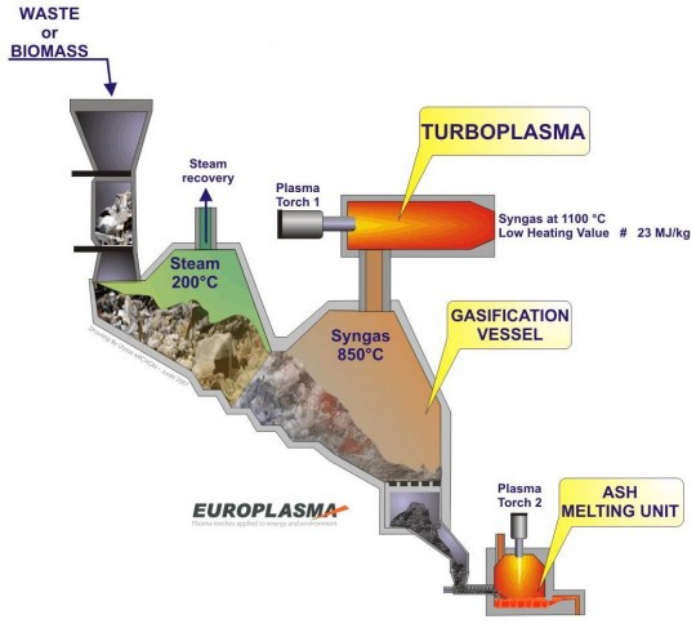

Figure 2.7: Illustration of the Europlasma gasification system including Turboplasma unit

The Canadian company **PyroGenesis Inc.** developed the Plasma Arc Waste Destruction System (PAWDS) to destroy combustible waste aboard ships. The system was installed in 2003 on the Carnival Cruise Lines M/S Fantasy ship and is able to treat ship waste such as food, paper, cardboard, plastics, wood and textiles. The typical feed rate of solid waste is 180-200 $\mathrm{kg\,h^{-1}}$. The key part of this gasifier is the patented Plasma Fired Eductor which uses a 300 kW non-transferred DC plasma torch [4, 5]. Since the focus of this system is waste elimination rather than energy generation, the syngas is simply combusted. PAWDS has been specified into all of the Gerald R. Ford Class air craft supercarriers, and has been ordered by their contracted shipyard for the first two ships in this class: the CVN-78 USS Gerald R. Ford and the CVN-79 USS John F. Kennedy [30, 98]. On land, the Plasma Resource Recovery System (PRRS) of PyroGenesis Inc. was commissioned in 2011 at Hurlburt Field, Florida (USA). The system at this US air force base can process up to 3100 metric tons per year (or 10.5 tpd) of municipal, industrial, hazardous and biomedical waste [161]. In this two-stage reactor, the material is first gasified in the plasma arc furnace by means of transferred DC graphite electrodes, after which the syngas is further treated in the second gasifier chamber by a plasma torch [157]. The output is electricity from a syngas-fueled internal combustion engine (420 kW) which is used internally. The unit was sold at a government liquidation auction in May 2013 [152]. Evolving from the plasma platform developed for the US Military, PyroGenesis developed the patented SPARC process for the complete destruction of ozone depleting substances (ODS), refrigerants and other hazardous gases. The steam plasma hydrolysis reaction breaks down the waste into CO_2 and H_2O with a destruction efficiency of 99.99999%. A unit capable of processing up to 50 $\mathrm{kg\,h^{-1}}$ of R11, R12, R134a and R141 was purchased in 2013 by Recyclage EcoSolutions (RES) located in Laval (Canada). PyroGenesis also designed and built a pilot demonstration system for the treatment of up to 50 $\mathrm{kg\,h^{-1}}$ hazardous waste at the National Technical University of Athens (Greece) in 2002 [153].

Plasco Energy Group has installed a pilot-scale plasma gasification plant in collaboration with Hera Plasma in Castellgali (Spain) [76]. This unit can process non-recyclable municipal and industrial solid waste at feed rates ranging from 34 to 86 $\mathrm{kg\,h^{-1}}$. The purpose of the 125 kW plasma torch is syngas refining by breaking down the tars after the gasification process [43]. The plasma gasification technology of Plasco Energy Group has been showcased in Ottawa (Canada) since 2008 by the Plasco's Trail Road (PTR) plant. At this commercial-scale demonstration facility up to 85 tpd of post-recycled MSW can be converted to

syngas which then generates 4 MW of electricity. The plasma torches are utilized to clean the syngas and to vitrify the non-gasified material. On February 12, 2015, Plasco Energy Group announced that it has obtained a court order approving the company's application under the Companies' Creditors Arrangement to enter bankruptcy protection [29].

A company that has published reliable experimental results from their plasma gasification demonstration unit is **Advanced Plasma Power**. The company was founded in 2005 to commercialize the patented Gasplasma technology initially developed by Tetronics and demonstrated at the first test facility in Farringdon (UK). Since 2007, APP is based in Swindon (United Kingdom) where they have performed several plasma gasification experiments with municipal solid waste, mined landfill RDF, contaminated wood and auto-shredder residue with maximum design material feed rate of $100\,\mathrm{kg\,h^{-1}}$. The technology relies on a separated oxy-steam gasification process followed by gas treatment by DC plasma torch and vitrification of the inorganic material into a vitrified slag under the trademark PlasmaRok [45].

Another patented plasma gasification technology, called Plasma Enhanced Melter (PEM), was developed by **Integrated Environmental Technologies (InEnTec)**. The primary power supply for the process is introduced by the DC plasma torch as plasma energy and by the AC joule heating system (see Figure 2.8). The plasma arc provides most of the energy for the gasification reactions, while the independent AC power heats and maintains the temperature of the molten glass bath. The demonstration unit (PEM model G100P) at the Columbia Ridge Facility in Arlington (Oregon, USA) owned by InEnTec (incl. S4 Energy Solutions) can convert up to 25 tpd of high carbon waste (medical, ASR, high plastic MSW, etc.) into syngas since 2011 [179]. InEnTec owns an identical installation in Richland (USA) where tests using various feedstock are being performed for treatability studies. Since 2010, a PEM model G500 owned by Dow Corning (in Midland, Michigan USA) has been transforming hazardous chlorinated organic liquids into aqueous hydrochloric acid (HCl) and syngas. This plant converts 6600 tpy of feedstock and produces syngas at a rate of 3 MW in terms of chemical energy content and 5500 tpy of HCl. Older versions of the PEM technology have been installed in Japan, Taiwan, Honolulu and Malaysia but were decommissioned after some period of time either after completion of the predetermined test campaign or prematurely because of financial reasons from the

customer-side [93]. In 2007, InEnTec constructed a fully contained, self-sufficient transportable model G30 PEM on two flat-bed trailers. The system was demonstrated in March 2007 at Fort Riley Army Base in Kansas, processing municipal solid waste. The syngas produced by the system was used as fuel in a dual-fired diesel engine mounted on the second trailer.

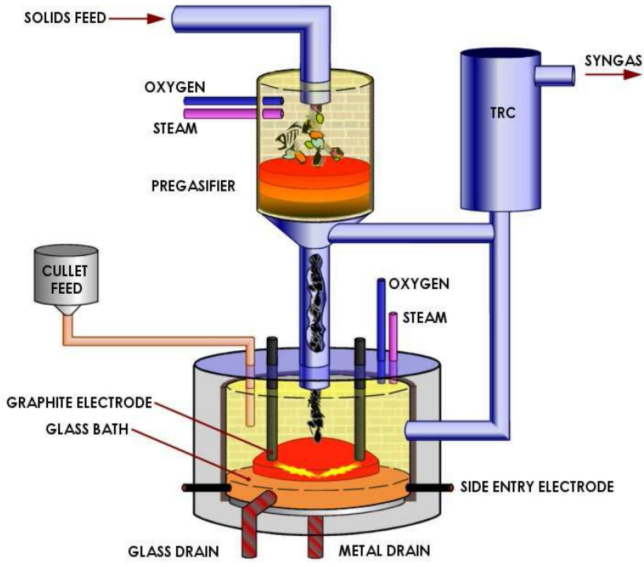

Figure 2.8: Illustration of the PEM reactor system [178]

After a proof of concept test campaign in Monterrey (Mexico) in 2006, **AdaptiveARC** has installed its patented CoolPlasma technology at two locations. In 2010, a commercial prototype (second generation) began operation in Mexico City. This unit can process 60 tpd of post-recycling mixed MSW and generates electricity from the syngas through a Caterpillar engine-generator (genset). In 2012 AdaptiveARC opened a third generation facility at the University of California at Riverside together with strategic partner NRG Energy. This system is aimed at commercial acceptance testing [3, 172].

A demonstration plant was constructed by **Envrionmental Energy Resources Ltd. (EER)** in Yblin (Israel) in 2007 with a designed capacity of 20 tpd of MSW.

In the fixed-bed updraft gasifier of their Plasma Gasification Melting (PGM) technology an electric arc with plasma power of 240 kW is maintained in an air/steam environment [215] (Figure 2.9). This facility is also used for academic research by the Royal Institute of Technology (Stockholm, Sweden) [216]. In 2002, another PGM reactor ('Pluton plant') was designed and built under EER's supervision at State Unitary Enterprise Scientific & Industrial Association 'Radon' (SIA Radon) for the treatment of low and intermediate-level radioactive waste (LILRW) with a capacity of 250 $\mathrm{kg\,h^{-1}}$ [94, 140, 151, 173].

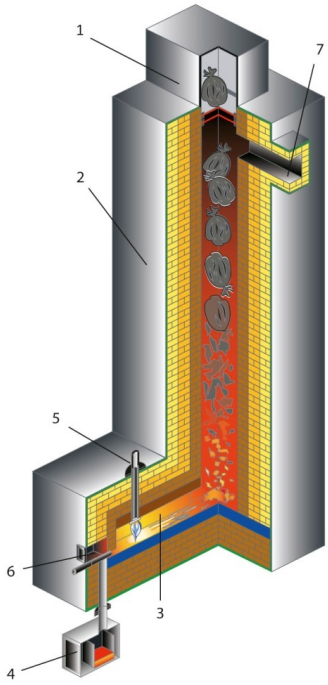

Figure 2.9: Illustration of the PGM reactor system with 1: feed loading, 2: reactor shaft, 3: molten slag bath, 4: slag reception, 5: plasma torch, 6: gas supply and 7: syngas outlet [140]

In 1992, **Plasma Energy Applied Technology (PEAT), Inc.** opened their research & development facility in Huntsville (Alabama, USA) using their plasma technology in a 50-100 $\mathrm{kg\,h^{-1}}$ plant. The company's Plasma Thermal Destruction & Recovery (PTDR) technology utilizes DC-powered graphite electrodes to create

the plasma arc and uses pure oxygen or steam as oxidizing media. The current installations of PEAT International are listed below [126].

- A PTDR-100 system with a capacity of $60\,\mathrm{kg\,h^{-1}}$ was commissioned in Northern China to treat mainly petroleum sludge in 2010 and is since 2013 permanently installed in Shanghai (China) to treat medical waste for Abada Plasma Technology Holdings.
- The same model was commissioned in 2010 at the commercial research and development foundry Technikon in Sacramento (California, USA). This PTDR-100 model uses a plasma heating system of 100 kW.
- In 2004, a 3 to 5 tpd facility began operation at the National Cheng Kung University in Tainan City (Taiwan). The processed materials include medical waste, fly ash and organic hazardous waste. A second system installed in Taiwan by PEAT International is at the Fooyin University in Kaohsiung wich has been treating a variety of hazardous and industrial waste streams at maximum $20\,\mathrm{kg\,h^{-1}}$.
- A $350\,\mathrm{kg\,h^{-1}}$ or 6 to 8 tpd demonstration plasma gasification system was built for the US Army in Lorton (Virginia, USA) in 1999 to process agricultural blast media and medical waste. This unit was dismantled in 2001 and reallocated to Georgia Tech Research Institute.

Additionally, according to their website a PTDR-100 model which was previously commissioned in Gujarat (India) in 2008, was re-commissioned in 2011 in Taichung (Taiwan), but no further information was found on this facility [150].

International Environmental Solutions (IES) Corp. delivered their proprietary pyrolysis system, the Advanced Pyrolytic System to Technikon [41]. The system has a capacity of 8 tpd and can treat MSW, tires, food wastes and biomass. The company filed for bankruptcy in 2012.

A plasma ordnance demilitarization system (PODS) was designed by **MSE Technology Associates, Inc.**, ordered by the US Department of Energy and Military, and was built at the facility at Hawthorne Army Depot (Nevada, USA) in 2006 [58]. The treated material includes small, fully assembled, smoke and pyrotechnic ordnance at a design capacity of $225\,\mathrm{kg\,h^{-1}}$ [127]. The furnace operates in an oxygen-enriched environment and contains a 1 MW plasma arc torch (which can operate in both transferred/non-transferred mode) and a

500 kW non-transferred torch. The mobile version, or Mobile Plasma Treatment System (MPTS) was implemented at Talon Manufacturing Company in Herndon (WV, USA). The furnace of the MPTS operates in an oxygen-deficient (reducing) environment and contains a 500 kW non-transferred plasma arc torch. This system was designed to process fuses and related components at feed rates of $140\,\mathrm{kg\,h^{-1}}$ and was entirely skid-mounted and transportable on eight flatbed trailers [208]. These technologies were included in an exclusive distribution and reseller agreement with Global Technologies Group Inc. in 2010 [187].

A plasma arc centrifugal furnace was developed by **Retech Systems LLC** at the US Department of Energy's Component Development and Integration Facility in Butte (Montana, USA) in 1991 [159]. The technology involves a centrifugal reactor volume equipped with two non-transferred plasma torches of 0.3 MW and 1.2 MW by Phoenix Solutions Co [102]. The feed rate during tests with metal-bearing soil at this site was approximately $55\,\mathrm{kg\,h^{-1}}$. A full-scale facility for the treatment of hazardous and toxic waste utilizing the plasma centrifugal furnace technology of Retech was operational in Muttenz (Switzerland) in 1991. This PLASMOX facility, designed to operate at a feed rate of 1 tonne per hour (tph) was owned and operated by MGC-Plasma AG (subsidiary of Burns and Roe Group). In 1994, MGC-Plasma AG in collaboration with Retech developed also a portable PLASMOX unit model RIF2 which could be moved by four standard tractor-trailers. Under a contract issued by the Naval Research Laboratory, Retech designed and constructed the Plasma Arc Hazardous Waste Treatment System (PAHWTS) at the US naval base in Norfolk. Successful tests were performed with soil, epoxy paint, latex paint, mixture of methanol with 1,1,1 trichloroethane (TCA) at 135-$225\,\mathrm{kg\,h^{-1}}$ and oily rags at $91\,\mathrm{kg\,h^{-1}}$ [166]. This plasma treatment system was sold through government auction in 2007 [69].

Another company specialized in plasma-based hazardous waste destruction is **SRL Plasma Pty Ltd** which operates, manufactures and markets the PLASCON process. The technology has been operating commercially since 1992 and has nine commercial plants operating. Four 150 kW Plascon units in Australia, two units which treat the liquid waste stream from 2,4 D manufacture, four plants in Japan for PCB destruction and 1 plant in United Kingdom for fire retardants and ODS [195]. Because of the lack of information on the location and details of these systems, they are not included in Table 2.1.

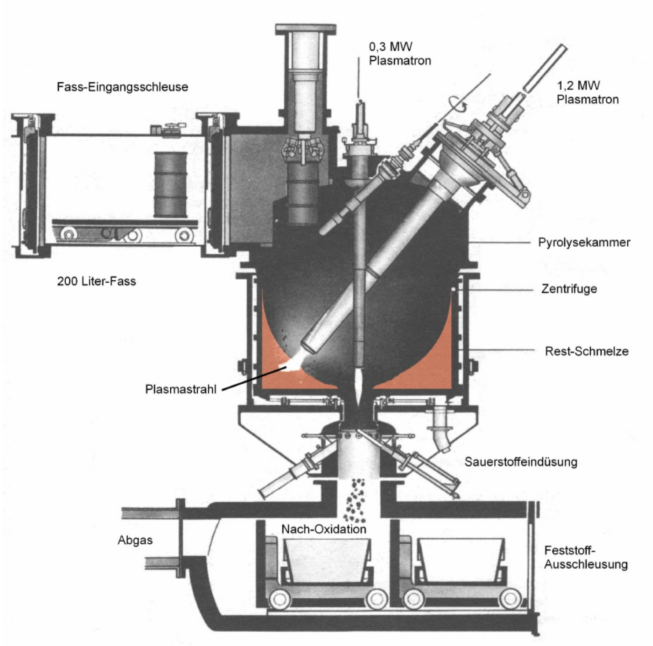

Figure 2.10: Illustration of the Retech gasification system

Enersol Technologies Inc. developed and demonstrated their stationary Plasma Energy Pyrolysis System (PEPS) in cooperation with the US Army at a 10 tpd test facility located in Springfield (Virginia, USA) in 1999. The plasma torch technology used in their system is supplied by Phoenix Solutions Co. Enersol also developed a mobile PEPS unit capable of processing 3 to 5 tpd of a variety of waste streams which can be mounted on six trailers [35].

It is clear that plasma gasification was originally employed for the destruction of hazardous waste. In these type of installations, such as the PGM reactor system by EER (Figure 2.9), the torches are almost exclusively positioned at the bottom of the reactor and are operated in batch mode. The evolution in plasma gasification projects shows that the focus in the last decade has shifted towards converting a wider variety of waste (incl. municipal and industrial waste) to useful secondary resources. With the focus on resource recovery, the quality of the syngas has become more important. Therefore, the plasma aspect is incorporated in such a way that it contributes to a cleaner syngas.
The plasma gasification industry is fast-growing and a lot of interesting projects

are currently being developed, which demonstrate that the emphasis lies on resource recovery:

- The plasma gasification unit of futureNrg is being constructed at the Sendayan Tech Valley (Serembam, Malaysia) to convert medical waste and waste pharmaceuticals. The produced syngas will be used to generate electrical power for the plant and thermal energy through combined heat and power [60].
- A 650 tpd energy from waste facility is being developed in Barbados by Cahill Energy. The company has selected Alter NRG to supply the plasma gasification technology. The start date is scheduled in 2019 [26].
- In Bijie (China), the WPC gasification technology is part of a plan by Green World Energy Solutions to construct a waste-to-energy facility. The first phase will have the capacity to process 600 tpd of MSW and 200 tpd of other waste. The vitrified slag by-product will be converted into useful foam insulation. Full commercial operation is expected to start in 2017 [147].
- Group Machiels has launched an ambitious project in 2008 to divert (incl. recycling) 16 million tonnes of landfill waste over a period of 20 years. The non-recycled excavated waste from the Remo site in Houthalen-Helchteren (Belgium) will be treated by plasma gasification technology supplied by Advanced Plasma Power. The required throughput is 450 000 tpy, which will generate in excess of 100 MW of net electricity [182].
- Another project being developed by APP is planned at Port of Hamilton in Ontario (Canada). The Gasplasma technology will be used to process up to 170 000 tpy of commercial and municipal waste, which will generate 20 MW of net electricity from syngas.
- Solena Fuels has committed to build a facility which will convert landfill waste to jet fuel at Thames Enterprise Park in Essex (UK). According to their website, Solena's Integrated Biomass-Gas to Liquid solution is based on an industry-proven Fischer-Tropsch platform coupled with Solena's proprietary high temperature plasma gasification [174].

As the plasma gasification technology is maturing, it is to be expected that future projects will opt for integrated plasma gasification processes (e.g. integrated plasma gasification combined cycle).

Besides the established plasma gasification facilities, there exists also a long list of launched projects which have been cancelled in the past. The reasons

these projects were scrapped are often financial when failing to secure the large investments needed for commercial plasma gasification developments. A second common reason is the intensive process of obtaining the necessary environmental permits.
One of the important elements of a project to become successful projects is the location of the plasma gasification unit. The location is crucial in securing a constant availability of waste for the plant. The development of a plasma treatment facility is therefore often a cooperative effort between local private and/or intercommunal (waste) syndicates, the technology providing company and possibly a company for the downstream use the gasification products. Similar to the availability of the input, there should also be a stable market for the output of the plant, whether it is electricity and/or heat, or chemicals.
It is clear that a well-defined structure and direction for the purpose of the plasma gasification unit from the input to the output is needed.

Not only financial, organisational and planning mistakes have failed some of the launched plasma gasification projects, there are also a number of technological bottlenecks which proved to be insurmountable in some cases.
Plasma gasification reactors need to be able to handle multiple tonnes of waste per hour in order to be financially viable. Because the technology is relatively new, many of the technology providers only have a pilot-scale installation capable of processing a couple of tonnes per day. This means that the capacity of the proposed reactor systems are often up to two orders of magnitude larger than the proven demonstration unit. One of the consequences of design flaws due to overambitious up-scaling are cold spots leading to incomplete gasification. Other technological problems can include the material for refractory lining and particulates build-up and clogging of piping and the afterburner.
Adding these challenges to the technological barriers inherent to plasma torches (such as torch efficiencies and electrode lifetime), it becomes evident that a plasma gasification project needs to be very-well engineered in order to benefit from the potential of the technology.

2.6.2 Academic

Besides the previously listed reactors from PEAT International at the National Cheng Kun University in Taiwan and at Georgia Tech Research Institute (USA) [122], from Pyrogenesis at the National Technical University of Athens (Greece) [1] and from AdaptiveARC at the University of California (USA) there

exists a number of additional plasma gasification unit for academic research purposes.

- A lab-scale plasma gasifier equipped with a steam plasma torch has been constructed and used for gasification experiments since 2005 by the Institute of Nuclear Energy Research (INER) in Taipei (Taiwan) in addition to their plasma melter facility for low-level radioactive waste [186]. The unit is equipped with a 100 kW non-transferred plasma torch and has a maximum material throughput of $10\,\mathrm{kg\,h^{-1}}$. Since 2009, a second 500 kW pilot-scale plasma gasification plant is operational and generates syngas from biomass for the production of DME [32].
- The pilot-scale installation at the Institute of Plasma Physics, Academy of Sciences of the Czech Republic (IPP-ASCR) in Prague was constructed in 2005. This realization was made possible by the financing of Envitech (Belgium) and via the collaboration with Ghent University (Belgium). Research on this plasma gasification system is presented in this work and the details of this configuration are discussed in Paragraph 5.2.1.
- The Institute of Electrophysics of the Russian Academy of Sciences (St. Petersburg) owns a shaft reactor with a 50 kW DC torch mounted on top. It can process up to $50\,\mathrm{kg\,h^{-1}}$ of solid industrial waste [21], low radioactive waste and medical waste.
- The Institute of Mechanics, Chinese Academy of Sciences (CAS-IMECH) in Beijing (China) developed a 150 kW DC plasma pyrolysis installation and a smaller laboratory-scale 30 kW DC plasma arc reactor for the destruction of chemical wastes [113].

2.7 Conclusions

Compared to the four main types of conventional gasifier design, the configuration of plasma gasification reactors is much more varied. The integration of a plasma element in a plasma gasification system is clearly strongly dependent on the type of material treated and the desired specifications of the end-products.
Some general design features which can be distinguished among the variety of plasma gasifier configurations are:

- Single-stage or two-stage. As mentioned previously, either the plasma jet enters in the same volume where the gasification process occurs (single-stage) or the plasma treatment can be a separate step for cleaning the syn-

gas and/or melting the inorganic residues downstream from the gasification chamber (two-stage).

- Continuous or batch material feeding. Most of the plasma gasification systems have a continuous material feeding mechanism. Hazardous material which needs to be well-contained during transport and/or pre-handling is most-likely loaded in batch-mode into the reactor.
- Position and type of plasma torch. In almost all of the plasma gasifiers, the plasma flow is positioned near the bottom of the reactor volume. Fresh material is gradually passing through the high-temperature region created by the plasma jet(s), where the gasification of the material is taking place. A shaft reactor is the matching gasifier shape for this torch configuration, in which the stack of material is slowly moving down as the bottom of the pile is being converted to syngas (see Figure 2.6).
  An exception to this set-up is the in-flight plasma gasification system. The exit of the plasma torch is located at the top of the reactor, next to the point-of-entry of the treated material. The waste stream falls freely under gravitational force into the volume, where it immediately passes the plasma jet region and is assumed to be instantaneously gasified. This type of plasma gasification system is operational at the Institute of Plasma Physics in Prague (Czech Republic) and has been proven successful for the treatment of fine homogeneous biomass particles.

The material of interest in the experimental part of this thesis is refuse-derived fuel (RDF). In a traditional gasification system, a fluidized bed or downdraft configuration would be selected to process this type of waste, because of their capability of handling coarse heterogeneous material and the higher operating temperatures.
Some plasma gasification facilities were listed in this chapter that are treating municipal solid waste (somewhat similar to RDF). Either their configuration is similar to a downdraft gasifier or they are two-stage systems, but no single-stage in-flight plasma gasification system. Therefore, it would be interesting to test the performance of the single-stage research unit at the IPP for gasifying material with a high inorganic content, such as RDF.

Table 2.1: List of existing plasma gasification facilities

Country	City	Company	Feedstock	Technology provider	Year	Downstream processing	Output
USA	Madison, Wisconsin	Coskata	biomass and waste	WPC	2009	fermentation	bio-ethanol
	Carnival cruise ship	Carnaval Cruise Lines	200 kg h^{-1} of shipboard waste	Pyrogenesis	2003	combustor	
	USS Gerald carrier	US Navy	200 kg h^{-1} of shipboard waste	Pyrogenesis	2012	combustor	
	Hurlburt Field, Florida	US military	3100 tpy of MSW, IW, hazardous & biomedical waste	Pyrogenesis	2011	gas engine	electricity intern
	Madison, Wisconsin	WPC	48 tpd of various waste	WPC	1984	combustor	
	Arlington, Oregon	InEnTec	25 tpd of high carbon waste	InEnTec	2011		
	Midland, Michigan	Dow Corning Corporation	6600 tpy of hazardous chlorinated organic liquids	InEnTec	2010		HCl + syngas
	Richland, Washington	InEnTec	25 tpd of various waste	InEnTec	2009		
	Riverside, California	NRG Energy	MSW, biomass, construction debris	AdaptiveARC	2012	Caterpillar genset	electricity
	Sacramento, California	Technikon	8 tpd of biomass and waste	IES			
	Sacramento, California	Technikon	60 kg h^{-1} of various waste	PEAT	2010		
	Atlanta, Georgia	Georgia Insitute of Technology	6-8 tpd of various waste	PEAT	2001		
Japan	Mihama - Mikata	Hitachi Metals	17.2 tpd of MSW and 4.8 tpd of sewage sludge	WPC	2002	boiler	heat to dry sewage sludge
	Utashinai	Hitachi Metals	2 trains of 83 tpd of ASR or 110 tpd of MSW	WPC	2003	steam turbine	1.5 MW net electricity
India	Pune	SMS Envocare Ltd.	72 tpd of hazardous waste	WPC	2009	steam turbine	1.6 MW net electricity
	Nagpur	SMS Envocare Ltd.	72 tpd of hazardous waste	WPC	2011	steam turbine	1.6 MW net electricity
UK	Teesside	Air Products	950 tpd of non-recyclable residaul waste	WPC	2014	combined cycle	45 MW net electricity

Table 2.1: List of existing plasma gasification facilities (continued)

Country	City	Company	Feedstock	Technology provider	Year	Downstream processing	Output
	Swindon	APP	100 kg h^{-1} of various waste	APP	2007	Liebher gas engine	60 kW electricity
Canada	Ottawa, Ontario	Plasco	85 tpd of post-recycle MSW	Plasco	2008	gas engine	4 MW net electricity
	Laval, Quebec	Recyclage EcoSolutions	50 kg h^{-1} of R11, R12, R134a and R141	Pyrogenesis	2013		CO_2 + H_2O
China	Shanghai	Abada Plasma Technology Holdings	60 kg h^{-1} of medical waste	PEAT	2013		
	Hubei	Wuhan Kaidi	150 tpd of biomass	WPC	2013	Fischer - Tropsch	liquid fuels
Mexico	Mexico City	Biosistemas Sustentables	60 tpd of post-recycling mixed MSW	AdaptiveARC	2010	Caterpillar genset	420 kW electricity intern
Taiwan	Tainan	National Cheng Kung University (NCKU)	3-5 tpd of industrial waste and toxic waste (incinerator fly ash, medical waste and inorganic sludge)	PEAT	2004		
Greece	Athens	National Technical University of Athens	50 kg h^{-1} of hazardous waste	Pyrogenesis	2002		
France	Morcenx	CHO Power	37 000 tpy of IW and 15 000 tpy wood chips	Europlasma	2014	gas engine + steam turbine	12 MW net electricity + heat for wood dryer
Spain	Castellgali	Hera Plasma	85 kg h^{-1} of non-recyclable MSW and IW	Plasco	2007	combustor	
Russia	Moscow	Sia Radon	250 kg h^{-1} of LILRW	EERE	2002		
Israel	Yblin	Environmental Energy Resources	20 tpd of MSW	EER	2007		

CHAPTER 3

Plasma Modelling

3.1 Background

Thermal plasmas provide opportunities for materials processing due to their high energy content and high energy density. Thermal plasma processing techniques of current interest include spraying, cutting, coating, synthesis, sintering, extractive metallurgy and waste treatment, among others (see Fauchais and Vardelle [56] for a detailed list of thermal plasma applications). The plasma system of choice for these processes is primarily a DC arc plasma torch. The apparent simplicity of this type of plasma torch is in contrast with the highly complex plasma flow phenomena. To gain a better understanding of the physical phenomena (electrical, chemical and thermal) and to drive the continuous development and improvement of thermal plasma based technologies, a large amount of computational fluid dynamics (CFD) modelling has already been done. The overall goal of these numerical studies is to develop models that can correctly predict the plasma flow characteristics (temperature, velocity and concentration fields) and consequently the interaction of the flow with solid or liquid materials in plasma processes (e.g. plasma gasification).

In all plasma jet simulations described in literature, independent of the specific case set-up, the same physical mechanisms and model aspects are included. The approach and assumptions used in their implementation strongly influences the accuracy of the simulation results. A short description of the main elements in-

volved in the CFD modelling of thermal plasma is given here. A full description of these elements can be found in the review by Trelles et al. [183].

3.2 Physical Phenomena

Several physical phenomena specific to thermal plasma problems need to be accurately accounted for in the CFD modelling.

3.2.1 Fluid Models

The thermal plasma flow can be assimilated to a fluid with Navier-Stokes equations describing its hydrodynamic movements. The conservation or continuity equations for an incompressible plasma, assuming negligible temporal and spatial pressure variations, are [136]:

The equation of mass continuity:

$$\frac{\partial \rho}{\partial t} + \nabla \cdot (\rho \boldsymbol{v}) = 0 \tag{3.1}$$

The equation of momentum conservation:

$$\frac{\partial (\rho \boldsymbol{v})}{\partial t} + \nabla \cdot (\rho \boldsymbol{v}\boldsymbol{v}) = -\nabla p + \nabla \cdot \boldsymbol{\tau} + \rho \boldsymbol{g} + \boldsymbol{j} \times \boldsymbol{B} \tag{3.2}$$

The energy conservation equation:

$$\frac{\partial (\rho h)}{\partial t} + \nabla \cdot (\rho \boldsymbol{v} h) = -\nabla \cdot \left(\sum_{i=1}^{q} h_i \boldsymbol{J_i} \right) - R + \nabla \cdot \left(\frac{k}{C_p} \nabla h \right) - \nabla \cdot \left(\frac{k}{C_p} \sum_{i=1}^{q} h_i \nabla Y_i \right) + \frac{\boldsymbol{j}^2}{\sigma} + \frac{5 k_B}{2 e C_p} \boldsymbol{j} \cdot \nabla h \tag{3.3}$$

in which the first four terms on the right-hand side describe respectively changes in enthalpy due to diffusion, net radiative emission and two thermal conduction terms.

The mass continuity equation of species i:

$$\frac{\partial (\rho Y_i)}{\partial t} + \nabla \cdot (\rho \boldsymbol{v} Y_i) = -\nabla \cdot \boldsymbol{J_i} + r_i \tag{3.4}$$

with r_i the net rate of production of species i due to chemical reactions if applicable. If electromagnetic effects are rigorously included in the calculations, besides adding the Lorentz force to the momentum equation and the Joule heating and electron enthalpy flux terms to the energy equation (coloured blue in the equations 3.2 and 3.3), two additional equations are required to describe the flow of charge, i.e. the current continuity equation and the Maxwell's equations:

$$\nabla \cdot \boldsymbol{j} = 0 \tag{3.5}$$

$$\nabla \times \boldsymbol{B} = \mu_0 \boldsymbol{j} \tag{3.6}$$

In the above equations, v is the mass-average velocity of the gas, p is the pressure, h is the plasma enthalpy per unit mass, $\boldsymbol{j}$ is the current density, $\boldsymbol{J}_i$ is the mass flux of species i relative to the mass-average velocity, Y_i is the mass fraction of species i, $\boldsymbol{B}$ is the magnetic field induced by the current, $\boldsymbol{\tau}$ is the stress tensor, R is the net energy loss by radiation, g is the gravity, k_B is the Boltzmann's constant, e is the electronic charge and μ_0 the permeability of free space. The gas properties are mass density ρ, thermal conductivity k, electrical conductivity σ and specific heat at constant pressure C_p.

The approach to solving the flow governing equations depends on the fluid description of plasma. The most frequently used thermal plasma models rely on the assumption of Local Thermodynamic Equilibrium (LTE). This requires that the velocity distribution function and population density of excited states for each species are described by a Maxwellian distribution, that the concentration of the species present can be calculated assuming chemical equilibrium and that the translational, excitation and the reaction temperatures are equal. This means that the plasma flow can be described as a reactive fluid in chemical equilibrium in which the internal energy of the fluid is characterized by a single temperature T [136, 183].
Departures from thermal equilibrium can be taken into account by solving two energy equations, one for the heavy particles at temperature T_H and the other for the electrons at temperature T_e. Hence, such thermodynamic non-equilibrium thermal plasma models (NLTE) are also known as two-temperature models.
An even more fundamental approach to the description of thermal plasma flow is to represent plasma as a multicomponent, chemically reacting ideal gas. In such chemical non-equilibrium models, neutrals, ions and electrons are considered as separate components or species of the plasma among which arbitrary numbers of kinetic and equilibrium chemical reactions can occur [155].

3.2.2 Turbulence

The plasma jets encountered in most thermal plasma applications are characterized by a turbulent flow state. The large velocity and temperature gradients together with electromagnetic effects cause the flow to become unstable and turbulent. One of the physical phenomena which causes turbulent instabilities is the changing anode attachment position of the arc caused by the interplay among thermal, magnetic and electrochemical forces within the plasma column. The resulting turbulent plasma jets are usually accompanied by strong entrainment

of ambient gas into the jet and with short high-temperature region lengths. In some materials processing techniques, these features are not desirable, which has triggered the development of (DC) laminar plasma jets [213]. Cheng et al. [28] compared the flow field characteristics of simulations of laminar and turbulent argon plasma jet issuing into ambient air. It was found that significant differences exist in the entrainment mechanisms, spreading angle of the jet and in the influence of parameters of the plasma boundary conditions.
In the majority of the plasma models in literature, the flow regime is turbulent. The modelling of turbulence can be done by several different approaches. The use of turbulence models in thermal plasma flows is significantly more involved than for most other industrial applications due to their inherent characteristics (mainly large property variations) [183]. The most accurate numerical description of turbulent flows is direct numerical simulation (DNS), in which no approximations for solving the flow equations are included. Due to the high computational cost of this technique for resolving the whole range of flow length scales, no DNS of a thermal plasma has been performed yet. Large Eddy Simulation (LES) is an alternative approach to DNS which resolves the large scale turbulent perturbations in the flow and models only the smaller scales. Accurate simulations with LES require accurate spatial and temporal discretization. The use of LES as turbulence model is gradually gaining popularity [12, 33, 128], but the most widely used methods for modelling turbulence are still the Reynolds-averaged Navier-Stokes (RANS) models. These models seek the solution of approximations of the time-averaged Navier-Stokes equations [183]. Many different types of models exist in this group, but the most popular RANS turbulence model is the k-ϵ model, where k stands for the turbulent kinetic energy and ϵ its rate of dissipation. This approach to modelling turbulence may provide an adequate description of the flow for transferred torches, whereas the LES approach is more appropriate for the highly unsteady non-transferred torches.

3.2.3 Radiation

Radiation is an important phenomenon in thermal plasmas as it represents the largest energy loss term in the hottest regions. The total radiative flux source term in the energy equation is a function of the spectral intensity, which is found by solving the radiative transfer equation (RTE). Because of the very complicated and exceedingly expensive computation, it is not possible to rigorously solve the RTE. Therefore, several types of simplified models are often employed to account for the radiative transport in thermal plasmas.
The most frequently used methods are the Discrete Ordinates Methods (DOMs),

the P-1 method (simplest case of the P-N method, which is based on the expansion of the radiation intensity into an orthogonal series of spherical harmonies [129]) and the Net Emission Coefficient (NEC) method [114]. The latter approach directly estimates the net radiation (i.e. the difference between emission and absorption) through the net emission coefficient, which for a given plasma forming gas can be expressed as function of temperature and an effective absorption radius R_p of an isothermal sphere in which re-absorption occurs. A more elaborate discussion on radiative transport in plasmas can be found in Trelles et al. [183].

3.2.4 Diffusion

The process of diffusion between different species (or group of species) can occur due to species concentration gradients, pressure gradients, temperature gradients and external forces. An example of the latter driver of diffusion is ambipolar diffusion, which is manifested between charged particles by an externally applied electric field and the electric field that arises because of the tendency of electrons to diffuse more rapidly than ions. In this paragraph the diffusion due to difference in concentration is briefly touched upon.

The most accurate way to model diffusion is to treat each species (molecular, atomic or ionic), derived from a given atomic or molecular gas, separately. The calculation of the diffusion flux then relies on multicomponent diffusion coefficients, dependent on the mole fractions and masses of all the species present and on the collision cross sections for interactions between all the species. This approach has the advantage that it does not require the assumption of local chemical equilibrium (LCE) and that chemical reactions between the species derived from the different gases can be treated. However, the complexity of implementation of this rigorous method for a large number of species (typical for plasma flows) has created the development of several different approximations to model diffusion. These approximations treat diffusion in terms of the binary diffusion coefficients D_{ij} which depend only on the properties of species i and j.

As mentioned above, in most plasma modelling problems, LCE is assumed. For these cases, the species derived from each gas are grouped together and the diffusion is described between the gases involved. The different approximations for the estimation of the diffusion coefficients for a mixture of two gases are comprehensively described by Murphy [133]. The expressions which are discussed are the binary diffusion coefficient approximation, the first and second viscosity approximation, the quasi-binary diffusion coefficient approximation and the combined diffusion coefficient method.

In the same publication by Murphy [133], a number of sample calculations were

performed to evaluate the accuracy of the diffusion coefficients calculated using each of the previously mentioned methods. It was concluded that the combined diffusion coefficient treatment is required for an acceptably accurate treatment of diffusion phenomena in plasmas in LCE [135].

3.3 Modelling Aspects

Besides the physical phenomena within the flow, there are also some aspects in plasma modelling which are inherent to the specific case set-up. These aspects are further elaborated upon.

3.3.1 Dimension of Space

One-dimensional (1D) stationary plasmas, corresponding to wall-stabilized arcs, are the simplest cases of thermal plasma models. In such models, the plasma is characterized by the temperature T, which depends only on the radial position r and can be calculated by solving the energy conservation equation [67]. For transient 1D plasma models, the cooling of the plasma is assumed to be instantaneously compensated by radial convection. For this type of model, two time-dependent conservation equations (mass and energy) are solved with temperature $T(r,t)$ and radial velocity $v(r,t)$ as unknowns.
More common is the development of two-dimensional (2D) plasma models. The two-dimensional formulation allows calculation of either planar or axisymmetric plasma flows [155]. Flows having axial symmetry are described by 2D cylindrical coordinates and its axisymmetric formulation permits the calculation of an azimuthal velocity component (or swirl).
A lot of plasma phenomena are inherently three-dimensional (3D) and are thus ignored by a 2D approach. This necessitates the use of 3D plasma models which can account more accurately for anode attachment fluctuations, three-dimensional turbulent structures, etc.
The difference in results between a 2D and 3D approach when modelling a non-transferred DC plasma torch was described by Bhuyan and Goswami [14]. They reported significant differences between the control parameters, caused by the inability of the 2D model to realistically simulate the arc which exhibits local attachments in the circumferential direction.

3.3.2 Computational Domain

First, the dimensions of the computational domain should be selected sufficiently large around the area of interest. The size of the domain can determine the sensitivity of the simulation results to the choice of boundary conditions. Furthermore,

the discretization of the domain into a computational grid allows to solve the set of partial differential equations. The mesh size should be sufficiently fine in order to obtain a solution which is invariant with finer mesh sizes. The correct grid size is evaluated through a grid independence study [209]. Besides the size of the mesh, the quality of the cells can also influence the convergence of the simulation and the final result.
The choice of geometry also strongly determines the boundary conditions of the calculation. This is well illustrated by Selvan and Ramachandran [168], who compared two three-dimensional arc plasma torch simulations with different geometries. In plasma modelling, the choice of the computational domain is dependent on the plasma area of interest. An important distinction is made between plasma arc models and plasma jet models. In the former type of models, the computational domain is predominantly the inner volume of the torch chamber in which the electromagnetic effects of the plasma column and the interaction with the stabilizing medium are often investigated. In plasma jet models, the computational domain is the area outside of the torch and the inlet boundary conditions for the plasma are imposed on the exit nozzle of the plasma torch.

3.3.3 CFD Software

A limited number of research groups has developed their own in-house fluid dynamics software for modelling plasma flows. One of the most complete and well-tested computational models is the computer code LAVA, developed by Ramshaw and Chang [155]. In this software, the governing equations for a multicomponent chemically reacting ideal gas are solved using standard finite-difference techniques with explicit temporal differencing. In Williamson et al. [209], the capability of reproducing the general features of the interaction of a plasma jet with its surrounding environment using the LAVA environment was demonstrated.
Most research efforts in the thermal plasma community are being performed using commercial software packages, such as FLUENT, COMSOL, PHOENICS, ESTET, etc. Boussagol et al. [19] presented a comparison of numerical simulations of a DC plasma jet flowing in air using two commercial three-dimensional computational fluid dynamics codes, ESTET and FLUENT. The flow fields computed by both codes exhibited significant differences despite using the same model setup. This shows that the numerical algorithms and the approach in modelling turbulence used by the commercial codes, which are not specialized for plasma problems, can affect the flow field.

3.3.4 Time Dependency

The CFD simulations of a plasma flow can be done assuming steady-state conditions or by a transient (unsteady/time-dependent) approach. Two successive sets of numerical simulations were performed by Mariaux and Vardelle [118] to investigate the effect of time-dependency on the flow field. The first calculations were done at steady-state conditions and the second set of calculations was dedicated to the unsteady-state calculations of the plasma flow. The results show that the flow fields are subjected to important time-variations close to the exit nozzle, which require accurate time-dependent boundary conditions. This is especially the case if the objective of the modelling is to study the turbulent behaviour of the plasma flow.

3.4 Thermophysical Properties

Thermodynamic and transport properties of the plasma are important inputs for the fluid dynamic modelling of plasma jets. In this paragraph, the description of the calculation of these properties (applicable to plasma systems in LTE) is presented.

Obtaining the equilibrium composition of the gas system is the first prerequisite step in the calculation of thermodynamic and transport properties. The local composition of a plasma in LTE is determined only by the local temperature, pressure and concentrations of the constituent chemical elements. The standard technique for calculating the composition is the Gibbs free energy minimization approach assuming the plasma is an ideal gas. The required thermodynamic data for the individual species are available in tables, such as the JANAF tables [27]. The main processes which occur in the temperature range from room temperature to 20 000 K are dissociation of molecules at low or intermediate temperatures, followed by partial ionization with the formation of ions and electrons and the disappearance of the molecules and finally, at high temperatures (T>15 000 K) the gas is almost totally ionized.

Once the species composition is known, the thermodynamic properties (enthalpy (H), density (ρ), molecular weight (M), speed of sound (c) and specific heat capacity (C_p)) of a closed gaseous system in thermodynamic equilibrium at constant pressure and temperature can be directly calculated from particle number densities (from the equilibrium composition) and internal partition functions [37, 38]. The calculation of the transport properties (thermal conductivity (k), viscosity (μ), etc.) is based on solving the Boltzmann integral-differential equation describing the evolution of the electron energy distribution function

by the well-known Chapman-Enskog method [104]. The transport coefficients are approximated using Sonine polynomials. The data necessary for these calculations are the particle number densities and the collision integrals [67]. Detailed information about the methods used for the equilibrium and transport properties calculation can be found in Murphy and Arundell [139].

In the modelling of plasma processes, the plasma gas from the torch is represented by either a pure gas, such as argon [48, 91, 110, 111, 201] or a gas mixture with fixed composition (e.g. 50 %Ar–50 %H_2) [12, 13, 49, 71, 118, 124, 125, 196]. LTE thermodynamic and transport properties are available for most of these plasma gases (either pure gases or gas mixtures with fixed composition) as a function of temperature and pressure [183].
In many thermal plasma problems, the medium rarely consists of a single gas, but is made up of a mixture of gases. The plasma gas can be defined as a variable mixture of different gases and additionally, the plasma gas can mix with other surrounding gases. For these multicomponent mixtures, the local gas composition cannot be known a priori and therefore it is necessary to solve the species conservation equation(s) in the CFD simulations. The properties of the gas mixture are then determined from the local species concentrations, temperature and pressure. There are two general methods of doing this.
In the rigorous method, the equilibrium composition is first determined considering the complete system of all gases considered, after which the thermodynamic and transport properties are calculated and stored in a multidimensional matrix as a function of gas concentrations and temperature (and pressure if applicable). This way, not only the products of ionization and dissociation of the pure gases, but also combined ions and molecules from the interactions between different gases are considered. The accurate thermodynamic and transport properties are then directly assigned to the gas mixture through interpolation of this pre-calculated matrix during flow calculations. Because all possible species, formed from the different gases are included in the calculation of the species composition of the complete system, this method is often referred to as the full multicomponent approach. This approach was applied by Vincent et al. [196], Trelles et al. [184] and Colombo et al. [34] in their plasma flow simulations.
In the second approach for calculating thermophysical properties of a gas mixture, first the equilibrium composition and the physical properties of each gas are determined separately. Consequently, these temperature-dependent properties of the pure gases are used with mixing rules to estimate the gas mixture properties. This method cannot take into account possible chemical reactions between the

various gases and therefore only the effect of dissociation and ionization of each individual gas is included in the properties of the gas mixture. Details of these mixing rules are discussed in the next paragraph.

3.4.1 Different Mixing Rules

The development of reliable mixing rules, which would allow the transport coefficients of gas mixtures to be determined from those of pure gases, has been a topic of interest for more than 50 years [137]. Several authors tend to use mixing rules because of the accessibility of the necessary data and because of the simple implementation and fast execution. Mixing rules based on simple species proportionality in terms of mass fractions or molar fractions are generally used for non-reactive mixture components and at low temperatures. For some of the thermodynamic and transport properties, the application of these rules at high temperatures is acceptable, while for other properties, the effects of dissociation and ionization at elevated temperatures cause significant deviations from the exact values.

An analysis of the influence of using mixing rules on the mixture properties has been published by Gleizes et al. [66], who identified large variations in properties of gas mixtures with metallic vapours depending on the chosen mixing rules. In the majority of CFD simulations, the gas concentrations are expressed in mass fractions. Since some mixing rules rely on molar proportions, considering a binary gas mixture, these can be calculated as:

$$x_i = \frac{\frac{y_i}{M_i}}{\sum_i \frac{y_i}{M_i}} \tag{3.7}$$

in which x_1 and x_2 are the molar fractions of the gases in the mixture, y_1 and y_2 are the mass fractions and M_1 and M_2 the molecular weights.

3.4.1.1 Density

The mass density (ρ in $\mathrm{kg\,m^{-3}}$) can be calculated from the plasma composition (expressed in number density n_i in $\mathrm{mol\,m^{-3}}$) and the molecular weights of the components:

$$\rho = \sum_i n_i M_i \tag{3.8}$$

By constructing a set of equations which describe the total number densities of the heavy species in terms of the molar fractions of the mixture elements, the density can be eventually calculated from the electron number density (n_e), which relates to the total number density (N) as:

$$N = \frac{p}{k_B T} - n_e \tag{3.9}$$

A good agreement between the exact values and this approximation via the electron number density was found [66]. However, it is generally not necessary to use this method as a simple molar interpolation (Equation 3.10) between the mass densities of the gases only leads to small departures from the exact solution.

$$\rho = \sum_i x_i \rho_i \tag{3.10}$$

3.4.1.2 Specific Heat

The specific heat at constant pressure (C_p in $\mathrm{J\,kg^{-1}\,K^{-1}}$) is derived from enthalpy. For a non-reacting gas mixture, the difference in enthalpy values between rigorous calculation and mass interpolation between the individual gases is small. However, the use of mixing rules for a reacting gas mixture omits the contribution of species combined from the constituent elements of the gases in the enthalpy calculation. Hence, the calculation of heat capacity via mass interpolation between the individual gas properties can lead to erroneous results. The mixing rules for specific heat should be evidentially expressed in mass proportions because C_p is defined in mass units.

$$C_p = \sum_i y_i C_{p,i} \tag{3.11}$$

3.4.1.3 Viscosity

The mixing rules developed by Wilke [207] are perhaps the best known formulas for the estimation of dynamic viscosity (μ in $\mathrm{kg\,m^{-1}\,s^{-1}}$) of a gas mixture.

$$\mu = \sum_i \frac{x_i \mu_i}{\sum_j x_j \phi_j} \tag{3.12}$$

with

$$\phi_{ij} = \frac{1}{\sqrt{8}} \left(1 + \frac{M_i}{M_j}\right)^{\frac{1}{2}} \left[1 + \left(\frac{\mu_i}{\mu_j}\right)^{\frac{1}{2}} \left(\frac{M_j}{M_i}\right)^{\frac{1}{4}}\right]^2 \tag{3.13}$$

Comparison of the mixing rule of Wilke with adapted formulas by Vanderslice et al. and Yun et al. [214] and molar and mass proportionality rules was done by Gleizes et al. [66], which revealed the best fit for the mixing rule of Yun et al. (Equation 3.14) and showed an inaccurate approximation by the Wilke's mixing rule.

$$\mu = \frac{\mu_1}{1 + \dfrac{15R\mu_1}{4\Lambda_{12}M_1}} + \frac{\mu_2}{1 + \dfrac{15R\mu_2}{4\Lambda_{12}M_2}} \tag{3.14}$$

where (R/Λ_{12}) is a parameter function of temperature depending on the viscosity of the equimolar mixture.

Similar results were obtained by Murphy [137] who compared the exact values for the temperature-dependent viscosity for a mixture of 25 % nitrogen and 75 % with the results obtained from the mixing rules of Yun et al. [214], Wilke [207] as well as with a mole-fraction-weighted average.
Palmer and Wright [148] also reviewed the performance and accuracy of four commonly used mixing rules (full multicomponent approach versus mixing rules of Gupta-Yos, Armaly-Sutton and Wilke) for determining viscosity of 11-species air and hydrogen-helium gas mixtures at high temperatures and found that the Gupta-Yos mixing rule gives acceptable results for weakly or non-ionized flows, while the Armaly-Sutton mixing rule is applicable to higher temperature, more strongly ionized flows by adequately tuning the parameters of the method.

3.4.1.4 Thermal Conductivity

The most popular mixing rule for thermal conductivity (k in $\mathrm{W\,m^{-1}\,K^{-1}}$) is the one proposed by Mason and Saxena [120]. Their method is an approximation to a more accurate method given by Hirschfelder [78]. This mixing rule is analogous to the mixing rule of Wilke, proposed for viscosity (Equation 3.12) with an additional empirical factor 1.065 to establish self-consistency for mixtures of identical species.

$$k = \sum_i \left[1 + \sum_{k=1, k\neq 1} G_{ik} \frac{x_k}{x_i} \right]^{-1} \tag{3.15}$$

with

$$G_{ik} = \frac{1.065}{2\sqrt{2}} \left(1 + \frac{M_i}{M_k} \right)^{-\frac{1}{2}} \left[1 + \left(\frac{\mu_i}{\mu_k} \frac{M_k}{M_i} \right)^{\frac{1}{2}} \left(\frac{M_i}{M_k} \right)^{\frac{1}{4}} \right]^2 \tag{3.16}$$

Similar to the mixing rule of Wilke for viscosity, the mixing rule for thermal conductivity by Mason and Saxena was derived for mixtures of non-ionized gases, considering only elastic collisions. They assume that the off-diagonal terms in the matrix that is inverted in calculating the respective transport properties is zero, and that all interactions between species belonging to different gases have the same cross-section [148]. They give reasonable results at lower temperatures, before dissociation and ionization occur, but are generally inaccurate at higher temperatures [66, 137, 148]. The dissociation peaks in the evolution of thermal conductivity as a function of temperature are caused by the contribution of inelastic collisions (called reactive thermal conductivity), which are not taken into account by the mixing rules.
Another mixing rule for thermal conductivity is the Wassiljewa approximation [149] which limitations were discussed by Fauchais et al. [50].

3.5 Conclusions

As mentioned in Section 1.4.4.3, the development and application of the previously described hybrid water/gas stabilized DC plasma torch would benefit significantly from a CFD model capable of correctly describing the plasma jet. Because of the combined stabilization effect of this unique torch, the physical properties of the plasma flow are distinctively different than a plasma generated by water or gas-stabilized torches. In order to adequately simulate the flow field and the entrainment processes at the fringes of the jet, extra attention needs to be given to the calculation of the thermodynamic and transport properties of the resulting plasma gas mixture.
Since the goal is eventually to incorporate the CFD description of this plasma jet into a larger model where the plasma interacts with other gases and/or material, it is very likely that the mixing rules which are fastest and easiest to implement will be used. The most common choices for the estimation of transport properties of a gas mixture are therefore the mixing rules of Wilke (Equation 3.12) and Mason and Saxena (Equation 3.15). Despite their advantages in simplicity, however, it is not clear how their inaccuracy might affect the simulated flow field of a plasma jet.

Two

CFD Modelling of Plasma Jet - Effect of Mixing Rules

CHAPTER 4

Numerical Modelling of Ar/H_2O Plasma Jet with Different Mixing Models

4.1 Introduction

The setting of thermal plasma applications is often in an environment containing a lot of different gases. A perfect example is the use of a non-transferred plasma torch in plasma gasification. In such a system, the plasma gases interact with gasifying agents, as well as with product gases from the gasification reactions. When modelling the entrainment of surrounding gas(es) into a plasma jet, the thermophysical properties of the resulting gas mixture need to be determined in each node of the computational grid. The rigorous approach to the calculation of thermodynamic and transport properties of the gas mixture, in which they are interpolated from a pre-calculated multidimensional matrix in terms of temperature and mass fractions of all gases involved (and possibly pressure) can become overly cumbersome due to the complexity of the calculation routines and the computational expense. Also, the large dataset needed to calculate the properties according to the full multicomponent approach is not always readily available.

Therefore, it is necessary to use mixing rules for the calculation of the thermodynamic and transport properties of the gas mixture in complex multi-gas systems at high temperatures. The importance of the accuracy of the mixing rules was emphasized by Murphy [139] who stated that accurate values of the transport

coefficients and the thermodynamic properties of high-temperature gases and gas mixtures are indispensable inputs in the CFD modelling of thermal plasma processes. Also Trelles [183] pointed out that the accuracy of results strongly depends on the use of suitable thermodynamic and transport properties. Hence, the accuracy of different mixing rules (especially for transport properties) has already been compared in literature, as presented in Paragraph 3.4.1.

From these comparative analyses of the mixing rules for transport properties, it was concluded that the expressions formulated by Wilke and Mason and Saxena are lacking in accuracy. Nevertheless, they are perhaps the best-known formulas and they continue to be used very frequently in plasma jet simulations [12, 19, 71, 124]. Their simplicity of implementation is often preferred over improved accuracy. The previous discussion about the mixing rules was strictly limited to the stand-alone evaluation of their accuracy compared to the exact values without a link to the implications on the simulated flow field.

In the literature, the possible effect of the errors introduced on the flow field from inaccurate values for viscosity and thermal conductivity (calculated with mixing rules) are frequently ignored by assuming that their contribution is negligible in relation to their turbulent counterparts [50, 209]. This might be the case in the main part of the computational domain where the flow field is characterized by a turbulent regime, but not necessarily in the region close to the torch exit. The onset of turbulence only occurs from roughly 20 mm downstream of the exit nozzle [55], so the molecular properties determine the flow field to a great extent in the high-temperature core and at the fringes of the plasma column in the laminar region of the plasma jet close to the exit nozzle.

It is therefore relevant to investigate the effect of the method for calculating thermodynamic and transport properties of a gas mixture on the simulated flow field of a plasma jet. The influence of using mixing rules on the accuracy of the simulation results has not yet been the subject of a quantitative study.

To that purpose, three plasma jet simulations were performed, which differ in the extent to which mixing rules are used for the calculation of the thermophysical properties of a gas mixture. The first model approach (model 1) uses mixing rules among all individual gases. The second model approach (model 2) uses mixing rules among a collection of gases (for which the properties are calculated rigorously) and the remaining individual gases. In the third model approach, without mixing rules, the thermodynamic and transport properties of the gas mixture are calculated rigorously. The influence of the mixing rules in the calculation of the thermophysical properties is evaluated via comparison of the resulting flow field between the three different simulations. These three mixing

model approaches or 'mixing models' are not to be confused with the previously discussed 'mixing rules' which they either incorporate or not.

In this chapter, first, the specifics of the plasma jet which serves as the case set-up for the comparative analysis of the different mixing models is presented. The development of this particular case model was performed in the framework of modelling a plasma gasification system. The model geometry, the boundary conditions, model assumptions and model equations are discussed. Secondly, the details of the three different mixing models are explained. Then the results of the simulations are presented and discussed.

4.2 Model Set-Up

The case set-up for the investigation of the effect of mixing laws in the calculation of thermodynamic and transport properties is based on the hybrid water/gas stabilized torch system developed at the IPP (described in detail by Hrabovský et al. [90]). The combined stabilization mechanisms of argon flow and water vortex create a low-density, high-velocity plasma jet. The substantially different characteristics of the resulting plasma flow (as mentioned in Paragraph 1.4.4.3) make it ideally suited for plasma spraying and waste treatment purposes. In these applications, the Ar/H_2O jet exiting the plasma torch mixes with the surrounding atmosphere, e.g. with air in plasma spraying applications. This situation serves as the baseline for the model case set-up, in which nitrogen gas was selected as the model substance for the ambient gas (closely resembling air). Thanks to this simplification, all chemical elements can be attributed to a single gas and an unambiguous comparison can be made between the different mixing models. The selection of nitrogen to resemble a surrounding atmosphere of air is acceptable since it makes up 79 % of the composition of air and since the collision integrals for oxygen and nitrogen species are similar, leading to similar diffusion rates for nitrogen and air.
The interaction of the H_2O/Ar plasma jet with surrounding nitrogen gas at atmospheric pressure was simulated with three different models. In the following sections, the details of the case set-up are explained, i.e. the computational domain and boundary conditions, the different mixing models, boundary conditions and model assumptions and model equations.

4.2.1 Computational Domain

The domain considered in the calculations represents the plasma jet region outside the plasma torch. The 3D geometry linked to the actual plasma torch structure is shown in Figure 4.1. The computational domain is cylindrical with a diameter of 10 cm and a length of 20 cm. These dimensions correspond well with the area of interest for plasma spraying and for interaction of plasma with biomass and/or waste in plasma gasification.

The exit nozzle of the plasma torch is located at the top of the domain with a radius of 3 mm (marked in red in Figure 4.2(a)). Around the plasma exit, a ring of 2 mm width marks the edge of the copper torch nozzle (marked in light blue in Figure 4.2(a)). The grid consists of 453 375 hexahedral cells and is more refined near the central axis and closer to the torch nozzle, especially at the interface between the plasma column and the surrounding environment (i.e. at the edge of the nozzle exit). The more refined mesh at the edge of the plasma outlet is put in evidence in Figure 4.2(b), which shows a zoom of the nozzle surface and the surrounding mesh.

This grid size was proven to be sufficiently fine using a grid independence study

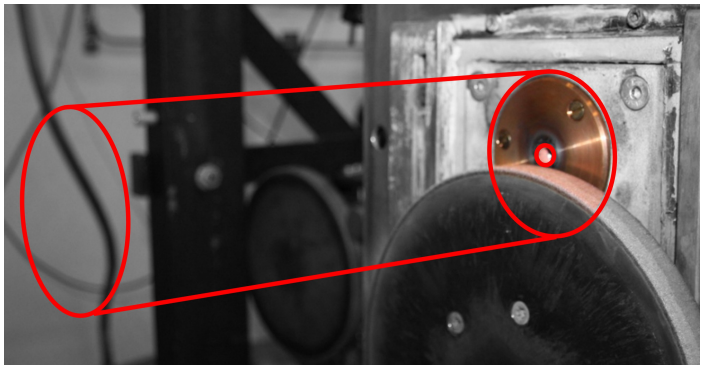

Figure 4.1: Geometry of the case set-up with outlining of the computational domain

between 135 000 (coarse), 453 375 (fine) and 1 881 000 (finest) cells. An extract of this study is shown in Figure 4.3, in which the time-averaged temperature profiles (over 7.5×10^{-4}s) at the position 5 mm downstream of the nozzle exit for the three different grid sizes were compared. The time step size was adapted so the Courant-Friedrichs-Lewy (CFL) number remained the same for the three grid sizes. Although there is still a small difference between the fine grid and the finest grid, the fine grid with 453 375 cells was selected because of computational time

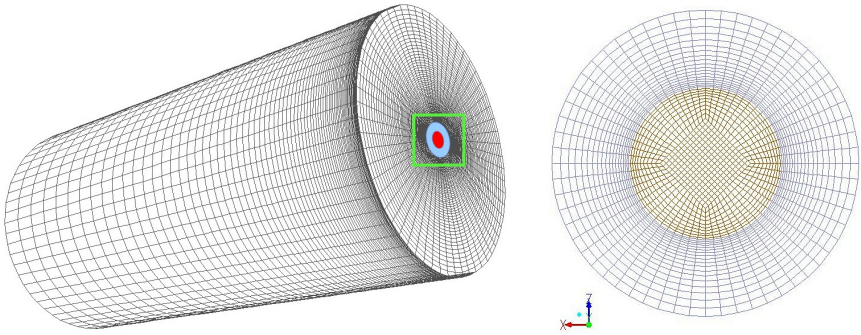

(a) Structured hexahedral mesh of the computational domain

(b) Mesh on nozzle exit surface (yellow) and surrounding copper ring (light blue)

Figure 4.2: Mesh

considerations.

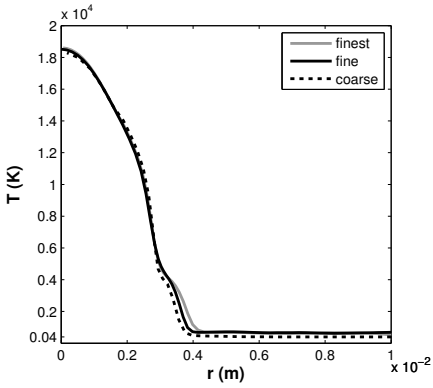

Figure 4.3: Extract of LES grid independence study of time-averaged radial temperature profiles at 5 mm downstream of the torch exit

4.2.2 Boundary Conditions

On the top surface, the copper back wall of the torch chamber is replaced by a pressure boundary with nitrogen gas at $P_{static} = 1$ atm and $T = 400\,\mathrm{K}$. The reason for this is the objective of the simulations, which is to identify the differences in mixing of the plasma with surrounding gas brought about by the

use of mixing rules in the calculation of the thermophysical properties of the gas mixture. It was believed that including the solid boundary condition for the back wall would limit the entrainment of the atmospheric gas. The solid structure of the torch wall was therefore reduced to the ring with an inner diameter of 3 mm and outer diameter of 5 mm, which has a wall boundary condition at a fixed temperature of 1300 K, which is close to the melting point of copper. This area is marked by the small blue line in Figure 4.4. Also the part of the anode copper disk (visible in Figure 4.1) is omitted.

Except for the torch nozzle surface, all the other borders of the computational domain were defined as pressure boundaries with nitrogen at $P_{static} = 1$ atm and $T = 400$ K, drawn by a black line in Figure 4.4.

The flow of plasma from the nozzle exit was defined by means of temperature,

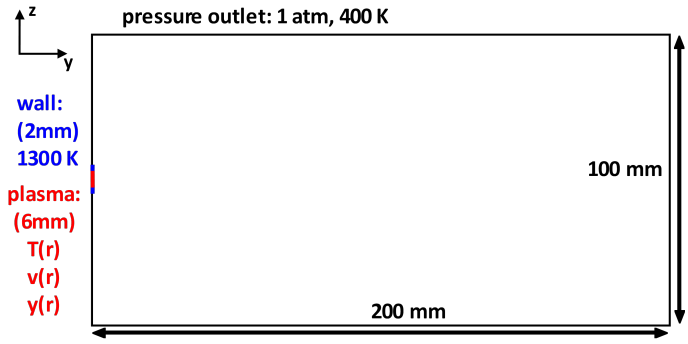

Figure 4.4: Cross section of the cylindrical domain in-plane through the central axis

velocity and concentration profiles (red line in Figure 4.4). These profiles were derived from previous measurements on the torch, which were published by Hrabovský et al. [90]. The selected results were those from torch operation at arc current (I) of 400 A and with an argon flow rate of 22 slm (i.e. 3.67×10^{-4}Nm^3/s). The plasma temperature and composition profile were determined by emission spectroscopy at position 2 mm downstream of the nozzle exit. The specifics of the diagnostic method and the procedure to derive the profiles from the emission spectra are explained in detail in the publication [90].

The species molar distribution over the nozzle radius was converted to a mass fraction profile of argon in the argon/steam mixture with the molecular weight of the gas mixture (M_{mix}) at each radial position as $Y_{Ar} = x_{Ar}M_{Ar}/M_{mix}$. This profile was approximated by a fourth order polynomial function (Figure 4.5(b)).

The temperature (Figure 4.5(a)) was expressed with the frequently used function [19, 28, 116, 209]:

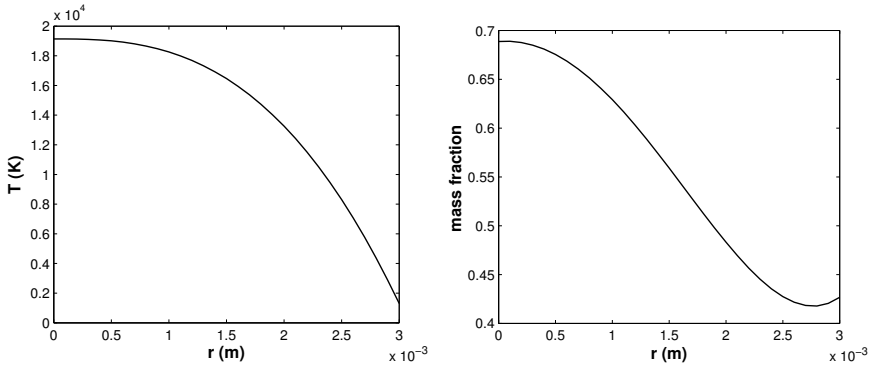

(a) Temperature (b) Argon mass fraction

Figure 4.5: Plasma inlet profiles

$$\text{Temperature:} \quad T_{in} = (T_0 - T_w)\left[1 - \left(\frac{r}{R_{in}}\right)^{n_T}\right] + T_w \tag{4.1}$$

$$\tag{4.2}$$

In this equation, the torch radius R_{in} is 0.003 m and T_w, the torch wall temperature, is set at 1300 K (i.e. the melting temperature of copper). The centreline temperature T_0 was 19 140 K and the parameter $n_T = 2.737$ to achieve the best fit with the experimental profile [90].

A remark about using these profiles is that they were measured at 0.002 m downstream of the exit nozzle (since it is not possible to perform these measurements closer to the exit nozzle), therefore, some assumptions need to be made in order to use these profiles at the nozzle surface:

- The temperature profile at 0.002 m downstream of the exit nozzle corresponds to the temperature profile at the nozzle surface. To argument this assumption it is important to know that the energy balance equation at the arc centre is dominated by a balance between radiation losses and ohmic heating [112]. The magnitude of both energy terms was evaluated:

– Radiation losses were calculated using the Net Emission Coefficient (NEC) approach, initially proposed by Lowke [117]. In this method, the net emission means the emission minus absorption, which is mathematically represented by the divergence of the radiative flux. The integration of this net emission over the whole spectrum (VUV, UV, visible and IR parts) is previously calculated for an isothermal spherical plasma with R_p is taken as the radius of the sphere. In practical applications, a cylindrical plasma is often assumed and the conducting radius R_p as the distance from the axis where the temperature is 70-80 % of the axis temperature [156]. For the fitted temperature profile, the estimated R_p was 0.0018 m. For this value of R_p, the net emission coefficients (with unit $W\,m^{-3}\,sr^{-1}$) as a function of temperature for an Ar/H_2O gas mixture with 30 % argon molar content at 1 atm were calculated by Vladimir Aubrecht [8]. A surface-weighted average of the net emission coefficient over the cross section of the torch nozzle was calculated:

$$\bar{\epsilon_N} = \frac{1}{\pi R^2} \int_0^R 2\pi r \epsilon_N \left(T\left(r\right)\right) dr \tag{4.3}$$

The total energy loss by radiation over the length l of 0.002 m from the exit nozzle was calculated as:

$$P_R = 4\pi \bar{\epsilon_N} A l \tag{4.4}$$

with A the surface of the plasma column cross section. The calculated value for this energy term was 4.334 kW.

– The Joule heating (P_{JH}) between the exit of the nozzle and the position 0.002 m downstream can be calculated as:

$$P_{JH} = IU = \frac{U^2}{R} = U^2 G = \frac{U^2 \sigma A}{l} \tag{4.5}$$

with I the arc current, U the potential difference over the length l, R the resistance, G the conductance and σ the electric conductivity.
For the selected operating conditions of the torch, the voltage between the nozzle and the arc attachment point at the anode (which is on average 0.0132 m downstream from the nozzle [31]) is 75 V [90]. About 20 V is produced in the region from the anode surface to the centre of the arc, so the voltage over the length l of 0.002 m from the torch exit is estimated to be: $U = \frac{0.002}{0.0132}\,(75 - 20)$.
For each radial position r along the radius of the plasma column cross section, the electrical conductivity was interpolated from pre-calculated tables as a function of temperature T and argon mass fraction Y_{Ar}.

The surface-weighted average of the electrical conductivity over the cross section is then determined as:

$$\bar{\sigma} = \frac{1}{\pi R^2} \int_0^R 2\pi r \sigma \left(T\left(r\right), Y_{Ar}\left(r\right)\right) dr \tag{4.6}$$

Finally, the calculated value for the Joule heating (Equation 4.5) was 4.349 kW.

The radiation loss of 4.334 kW is almost exactly compensated by the Joule heating of 4.349 kW in the plasma volume till 0.002 m, which justifies the assumption that the temperature profile measured at 0.002 m can be imposed as the boundary condition at the torch exit.

- The mass fraction profile of argon at the nozzle surface is the same as the profile at 0.002 m downstream of the torch exit. It is assumed that in this high-temperature, high-velocity region, the de-mixing of argon and water species by diffusion in the radial direction is negligible.

The velocity profile at the plasma inlet is assumed to follow a similar expression as the temperature profile:

$$\text{Velocity:} \quad v_{in} = v_0 \left[1 - \left(\frac{r}{R_{in}}\right)^{n_v}\right] \tag{4.7}$$

The centreline velocity v_0 in this equation was chosen as $4300\,\mathrm{m\,s^{-1}}$ from measurements of speed of propagation of disturbances in the plasma jet [89]. The parameter n_v can be determined from the energy balance over the torch nozzle. The potentials of the cathode nozzle and the exit nozzle were measured by high-resistance voltage dividers and the energy losses were determined from calorimetric measurements on cooling loops of the cathode and of the water stabilizing system. The total energy exiting the torch can then be calculated from volt-ampere characteristics and power losses in the torch chamber. The energy loss to the cooling water is taken into account by an efficiency factor η (61 %). This net energy should correspond to the enthalpy flux of the plasma at the exit nozzle:

$$\begin{aligned} \eta IU = & \int_0^R 2\pi \rho \left(Y_{Ar}\left(r\right), T\left(r\right)\right) H\left(Y_{Ar}\left(r\right), T\left(r\right)\right) v\left(r\right) dr \\ & - H^{\circ}{}_{Ar}\left(T_0\right) \int_0^R 2\pi Y_{Ar}\left(r\right) \rho \left(Y_{Ar}\left(r\right), T\left(r\right)\right) v\left(r\right) dr \\ & - \int_0^R 2\pi \left(1 - Y_{Ar}\left(r\right)\right) \rho \left(Y_{Ar}\left(r\right), T\left(r\right)\right) v\left(r\right) dr [H^{\circ}{}_{H_2O_{(g)}}\left(T_b\right) \\ & - C_{p,H_2O(l)}\left(T_b - T_0\right) - \lambda_w] \end{aligned} \tag{4.8}$$

$\rho(Y_{Ar}, T)$ and $H(Y_{Ar}, T)$ are respectively the density and enthalpy for the plasma mixture (Ar/H_2O) as a function of mass fraction of argon and temperature.

The latter two variables are function of radial position (r) (see Figures 4.5(a) and 4.5(b)).
The enthalpy values of the plasma mixture were calculated as:

$$H\left(T\right) = \frac{1}{M_{mix}} \sum_{i}^{n} x_i \left(H°_i\left(T\right) - H°_i\left(0\right)\right) \tag{4.9}$$

with i one of the n species in the gas composition from water vapour and argon at temperature T. x_i is the molar fraction of species i, H_i° the standard enthalpy in kJ/mol and M_{mix} is the molecular weight of the gas mixture in kg/mol.
Because only the sensible heat supplied to the carrier gas should be used in this equation, the following energy terms should be taken into account:

- Since argon and water vapour, which make up the plasma gas were fed to the torch at temperature T_0 (300 K), their enthalpies should be subtracted from the energy balance. The second term on the right-hand side of the balance (Equation 4.8) is this energy term from argon.
- Water vapour is originally supplied as liquid water, therefore the enthalpy of water vapour at boiling temperature T_b (373.15 K) should be subtracted from the balance (first term in square brackets).
- The second and third term in the square brackets in Equation 4.8 are the sensible heat of the liquid water from inlet temperature till boiling temperature and the latent heat of evaporation respectively to correct for the excess energy subtracted by the first in brackets.

After taking all these elements into consideration, the energy balance equation 4.8 can be solved for *v(r)*, which gives a value of 1.688 for the parameter n_v. The resulting velocity profile is shown in Figure 4.6.

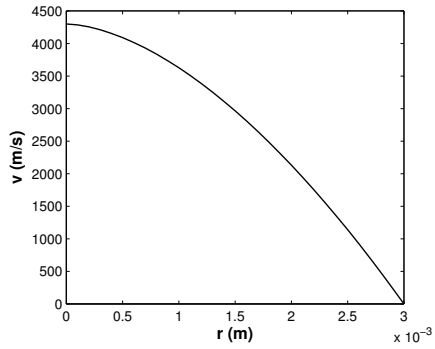

Figure 4.6: Velocity profile

4.3 Description of the Mixing Models

Three different methods for calculating thermodynamic and transport properties of the gas mixture were compared to investigate the influence on the flow field of using mixing rules. The formulas for the mixture density (in $\mathrm{kg\,m^{-3}}$) and speed of sound (in $\mathrm{m\,s^{-1}}$) were expressed in terms of molar fraction, for enthalpy (in $\mathrm{kJ\,kg^{-1}}$) in terms of mass fraction and for dynamic viscosity (in $\mathrm{kg\,m^{-1}\,s^{-1}}$) and thermal conductivity (in $\mathrm{W\,m^{-1}\,K^{-1}}$) the respective mixing rules of Wilke [207] and of Mason and Saxena [120] were used. As mentioned previously, these mixing rules are often selected by researchers/authors because of their simplicity. The fact that these mixing rules are the least accurate ones, is advantageous to the study, since their effects on the flow field (if any) will be more pronounced.
The specific heat (in $\mathrm{J\,kg^{-1}\,K^{-1}}$) was calculated as the numerical derivative of enthalpy over an interval of 0.2 K. The thermodynamic properties and transport coefficients of the different gases and gas mixtures were calculated using the methods presented by Murphy in previous publications [134, 137–139].

Pure gas data were tabulated as a function of temperature from 400 K to 20 000 K with intervals of 100 K. Properties of the plasma gas (Ar/H_2O) and the complete gas mixture ($Ar/H_2O/N_2$) are also function of species mass fraction(s) and were stored in a multidimensional matrix with mass fraction step size(s) of 0.02. Except for enthalpy, for which 0.01 was used as the mass fraction step size. All properties were calculated at a pressure of 1 atm. The details of the three different models are now explained and are summarized in Table 4.1 (where x and y denote respectively mole fraction and mass fraction).

Table 4.1: Details of the three mixing models

Property	MODEL 1 n=3; i=1: Ar, i=2: H_2O, i=3: N_2	MODEL 2 n=2; i=1: plasma (Ar/H_2O), i=2: N_2	MODEL 3
Density (ρ)	$\rho_{mix} = \sum_i^n x_i \rho_i$ with ρ_i = f(T)	$\rho_{mix} = \sum_i^n x_i \rho_i$ ρ_{pla} = f(y_{Ar} ,T) and ρ_{N2} = f(T)	ρ = f(y_{Ar} , y_{N2} , T)
Enthalpy (H)	$H_{mix} = \sum_i^n y_i H_i$ with H_i = f(T)	$H_{mix} = \sum_i^n y_i H_i$ H_{pla} = f(y_{Ar} ,T) and H_{N2} = f(T)	H = f(y_{Ar} , y_{N2} , T)
Heat capacity (cp)	$C_{p,mix} = \sum_i^n y_i C_{p,i}$ with $C_{p,i} = \frac{dH_i}{dT}$	$C_{p,mix} = \sum_i^n y_i C_{p,i}$ with $C_{p,i} = \frac{dH_i}{dT}$	$C_p = \frac{dH}{dT}$
Speed of sound (c)	$c_{mix}{}^2 = RT \frac{\sum_i^n x_i C_{p,i}}{\sum_i^n x_i M_i \sum_i^n x_i (C_{p,i} - R)}$ with $C_{p,i}$, M_i = f(T)	$c_{mix}{}^2 = RT \frac{\sum_i^n x_i C_{p,i}}{\sum_i^n x_i M_i \sum_i^n x_i (C_{p,i} - R)}$ with M_{pla} , $C_{p,pla}$ = f(y_{Ar} ,T) M_{N2} , $C_{p,N2}$ = f(T)	c = f(y_{Ar} , y_{N2} , T)
Viscosity (μ)	$\mu_{mix} = \sum_{i=1}^n \frac{x_i \mu_i}{\sum_j x_j \phi_{ij}}$ with μ_i , M_i = f(T) with $\phi_{ij} = \frac{1}{\sqrt{8}} \left(1 + \frac{M_i}{M_j}\right)^{-\frac{1}{2}} \left[1 + \left(\frac{\mu_i}{\mu_j}\right)^{\frac{1}{2}} \left(\frac{M_j}{M_i}\right)^{\frac{1}{4}}\right]^2$	$\mu_{mix} = \sum_{i=1}^n \frac{x_i \mu_i}{\sum_j x_j \phi_{ij}}$ with μ_{pla} , M_{pla} = f(y_{Ar} ,T) μ_{N2} , M_{N2} = f(T) with $\phi_{ij} = \frac{1}{\sqrt{8}} \left(1 + \frac{M_i}{M_j}\right)^{-\frac{1}{2}} \left[1 + \left(\frac{\mu_i}{\mu_j}\right)^{\frac{1}{2}} \left(\frac{M_j}{M_i}\right)^{\frac{1}{4}}\right]^2$	μ = f(y_{Ar}, y_{N2}, T)
Thermal conductivity (k)	$k_{mix} = \sum_{i=1}^n k_i \left[1 + \sum_{\substack{k=1 \\ k \neq i}}^n G_{ik} \frac{x_k}{x_i}\right]^{-1}$ with k_i, μ_i , M_i = f(T) with $G_{ik} = \frac{1.065}{2\sqrt{2}} \left(1 + \frac{M_i}{M_k}\right)^{-\frac{1}{2}} \left[1 + \left(\frac{\mu_i}{\mu_k} \frac{M_k}{M_i}\right)^{\frac{1}{2}} \left(\frac{M_i}{M_k}\right)^{\frac{1}{4}}\right]^2$	$k_{mix} = \sum_{i=1}^n k_i \left[1 + \sum_{\substack{k=1 \\ k \neq i}}^n G_{ik} \frac{x_k}{x_i}\right]^{-1}$ with k_{pla}, μ_{pla} , M_{pla} = f(y_{Ar} ,T) k_{N2}, μ_{N2} , M_{N2} = f(T) with $G_{ik} = \frac{1.065}{2\sqrt{2}} \left(1 + \frac{M_i}{M_k}\right)^{-\frac{1}{2}} \left[1 + \left(\frac{\mu_i}{\mu_k} \frac{M_k}{M_i}\right)^{\frac{1}{2}} \left(\frac{M_i}{M_k}\right)^{\frac{1}{4}}\right]^2$	k = f(y_{Ar}, y_{N2}, T)

4.3.1 Model 1

The thermophysical properties of respectively Ar, H_2O and N_2 were calculated by considering only the interactions of species within each individual gas (which includes hydrogen-oxygen interactions for water vapour) [134, 137–139]. At every iteration of the model, the properties in each point were approximated as a function of temperature by linear interpolation. The mixture properties were then calculated by using mixing rules. Consequently, only the dissociation and ionization products (ions, atoms and molecules) of each individual gas are considered: e^-, Ar, Ar^+, Ar^{++}, Ar^{+++}, Ar^{++++}, $H_2O_{(g)}$, H_2, O_2, O, O^+, O^{++}, O^{+++}, O^-, O_2^+, O_2^-, O_3, O_3^+, O_3^-, H, H^+, H^-, H_2^+, H_2^-, H_3^+, OH, OH^+, OH^-, HO_2, HO_2^+, HO_2^-, H_2O^+, H_2O_2, $H_2O_2^+$, H_3O^+, N_2, N^+, N^{++}, N^{+++}, N_2^+, N_2^-, N_3, N_3^+, N_3^-.

4.3.2 Model 2

The mixing rules were only applied between two gases, nitrogen and 'plasma gas'. The properties of the plasma gas mixture of argon and steam were calculated rigorously (considering the argon-water vapour, argon-hydrogen, argon-oxygen and hydrogen-oxygen interactions) [134, 139]. At every iteration of the model, bilinear interpolation as a function of argon mass fraction and temperature from this pre-calculated table was performed. The same species as in model 1 were included in the property calculation, but the resulting properties of the Ar/H_2O mixture differ from the properties calculated using mixing rules because of additional interactions and consequently a change in Gibbs free energy of this binary system.

4.3.3 Model 3

In this full multicomponent model, no mixing rules were used to calculate the thermodynamic and transport properties of the ternary mixture of argon, steam and nitrogen. Thermodynamic and transport properties were interpolated from a pre-calculated matrix as a function of argon mass fraction, nitrogen mass fraction and temperature. In the calculation of these properties all possible interactions (i.e. argon-water vapour, argon-hydrogen, argon-oxygen and hydrogen-oxygen, nitrogen-water vapour, nitrogen-oxygen and nitrogen-hydrogen) were taken into account [132, 134, 137]. This means that the combined products of H_2O and N_2 (NO, NO^+, NO^-, NO_2, NO_2^+, NO_2^-, N_2O, N_2O^+, N_2O^-, N_2O_3, N_2O_4, NO_3, NO_3^-, NH^+, NH, NH^-, NH_2, NH_3, NH_4^+, N_2H_2, N_2H_4, HN_3, HNO, HNO_2, HNO_3, NH_2OH, NH_2NO_2) were also included in the properties calculation together with the list of species listed for model 1. Although the concentration of these additional components is low, it can change the resulting thermophysical

properties of the gas mixture.

The definitions of the different gas mixtures in all three models are illustrated in Figure 4.7. The blue sets of species correspond to the three gases in model 1, which properties were individually calculated and among which mixing rules were applied. The red circles show the approach for model 2 where the properties of the gas mixture Ar-H_2O were rigorously calculated and then combined with the properties of nitrogen through mixing rules to estimate the ternary gas mixture properties. For model 3 (the green circle), no subdivision was made and the properties of the gas mixture comprised of all species from the three gases was rigorously calculated in the full multicomponent approach.

In model 2, the combination of two non-reacting gases (argon and water vapour)

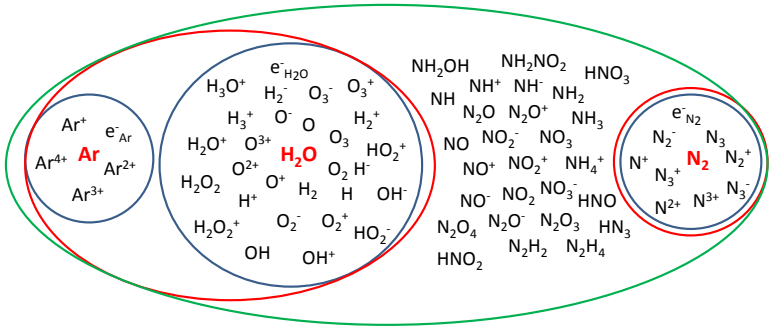

Figure 4.7: Illustration of the different mixing model approaches. blue for Model 1, red for Model 2 and green for Model 3

does not lead to additional combined species from the constituent elements of the two gases. Nevertheless the presence of the chemical species from both gases alters the outcome of the minimization of the Gibbs free energy of the system and leads to a different equilibrium conditions than when the equilibrium compositions of the individual gases are combined. This change in equilibrium composition can be seen in Figure 4.8(a), which shows the difference between the molar fractions of each species considering the complete system of a 50 wt% Ar-50 wt% H_2O gas mixture, and the molar fractions of each species when combining the separately determined equilibrium compositions of the individual gases as a function

of temperature:

$$\Delta x_i = x_i^{(2)} - \frac{\left(\dfrac{x_i}{\sum_j^{Ar} x_j^{Ar} M_j} + \dfrac{x_i}{\sum_j^{H_2O} x_j^{H_2O} M_j} \right)}{\dfrac{1}{\sum_j^{Ar} x_j M_j} + \dfrac{1}{\sum_j^{H_2O} x_j M_j}} \tag{4.10}$$

with i representing a species in the binary gas mixture of Ar and H_2O and j a species in the equilibrium composition of the individual gas (either argon or water vapour). The molar fraction of species i from the equilibrium composition calculation of the system comprising both gases is denoted by $x_i^{(2)}$.

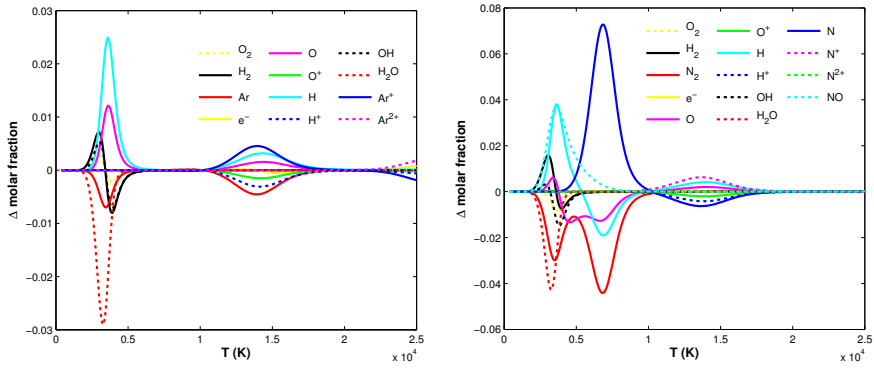

(a) 50 wt% Ar–50 wt% H_2O

(b) 50 wt% H_2O–50 wt% N_2

Figure 4.8: The difference in molar composition as a function of temperature for a certain gas mixture

The difference in composition is limited to 0.03 in terms of molar fraction of a certain gas species. The differences in molar fractions are distinctively noticeable in the dissociation region of H_2O and to a lesser extent in the ionization region (around 15 000 K).

In model 3, by definition, the full multicomponent approach takes into account all product species from the three gases. This includes the combination species between nitrogen and water vapour (i.e. the species outside of the red circles in

Figure 4.7). It is obvious that the equilibrium composition which includes chemical reactions between the gases differs from the one combined from the separate equilibrium compositions of the individual gases. In Figure 4.8(b), the difference between the molar fractions of each species considering the complete system of a 50 wt% H_2O-50 wt% N_2 gas mixture, and the molar fractions of each species by combining the separately calculated equilibrium compositions of the individual gases as a function of temperature. The formula for this expression is similar to Equation 4.10, but argon is interchanged by nitrogen gas. To avoid Figures 4.8(a) and 4.8(b) from becoming too cluttered, only the species at molar fractions higher than 0.01 were considered.
The only significant product species from combination of elements from N_2 and H_2O is nitrogen monoxide (NO). The biggest differences (up to almost 0.08) in terms of molar fraction were found in the temperature range of nitrogen dissociation.

4.4 Model Assumptions and Equations

Ansys FLUENT 14.0 was used as the CFD software, complemented with user-defined functions (UDF) for plasma inlet boundary conditions, thermodynamic and transport properties (including diffusion) and for post-processing purposes. Large Eddy Simulation (LES) was chosen as the turbulence model with Dynamic Smagorinsky-Lilly for the subgrid-scale model in combination with the pressure-based solver.
The time-step size was 1.5×10^{-7} s, bounded central differencing was selected as the spatial discretization scheme and second order implicit scheme was selected for temporal discretization. The simulations presented in this study were based on the following main assumptions:

- Effects of gravity and the effect of viscous dissipation on the temperature were neglected.
- The system is assumed to be in LTE [18]. This assumption is generally accepted in the modelling of atmospheric plasma jets [118]. Effects from ionization, dissociation and chemical reactions of gas species are included in the calculation of the gas properties (see Paragraph 4.3).
- No electromagnetic effects were taken into account.
- Compressibility effects were neglected. This means the density did not change with pressure, but was only a function of gas composition and temperature.

For this 3D time-dependent flow, the governing equations can be represented by mass continuity equation, the conservation equation of momentum, species conservation equation and energy conservation equation:

Mass continuity equation:

$$\frac{\partial \rho}{\partial t} + \bigtriangledown \cdot (\rho \boldsymbol{v}) = 0 \tag{4.11}$$

where ρ is the local density of the gas mixture and $\boldsymbol{v}$ the gas velocity vector.

Momentum conservation equation:

$$\frac{\partial (\rho \boldsymbol{v})}{\partial t} + \nabla \cdot (\rho \boldsymbol{v}\boldsymbol{v}) = -\nabla p + \nabla \cdot \boldsymbol{\tau} \tag{4.12}$$

where p is the pressure and $\boldsymbol{\tau}$ is the stress tensor, calculated from components with respectively molecular and turbulent viscosity.

Species:

$$\frac{\partial (\rho Y_i)}{\partial t} + \nabla \cdot (\rho \boldsymbol{v} Y_i) = -\nabla \cdot \boldsymbol{J_i} \tag{4.13}$$

The diffusion flux of species i, $\boldsymbol{J_i}$, includes a laminar and a turbulent contribution to diffusion. The laminar diffusion was described by the combined diffusion approach of Murphy [131]. This method describes the diffusion of high-temperature gases relative to one another. Combined diffusion coefficients allow the diffusion of one gas (e.g., argon) with respect to another (e.g., nitrogen) to be defined. A gas is defined as comprising all species derived from that gas; e.g. nitrogen gas comprises N_2, N, N^+, N_2^+, etc., and electrons derived from the nitrogen species. The use of combined diffusion coefficients has the advantage that only one 'gas' conservation equation needs be solved, rather than N - 1 species conservation equations for a plasma containing N species [137]. They are linear combinations of the multicomponent diffusion coefficients. More details on the theory of the combined diffusion coefficient method can be found in publications by Murphy [131]. With some additional assumptions on this approach, the expression for the diffusion flux in a three-component mixture could be written in terms of binary combined diffusion coefficients (see Appendix A).

The diffusion flux of species i could then be defined as:

$$J_i = \sum_{j}^{n-1} \left(\frac{\rho}{\overline{M}^2} \overline{m_i m_j} \overline{D_{ij}^x}(\overline{x_j}, T) \nabla \overline{x_j} - \overline{D_{ij}^T}(\overline{x_j}, T) \nabla \ln T \right) + \frac{\mu_t}{Sc_t} \nabla Y_i \tag{4.14}$$

The first term on the right-hand side describes the laminar diffusion by using the combined diffusion approach and was calculated with a user-defined function in FLUENT as a source term in the species conservation equation. $\overline{M}$ is the average mass of all species in the gas mixture, $\overline{m_i}$ and $\overline{m_j}$ are respectively the average masses of the heavy species of the gas i and j, $\overline{x_j}$ is the sum of the mole fractions of the species of gas j and $n = 3$ is the number of gases in the mixture. The combined ordinary diffusion coefficient $\overline{D_{ij}^x}$ and combined temperature diffusion coefficient $\overline{D_{ij}^T}$ (as functions of the mole fraction of gas j and temperature) describe, respectively, diffusion due to mole fraction gradients and temperature gradients.
The second term on the right-hand side was calculated by the standard FLUENT code and describes turbulent diffusion with Sc_t the turbulent Schmidt number and μ_t the turbulent viscosity.
The original expression for the diffusion flux (Equation 4.14) with combined diffusion coefficients introduced by Murphy also contains two additional terms. One term describing the diffusion due to pressure gradients (∇p) and a second term describing ambipolar diffusion due to an electric field (∇e). Both terms were neglected in the calculation because of the negligible pressure differences and because the electromagnetic effects were omitted.

Energy conservation equation:

$$\frac{\partial (\rho E)}{\partial t} + \nabla \cdot (\boldsymbol{v} (\rho E + p)) = \nabla \cdot \left(k_{eff} \nabla T - \sum_j h_i \boldsymbol{J_i} \right) - R \qquad (4.15)$$

where k_{eff} is the effective conductivity ($k + k_t$, with k and k_t the laminar and turbulent thermal conductivity respectively) and E the specific total energy ($\mathrm{J\,kg^{-1}}$) as $E = h - \frac{p}{\rho} + \frac{v^2}{2}$ in which h is the enthalpy. The turbulent thermal conductivity is obtained with the constant turbulent Prandtl number hypothesis. The energy term for species diffusion was calculated through a user-defined function and added to the energy equation as a source term. The expression for the diffusion flux of species i, $\boldsymbol{J_i}$ is the same as for the species conservation equation (Equation 4.13).
h_i is the enthalpy of gas i, defined as the sum of the enthalpies of the species making up the respective gas. For model 2 and 3, h_i was defined from the directly calculated enthalpy h of the binary and ternary mixture, respectively, so that: $h(Y_i, ..., Y_{n-1}, T) = \sum_i^n h_i(Y_i, ..., Y_{n-1}, T) Y_i$ with $\sum_i^n Y_i = 1$ and with n = 2 (Ar and H_2O) for model 2 and n = 3 (Ar, H_2O and N_2) for model 3. The contribution of the enthalpies of the combined ions and molecules from the interactions between

H_2O and N_2 in model 3 were included in the enthalpy of N_2. Their contribution to the enthalpy value, however, is very small because of the low concentration of these species.
The last term on the right-hand side of Equation 4.15 is the net radiation power R and represents the energy loss from the hot arc core by radiation. R was modelled with the net emission coefficient (NEC) approach by $R = 4\pi\epsilon_N$ where ϵ_N is the net emission coefficient ($\mathrm{W\,m^{-3}\,sr^{-1}}$). Approximate values for the net emission coefficients for an argon/water plasma mixture with 30 % argon molar content at a pressure of 1 atm and for a plasma radius of 0.0018 m were used, taken from Aubrecht et al. [8].

4.5 Results

The flow variables selected for comparing the three mixing models are temperature, velocity and nitrogen mole fraction. These variables were statistically averaged in time by taking the arithmetic mean over 130 000 time steps or 19.5 ms. Figure 4.9 shows the comparison between an instantaneous temperature profile and the time-averaged temperature profile along a cross section in the x-direction for Model 1. The unstable flow of the plasma jet illustrates the need for a sufficiently long period of averaging in order to obtain a reliable statistical average.

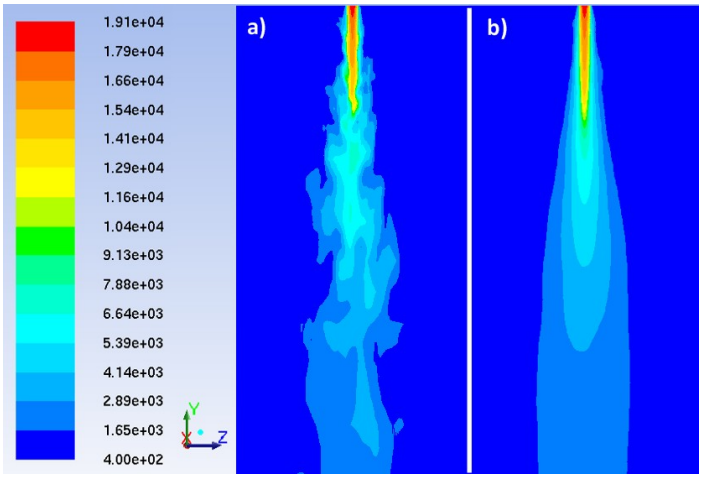

Figure 4.9: Temperature contours on a cross section at x=0 mm for Model 1 of a) the instantaneous flow field and b) the averaged flow field

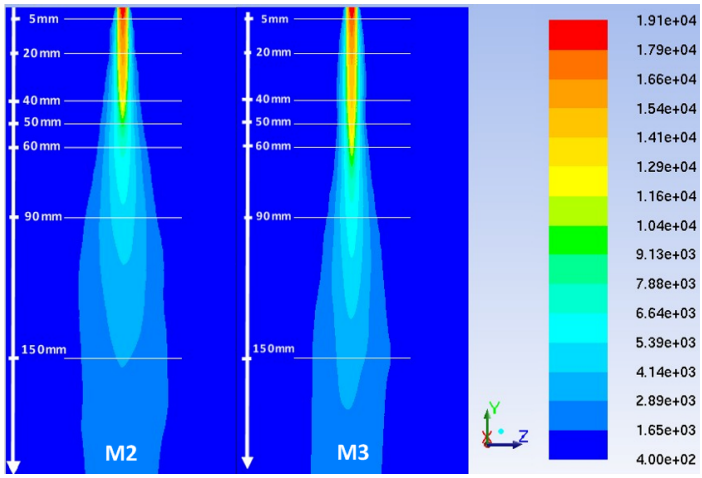

Figure 4.10: Averaged temperature contour profiles of model 2 versus model 3 with mark-ups of the different downstream positions of sampling for the radial profiles

For comparison of the three mixing models, instead of comparing full contours along x- or z-direction cross sections, the data is sampled at particular cross sections in the y-directions downstream of the torch exit nozzle (5, 20, 40, 50, 60, 90 and 150 mm). This is well illustrated by Figure 4.10.
In the plane at the marked positions, the variables are averaged in space along circles. The obtained average radial profiles for the different simulations were compared over a length of 1 cm radial from the jet centreline. The negative radius values were used to plot results of a chosen model against the output of a second model, plotted on the positive radius values.

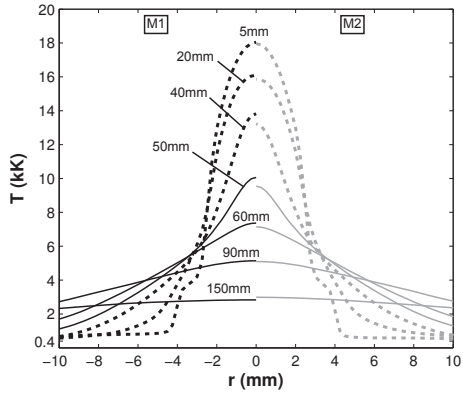

Figure 4.11: Temperature profiles of model 1 (black) versus model 2 (grey)

In Figure 4.11, the radial temperature profiles of model 1 versus model 2 are plotted. The temperature values at every position are almost identical with only small differences at the positions 40 mm, 50 mm and 60 mm where the temperatures from model 2 are smaller than those from model 1. Overall, there are no big differences in the temperature field between model 1 and model 2. A different trend can be seen in Figure 4.12, where for model 2 and model 3 only the temperatures in the high-temperature region of the plasma jet (dotted lines for 5 mm and 20 mm) are in good agreement. From 40 mm downwards, the radial temperature profiles of model 3 clearly show much higher temperatures than the profiles from model 2. The differences in centreline temperatures between model 2 and model 3 can be up to 55 % of the values calculated in model 2.

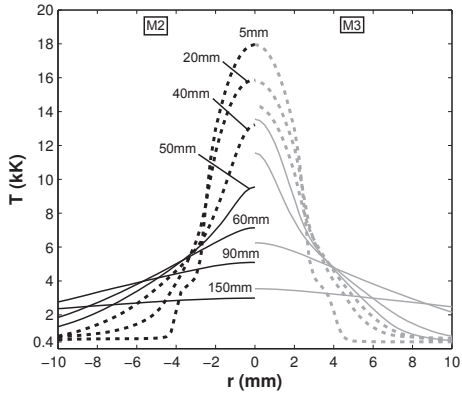

Figure 4.12: Temperature profiles of model 2 (black) versus model 3 (grey)

The comparison of axial velocity profiles from simulations with model 1 and model 2 is plotted in Figure 4.13. Similar to the comparison of the temperature field of

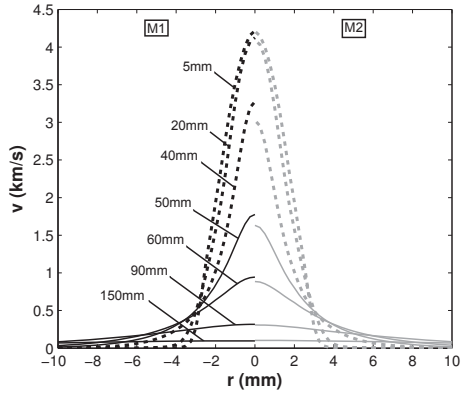

Figure 4.13: Velocity profiles of model 1 (black) versus model 2 (grey)

these two models (Figure 4.11), there are some small differences in the velocity fields noticeable between 40 mm and 60 mm downstream of the torch exit. The velocities at these positions are slightly lower for model 2 compared to model 1. In Figure 4.14, it can be seen that the velocity profiles from the simulation with model 3 show significantly higher values than the velocity profiles from the simulation with model 2 starting at 40 mm downstream of the exit nozzle. These

differences increase further downstream and calculated velocities of the jet with model 3 can become more than twice as high as the ones with model 2 at the same positions (50, 60 and 90 mm).

Finally, nitrogen mole fraction is the last variable evaluated to make the compar-

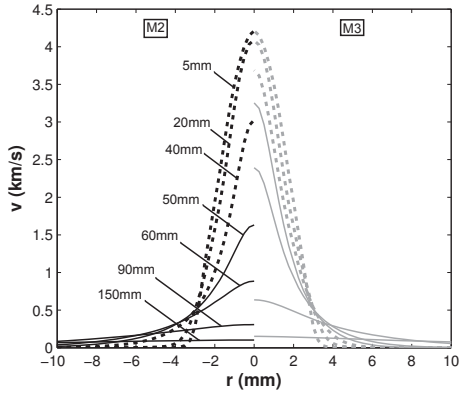

Figure 4.14: Velocity profiles of model 2 (black) versus model 3 (grey)

ison between the three mixing models. This parameter characterizes the level of entrainment of surrounding gas into the plasma jet. The profiles of nitrogen mole fraction of model 1 and model 2 are plotted in Figure 4.15. The concentration profiles of nitrogen gas in the gas mixture are almost identical for both models.

The comparison between model 2 and model 3 on the basis of nitrogen mole fraction in Figure 4.16 shows different results than those in Figure 4.15.

In the high-temperature region (5 mm and 20 mm), the concentrations of nitrogen gas in the gas mixture are nearly identical for the two models, but at 40 mm and further downstream of the torch exit the profiles of nitrogen mole fraction from the simulation with model 2 are much higher than those from the simulation with model 3. As shown by the rapid increase in nitrogen concentration in the downstream direction in model 2, it is clear that the entrainment of the surrounding atmosphere occurred much faster (i.e. closer to the torch exit) with model 2 than with model 3.

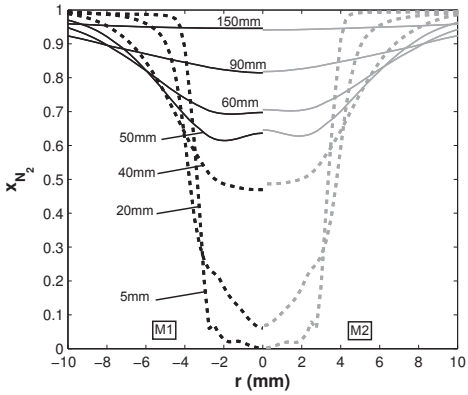

Figure 4.15: Nitrogen mole fraction profiles of model 1 (black) versus model 2 (grey)

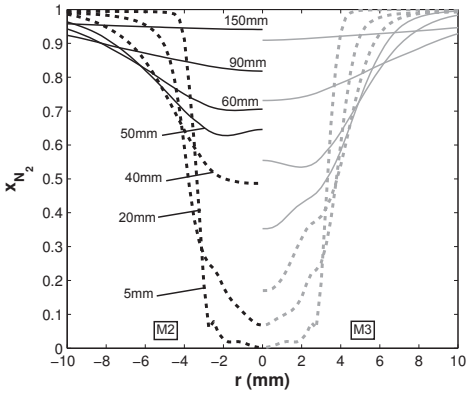

Figure 4.16: Nitrogen mole fraction profiles of model 2 (black) versus model 3 (grey)

4.6 Discussion

The comparison of model 1 with model 2 in Figures 4.11, 4.13 and 4.15 showed little difference in the temperature, velocity and nitrogen mole fraction profiles. This means that the correct calculation of the thermodynamic and transport properties of the plasma gas (Ar/H_2O) has only a limited influence on the flow characteristics. The full multicomponent approach (model 3), on the other hand, gave a significantly different flow field than model 2 (see Figures 4.12, 4.14

and 4.16). Up to 20 mm from the torch exit, the profiles of temperature, velocity and nitrogen concentration are quasi-identical with model 2 and model 3. The big differences start from 20 mm downwards, where a steep increase of nitrogen mole fraction at 40 mm for model 2 can be seen. This is caused by an intense entrainment of nitrogen into the jet, which indicates turbulent mixing of the jet with the surrounding atmosphere. This is accompanied by the sharp decrease of velocity and temperature (i.e. cooling with cold nitrogen) in the simulation with model 2 from 20 mm downwards. For model 3, the increase in nitrogen mole fraction in the jet occurs more gradually, suggesting a longer, more stable jet with a delayed onset of turbulence. The observation that the jet calculated with model 3 remains quasi-laminar for a longer time than the jet calculated with model 2 is confirmed by looking at the evolution of the root-mean-square (RMS) of the velocity fluctuations at different axial positions (Figure 4.17).

This parameter is an indicator of the velocity fluctuations and stability of

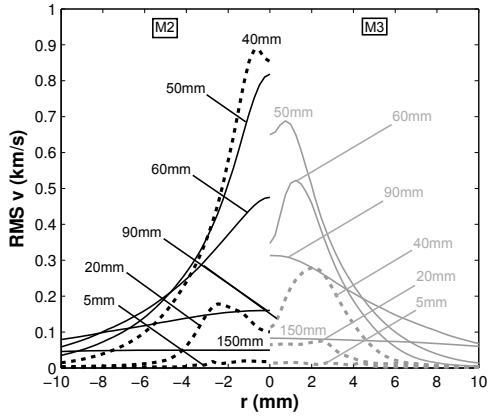

Figure 4.17: Root-mean-square velocity profiles of model 2 (black) versus model 3 (grey)

the jet, or level of turbulence. The values of this variable are much higher at positions closer to the torch exit for model 2 than for model 3. The difference is especially large at 40 mm downstream of the torch exit, which corresponds to the region where the sharp increase in nitrogen mole fraction in the jet and the decrease in velocity and temperature with model 2 can be observed. Including all interactions of the ternary gas mixture in the calculation of thermodynamic and transport properties clearly has a large impact on the flow variables. In the following section, the significant differences in results and the difference in

transition from laminar to turbulent flow between the different simulations will be explained by the differences in thermodynamic and/or transport properties of the mixing models .

The thermodynamic and transport properties of the gas mixture with composition 25 wt% argon, 25 wt% steam and 50 wt% nitrogen are plotted to examine which differences between the calculated values by the three models cause the differences in the resulting flow fields. Values of molecular weight and enthalpy of the selected mixture composition are displayed as a function of temperature in Figures 4.18 and 4.19 respectively. Density values are not reported because no significant differences were identified between the models. In these figures, the lines for model 1 and model 2 overlap (full lines), because no errors were introduced by using mixing rules for the calculation of thermodynamic properties of the plasma gas mixture. The properties calculated by model 3 are represented by the dotted lines.

The molecular weights and enthalpies calculated with model 3 are respectively

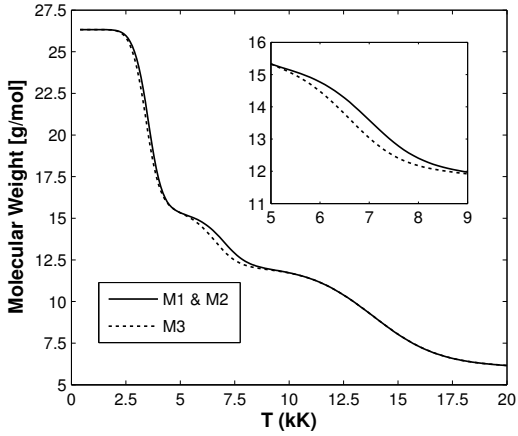

Figure 4.18: Difference in molecular weight between model 1 and 2 (solid line) and model 3 (dotted line) for a mixture of 25 wt% Ar, 25 wt% H_2O and 50 wt% N_2

lower and higher than the ones from model 1 and 2 between 5000 K and 9000 K. In model 3, the products from combination of elements of water vapour and nitrogen are taken into account in the mixture composition. In this temperature range, nitric oxide (NO) and other combination species in smaller concentrations

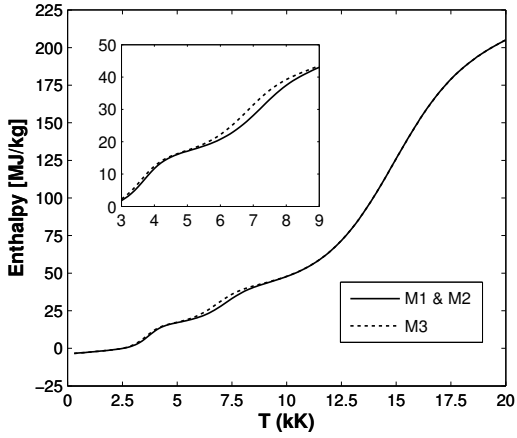

Figure 4.19: Difference in enthalpy between model 1 and 2 (solid line) and model 3 (dotted line) for a mixture of 25 wt% Ar, 25 wt% H_2O and 50 wt% N_2

are formed and cause the differences in molecular weight and enthalpy values. However, they do not explain the large changes in the flow field calculated with model 3 compared to that calculated with model 2. The reason for this can be found in the differences in transport properties between the three mixing models. The thermal conductivity and viscosity of the three models for the same mixture composition are compared as a function of temperature respectively in Figures 4.20 and 4.21.

The full multicomponent approach for the calculation of the transport properties (model 3) clearly generated different values than the other two models, which used the mixing rules of Wilke [207] and Mason and Saxena [120] for the respective properties. As noted above, these formulas were proposed for mixtures of non-ionized gases, considering only elastic collisions and employing several approximations. This does not give satisfactory results for thermal conductivity where the contribution of the inelastic collisions is important because they are responsible for the dissociation and ionization peaks apparent in Figure 4.20.
Consequently, the use of the mixing rule of Mason and Saxena leads to an underestimation of the actual values of thermal conductivity, especially at the ionization temperatures (between 10 000 and 20 000 K). It is clear that the differences in thermal conductivities between model 2 and model 3 are much

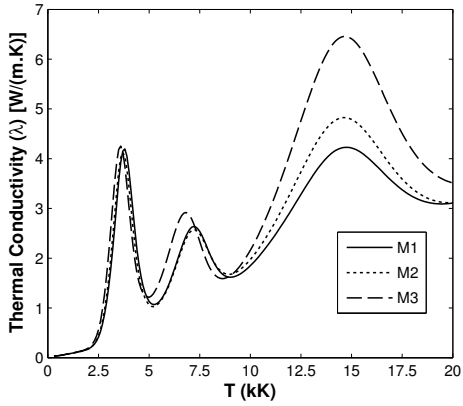

Figure 4.20: Difference in thermal conductivity between model 1 (solid line), model 2 (dotted line) and model 3 (dashed line) for a mixture of 25 wt% Ar, 25 wt% H_2O and 50 wt% N_2

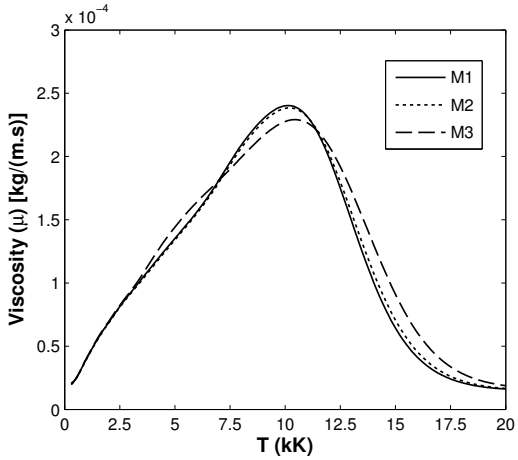

Figure 4.21: Difference in dynamic viscosity between model 1 (solid line), model 2 (dotted line) and model 3 (dashed line) for a mixture of 25 wt% Ar, 25 wt% H_2O and 50 wt% N_2

higher than those between model 1 and model 2. In the calculation of thermal conductivity in model 2, the only additional interactions taken into account by rigorous calculation, relative to the calculation in model 1, are those between species derived from argon and water vapour. Interactions between all species in the ternary mixture are considered in the full multicomponent approach of model

3, leading to much larger differences.

In the previous figures, the differences between the different models were plotted for a specific gas mixture as a function of temperature. To get a complete overview of the differences in thermodynamic and transport properties, they can be visualized over the whole range of argon mass fraction, nitrogen mass fraction and temperature. In the following plots (Figure 4.22), the values of the different properties calculated by model 2 are divided by the values of the respective properties calculated by model 3. The data field is displayed by cross sections at different temperatures. The values of the ratio of the properties calculated using model 2 to those calculated using model 3 are coloured according to the corresponding colour map:

- Values equal to 1: properties of model 2 equal properties of model 3.
- Values <1: properties of model 2 are estimated smaller than properties of model 3.
- Values >1: properties of model 2 are estimated larger than properties of model 3.

In Figures 4.22(a) and 4.22(b), significant differences between model 2 and model 3 are shown for the transport properties. The large differences in thermal conductivity in the temperature region from 6000 to 8000 K coincide with the shift in dissociation peak for nitrogen gas, visible in Figure 4.20. This shift in dissociation peak is also responsible for the large differences in heat capacity between the two models in the same temperature region. To illustrate this, the evolution of heat capacity calculated by the three mixing models is plotted as a function of temperature for 6 different gas compositions in Figure 4.23.

There exists a strong connection between the heat capacity C_p (derivative of the enthalpy) and the reactive thermal conductivity. This is particularly clear at temperatures around the dissociation of molecules (T <8000 K for the gaseous system in this case). The use of mixing rules can possibly lead to a loss of consistency between both properties and thus may produce artificial changes on the resulting flow field. Therefore, it was confirmed that the positions of the dissociation peaks within the temperature field for thermal conductivity and heat capacity are identical and that the physical meaning of their correlation was not impaired.

The comparative plots between the two properties for six different gas mixture compositions as a function of temperature was added in Appendix B.

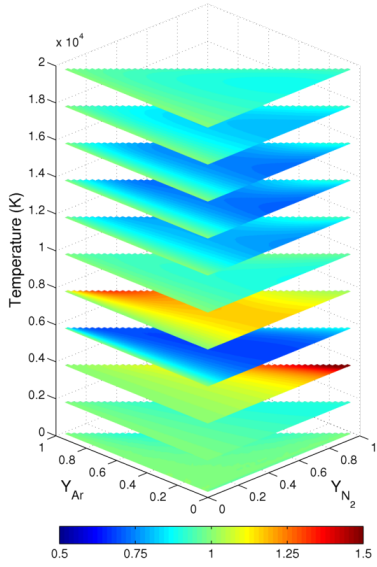

(a) Thermal conductivity

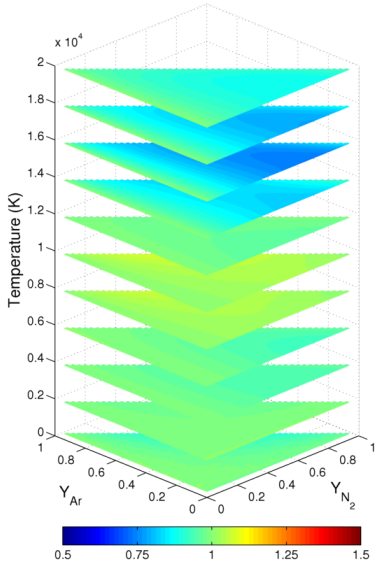

(b) Viscosity

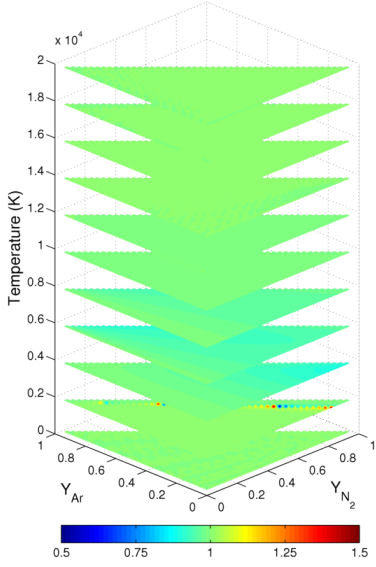

(c) Enthalpy

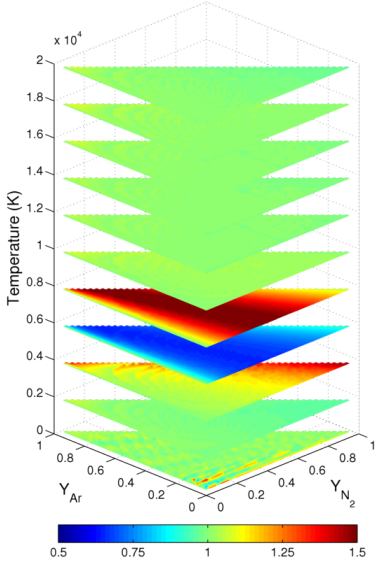

(d) Heat capacity

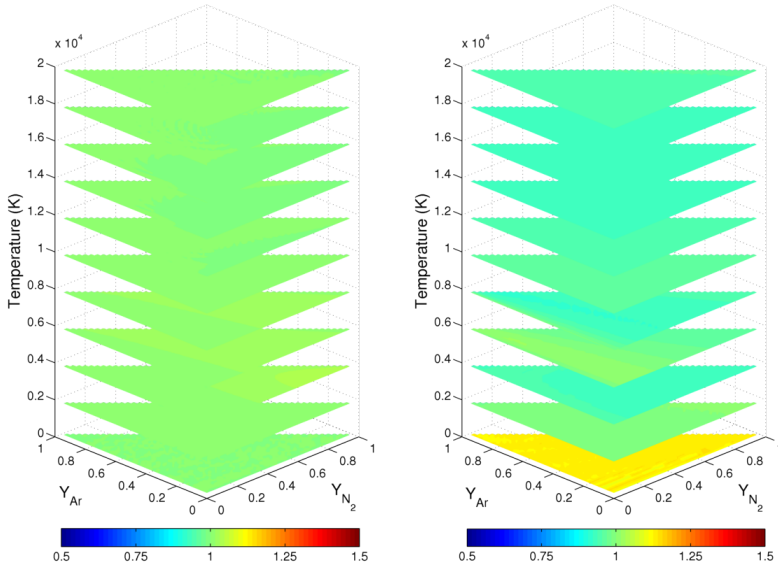

(e) Density (f) Speed of sound

Figure 4.22: Ratio of the values calculated with model 2 over the values calculated with model 3 for the specific thermodynamic or transport property

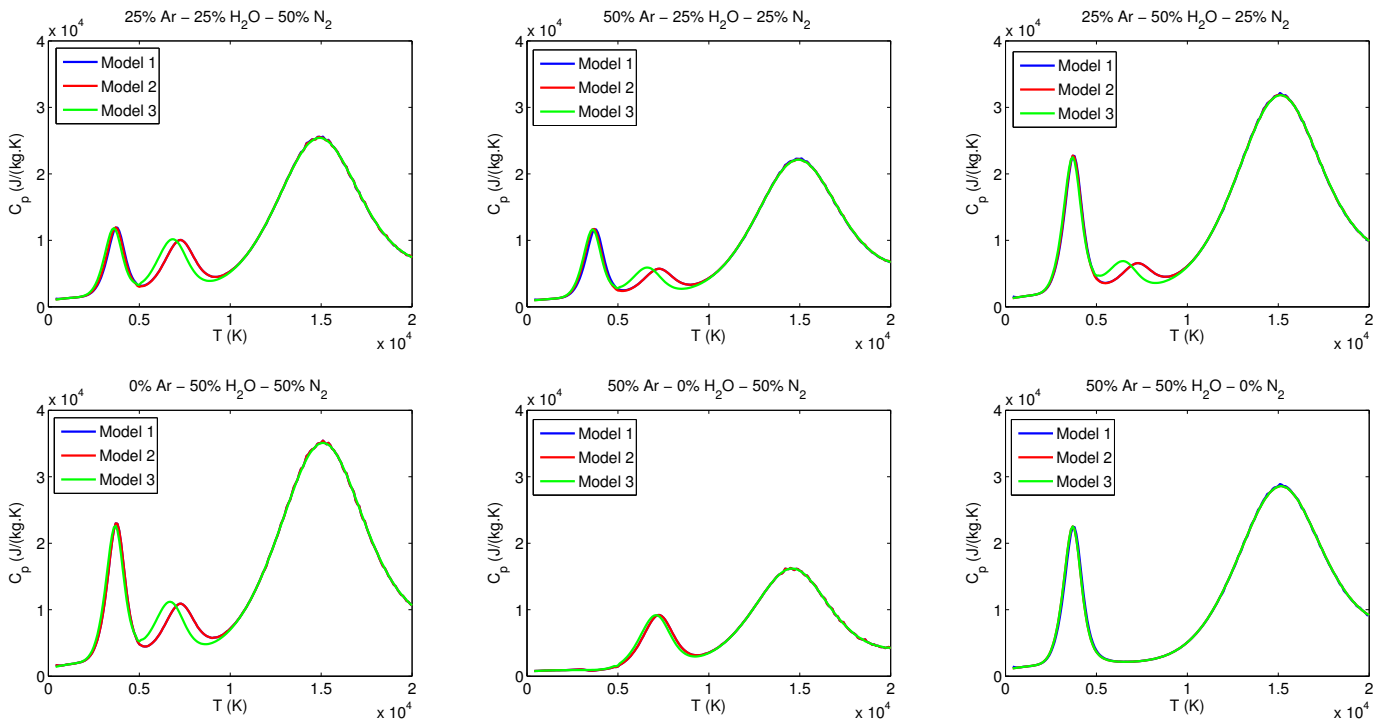

Figure 4.23: Heat capacity calculated by the three mixing models as a function of temperature for 6 different gas mixture compositions

The higher thermal conductivities of model 2 in the high-temperature region, compared to model 1, lead to lower temperature profiles in the center of the jet (Figure 4.11) because of a higher conductive heat transfer in radial direction. These lower temperatures in model 2 in turn lead to higher viscosities in the centre of the jet and therefore lower velocities (Figure 4.13).
In the explanation for the differences in flow fields between model 2 and model 3, the processes at the fringes of the jet are more important, since it is the delayed onset of turbulence in model 3 that leads to the large differences observed. The influence of each of the thermodynamic and transport properties on this delayed onset was assessed by exchanging one-by-one, each property used in model 2 for the rigorously-calculated property used in model 3. It was found that only by changing the thermal conductivity were large differences in the flow fields obtained; changing all the other properties led to only small differences. It is therefore concluded that the different thermal conductivity values used in model 3 are primarily responsible for the delayed onset of turbulence, and the consequent changes in jet properties.

In the region close to the torch exit, the temperature at the core of the jet ranges from 10 000 to 20 000 K (Figure 4.12). It is clear from the analysis of the thermal conductivity calculations that its value in this temperature range is strongly underestimated by the mixing law of Mason and Saxena with model 2. The higher average thermal conductivities obtained with model 3 (Figure 4.24(b)) cause higher conductive heat transfer in radial direction and higher temperatures at the edge of the jet compared to model 2. Higher temperatures in the temperature range at the jet boundary lead to higher viscosities in this temperature range ($<$10 000 K in Figure 4.21). The average viscosities in the region close to the exit nozzle (Figure 4.25(b)) indeed show higher values of viscosity for model 3 compared to model 2. The higher values for viscosity in the shear layer, stabilizes the shear layer. This limits the entrainment of nitrogen gas in the plasma jet, which is predominantly due to turbulent mixing, and results in a more stable jet (i.e. a longer transition to turbulence). This delays the cooling of the jet with cold nitrogen gas and slows down the decrease in velocity of the plasma jet.

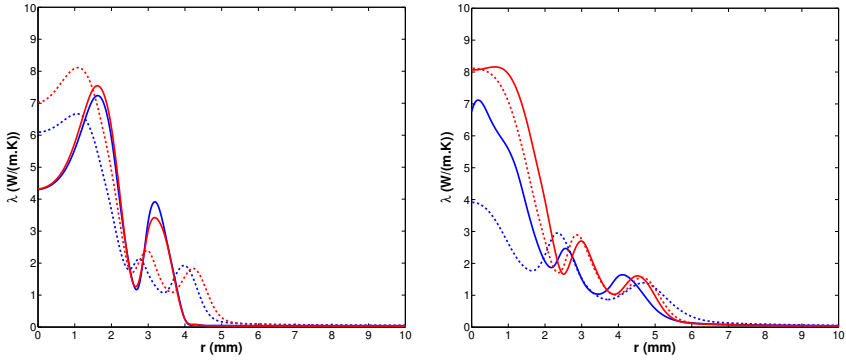

(a) 5 mm: full line; 20 mm: dashed line (b) 30 mm: full line; 40 mm: dashed line

Figure 4.24: Average thermal conductivity profiles of model 2 (blue) versus model 3 (red)

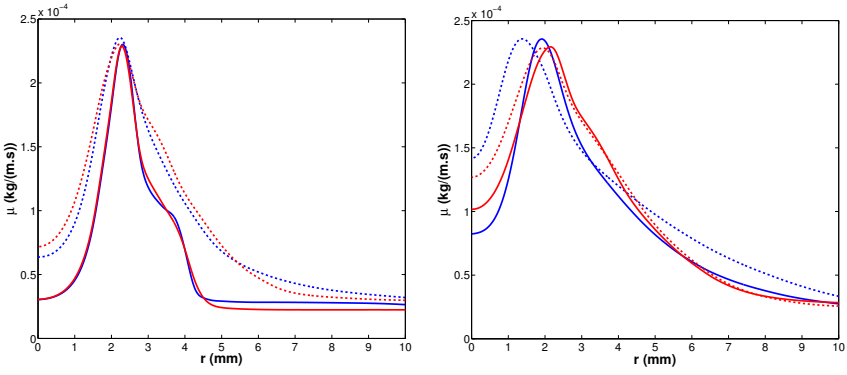

(a) 5 mm: full line; 20 mm: dashed line (b) 30 mm: full line; 40 mm: dashed line

Figure 4.25: Average viscosity profiles of model 2 (blue) versus model 3 (red)

4.7 Conclusion

The influence of the use of mixing rules in assigning thermodynamic and transport properties to a high-temperature gas mixture in plasma jet modelling was investigated. CFD simulations of an argon/water plasma jet issuing into ambient nitrogen gas with three different mixing models were compared on the basis of

the temperature, velocity and nitrogen concentration profiles in the resulting flow field.
It was found that the use of approximate mixing rules can greatly influence the calculated flow of a plasma jet. As already mentioned by Gleizes et al. [66], the specific differences in flow fields between a simulation with rigorous calculation of thermodynamic and transport properties of a gas mixture and simulations with estimation of the mixture properties by mixing rules are particular to the individual case that is modelled. However, it can be concluded that the main cause of the differences are the deviations from exact values of transport properties, calculated in this case with the mixing rules of Wilke and of Mason and Saxena. The more important the interactions between the different gases (e.g. inelastic collisions between water vapour and nitrogen), the larger the error in the calculation of the transport properties, especially thermal conductivity.
It was found that the entrainment of surrounding gas and the onset of turbulence occurs more rapidly for the simulations in which the thermophysical properties were estimated with mixing rules.

In the literature, the possible effect of the errors introduced on the flow field from inaccurate values for viscosity and thermal conductivity (calculated with mixing rules) are frequently ignored by assuming that their contribution is negligible in relation to their turbulent counterparts. However, in plasma jet modelling, the level of turbulence in the high-temperature region close to the torch exit is often low and the jet can be considered as quasi-laminar. In that region, the values of the molecular transport properties are much higher than those of the turbulent transport properties. Our results demonstrate that these effects can strongly influence the onset of turbulence, and consequently the properties of the flow in the turbulent regions, calculated from CFD simulations. Exact calculation of the transport properties is therefore necessary for a correctly calculated plasma flow.

The conclusions of this chapter are very relevant for the modelling of plasma-based applications. Such models are being developed to optimize the interaction of a plasma flow with solid particles, liquids or other gases. The heat- and mass transfer rates and chemical kinetics during these interactions strongly depend on temperature, velocity and gas composition. Although the results of this study are specific to the modelled case, it is clear that an inaccurate estimation of the thermodynamic and transport properties of a gas mixture, especially in a reacting gaseous environment, can lead to an incorrect flow field.
An example of a plasma-based application in which this can directly affect

the outcome of a simulation is plasma spraying. Plasma (jet) models are being increasingly used for choosing the optimal point of entry for the material powder. The velocity by which the powder is being accelerated by the plasma jet determines the distance of the receiving surface from the plasma torch, the temperature influences the melting (and spheroidization) characteristics and most importantly, the entrainment of the surrounding atmosphere (especially in the case of air or oxygen) is critical for the level of oxidation that the particles undergo in-flight. All these elements determine the quality of the plasma spraying result.

The application of interest in this research, however, is plasma gasification. The outcome of this theoretical modelling study can also be useful for the development of a CFD model of a plasma gasification system. A correctly simulated flow field of a plasma jet will primarily be of importance for the engineering and the configuration of the plasma torch(es) mounted to the reactor volume. Especially the predicted temperature will determine the choice of material for the connection between the plasma torch and the reactor, the shape of the connection, the distance of the exit nozzle to the walls of the connection and the required specifications for the incorporated water-cooling circuits.
It is assumed that effect on the actual gasification process of the use of mixing rules for the calculation of thermodynamic and transport properties of the multicomponent gas mixture will be negligible. After all, the deviations from the actual thermophysical values were manifested on the flow field by an accelerated onset of turbulence, which in turn increased the entrainment of surrounding gas, which resulted in a faster decrease in temperature (and velocity). In the case of a plasma gasification process, the explosive release of devolatilization gases and the intense mixing of gasifying agents with the produced syngas will cause an extremely turbulent regime. Consequently, the evolution of the plasma flow will be influenced much stronger by these turbulent mixing motions inside the reactor than by the effect of an inaccurate estimation of its thermophysical properties.

Three

Thermal Plasma Processing of Waste

CHAPTER 5

Single-Stage Plasma Gasification of Refuse-Derived Fuel

5.1 Background

The development of plasma gasification as a solution for waste materials treatment is situated in the broader framework of contemporary global challenges. Since the industrial revolution, the exploitation of fossil resources has continuously increased at an exponential rate [119]. The combustion of these fossil fuels for energy and transportation purposes has released approximately 350 billion tonnes of carbon into the atmosphere over the course of the last 50 years [11]. Although about half the carbon dioxide emitted into the atmosphere by human activities is absorbed by the Earth's oceans, forests and other ecosystems, their increasing concentrations pose serious risks for these ecosystems (e.g. acidifying oceans) and to human health. Moreover, this pollution is threatening to cause an anthropogenic climate change.

Another issue related to fossil fuels is its security of supply. Kruyt et al. [105] identified four dimensions of (fossil-based) energy security that relate to the availability, accessibility, affordability and acceptability of energy. The global availability is finite and it was shown that the rate of depletion of currently known reserves is accelerated by the increased global demand of fossil resources, driven by the fast-expanding world population and urbanization. Concurrently, this makes the extraction of raw materials more difficult and more energy-intensive,

resulting in additional environmental burden [80], which can be linked to the dimension acceptability. Also the accessibility of energy, related to geopolitical elements is a matter of concern, considering the recent political instabilities of the regimes in a number of supplier countries.
Among others, the environmental impact and the security of supply of fossil fuels have initiated a shift towards heat and electricity generation systems based on renewable energy sources [42].

Besides energy and transportation end-uses, fossil fuels are also widely used as a feedstock in industrial product manufacturing. In the context of depleting reserves of natural resources (including also other raw materials besides fossil fuels) and increasing material demands, there is a broad consensus that a transition towards a resource efficient circular economy is necessary. Sustainable waste management is an important aspect in this transition as it aims at the integral valorization of waste streams and at closing the material loop [211]. Waste is considered a very promising renewable resource, both for energy and for material purposes. It will be an abundant resource for the future, since the global solid waste generation is rapidly accelerating, due to the economic development and increased buying power in present developing countries.
Nowadays a large amount of waste is still being landfilled. One of the reasons for this is the limited range of waste streams which can be processed with the currently available conversion technologies. The most common method to process waste is incineration, which mainly focuses on energy recovery (electricity and heat production), but it is associated with the generation of SOx, NOx and other hazardous emissions. The aforementioned factors have led the waste industry to phase out unsustainable waste-management practices (e.g. landfills) and move towards more resource-efficient and environmental-friendly technologies [16].

Plasma gasification is a promising alternative for conventional thermochemical conversion technologies as it offers a substantially higher resource recovery potential.
Several advantages of plasma gasification compared to combustion, such as a less extensive gas cleaning and a lower amount of residue material to be treated have already been discussed in Paragraph 2.3. The overall advantage of plasma gasification, however, is its versatility of implementation in a waste management system. This versatility stems from the flexibility of all elements of the technology. At the input side, a wide range of waste- and material types can

be processed, including hazardous wastes, low-level radioactive wastes and wastes with a high inorganic fraction. At the output side, the main product is syngas which can be used for heat and/or electricity production, hydrogen production or as a feedstock for ammonia or liquid hydrocarbons synthesis. Above all, the process conditions can be tuned according to the type of waste material and to the desired syngas characteristics for a specific end-use. The syngas composition, for example, can be influenced by the combination of gasifying agents, added to the process. The plasma power on the other hand controls the temperature of the reactor and can easily be adjusted to the material load.
Because of the flexibility of the plasma gasification process, the operating parameters should be carefully selected for each specific implementation to ensure optimal performance.

In this chapter, the plasma gasification of refuse-derived fuel (RDF) is analyzed. Refuse is a general term for municipal solid and commercial wastes and the terms 'Refuse-Derived Fuel (RDF)' and 'Solid Refuse Fuel (SRF)' usually refer to the segregated high calorific fraction of municipal solid waste (MSW), commercial or industrial process wastes. According to a study ordered by the European Commission [63], the total quantities of RDF produced from MSW in the European Union in 2003 were estimated to amount to approximately 3 million tonnes per year. In a draft document published by the European Committee for Standardization (CEN) Task Force 118 on solid recovered fuels [52], this amount was expected to increase to about 13 million tonnes per year by 2005. More recent data about the quantities of RDF are not available.
Since RDF has a high calorific value, its treatment focuses on energy valorisation. The amount of dedicated RDF treatment plants (mainly combustion/incineration facilities based on fluidised bed technology), however, is very low. Alternatively, the processes in which the energetic content of RDF is utilized as a secondary fuel can be divided into two major categories. The first category encompasses heat or power generating plants or both, in which approximately 70 % of the RDF is co-incinerated:

- Multi-fuel district heating plants in Scandinavian countries are co-incinerating RDF for heat production through grate combustion or fluidised bed technology.
- Coal-powered combined heat and power (CHP) plants for electricity production are co-combusting RDF as a secondary fuel.

The second category includes industrial processes, in which RDF is mainly co-incinerated in cement kilns. RDF can also be co-incinerated in blast furnaces, brick kilns or used in the paper industry [63, 70]. These industrial processes are also the predominant choice for co-incineration of secondary fuels processed from industrial wastes, such as spent solvents, waste oils, industrial sludge, automotive shredder residue, waste textiles, impregnated sawdust, etc.
Most of these valorisation options were also listed in a report by the Flemish Institute for Technology Research (VITO) in 2001, in which different scenarios for the treatment of municipal solid waste and non-hazardous industrial waste [44] were compared in terms of environmental impact, resources (materials and energy) recuperation and costs [197]. The study started off considering a broad spectrum of pathways from waste material to valuable end-products (heat, electricity and syngas) (Figure 5.1), including a processing step of RDF to syngas through pyrolysis and gasification systems.

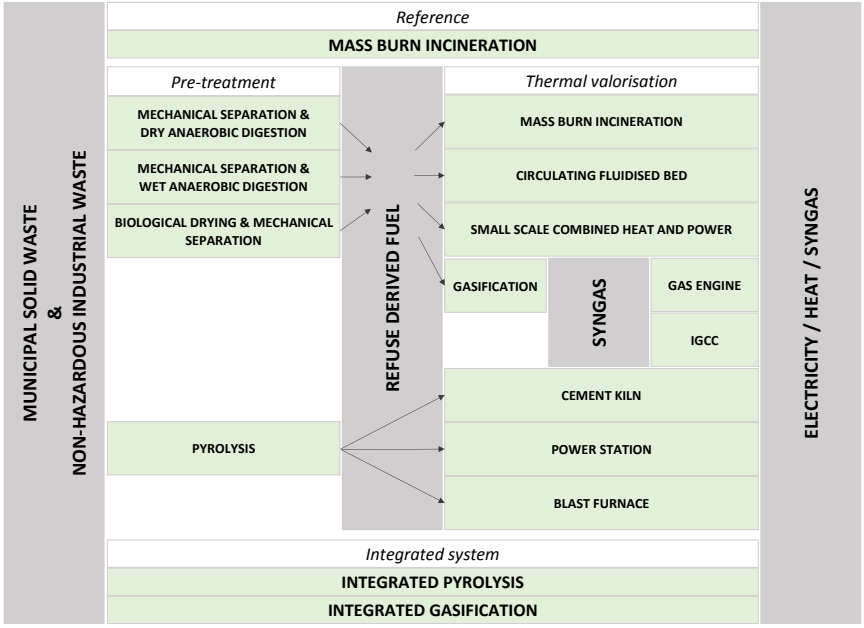

Figure 5.1: Overview of the pathways for conversion of MSW to end-product(s)

After evaluation of the technical feasibility of the different techniques, a selection was made of waste treatment scenarios which could be implemented at the time in the Flemish waste market within a short term (two years) and which are in

conformity with the Flemish legal framework (Figure 5.2). The techniques which did not make the short list were either not available on a pilot- or industrial scale (and not deployable in the Flemish market within two years) or unproven for the treatment of the waste material or did not comply with emission limits.

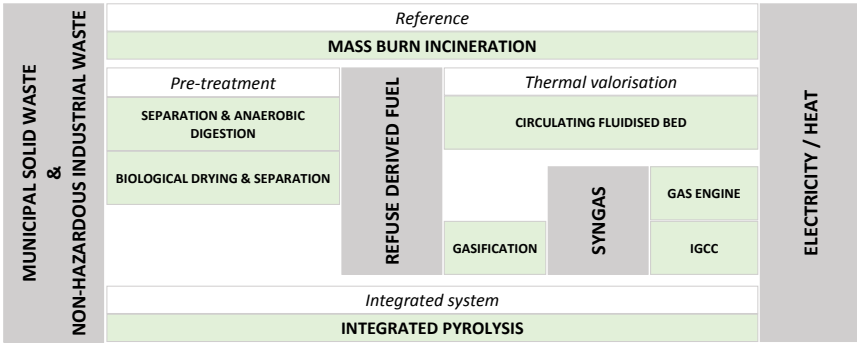

Figure 5.2: Selection of waste treatment scenarios

Although an advantage of co-incineration of RDF in industrial processes is saving non-renewable resources by substituting fossil fuels in high-demand energy processes, regulations regarding their use may not be well-defined and can be cause for concern. On the other hand, large scale incineration of RDF requires a constant throughput of material, which could hinder the development of prevention or recycling initiatives. Such issues are unlikely to present themselves when RDF is converted to syngas through plasma gasification due to its easy and fast-responding process control.

The research on plasma gasification of RDF is limited. In a pilot installation adapted from a system for metallurgical applications, Lemmens et al. [109] treated RDF with a transferred arc. The residual slag from the experiment was characterized to comply with the Flemish legislation for use as a secondary building material, however, no conclusive results were obtained about the performance of syngas production, because of the non-optimal design. Taylor et al. [181] treated RDF from MSW with the Gasplasma process, which comprises an oxy-steam bubbling fluidised bed gasifier and the subsequent plasma converter. The results of experiments on this two-step system show the effective generation of a clean syngas with high carbon and energy conversion efficiencies, which compares well with theoretical predictions. Other research [2, 61] focused on analysing the performance of RDF plasma gasification with thermodynamic

equilibrium models. Galeno et al. [61] discussed the integration between a fluidized bed plasma torch gasification unit and a solid oxide fuel cell, which was calculated to produce a net energy output of about 4.2 MJ kg^{-1} and would have a net electric efficiency of 33 %.
Since 2005, research on the plasma gasification unit at the Institute of Plasma Physics (IPP) of the Academy of Sciences of the Czech Republic (ASCR) has been performed [193]. This reactor is equipped with a unique DC hybrid water/gas stabilized torch, creating a high enthalpy, high velocity plasma, ideal for waste treatment [22]. In this single-stage system, the material fed to the reactor is partially gasified in-flight when it passes the high-temperature region created by the plasma. With this set-up, different types of material, i.e. biomass (sawdust and pellets) [84, 88, 191, 192], oil [85] and plastics [86] have been successfully converted to syngas in which the sum of carbon monoxide and hydrogen amounted up to 90 vol%.

In this chapter, the performance of the plasma gasification of RDF using different combinations of gasifying agents is assessed. Several experiments on the single-stage plasma gasification reactor at the IPP were performed with different sets of process parameters. In Paragraph 5.2.1, the specifics of the reactor configuration and the composition and characteristics of the refuse-derived fuel are presented. Additionally, the method for calculating the required energy for gasification and the maximum capacity of the system is documented. Nine experimental cases with different operating parameters were identified during steady state operation. In Paragraph 5.3, the measured compositions of the produced syngas of the different cases are mutually compared and the influence of the type of gasifying agent identified. Furthermore, the syngas compositions are compared to the theoretical compositions at thermodynamic equilibrium, and process yields (e.g. carbon conversion efficiency) and energy efficiencies are calculated. In the discussion, the influence of the type of material to be gasified on the performance of the plasma gasification system is examined by comparing the results of RDF experiments with previously published results from experiments with biomass. Finally, a comparative analysis is made of the output of these experiments to that of experiments with RDF from other plasma gasification facilities and to that of conventional RDF treatment options.

5.2 Materials and Methods

5.2.1 The Reactor System

The experiments were performed on the plasma gasification reactor PLASGAS at the IPP. A schematic overview of the system is shown in Figure 5.3, reproduced from Hrabovský et al. [87]. The reactor has an inner volume of 0.22 m^3 and is coated with special refractory ceramics. Four layers of different insulation materials with a total thickness of 400 mm separate the inner surface of the reactor from the water-cooled outer walls to reduce the heat losses from the reactor. The temperature of the inner wall of the reactor is measured at six locations by thermocouples (WRe5–WRe26 and PtRh30–PtRh6) in a ceramic sheath. To prevent destruction of the ceramic coating, the reactor is pre-heated by an electric rod prior to the experiments for 24 h to temperatures of about 1200 K. Further heating is produced by the plasma torch, which is mounted on top of the reactor vessel.

The plasma torch used in the plasma gasification experiments was the previously

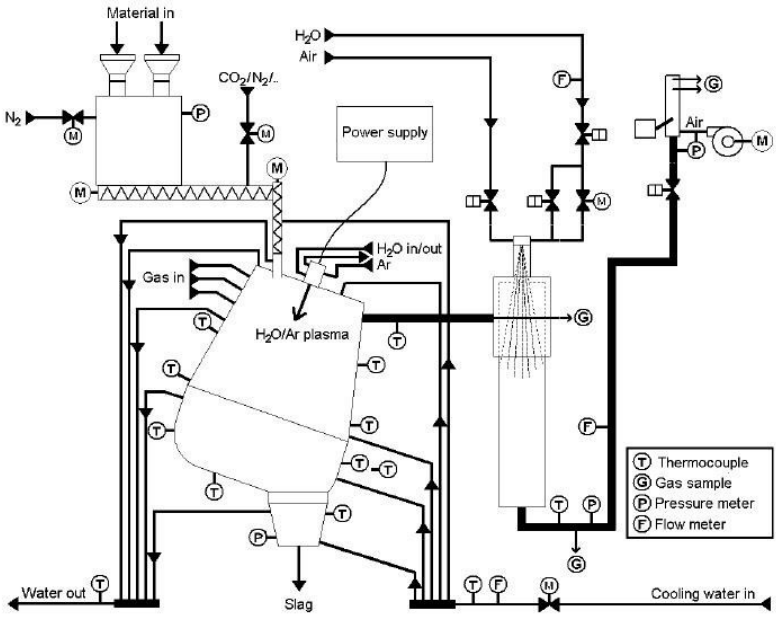

Figure 5.3: Schematic of the reactor system

presented hybrid DC water/argon stabilized torch (Paragraph 1.4.4.3). Both the

heat losses from the reactor wall and the energy losses inside the arc chamber are determined from calorimetric measurements on the respective cooling circuits.
The material to be gasified is continuously supplied from the material container by a screw conveyer and falls into the reactor volume under gravitational force. This Archimedes-type screw feeder is designed to handle homogeneous fine material streams, such as sawdust, wood chips, pellets, polyethylene beads, etc.. The gas inlets for the gasifying agents (O_2 and CO_2) are located in the upper part of the reactor. The volumetric flow rates of these oxidizing gases (F_{O_2} and F_{CO_2}) are set using thermal gas mass flow controllers (Aalborg GFC–57 and Aalborg GFC–47 respectively). These units are calibrated for a default gas and operate in a certain gas flow range. The gas flow rate is controlled by setting a desired percentage of the full flow range of the unit. Calibration of these gas flow controllers was performed prior to the experiments to obtain the correlations between the percentage of full range of the specific gas flow controller used and the gas flow rate of the added gas.
Inflow of liquid water as gasifying agent is positioned at the top of the reactor and enters the reactor volume together with the material feed. The water reservoir at room temperature was positioned on a scale and the flow of water was accomplished with a pump. The mass flow rate ($\dot{m}_{H_2O}$) was accurately determined from the time derivative of the weight difference.
The outlet for the produced gas is positioned in the upper part of the reactor, so that the syngas passes through the high-temperature plasma jet region before exiting the volume. The gas then flows to a cylindrical quenching chamber with a length of 2 m and a diameter of 0.3 m. The flow rate of the water spray is automatically controlled to keep the gas temperature at the output of the quenching chamber at 550 K. The gas temperatures are measured at the input and output of the quenching chamber by thermocouples (NiCr–NiAl with Inconel sheath and resistance thermometer Pt 100, respectively). The syngas is filtered through basalt filter bags before entering the combustion chamber where it is combusted by air flow. The produced syngas is collected for on-line composition analysis at the output of the reactor by a sampling tube which is cooled by water spray when it crosses the quenching chamber. To prevent blocking or damaging the inputs of the mass spectrometer, the gas sample circuit first passes a microfilter (Vesta MF M14). The sampled gas is then sent to the sample gas cooler (EGK 4S from Bühler Technologies) by a membrane pump (KNF) to condensate any steam in the syngas. In a final step, the sampled gas is prepared by a conditioning system (Perma Pure AmbiGASS) before being sent to the quadrupole mass spectrometer (Pfeiffer Omnistar GSD 301 T3). The mass spectrometer is calibrated to measure

the relative concentrations of CO, H_2, CO_2, CH_4, O_2 and Ar.

5.2.2 Refuse-Derived Fuel (RDF) Characteristics

The refuse-derived fuel (RDF) treated during the plasma gasification experiments is processed from waste excavated from landfill sites. It is composed of municipal solid waste (MSW, 59 %) and industrial waste (IW, 41 %). The proximate and ultimate analyses are summarized in Table 5.1. The composition of the ash fraction is given in Table 5.2.

The compositional analysis is also shown, it provides a rough estimation of the

Table 5.1: Proximate, ultimate and compositional analysis of RDF processed from excavated waste (59 % municipal waste, 41 % industrial waste).

Proximate analysis		Ultimate analysis		Compositional analysis	
	wt% dry		wt% dry		wt% dry
fixed carbon	8.6	C	46.8	plastics	47
volatile matter	69.3	H	5.7	wood+paper	24
ash	22.1	O[a]	22.3	textiles	10
moisture	*4.6*	Cl	1.60	fines	18
		N	1.25		
		S	0.26		

[a] by difference

different material types the waste is composed of. The material has a net calorific value (NCV) of 22.37 MJ/kg_{dry}. This material is rightfully termed refuse-derived fuel, in view of the treatment steps the original landfilled waste was subjected to. During the residence time in the landfill, the organic material was degraded due to chemical reactions and microbes. This decomposition process is similar to an anaerobic digestion pre-treatment step. Consequently a mechanical-biological pre-treatment step followed, since after excavation, the collected waste was dried and reduced in size [154]. All methods used to excavate and characterize the landfill waste are thoroughly explained in a case study [154].

It was determined that the storage time of the MSW varied from 14 to 29 years; while for the IW, storage time varied from 14 to 24 years. More detailed information can be found in the study, performed by Quaghebeur et al. [154]. The compositional analysis of the mixed RDF material indicates a plastics content of 47 % (see Table 5.1), a relatively large fraction when compared to the RDF materials studied by other researchers [40, 162] who report plastic fractions varying

from 16 % to 26 %. However, this is a logical consequence of the high plastics fraction present in the industrial waste (66 %), in combination with the high amount of industrial waste (41 %) used to produce the mixed RDF material. The fines fraction contains all particles smaller than 4 mm, while the maximum particle size of the RDF is 25 mm.

5.2.3 Procedure for Gas Tar Analysis

At certain instances during the experiment, gas samples of 600-900 ml are taken from the produced syngas flow. The solid phase adsorption/extraction (SPA/SPE) method is used for tar sampling. Tar vapors are adsorbed on to aminopropyl-bonded silica (Discovery DSC-NH2, 500 mg/3 ml). The SPE tubes are preconditioned with 2.5 ml of dichloromethane (DCM). Analytes are desorbed by DCM and the fractions analysed by gas chromatography with flame ionization detector (GC-FID).

5.2.4 Procedure for Residual Ash Analysis

A solid/liquid extraction with DCM is performed and the extracts were analyzed by means of GC-MS. Additionally, a thermogravimetric analysis was performed in order to determine the ratio of volatile organic components (VOCs), fixed carbon and mineral ash residue contained in the samples. A representative sample is heated from room temperature up to 600 °C (20 °C min^{-1}) with nitrogen as carrier gas. After an isothermal period of 30 min, the sample is heated further (20 °C min^{-1}) to 900 °C in air.

5.2.5 Calculation of the Theoretical Gasification Energy from Thermodynamic Equilibrium

In this section, the theoretical required energy to achieve complete gasification and the corresponding theoretical maximum capacity of the plasma gasification system treating RDF are assessed. The upper limit of the amount of material which can be treated is determined by the energy necessary to achieve complete gasification and the amount of added energy from plasma available to the process. The general procedure for this calculation is illustrated for plasma gasification with water as gasifying agent, but is similar for plasma gasification cases with other gasifying agents. The energy necessary for complete conversion of 1 kg of material to the equilibrium composition at temperature T can be calculated from the energy balance over the gasification system by:

$$\begin{aligned} E_{gas} =& E_{f,SG} + E_{f,ash} + E_{q,SG} + E_{q,ash} \\ & -(E_{f,RDF_{dry}} + E_{f,moist} + E_{f,pla} + E_{f,H_2O}) \end{aligned} \tag{5.1}$$

The terms E_f denote the total energy comprised in a material stream at standard conditions, expressed by the enthalpy of formation, and the terms E_q encompass the sensible heat within a material stream. The abbreviations 'SG', 'moist' and 'pla' stand for syngas, moisture content of the RDF and plasma, respectively.
The unit of the variable E_{gas} is kJ/kg$_{RDF}$ and its value is largely dependent of the composition of the RDF (Table 5.1) and the equivalence ratio (ER), determining the flow rate of water added as gasifying agent. The moisture content (w_{H_2O}) listed in Table 5.1 is expressed in dry wt%, but for convenient use in further analysis, the amount of moisture in RDF will be expressed as its weight fraction on as-received basis:

$$y_{H_2O} = \frac{w_{H_2O}}{(100.0 - w_{H_2O})} \tag{5.2}$$

The composition of the ash fraction was also analysed and the weight distribution of the ash components is shown in Table 5.2. The total weight fraction of ash in the RDF will be addressed as y_{ash}.

Table 5.2: Proximate analysis of the ash fraction of RDF

Component i	$y_{i,ash}$ ($\times 10^2$)	$M_{i,ash}$ (kg/mol)	$H°_{f,i,ash}$ (kJ/mol)
SiO_2	27.58	0.060	-911.3
Al_2O_3	9.46	0.102	-1674.4
Fe_2O_3	19.8	0.160	-825.9
CaO	17.12	0.056	-634.6
MgO	5.01	0.040	-601.5
TiO_2	3.01	0.080	-945.2
Na_2O	0.85	0.062	-414.2
K_2O	0.64	0.094	-363.0
P_2O_5	0.9	0.142	-1506.0
SO_3	3.01	0.080	-437.9
CuO	2.36	0.080	-156.06
ZnO	2.21	0.081	-350.46

5.2.5.1 Heat of Formation of Ash

From proximate analysis of the ash fraction (Table 5.2), the molecular weight (in

kg/mol) and heat of formation of ash (in kJ/mol) can be calculated as follows:

$$M_{ash} = \left(\sum_{i=1}^{n_{ash}} \frac{y_{i,ash}}{M_{i,ash}} \right)^{-1} \tag{5.3}$$

$$H^{\circ}{}_{f,ash} = M_{ash} \sum_{i=1}^{n_{ash}} \frac{y_{i,ash} H^{\circ}{}_{f,i,ash}}{M_{i,ash}} \tag{5.4}$$

with n_{ash} the total number of ash components.

The term in Equation 5.1 expressing the heat of formation of ash per kilogram of RDF (in kJ/kg$_{RDF}$) becomes:

$$E_{f,ash} = y_{ash}(1.0 - y_{H_2O}) \frac{H^{\circ}{}_{f,ash}}{M_{ash}} \tag{5.5}$$

with y_{ash} and y_{H_2O} the weight fractions of ash and moisture in the RDF, respectively.

5.2.5.2 Heat of Formation of RDF

Knowing the heat of formation of ash, the heat of formation of dry RDF can be estimated from its full oxidation reaction (Equation 5.6):

$$\mathrm{C}_{a_1}\mathrm{H}_{\ a_2}\mathrm{O}_{a_3}\mathrm{Cl}_{a_4}\mathrm{N}_{a_5}\mathrm{S}_{a_6}\mathrm{A}_{a_7} + z\mathrm{O}_2 \rightarrow q_1\mathrm{CO}_2 + q_2\mathrm{H}_2\mathrm{O}_{(g)} + q_3\mathrm{HCl} + q_4\mathrm{NO} + q_5\mathrm{SO}_2 + q_6\mathrm{A} \tag{5.6}$$

with element A representing ash.
The elements in the empirical formula for RDF are copied from the ultimate analysis of the material and the subscripts a_i are calculated as:

$$a_i = \frac{y_i}{y_C} \frac{M_C}{M_i} \tag{5.7}$$

with M_i and y_i, respectively the molecular weight (in kg/mol) and the weight fraction of the corresponding element i in the ultimate analysis of dry RDF. Thus, M_C and y_C denote the molecular weight and the weight fraction of carbon in dry RDF. From these subscripts, the molecular weight of the molecule with the generic chemical formula for RDF (in kg/mol) can be easily calculated:

$$M_{RDF} = \sum_{i=1}^{n_{RDF}} a_i M_i \tag{5.8}$$

with n_{RDF} the total number of elements in the generic formula for RDF. The balanced stoichiometric coefficients of the products of Reaction 5.6 are given in

Table 5.3: Stoichiometric coefficients and standard enthalpy changes of formation for the products of full oxidation of RDF (reaction 5.6)

Species	CO_2	$H_2O_{(g)}$	HCl	NO	SO_2	Ash
Stoichiometric coefficient (q_i)	a_1	$(a_2–a_4)/2$	a_4	a_5	a_6	a_7
$H°_{f,i,ox}$ (kJ/mol)	-393.51	-241.83	-92.31	90.29	-296.81	$H_{f,ash}$

Table 5.3.

From the standard enthalpy change of reaction of the full oxidation of dry RDF, the heat of formation of RDF (in kJ/mol) can be estimated:

$$\begin{aligned} \Delta H°_r &= -LHV_{RDF} M_{RDF} = \sum_{i=1}^{n_{prod}} q_i H°_{f,i,ox} - H°_{f,RDF} \\ H°_{f,RDF} &= \sum_{i=1}^{n_{prod}} q_i H°_{f,i,ox} + LHV_{RDF} M_{RDF} \end{aligned} \tag{5.9}$$

with n_{prod} the number of products of the full oxidation reaction of RDF.
The actual heat of formation of dry RDF in one kilogram of RDF (kJ/kg$_{RDF}$), as denoted by $E_{f,RDF}$ in Equation 5.1 is:

$$E_{f,RDF_{dry}} = (1.0 - y_{H_2O}) \frac{H°_{f,RDF}}{M_{RDF}} \tag{5.10}$$

5.2.5.3 Heat of Formation of H_2O as Moisture in RDF

The weight fraction of moisture in one kilogram of RDF was calculated in Equation 5.2. The heat of formation of liquid water ($H°_{f,H_2O_{(l)}}$) is 285.8 kJ/mol and with the molecular weight of water (M_{H_2O} = 0.01802 kg/mol), the term expressing heat of formation of water per kilogram of RDF (in kJ/kg$_{RDF}$) is calculated as:

$$E_{f,moist} = y_{H_2O} \frac{H°_{f,H_2O_{(l)}}}{M_{H_2O}} \tag{5.11}$$

5.2.5.4 Heat of Formation of H_2O from Plasma

The DC hybrid water/argon stabilized torch produces an O-H-Ar plasma jet which adds approximately 6 standard litres per minute (slm) of argon ($F_{Ar,pla}$) and 0.25 g/s of water vapour ($\dot{m}_{H_2O,pla}$) to the system. The term in Equation 5.1 expressing the heat of formation of the plasma content contains only that of the

water vapour fraction since the heat of formation of argon is zero. The flow of water vapour from the torch is constant in time, so its value will be divided by the material feed rate ($\dot{m}_{RDF}$ in kg/h) to obtain the amount of water vapour from plasma per kilogram of material. The heat of formation of water vapour ($H^\circ_{f,H_2O,(g)}$) was previously given in Table 5.3, so the term in Equation 5.1 becomes:

$$E_{f,pla} = 3.6 \frac{\dot{m}_{H_2O}}{\dot{m}_{RDF}} \frac{H^\circ_{f,H_2O_{(g)}}}{M_{H_2O}} \tag{5.12}$$

5.2.5.5 Heat of Formation of H_2O as Gasifying Agent

The portion of energy added to the system through water as gasifying agent is dependent of the desired equivalence ratio (ER) for the process. The equivalence ratio is defined as the ratio of the total amount of available moles of oxygen added to the process to the stoichiometric required amount of moles for the complete oxidation of material. The denominator in this ratio can be calculated from the stoichiometric coefficient for oxygen (z) in the full oxidation of RDF (Reaction 5.6). The molar amount of oxygen gas for full oxidation of one mole of dry RDF can be found from balancing Reaction 5.6:

$$z = a_1 + \frac{(a_2 - a_4)}{4} - \frac{a_3}{2} + \frac{a_5}{2} + a_6 \tag{5.13}$$

This amount is multiplied with the equivalence ratio and converted to the unit $\text{mol}_O/\text{kg}_{RDF,dry}$. Subsequently, the amount of oxygen added as moisture and from plasma is deducted to obtain the amount of monoatomic oxygen that needs to be added to the process per kilogram of dry RDF (O_{req}):

$$O_{req} = \frac{ER * 2z}{M_{RDF}} - \frac{y_{H_2O}}{M_{H_2O}} - 3.6 \frac{\dot{m}_{H_2O}}{\dot{m}_{RDF} M_{H_2O}} \tag{5.14}$$

One mole of monoatomic oxygen translates to one mole of water and the energy term for the heat of formation of H_2O as gasifying agent is derived as:

$$E_{f,H_2O} = (1.0 - y_{H_2O}) O_{req} H^\circ_{f,H_2O,(l)} \tag{5.15}$$

5.2.5.6 Heat of Formation of Syngas

From all the aforementioned input streams to the system, is possible to calculate the theoretical syngas composition at thermodynamic equilibrium at the temperature of the reactor T (K). The calculation procedure was previously explained in Paragraph 3.4. This calculation requires the total molar amount of each element

added to the system per kilogram of RDF.

$$\begin{aligned}
n_C &= \frac{y_C(1.0 - y_{H_2O})}{M_C} \\
n_H &= \frac{y_H(1.0 - y_{H_2O})}{M_H} + 2\frac{ER * 2z}{M_{RDF}}(1.0 - y_{H_2O}) \\
n_O &= \frac{y_O(1.0 - y_{H_2O})}{M_O} + \frac{ER * 2z}{M_{RDF}}(1.0 - y_{H_2O}) \\
n_{Cl} &= \frac{y_{Cl}(1.0 - y_{H_2O})}{M_{Cl}} \\
n_N &= \frac{y_N(1.0 - y_{H_2O})}{M_N} \\
n_S &= \frac{y_S(1.0 - y_{H_2O})}{M_S} \\
n_{Ar} &= \frac{60F_{Ar,pla}}{\dot{m}_{RDF}V_m}
\end{aligned} \tag{5.16}$$

with V_m the molar volume at standard conditions (=22.414 l/mol).
For the plasma gasification of RDF, the gas species which can be present at volumetric percentages higher than 0.1 % in the theoretical syngas at thermodynamic equilibrium are H_2, CO, CO_2, $H_2O_{(g)}$, Ar, N_2 and HCl. The molecular weights and the enthalpies of formation of these gas species are listed in Table 5.4

Table 5.4: Syngas composition and the molecular weight and heat of formation of the constituent species

Syngas species	H_2	CO	CO_2	H_2O	Ar	N_2	HCl
$M_{i,SG}$ (g/mol)	2.02	28.01	44.01	18.02	39.95	28.01	36.46
$H°_{f,i,SG}$ (kJ/mol)	0	-110.53	-393.51	-241.82	0	0	-92.30

The yield of the theoretically produced syngas (F_{SG} in m^3/kg of RDF) can be calculated from the flow rate of argon to the system ($F_{Ar,pla}$ in slm) and the volumetric fraction of argon in the syngas:

$$F_{SG} = \frac{100}{x_{Ar,SG}}\frac{60F_{Ar,pla}}{\dot{m}_{RDF}} \tag{5.17}$$

The total heat of formation of the syngas mixture becomes:

$$E_{f,SG} = \frac{F_{SG}}{V_m}\sum_{i=1}^{n_{SG}}\frac{x_i H°_{f,i,SG}}{100} \tag{5.18}$$

with n_{SG} the number of species in the syngas.

5.2.5.7 Sensible Heat of Syngas

The sensible heat of a gas (in kJ/mol) can be calculated using the Shomate equation (from NIST):

$$\Delta H°(T) = H°_T - H°_{298.15} = At + \frac{Bt^2}{2} + \frac{Ct^3}{3} + \frac{Dt^4}{4} - \frac{E}{t} + F - H \qquad (5.19)$$

with t=$T/1000$.
The coefficients of this equation are defined according to different temperature ranges. The coefficients for syngas species i can be found in the NIST database. The term for the sensible heat of the syngas is described by:

$$E_{q,SG} = \frac{F_{SG}}{60V_m} \sum_{i=1}^{n_{SG}} x_{i,SG} \Delta H°_{i,SG}(T) \qquad (5.20)$$

5.2.5.8 Sensible Heat of Ash

To calculate the sensible heat of the ash at temperature T, the heat capacity of the mineral ash fraction fist needs to be determined. The heat capacities of eight of the constituent species of ash (in kJ/kmol) are calculated according to the formula used by Mehmood et al [123]:

$$C_{p,i,ash} = K_0 + K_1 \text{x} 10^{-2} T^{-0.5} + K_2 \text{x} 10^{-5} T^{-2} + K_3 \text{x} 10^{-7} T^{-3} \qquad (5.21)$$

The coefficients K_0, K_1, K_2 and K_3 for the relevant species are listed in Table 5.5.

Table 5.5: Coefficients for the calculation of heat capacity of the first eight ash species

Ash species	K_0	K_1	K_2	K_3
SiO_2	80.01	-2.403	-35.47	49.16
Al_2O_3	155.02	-8.28	-38.61	40.91
Fe_2O_3	146.86	0	-55.77	52.56
CaO	58.79	-1.34	-11.47	10.3
MgO	58.179	-1.61	-14.05	11.27
TiO_2	77.84	0	-33.68	40.29
Na_2O	95.148	0	-51.04	83.36
K_2O	105.4	-5.77	0	0

For CuO, the enthalpy change ($\Delta H°_{CuO}$ in kJ/kg) from 298.15 K to T is calculated

Table 5.6: Shomate coefficients for CuO

Shomate coefficients	A	B	C	D	E	F	H
CuO	48.565	7.499	-0.056	0.014	-0.7601	-173.427	-156.063

with the Shomate equation (Equation 5.19). The coefficients used for solving this equation were taken from the NIST Webbook and are summarized in Table 5.6. The change of enthalpy of ZnO (in kJ/mol) is calculated according to the equation found in Sun et al. [177]:

$$\Delta H^{\circ}{}_{ZnO}(T) = (49.523 * (T - 298.15) + 0.0025/2 * (T^2 - 298.15^2))/1000 \quad (5.22)$$

The ash components P_2O_5 and SO_3 are not included in the calculation of the sensible heat of ash because they reach their boiling temperature at 44.8 °C and 360 °C, respectively. Therefore, the contribution of these inorganic compounds in the calculation of the sensible heat of the ash will be neglected, and the weight fraction of the other ash species will be normalized to:

$$w_{i,ash} = \frac{y_{i,ash}}{1 - y_{P_2O_5} - y_{SO_3}} \quad (5.23)$$

Taking all the previous calculated elements of the sensible heat of ash together gives the change of enthalpy for the ash fraction (in kJ/kg) as follows:

$$\Delta H^{\circ}{}_{ash}(T) = \sum_{i=1}^{n_{ash}-4} \frac{w_{i,ash} \int_{298.15}^{T} C_{p,i,ash} dT}{1000 M_{i,ash}} + w_{CuO,ash} \Delta H^{\circ}{}_{CuO} + w_{ZnO,ash} \frac{\Delta H^{\circ}{}_{ZnO}}{M_{ZnO}} \quad (5.24)$$

The energy term in Equation 5.1 denoting the sensible heat of the unreacted ash fraction is simply:

$$E_{q,ash} = y_{ash}(1.0 - y_{H_2O}) \Delta H^{\circ}{}_{ash}(T) \quad (5.25)$$

This last paragraph concludes the description of all terms in the calculation of the theoretical energy required for the complete gasification process (Equation 5.1). The maximum capacity of the plasma gasification system (in kg/h) is then determined by the calculated energy required for complete gasification (in kJ/kg) and the amount of energy from plasma available to the process (in kJ/h):

$$\dot{m}_{RDF,max} = \frac{P_{pla,net}}{E_{gas}} \quad (5.26)$$

Some additional remarks need to be made about the calculations in this paragraph:

1. An element in the calculation of the energy terms for heat of formation of H_2O from plasma and from the flow as gasifying agent, is the mass flow rate of RDF. This is to determine the amount of steam from plasma per kilogram of RDF. The difference of the desired amount of water preset by the selected equivalence ratio and that from moisture and plasma is the amount added as liquid water. With a higher material feed rate, a marginally higher amount of liquid water is added in stead of water vapour (from plasma). The resulting change in energy needed for the complete gasification process, originating from the difference between the heat of formation of liquid and gaseous water, is negligible. However, this difference in gasification energy with different material feed rates may be more significant for gasification with different gasifying agents.
2. The equilibrium composition at a certain temperature from the total amount of material is in fact calculated for a heterogeneous system. This means that for certain cases, a solid phase with some solid carbon (or soot) is present at equilibrium conditions. This amount, x_{soot} is expressed in moles per mole of gaseous phase. The sensible heat of this soot fraction which is formed needs to be taken into account. The sensible heat is calculated with the coefficients and empirical equations from Sheindli et al. [170]. The enthalpy change of soot (in kcal/kg) from 298.15 K to T amounts to:
$$\begin{aligned}\Delta H^\circ{}_{q,soot}(T) =& 0.464T + 0.123 \cdot 10^{-4}T^2 + 6.1 \cdot 10^4 T^{-1} \\ &+ 2.8 \cdot 10^6 \exp(-\frac{36600}{T}) - 184.6 \end{aligned} \tag{5.27}$$
and the energy term (in kJ/kg_{RDF}) which should be deducted in Equation 5.1 becomes:
$$E_{q,soot} = \frac{4.184 x_{soot} F_{SG} \Delta H^\circ{}_{q,soot}}{V_m M_C} \tag{5.28}$$
with M_C in kg/mol.
3. In the procedure unrolled above, the amount of oxygen required for complete gasification is entirely supplied through H_2O. However, the plasma gasification process can also be performed using combinations of different gasifying agents. In such case, the molar amount of oxygen is divided according to the selected molar ratio of the gasifying agents used. In determining the required flow of these gasifying agents from this ratio and the equivalence ratio, one mole of O_2 supplies two mole of available mono-atomic oxygen, and H_2O and CO_2 both one.

5.3 Results and Discussion

5.3.1 Experimental Parameters

Prior to the experiment, the reactor was gradually heated for 24 h to 1200 K. The total duration of the experiment, starting with the ignition of the torch after pre-heating was 4 h and the total amount of RDF added to the reactor volume during this period was 71.4 kg. The flow rate of the RDF feed is controlled by the intensity setting of the screw feeder. Three different signal intensities of 7.3, 9.9 and 19.4 were set during the experiment. By assuming a linear correlation between the signals and the feed rates and with the condition that the sum of the products of the resulting feed rates with their respective feeding times over the entire duration of the experiment equal the total amount of RDF added to the reactor, respective values of 21.3, 28.9 and 56.7 $\mathrm{kg\,h^{-1}}$ were obtained.
The screw feeder was not designed for heterogeneous material types, such as RDF. Consequently, some difficulties and fluctuations in the material feed rate were encountered, because of the inhomogeneity in size, shape, weight and density of the RDF. This means there is a possible error margin on the instantaneous feed rate, which can be of importance for experimental cases with short sampling periods.
The electrical current of the torch was about 420 A and the voltage drop between the cathode and the anode was around 288 V throughout the experiments, resulting in a relatively constant torch power of 120 kW.
The gas flow rates are expressed in the unit standard litres per minute (slm), which is the volume that a gas embodies at a pressure of 101.325 kPa and temperature of 0 °C. Argon was added to the reactor as internal standard at a flow rate of 87 slm. From the total amount of argon entering the reactor (i.e. internal standard and argon from the torch) and the concentration of argon in the syngas, the total flow rate of syngas can be calculated.

Within the duration of the experiment, several cases with different process parameters are identified. The time spans of these cases, over which the process output variables are averaged, are identified by stable syngas compositions, denoting pseudo steady-state operation. The time period of the experimental cases is minimum one minute and ranges up to 4 minutes. These short periods of pseudo steady-state operation are justified by the short response time of the system. This is illustrated in Figure 5.4 which shows the evolution of the added gases to the reactor and the syngas volumetric composition over time. The line marks show that the change in operational conditions is manifested in the syngas composition

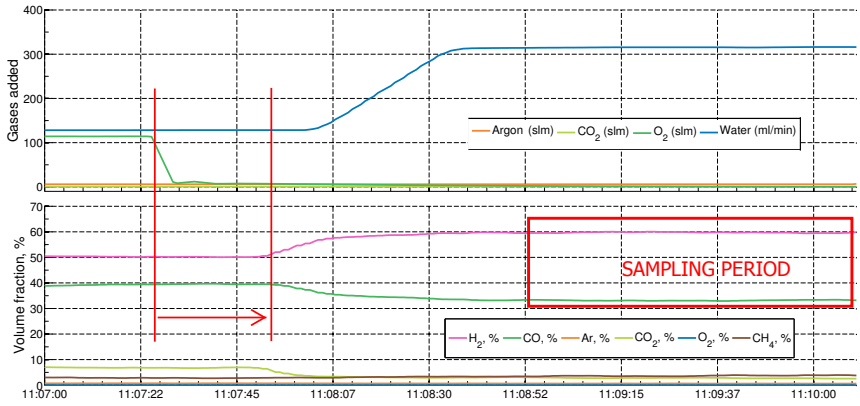

Figure 5.4: Time evolution of the flow rates of gasifying agents and volumetric syngas composition

within approximately 30 s. A typical time frame for the sampling period of the pseudo steady-state process variables is also shown.

The process parameters, including the material feed rate and the different combinations of gasifying agents for the selected cases are summarized in Table 5.7. Due to blockage of the material feeding system and the mass spectrometer sampling, no periods with steady-state operation for the material feed rate of 56.7 $\mathrm{kg\,h^{-1}}$ could be identified.

Table 5.7: Process parameters of the gasification cases with RDF.

Case number	$\dot{m}_{RDF}$ ($\mathrm{kg\,h^{-1}}$)	F_{H_2O} ($\mathrm{ml\,min^{-1}}$)	F_{CO_2} (slm)	F_{O_2} (slm)	ER	T (K)
1	28.9	0	216	118	0.52	1554
2	28.9	0	215	93	0.46	1538
3	28.9	0	177	93	0.43	1536
4	28.9	300	0	0	0.44	1429
5	28.9	385	0	0	0.55	1395
6	28.9	144	178	0	0.42	1446
7	28.9	113	0	114	0.43	1490
8	21.3	149	0	0	0.32	1574
9	21.3	0	167	0	0.30	1464

The equivalence ratio (ER) is defined as the ratio of the total amount of available moles of oxygen added to the process to the stoichiometric required amount of

moles for the complete oxidation of material. The amount of oxygen from the moisture content of the material and from the steam fraction in the plasma were included in the total amount of oxygen added to the reactor. The oxidation reaction considered was presented in the previous paragraph by Equation 5.6.
The temperature column in Table 5.7 shows the average value of the temperature measurements at the inner reactor wall surface. The thermocouples registered lower values than the actual temperature inside the reactor volume because of their shielded position in the water-cooled reactor wall. Nevertheless, the average of these measured temperatures will be used for the calculation of the theoretical syngas composition at thermodynamic equilibrium. Cases 4 and 5 and 8 can also be referred to as steam plasma gasification, and Case 7 as oxy-steam plasma gasification.

5.3.2 Theoretical Results

According to the method described in Paragraph 5.2.5, the energy required to achieve complete conversion of the solid material to syngas and ash at temperature T was calculated for all cases with their specific process parameters. The plasma mass content was estimated at 0.25 g/s of water vapour and 6 slm of argon. In these calculations, the actual amount of energy which is available to the process was used by taking into account the heat losses inside the torch, the losses to the section connecting the torch to the reactor and the losses to the reactor walls. These losses were determined from the calorimetric measurements of the respective water-cooling circuits. In Table 5.8, the net power available to the process (P_{net}), the theoretical syngas composition, the energy required for complete gasification, the maximum process rate of RDF ($\dot{m}_{RDF,max}$) and the molar ratio of gasifying agents (r: CO_2/O_2 for Cases 1 to 3, CO_2/H_2O for Case 6 and H_2O/O_2 for Case 7), if applicable is shown. Nitrogen gas and hydrogen chloride fractions both ranged between 0.4 % to 0.6 % for all cases and were not included in the table.
For cases 1 to 3 in which a mixture of CO_2 and O_2 is added as gasifying agent, Case 1 with the highest equivalence ratio shows the lowest value for the required energy for the gasification process. This is because of the higher flow rate of O_2 than in the other cases, which reacts exothermally with the waste material through the partial oxidation reaction (Equation 5.29), making energy available to the process.

$$C + \frac{1}{2}O_2 \rightarrow CO \tag{5.29}$$

The influence of this effect can be observed when comparing E_{gas} of Case 1 to that of Case 2, in which 25 slm less O_2 added. This reduction in O_2 flow rate more than doubles the required gasification energy. Reducing the CO_2 flow rate

Table 5.8: Theoretical results for all cases

Case No.	P_{net} (kW)	r	Syngas content (vol%)					E_{gas} $\frac{kJ}{kg_{RDF}}$	$\dot{m}_{RDF,max}$ (kg/h)
			CO	H_2	CO_2	$H_2O_{(g)}$	Ar		
1	46.6	1.83	52.0	21.1	11.8	13.5	0.6	895	187.6
2	46.3	2.32	54.7	23.7	9.1	10.9	0.6	1992	83.7
3	48.5	1.91	55.1	26.5	7.2	9.5	0.6	1708	102.2
4	46.4	-	32.4	51.5	3.2	11.6	0.5	7049	23.7
5	50.6	-	27.9	48.8	4.6	17.4	0.5	7702	23.6
6	47.3	1.01	47.6	37.5	4.7	8.8	0.5	6925	24.6
7	43.9	1.23	39.8	40.3	5.0	13.0	0.7	386	671.6
8	43.4	-	38.3	54.6	1.0	4.3	0.8	6683	23.4
9	50.9	-	62.4	32.7	1.3	1.7	0.8	6085	30.1

with 38 slm from Case 2 to Case 3 causes a small decrease in the energy variable accordingly.

It is evident that the higher equivalence ratio for the plasma gasification with H_2O in Case 5 compared to Case 4, leads to a higher value of E_{gas}, mainly because of the extra amount of energy needed to bring the additional flow of liquid water to the process temperature as water vapour. Case 6, in which a mixture of CO_2 and H_2O is added as gasifying agent to the process, shows a similar value for E_{gas} as the steam plasma gasification case, Case 4, with a similar equivalence ratio. The CO_2/H_2O ratio of Case 6 means that about half of the oxygen supplied as water in Case 4 is interchanged by CO_2. The theoretical overall heterogeneous gasification reaction of RDF with a stoichiometric amount of oxygen, z, can be written as:

$$\mathrm{C}_{a_1}\mathrm{H}_{\ a_2}\mathrm{O}_{a_3}\mathrm{Cl}_{a_4}\mathrm{N}_{a_5}\mathrm{S}_{a_6}\mathrm{A}_{a_7} + z\mathrm{O} \rightarrow q_1\mathrm{CO} + q_2\mathrm{H}_2 + q_3\mathrm{HCl} + q_4\mathrm{N}_2 + q_5\mathrm{H}_2\mathrm{S} + q_6\mathrm{A} \tag{5.30}$$

The standard enthalpies of this reaction with CO_2 and with H_2O as oxygen suppliers are both endothermic with values of $65.0\,\mathrm{kJ/mol_{RDF,dry}}$ and $66.8\,\mathrm{kJ/mol_{RDF,dry}}$, respectively. These similar values explain why CO_2 and H_2O can be easily exchanged as gasifying agents without a significant alteration in the energy required for the gasification process.

The energy variable E_{gas} is lowest for oxy-steam plasma gasification, Case 7. The same explanation of the exothermic reaction with O_2 as for cases 1 to 3 applies here. Also the interchangeability of CO_2 and H_2O as gasifying agents can be illustrated by comparing Case 3 (CO_2+O_2) and Case 7 (H_2O+O_2) with identical

equivalence ratios. The lower molar amount of secondary gasifying agent (CO_2 in Case 3 and H_2O in Case 7) relative to O_2, however, leads to a significantly lower amount of required energy for the gasification process in Case 7 in comparison to Case 3.
The discussion of the results for Cases 8 and 9 (Table 5.8) and their relation to the other cases introduces no new elements compared to the explanations above.

In the next paragraph, the measured syngas composition is compared to the equilibrium composition, in which the flow of argon, added as an internal standard is also taken into account, in contrast with the previously calculated theoretical syngas content in which only the argon from plasma was included. The flow rate of added argon is constant at 87 slm in all cases and so is the additional required energy to heat this volume to the operating temperature. For example, this value is round about $200\,\mathrm{kJ\,kg^{-1}}$ for a temperature of 1500 K and a material feed rate of $28.9\,\mathrm{kg\,h^{-1}}$.

5.3.3 Syngas Composition

The syngas composition registered by the mass spectrometer for the different cases is shown and compared with the calculated theoretical composition, assuming thermodynamic equilibrium. Based on the amount of C, H, O, N, S, Cl and Ar added to the system (waste material, argon as internal standard, gasifying agents and plasma gas), the equilibrium composition of this heterogeneous system was calculated at the given temperature using the method described by Coufal and Živný [39].
The calculated syngas composition contains a percentage of water vapour, but because the water vapour was removed from the produced syngas during the experiment to prevent blocking of the mass spectrometer, the theoretical volumetric percentages were normalized to a dry syngas comprising only the following five syngas components, i.e. CO, H_2, CO_2, CH_4 and Ar. The mass spectrometer is also calibrated for O_2, but as could be expected, there was no O_2 detected in the syngas exiting the reactor. Carbon monoxide and nitrogen gas have the base peak at the same mass number in the mass spectrum and can not be differentiated at the resolution of the mass spectrometer used for the analysis. Since no nitrogen is added to the system and the reactor operates at overpressure, it is valid to link the peak at 28 exclusively to CO.
The argon concentration in the dry syngas content (which can amount up to 10 vol%) is specific to the set-up of the experimental system, in which it is used

for estimating the syngas flow rate (through adding an internal standard of argon). The argon content should not be taken into account when assessing the syngas composition from plasma gasification of RDF for industrial applications. The syngas compositions from the nine experimental cases are arranged according to the material feed rate and the type of gasifying agent used. For the material feed rate of 28.9 kg/h, Figure 5.5 shows the cases in which a mixture of CO_2 and O_2 was used as gasifying agent, Figure 5.6 depicts the steam plasma gasification cases and the experiments with a combination of CO_2 and H_2O and a combination of O_2 and H_2O are grouped in Figure 5.7. Figure 5.8 shows the cases with material feed rate of 21.3 kg/h and respectively H_2O and CO_2 as gasifying agents. The standard deviation on the volumetric percentages of all syngas components is smaller than 0.5 % in all nine cases. This shows the very stable operation of the reactor.

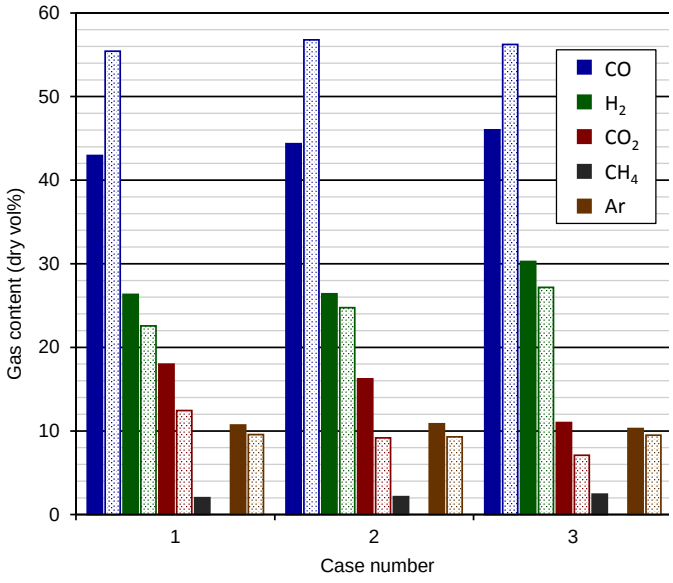

Figure 5.5: Measured (full colour) and theoretical (patterned) syngas composition for Cases 1, 2 and 3, with a combination of CO_2 and O_2 as gasifying agent

Specific reasons for the lower CO, higher H_2 and higher CO_2 concentrations than theoretically expected for Cases 1 to 3 in Figure 5.5 can be the following:

- The complete oxidation of some of the RDF (Equation 5.6) can have taken place, producing CO_2 and H_2O in stead of CO and H_2.
- Part of the produced CO can be further oxidized to CO_2:

$$CO + \frac{1}{2}O_2 \rightarrow CO_2 \tag{5.31}$$

- The water-gas shift reaction can have also occurred (Equation 5.32), reducing the amount of CO and yielding CO_2 and H_2.

$$CO + H_2O \leftrightarrow CO_2 + H_2 \tag{5.32}$$

According to the theoretical syngas compositions, before normalization to dry syngas, the water vapour contents for Case 1 to 3 were 13.5 vol%, 10.9 vol% and 9.5 vol% respectively. The theoretical presence of water vapour imposes the supposition that the water-gas shift reaction occurs.
In comparison to Case 1, there was 25 slm less O_2 added to the process in Case 2, which results in higher CO and lower CO_2 concentrations. Since less O_2 was available, more CO_2 was consumed in the gasification process, and additionally, less CO_2 was produced via the CO oxidation reaction (Reaction 5.31). By reducing the CO_2 flow rate in Case 3 by 38 slm compared to the value in Case 2, the CO content is increased and the CO_2 concentration reduced to 11.0 vol%. The hydrogen content is also significantly higher than in the two other cases, most likely because the lower amount of CO_2 present in the system shifts the equilibrium of the water-gas shift reaction to the right. Also, less energy is consumed for heating up the gasifying agents.
Based on the evaluation of these three cases, it is clear from the high concentrations of CO and H_2 and the low concentrations of CO_2 that Case 3 yields the most desirable syngas composition.
The measured syngas content in Figure 5.6 corresponds well to the theoretically expected composition (patterned bars), except for the presence of CH_4 ($\sim$4 %) in the produced syngas. Steam plasma gasification clearly yields a high hydrogen gas fraction in the composition with about 53 vol% for both cases. The difference between Case 4 and 5 is the increase in water flow rate from 300 ml min^{-1} to 385 ml min^{-1}, increasing the equivalence ratio from 0.44 to 0.55. With the extra addition of H_2O to the system, the CO concentration drops from 30.1 vol% to 27.2 vol%, the CO_2 concentration increases from 3.3 vol% to 5.9 vol% and the H_2/CO ratio increases from 1.75 to 1.95. This is possibly due to a shift in equilibrium of the water-gas shift reaction (Equation 5.32) towards the right according to Le Chatelier's principle. This shift in equilibrium is slightly promoted by the marginally lower temperature in Case 5 compared to Case 4.

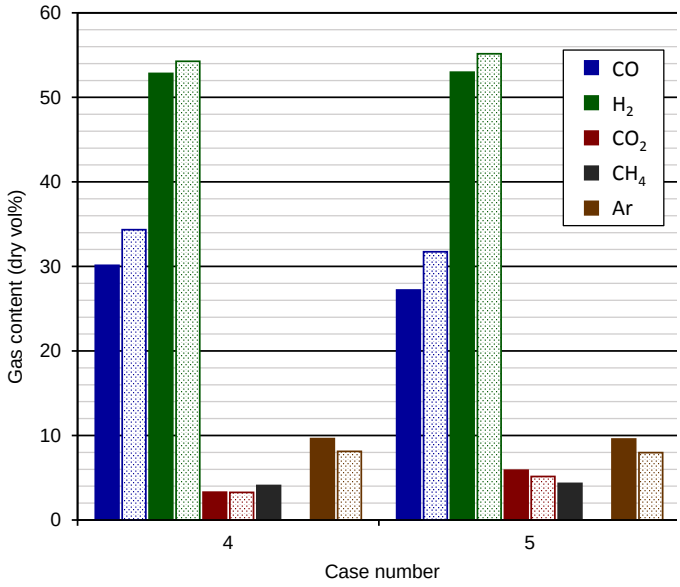

Figure 5.6: Measured (full colour) and theoretical (patterned) syngas composition for Cases 4 and 5, with H_2O as gasifying agent

The syngas composition analysis of the plasma gasification with a mixture of CO_2 and H_2O (Case 6) and a mixture of O_2 and H_2O (Case 7) is displayed in Figure 5.7. For Case 6, the measured volume fractions of CO and of H_2 are lower and the volume fraction of CO_2 is higher than expected from theoretical calculation.

The standard enthalpies of the gasification reaction (Equation 5.30) with CO_2 and with H_2O are nearly identical. As a result of these two competing reactions, the volumetric percentages of CO and H_2 are similar (H_2/CO ratio of 0.88), in contrast to previous cases in which either CO or H_2 is predominantly present.

In Case 7, the calculated concentrations of CO and H_2 are almost identical. The measured CO concentration is lower and the H_2 concentration higher than their theoretical counterparts. The fact that the measured argon volume percent is lower than the calculated value implies that the total produced volume of dry syngas is higher than theoretically expected, suggesting a very high solid-to-gas conversion efficiency. The variables which indicate the performance of the gasification process will be discussed in detail in the next paragraph.

The syngas composition of Cases 8 and 9 with a material feed rate of 21.3 kg/h

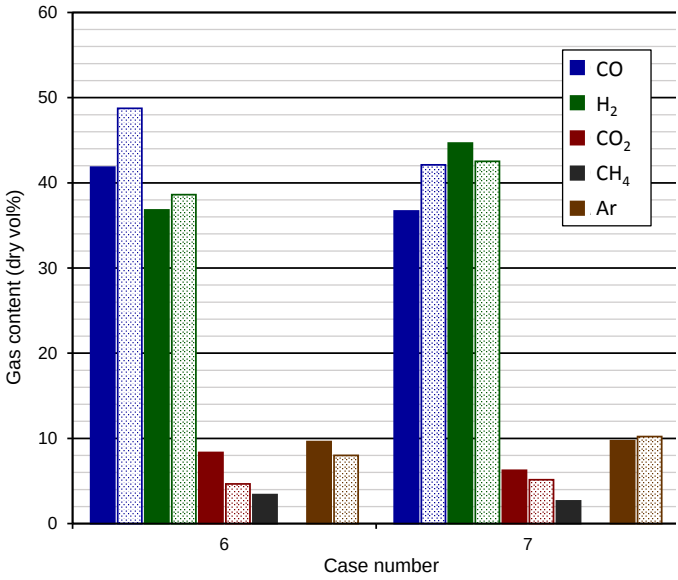

Figure 5.7: Measured (full colour) and theoretical (patterned) syngas composition for Cases 6 and 7, with a combination of CO_2 and H_2O and a combination of O_2 and H_2O as gasifying agent, respectively

and respectively H_2O and CO_2 as gasifying agent, is shown in Figure 5.8. Similar to the other steam plasma gasification cases, numbers 4 and 5, the measured syngas composition of Case 8 is very close to the equilibrium composition. The values of the volumetric percentages of the syngas components of Case 9 are also close to the theoretical values. Although the differences are relatively small, the lower CO and higher CO_2 concentrations suggest that a part of the added CO_2 did not partake in the gasification reactions.
At similar equivalence ratios of respectively 0.32 and 0.30, the change in gasifying agent from H_2O in Case 8 to CO_2 in Case 9, lead the H_2/CO ratio of 0.64 for the latter case to be practically the inverse of the H_2/CO ratio of 1.62 for Case 8.

In the above comparative analysis of the measured syngas composition with the equilibrium composition, no attention has been given to the argon concentration. The argon concentration is only influenced by the total volume of syngas produced and is independent of the process chemistry leading to the syngas composition. With the theoretical composition representing the dry syngas content for complete

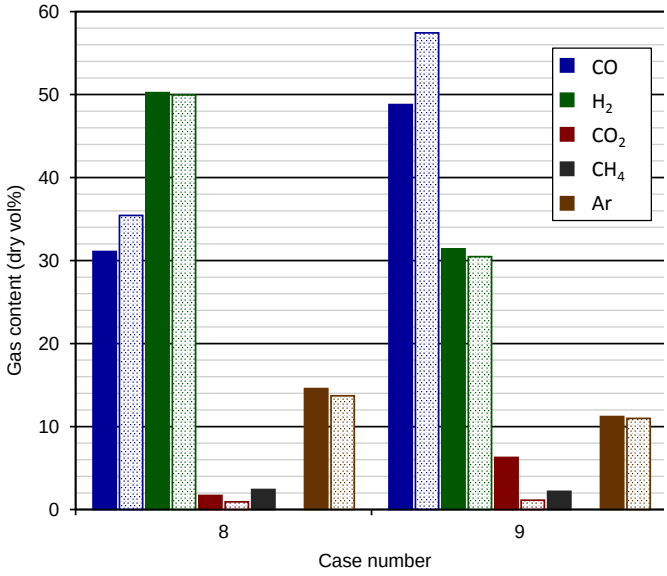

Figure 5.8: Measured (full colour) and theoretical (patterned) syngas composition for Cases 8 and 9, with a reduced RDF feed rate and with H_2O and CO_2 as respective gasifying agents

RDF to syngas conversion, the smaller the difference between actual and theoretical argon concentration, the higher the efficiency of the gasification process.
For Cases 1 to 6, the actual syngas composition shows a higher argon concentration than the theoretical composition, while the exact same amount of argon (i.e. the sum of argon from plasma and argon added as internal standard) is represented by the argon fraction in both compositions. This means that the total volume of produced syngas is lower than the theoretical calculated volume considering complete conversion. The ratio of the theoretical argon volume percent to the measured argon volume percent (i.e. the ratio of the produced volume to the theoretical maximum volume of dry syngas) for Cases 1 to 3 is 89.5, 85.5 and 92.2 %, respectively. The measured syngas composition for Case 3 (with the lowest equivalence ratio) is also closest to the equilibrium composition.
The gasification process in Cases 4 and 5 achieves 84.2 % and 83.1 % of the theoretical maximum conversion to dry syngas, respectively. A similar value of 83.1 % for Case 6 was calculated. Case 7 is the only experiment in which a lower argon concentration in the dry syngas was measured than the theoretical value. The volume of dry syngas produced was estimated (through the internal stand-

ard of argon) at 105 % the theoretical volume at equilibrium conditions. Possible explanations for this high value are:

- Small error margins on the material feed rate and/or gas flow rates.
- Part of the added water as gasifying agent could have reacted through the water-gas shift reaction, which would augment the volume of dry syngas.
- Because of the favourable process conditions (see Table 5.8), the oxy-steam plasma gasification converted some additional previously unreacted material to syngas during the sampling period.

The differences between the volume of dry syngas produced and the theoretical maximum for Cases 8 and 9 are small. Respectively 93.9 % and 98.0 % of the theoretical volume was produced.

This comparison between the produced volume of dry syngas and the theoretical value already leans towards the performance analysis of the experiments, which is discussed in the next paragraph.

5.3.4 Performance Yields and Energy Efficiencies

Besides syngas composition, other frequently used indicators for analysing the performance of plasma gasification processes are carbon conversion efficiency (CCE), CO yield and H_2 yield. Carbon conversion efficiency is defined as the ratio of the amount of carbon in the syngas to the amount of carbon in the feed (i.e. from waste and from CO_2 as gasifying agent):

$$CCE = \frac{\dot{m}_{C,SG}}{\dot{m}_{C,RDF} + \dot{m}_{C,CO_2}} \tag{5.33}$$

where $\dot{m}_{C,SG}$ = mass of carbon exiting with the syngas (CO, CO_2 and CH_4)
$\dot{m}_{C,RDF}$ = mass of carbon entering with the RDF
$\dot{m}_{C,CO_2}$ = mass of carbon entering with CO_2 as gasifying agent

CO yield is defined as the ratio of the amount of carbon in the CO fraction of the syngas to the total amount of carbon injected:

$$\text{CO yield} = \frac{\dot{m}_{C,CO}}{\dot{m}_{C,RDF} + \dot{m}_{C,CO_2}} \tag{5.34}$$

where $\dot{m}_{C,CO}$ = mass of carbon exiting as carbon monoxide

H_2 yield is defined as the ratio of the amount of hydrogen in the H_2 fraction of the syngas to the total amount of hydrogen injected:

$$H_2 \text{ yield} = \frac{\dot{m}_{H,H_2}}{\dot{m}_{H,RDF} + \dot{m}_{H,H_2O}} \tag{5.35}$$

where $\dot{m}_{H,H_2}$ = mass of hydrogen exiting as hydrogen gas
$\dot{m}_{H,RDF}$ = mass of hydrogen entering with the RDF
$\dot{m}_{H,H_2O}$ = mass of hydrogen entering with water as gasifying agent

The values of these performance indicators for all nine cases are plotted in Figure 5.9.

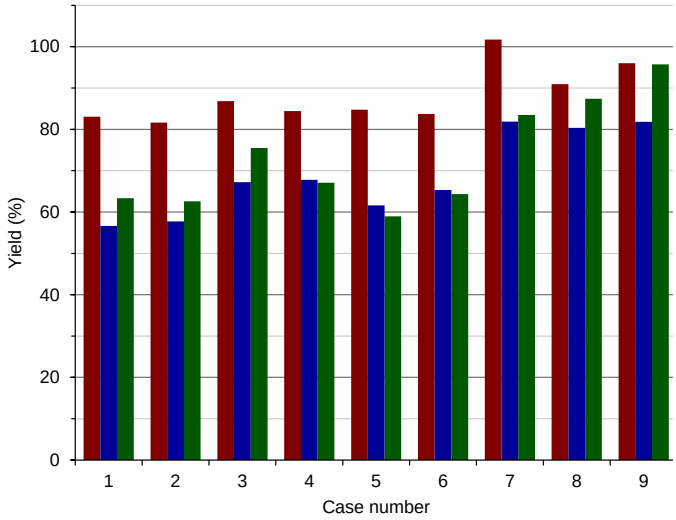

Figure 5.9: Carbon conversion efficiency (red bar), CO yield (blue bar) and H_2 yield (green bar)

Case 1 with the lowest theoretical value or the required energy for the gasification process (Table 5.8) is expected to be the most performant case. However, Case 3 shows the highest values for all three performance indicators at 86 % for the carbon conversion efficiency and 67 % and 76 % for the CO yield and H_2 yield, respectively. The comparative analysis of the measured syngas composition and the theoretical values already showed that the gasification process in Case 3 was performing close to equilibrium conditions, whereas Case 1 showed a larger deviation from equilibrium operation.

The CO and H_2 yield are nearly identical for Case 1 and 2, which indicates that only a limited additional amount of CO_2 is participating in the gasification reactions after reduction of the O_2 flow rate in Case 2. The carbon conversion efficiency is slightly lower, probably because of the lesser amount of energy released from the oxidation reactions with excess oxygen.
The lower flow rate of CO_2 for Case 3, compared to Case 2 leads to a lower value of the denominator in the CO yield and hence a higher value for the CO yield. The higher H_2 concentration in the syngas for Case 3, due to the water-gas shift reaction, significantly increases the H_2 yield. The higher CCE for Case 3 compared to Case 2 is in line with the lower theoretical gasification energy for Case 3 (less CO_2 needs to be heated to process temperature), making more energy available for the gasification reactions.

For the steam plasma gasification, after supplying an additional $85\,\mathrm{ml\,min^{-1}}$ of water in Case 5, the change in carbon conversion efficiency (from 84 to 85 %) is negligible. The H_2 yield decreased from 67 % to 59 %, because of the extra water added, which was not converted to syngas to a sufficient extent. The additional water flow shifted the water-gas shift reaction to the right, converting some of the CO to CO_2, which dropped the CO yield from 68 % to 61 %.
It is interesting to observe that the performance indicators of Case 4 and Case 6 are similar. Although these cases showed very different syngas compositions, the similar equivalence ratio and similar enthalpies of reaction for the overall gasification reaction with H_2O and with CO_2 resulted in only slightly lower process efficiencies for Case 6 than for Case 4. For Cases 1 to 6, the different (combinations of) gasifying agents and equivalence ratios do not seem to impact the carbon conversion efficiency to a great extent. The values of the CCE for these cases stay in the limited range from 82 % to 87 %.

Case 7 shows distinctively different values for the parameters in Figure 5.9 than the other cases. The CO and H_2 yield reach 82 % and 83 %, respectively, and the CCE exceeds 100 %. The high values for these performance criteria, especially the latter, are in line with the result of a higher volume of produced syngas than the theoretical maximum (Paragraph 5.3.3) and the low energy requirement for complete gasification (Paragraph 5.3.2). The possible explanations for the slight overestimation of carbon conversion efficiency exceeding 100 % were previously discussed (Paragraph 5.3.3). Despite the small incongruity, these results demonstrate the high performance of the process of

plasma gasification of RDF with a combination of O_2 and H_2O as gasifying agents.

In terms of energy efficiency, the cold gas efficiency (CGE) and mechanical gasification efficiency (MGE) for the different cases are summarized in Table 5.9, together with syngas yield and lower heating value (LHV) of the syngas.
The cold gas efficiency is the ratio between the chemical energy content in the syngas, and the sum of the chemical energy in the fuel and the electric power consumed by the plasma torch:

$$CGE = \frac{LHV_{syngas} F_{syngas}}{LHV_{RDF} \dot{m}_{RDF} + P_{plasma}} * 100 \tag{5.36}$$

with F_{syngas} the volumetric flow rate of syngas, $\dot{m}_{RDF}$ the mass flow rate of RDF and P_{plasma} the torch power. The lower heating value of syngas is expressed in volumetric units and that of RDF in mass units.
The mechanical gasification efficiency is the ratio between the chemical energy content in the produced syngas compared to the chemical energy in the fuel:

$$MGE = \frac{LHV_{syngas} F_{syngas}}{LHV_{RDF} \dot{m}_{RDF}} * 100 \tag{5.37}$$

The sensible heat of the syngas is not included in these efficiencies. The value of this term is relatively constant for all cases and ranges from 20 kW to 22 kW for the cases with a material feed rate of 28.9 kg h^{-1} and amounts to 16 kW for a material feed rate of 21.3 kg h^{-1}. In this experimental set-up, the produced syngas exiting the reactor at temperatures up to 1550 K is rapidly quenched. In an industrial facility however, part of the sensible heat of the syngas can be recovered and either recirculated into the system, or applied externally (for heat or electricity production).
Furthermore, only the power used for generating the plasma is included in the calculation of the cold gas efficiency. Any auxiliary power necessary for operating the complete system is neglected, since it was only marginal to the torch power. However, in an industrial-sized facility, the additional energy sinks outside of the actual plasma gasification reactor become more pronounced and need to be taken into account when evaluating the energy efficiencies of the system.
In all cases, the single-stage plasma gasification of RDF produced a medium calorific value syngas with a lower heating value (or net calorific value) ranging from 9.0 MJ/Nm^3 to 11.0 MJ/Nm^3. For the plasma gasification of RDF with a mixture of CO_2 and O_2 (Cases 1 to 3), the calorific values of the produced syngas are the lowest, mainly because of the high levels of CO_2 in the syngas composition. Case 3 with the lowest equivalence ratio and lowest CO_2 concentration in the syngas

Table 5.9: Syngas characteristics and energy efficiencies

Case No.	Syngas yield (Nm^3/kg)	LHV (MJ/Nm^3)	CGE (%)	MGE (%)
1	1.69	9.0	42	72
2	1.66	9.2	42	72
3	1.75	9.9	48	82
4	1.88	11.0	57	97
5	1.88	10.7	56	95
6	1.87	10.5	54	92
7	1.86	10.4	53	91
8	2.15	10.2	53	104
9	2.18	10.3	54	106

of the first three cases, yielded the highest CGE and MGE with respective values of 48 % and 82 %.

The energy efficiencies for steam plasma gasification are significantly higher with values of 56 % and 94–95 % for CGE and MGE, respectively. Up to 1.88 Nm^3/kg of syngas is produced with the highest calorific values of all cases (10.7–11.0 MJ/Nm^3).

An important aspect in the analysis of the steam plasma gasification cases is the fact that only the dry syngas content is considered in the syngas characteristics. The flow of unreacted gasifying agent leaving the reactor as water vapour for Case 4 and 5 (and Case 7) is not taken into account. In contrast, when CO_2 is added as gasifying agent, the (excess) CO_2 is registered by the mass spectrometer and included in the calculation of syngas heating value, which lowers its value.

Cases 1 to 3 display significant lower syngas yields than Cases 4 to 7, which have the same material feed rates, despite showing comparable (and even higher) carbon conversion efficiencies. Additionally it is expected that lower volumes of water vapour are neglected in the dry syngas flow for Cases 1 to 3. The reason for the lower syngas yields is the use of O_2 as gasifying agent which harbours two moles of mono-atomic oxygen available to the process per mole of oxygen gas. Hence, the volumes of CO_2 and H_2O as gasifying agents supplied to the system need to be twice as high in order to add the same amount of available oxygen, augmenting the total volume of gas in the system.

This explanation also applies for the difference in syngas yield between Case 7 and Cases 8 and 9. However, the syngas yields for Cases 8 and 9 seem disproportionately high considering the lower equivalence ratios and lower gasification

efficiencies, compared to those from Case 7. The calculated theoretical energy for the gasification process for Case 8 and 9 was also not significantly lower than for example Cases 4 to 6.
Two possible interpretations of these apparent discrepancies in syngas yield are either that the material feed rate in Case 7 was in fact lower than 28.9 kg/h or that the material feed rate in Cases 8 and 9 were higher than the estimated 21.3 kg/h. The latter explanation is considered more acceptable since a lower material feed rate for Case 7 would increase its carbon conversion efficiency even more (significantly exceeding 100 %), which seems unlikely.

5.3.5 Tar Analysis

Gas samples were taken at three instances during the experiment. The gas sampling for Sample 1 was done in the time period selected for Case 8, but the time instances of Samples 2 and 3 do not coincide with any identified time periods at steady state operation. Samples 2 and 3 were taken during material feed rates of $56.7\,\mathrm{kg\,h^{-1}}$ with a combination of 192 slm CO_2 and $293\,\mathrm{ml\,min^{-1}}$ H_2O and with $463\,\mathrm{ml\,min^{-1}}$ H_2O, respectively.
The total tar content in the three gas samples increases from 132 to 370 and $543\,\mathrm{mg/Nm^3}$, with ascending sample number. The tar species with the highest concentrations are shown in Table 5.10. The concentration of the BTX fraction

Table 5.10: Concentrations of the most abundant tar species

Tar species	Sample number		
(mg/Nm^3)	1	2	3
BTX	0	1.4	1.1
Naphthalene	78.6	205.8	155.5
Acenaphthylene	7.4	90.7	35.8
Phenanthrene	8.4	67.3	51.6
Pyrene	7.2	31.9	29.6
Fluorene	1.8	12.6	3.9
Fluoranthene	6.7	32.3	32.9
Biphenyl	3.2	21.1	12.4

(benzene, toluene and xylene) is very low. This is in line with the chemical components generally found with high-temperature steam gasification, as reported by Elliot [51].
Naphthalene is by far the most abundant tar component. The total tar level is significantly lower for the case with the lowest material feed rate.

Plasma gasification experiments performed on wood resulted in a lower tar content ($< 10\,mg/Nm^3$) [79]. This is most likely because of the heterogeneous nature of the RDF and the coarser particle size. On the other hand, the tar level was lower than in the syngas obtained from conventional RDF gasification, which is typically in the range of 1-100 g/Nm^3, depending on the type of gasifier. Nevertheless, a cleaning step would be necessary prior to downstream application of the syngas in a gas engine, gas turbine or fuel cell, which have tar tolerance levels of about 50, 5 and 1 mg/Nm^3, respectively.

5.3.6 Residue Analysis

After the experiment, the reactor was opened and the solid residue was collected. The total mass of the residue from the reactor volume was 12.6 kg and an additional 1.65 kg of solids was recovered from the filter. There was also an unknown amount of material found in the pipes. Samples of the material from the bottom and top of the reactor were taken. The main part of the residual ash was in the form of particulates (Figure 5.10(a)), but at the bottom molten solids could be seen (Figure 5.10(b)).

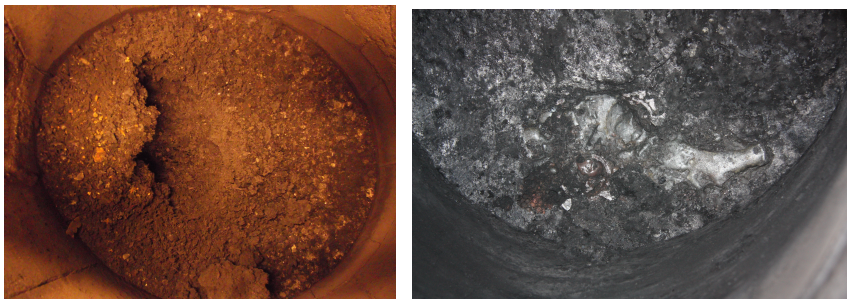

(a) Residue as particulates

(b) Molten residue at the bottom

Figure 5.10: Visualization of the residual ash fraction in the reactor volume

A summary of the results from the thermogravimetric analysis is depicted in Table 5.11. The results show that during the experiments, unreacted material collects at the bottom of the reactor. There is a small deviation of 3 % on the sum of volatile organic compounds (VOC), fixed carbon and mineral ash, but this is because of the accuracy of the thermogravimetric analysis. The VOC in the accumulated residue at the top is lower than at the bottom, since this material was more directly exposed to the high-temperature flow of plasma.

Table 5.11: Proximate analysis of solid residue samples based on TGA

	Bottom wt%	Top wt%
VOC	34	5
fixed carbon	16	39
mineral ash	53	53

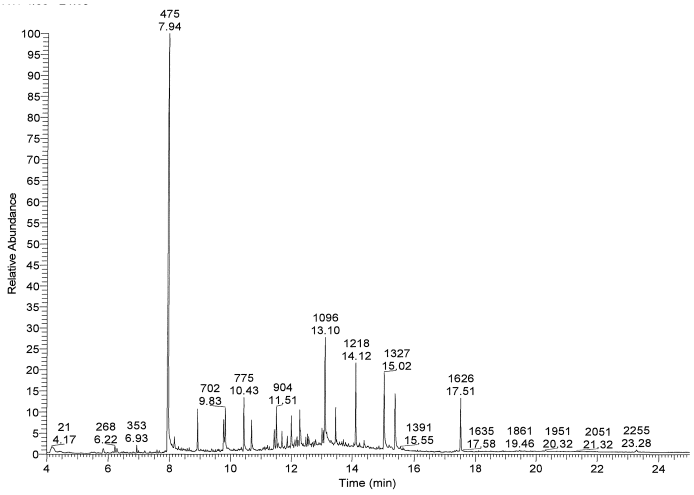

Figure 5.11: Chromatogram of top sample

The chromatograms of both samples are displayed in Figure 5.11 and 5.12.
A short list of identified chemical compounds with the highest peaks is shown in Table 5.12 with their relative concentration expressed in µg/g.
Similar compounds as in the results from the gas tar analysis are found, with naphthalene present in the highest concentration.

5.3.7 Comparison with Single-Stage Biomass Plasma Gasification

A number of experiments with various materials have been performed on the single-stage reactor at IPP. Besides polyethylene, pyrolysis oil from waste tyres and plastic waste, biomass (spruce) in the shape of pellets or as sawdust has been the material of choice. Adapted results from experiments previously published in Hrabovský et al. [83] are qualitatively compared to the results from the RDF experiments.

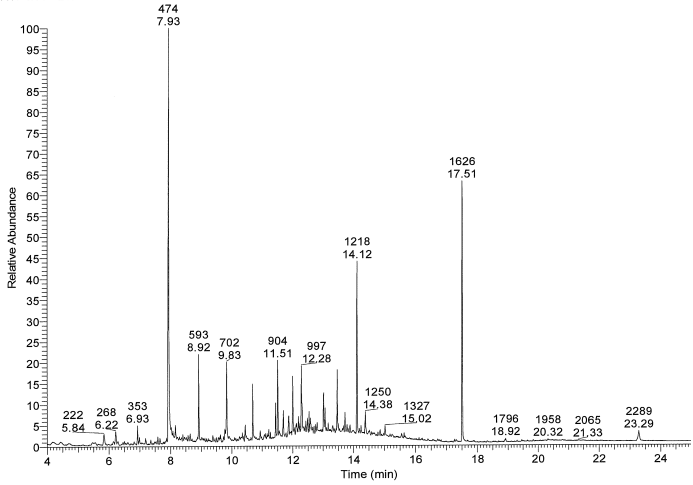

Figure 5.12: Chromatogram of bottom sample

Table 5.12: List of the most abundant chemical compounds from GC of ash samples

Scan No.	Chemical compound	Bottom	Top
474	naphthalene	54.75	118
593	C13H28	11.17	7.91
702	C14H30	13.52	12.19
775	acenaphthylene	2.02	11.5
997	C17H36	11.3	6.26
1096	anthracene	-	25.4
1218	diisobutyl phthalate	24.32	23.23
1327	fluoranthene	-	22.48
1370	pyrene	-	14.2
1626	diisooctyl phthalate	29.9	9.89

The biggest differences in the material composition between biomass and RDF are the higher moisture content (12.2 wt%), the very low ash fraction and a much higher oxygen content. No quantitative comparison can be made about the syngas composition because of the different material composition, material feed rate ($44\,\mathrm{kg\,h^{-1}}$) and equivalence ratios. Three experimental cases of sawdust gasification with respectively H_2O, a mixture of CO_2 and H_2O and a mixture of O_2 and H_2O as gasifying agents are therefore qualitatively compared with Case 4, Case

6 and Case 7. The operational parameters for these experiments are summarized in Table 5.13.

Table 5.13: Process parameters of the gasification cases with sawdust.

Case number	T (K)	F_{H_2O} (ml min^{-1})	F_{CO_2} (slm)	F_{O_2} (slm)	ER
B1	1460	70.4	0	0	0.17
B2	1418	70.4	87.8	0	0.24
B3	1443	70.4	0	44.2	0.24

The syngas composition (coloured bars) and the calculated equilibrium composition (patterned bars) for these biomass cases are shown in Figure 5.13.

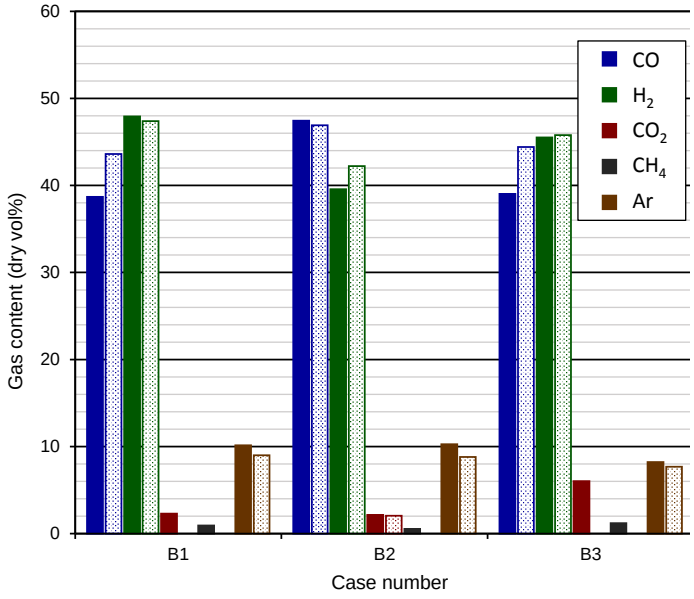

Figure 5.13: Measured (full colour) and theoretical (patterned) syngas composition for the biomass cases

Overall, the CH_4 concentrations are lower in the syngas from biomass gasification than in that from RDF gasification. The measured gas content does not necessarily match the theoretical composition to a greater degree than for the RDF experiments. The same trends in the H_2/CO ratio depending on the type of gasifying agent(s) used can be observed (Table 5.14).

Table 5.14: Comparison of performance parameters of RDF experiments Cases 4, 6 and 7 and biomass experiments Cases B1, B2 and B3.

Parameter	Material	Gasifying agents		
		H_2O	CO_2+H_2O	O_2+H_2O
H_2/CO	RDF	1.75	0.88	1.22
	Biomass	1.24	0.83	1.17
CCE	RDF	84	84	102
	Biomass	85	88	93
CO yield	RDF	68	65	82
	Biomass	79	83	78
H_2 yield	RDF	67	64	84
	Biomass	89	73	84

For both materials, the values of the H_2/CO ratio are very similar for the gasification with a combination of CO_2 and H_2O and with a combination of O_2 and H_2O. For steam plasma gasification, the value for RDF was significantly higher than for biomass, caused by the even larger difference in equivalence ratio and the much larger amount of water added to the system. Hwang et al. [92] suggested an accelerated degradation of RDF in the presence of steam due to a catalytic effect of ash. Although no prove for this assertion was found in their reported reference, other research has confirmed the promoting effect of mineral matter on the steam gasification of coal [101, 160].

The CCE, CO and H_2 yields are higher for biomass than for RDF, except for the case with O_2 and H_2O. The difference in carbon conversion efficiency between the two material types is not as high as the differences in the other yields. The cold gas efficiencies and mechanical gasification efficiencies are higher with biomass than with RDF at values of 65–66 % and 105–107 %, respectively. Despite the lower ER and the higher material feed rate, the plasma gasification of the single-type material (biomass) proves more performant than the plasma gasification with RDF. The small particle size (i.e. high surface area) allows better mass and heat transfer, the high oxygen and moisture content in the material means an evenly distributed oxygen availability throughout the material and more energy is available for the gasification process because less energy is spent on heating a considerable ash fraction and a larger volume of gasifying agents.

5.3.8 Comparison with Two-Stage RDF Plasma Gasification

Publicly available results from plasma gasification experiments with RDF are very scarce. An interesting plasma gasification facility, which is well-documented in literature is the demonstration plant of Advanced Plasma Power (APP) in Swindon (UK). This two-stage system consists of an oxy-steam bubbling fluidised bed gasification step followed by a plasma converter, in which the syngas and the solid residue from the former step are treated.
Experiments in which RDF is converted to syngas in this system are published by Materazzi et al. [121]. The main differences in RDF composition are compared in Table 5.15.

Table 5.15: Comparative analysis of RDF composition between the RDF used in the experiments (RDF_{IPP}) and the RDF from Materazzi et al. [121] (RDF_{APP})

Proximate analysis (wt%dry)			Ultimate analysis (wt%dry)		
	RDF_{IPP}	RDF_{APP}		RDF_{IPP}	RDF_{APP}
Moisture	4.6	6.3	C	46.8	58.65
Ash	22.1	13.7	H	5.7	8.35
			O	22.3	16.03

The RDF used in the two-stage plasma gasification experiments has a lower ash content, higher carbon content, higher hydrogen content and lower oxygen content. The moisture content is similar and the net calorific value is slightly higher ($24.92\,MJ\,kg^{-1}$ as received compared to $22.37\,MJ\,kg^{-1}$ dry).
All process parameters of the two-stage plasma gasification experiments are higher than those from the single-stage oxy-steam plasma gasification experiment (Case 7) (Table 5.16). In the two-stage gasification, the heat necessary for the gasification reactions is produced from complete oxidation of part of the material. This results in the higher CO_2 content and lower CO/CO_2 ratio compared to the single-stage case. This also affects the H_2/CO ratio, which is only slightly higher, despite the higher hydrogen content in the material and the higher steam to oxygen ratio.
In Taylor et al. [181], the carbon conversion efficiency and mechanical energy of an experiment with RDF, similar to the one described by Materazzi et al. [121] is reported to be 99 and 94 %. These values correspond well with the ones for the oxy-steam single-stage plasma gasification in Case 7 (101 and 91 %). Because of the lack of publicly available data about the plasma power used in the plasma

Table 5.16: Comparative analysis of process parameters and syngas characteristics between the single-stage experiments (EXP) and the two-stage experiments from Materazzi et al. [121] (REF)

Process parameters	EXP	REF	Syngas characteristics	EXP	REF
RDF feed rate (kg/h)	29	50–60	CO	40.6	31.5
O_2/fuel (w/w)	0.34	0.5–0.6	H_2	49.5	41.2
H_2O/O_2 (mol/mol)	1.64	2.4–3.6	CO_2	6.9	16.4
			CH_4	2.9	1.6
			Inerts[a]	–	9.3
			CO/CO_2	5.88	1.92
			H_2/CO	1.22	1.31
			GHV[b] (MJ/Nm^3)	12.62	9.49

[a] The inert argon fraction in the syngas from single-stage experiments is not considered because it is not inherent to the gasification process (except the negligible amount of argon from plasma)

[b] The gross heating value (GHV) is given for a dry, inert-free syngas

converter step, no quantitative comparison can be made between the cold gas efficiency of the two-step and single-step plasma gasification systems.

Although no value for the total tar content in the syngas leaving the plasma converter is published, it is clear from the negligible levels of benzene, toluene, phenol and hexane after the plasma converter, that tar removal is effective in the two-stage system. The maximum concentration of the BTEX aromatics (benzene, toluene, ethylbenzene and xylene) in the syngas samples from in-flight single-stage plasma gasification system was very low at $1.4\,mg/Nm^3$. The largest tar substance groups detected in the produced syngas were naphthalenes and other polyaromatic hydrocarbons with concentrations of two orders of magnitude higher, unfortunately no data about those tar components were reported for the two-stage system.

An obvious advantage of the two-stage system is that the residual inorganic fraction leaving the plasma converter was successfully vitrified into a slag, whereas the non-gasified fraction in the single-stage system did not reach its melting point and was for the most part recovered as solid particulates. The vitrified slag is suitable for further materials processing (e.g. fabrication of ceramic glass products or road construction material), while the unmelted residue has little to no value as a by-product from gasification.

5.3.9 Comparison with Conventional RDF Conversion Methods

The two main thermochemical conversion methods which are considered for dedicated RDF treatment are fluidised bed incineration and (conventional) gasification. For fluidised bed combustion, a net electrical efficiency of 25.1 % was reported by VITO [197]. An industrial example of this technology is the largest circulating fluidized bed incinerator in Germany, located in Höchst. This plant operates in co-generation mode and produces approximately 70 MW of power and 250 metric tons of steam per hour from 678 000 metric tons of RDF (i.e. a thermal throughput of 270 MW). This is a net electrical efficiency of almost 26 %. The renewed interest in gasification technology has initiated a large number of (research) projects and realizations. Since 2012, the world's largest RDF gasification power plant is commercially operational in Lahti, Finland. It processes 250 000 tons of RDF per year and produces 50 MW of electricity and 90 MW of district heat from 160 MW of solid waste fuel power. The produced syngas is sent to a gas boiler from which a steam turbine is fed. The design power production efficiency is 31 % in combined heat and power mode with fuel utilization ratio of 87.5 %. The reported electrical efficiency of the RDF gasification facility is higher than for fluidized bed incineration.

These efficiencies can be compared to the performance of the single-stage plasma gasification experiments with RDF presented above. With the combinations of the process conditions, i.e. material feed rates, torch power, type of gasifying agent(s) and equivalence ratio, employed in the different cases, no net energy production from the syngas would be possible. In general, the material throughput was too low with respect to the torch power. The system did not perform at its maximum capacity for half of the cases according to the theoretical calculation of the required energy for the gasification process (Table 5.8). Especially the energy requirements for the cases with O_2 as gasifying agent in combination with CO_2 (Cases 1 to 3) or H_2O (Case 7) leave room for significantly higher material feed rates and consequently higher energy outputs.
Arena [7] reports that a plasma gasification facility typically requires about $1200\,\mathrm{MJ/t_{waste}}$ to $2500\,\mathrm{MJ/t_{waste}}$ to operate the plasma torch. In the presented experiments, this value was about $15\,\mathrm{MJ\,kg^{-1}}$. It is clearly important to adjust the power of the torch and the material feed rate and test the performance of the system with conditions which can yield a more positive energetic balance.

A low energy use is not only a prerequisite for becoming competitive in the waste-to-energy sector, but it is equally important for the implementation of plasma gasification as a waste-to-materials technology. The application of syngas as feedstock for the production of hydrogen, ammonia, methanol or liquid hydrocarbons (via Fischer-Tropsch process) are perhaps more interesting routes in terms of resource recovery than energy production. The description of these valorization pathways was previously presented in Section 2.5.1.2 and a detailed overview of these processes can be found in a technical report from 2003 by the National Renewable Energy Laboratory [176]. It is necessary to conduct a life-cycle assessment, which takes, among others, the environmental impact, land-use and economic aspects in account for the possible end-uses in each specific project in order to assess the viability of plasma gasification of waste as the most suitable production pathway.

The assessment of the feasibility of plasma gasification compared to other traditional treatment methods should not be limited to the comparison of the energy balance, but the performance of the entire system should be considered. This includes all aspects including ash-handling, (syn)gas cleaning, pretreatment steps, fuel flexibility, environmental impact, etc. While the presented plasma gasification experiments underperformed in energy terms, one of the added values of plasma gasification is the production of a much cleaner syngas. This reduces the extent and cost of the gas cleaning step. Furthermore, the energy content of the product gas is higher because a larger part of the heating value of the waste is converted to syngas in stead of being consumed to supply the necessary heat for the gasification reactions. The higher quality syngas can be either converted to electricity with more advanced technologies, such as gas turbines or fuel cells, or used for the production of chemicals with less pretreatment.
The residual ash fraction after plasma gasification is generally recovered as a non-leachable, inert, molten slag. In the current configuration of the single-stage plasma gasification system, this was achieved to only a very small extent. The vitrified slag can be valorized as a by-product, which omits the need of ash-handling and disposal as in conventional gasification. This can achieve a significant cost-saving by the elimination of the different sorting, cleaning, stabilization and solidification steps of the bottom ash.

Finally, it should be noted that the environmental benefits of plasma gasification in all steps of a waste conversion system compared to traditional RDF treatment

technologies (incineration and conventional gasification) are only relevant if the electricity used for generating the plasma is coming from renewable sources.

5.4 Conclusions

In this chapter, the results from a plasma gasification experiment with RDF were presented. The tests were conducted on the single-stage plasma gasification unit at IPP using five different combinations of gasifying agents (CO_2+O_2, H_2O, CO_2, CO_2+H_2O and O_2+H_2O). The composition of the produced syngas was compared with the theoretical composition, assuming thermodynamic equilibrium and the performance of the different cases was assessed based on process yields and energy efficiencies. The plasma gasification of RDF yielded a medium calorific value syngas for all cases with a lower heating value up to 11.0 MJ/Nm^3.
The carbon conversion efficiency was relatively insensitive to the type of gasifying agent used and to the equivalence ratio, and maintained a value between 82 and 87 % for Cases 1 to 6 with a material feed rate of 28.9 kg/h. The CO yield, H_2 yield and CCE for the oxy-steam gasification were significantly higher than for the other cases. It is assumed that these much larger values (e.g CCE exceeding 100 %) were caused by some previously unreacted material which was gasified during the sampling period. It is also possible that small error margins on the material feed rate and/or gas flow rates should be taken into account.
From the three cases using a combination of CO_2 and O_2 as gasifying agents, the influence of the amount of oxygen added as gasifying agent on the process performance was identified.
The syngas yield in Cases 8 and 9 with a material feed rate of 21.3 $kg\,h^{-1}$ are significantly higher than those in the other cases. From the comparison with Case 7, it can be concluded that the material feed rates are likely to be somewhat higher than the set value.

Overall, the measured syngas composition was relatively close to the theoretical composition, suggesting that the conditions inside the reactor during the plasma gasification process were close to thermodynamic equilibrium. The best similarity between measured and calculated syngas composition was found for steam plasma gasification. Additionally, the energy efficiencies of Cases 4 and 5 were the highest with values of 57 % and 97 % for cold gas efficiency and mechanical gasification efficiency, respectively. The H_2/CO ratio of the syngas from Case 5 was 1.95, which is close to the optimum ratio needed by the Fischer-Tropsch process.
From the comparative analysis of Case 4 and Case 6, it was shown that at a

constant equivalence ratio, CO_2 and H_2O as gasifying agents can be interchanged to control the syngas composition while maintaining a relatively constant performance of the process. The theoretical estimation of the energy required for the gasification process showed that the available energy to the system by the plasma torch was not sufficient to achieve complete conversion for the cases with CO_2 and H_2O or combinations thereof as gasifying agents. The gasification processes with O_2 as gasifying agent in combination with CO_2 or H_2O need less energy and did not reach their maximum capacity during the experiments.
The tar analysis of syngas samples showed low total tar content varying from 132 to 543 mg/Nm^3 with napthalene as the most abundant tar species. These tar levels are lower than for conventional gasification, but higher than previous tar measurements during biomass plasma gasification. Napthalene was also found in the highest concentrations in the two ash samples. The mineral ash content was 53 % throughout the collected residual fraction of the gasified material. Most of the material was recovered as particulates and a small portion of the ash was molten in the slip stream of the plasma jet.

Further comparative analysis between RDF and biomass plasma gasification revealed similar trends in syngas composition (H_2/CO ratio) depending on the type of gasifying agent(s) used. Despite more favourable process conditions for the RDF experiments (lower material feed rate and higher ER), the performance of the gasification of the single-type biomass material was higher than that of RDF gasification. This suggests the influence of particle size, ash and moisture content, and oxygen distribution of the material on the gasification efficiency.
Finally, it can be concluded that the syngas from single-stage oxy-steam plasma gasification has some advantageous characteristics over the syngas from two-stage oxy-steam plasma gasification. The high level of CO_2 from complete oxidation of the material in the latter process leads to a lower sum of carbon monoxide and hydrogen and a lower CO/CO_2 ratio. In both systems, the high-temperature and high level of radiation from plasma successfully broke down the tar content to very low levels. In the plasma converter step of the two-stage plasma gasification system, the solid residue was melted to a vitrified slag which can be valorised. In contrast, the residual material in the single-stage gasification reactor did not reach its melting point and was recovered as particulates, not suitable for further applications.

The current conversion methods for dedicated RDF treatment are predominantly

conventional gasification and (circulating) fluidised bed incineration. Based on information of two commercial installations using these technologies, it can be concluded that the gasification plant yields a higher net electrical efficiency at 31 %. The material feed rates in the plasma gasification experiments were not high enough and the process parameters not optimized to allow any net electricity production from the produced syngas. However, given the high performance of the gasification with O_2 and H_2O as gasifying agents and the low theoretical values for the energy required for complete gasification, similar efficiencies for plasma gasification are definitely possible. The potential advantages of the plasma element in the process (such as valorisation of the mineral fraction) should be evaluated in a holistic approach, preferably on a demonstration unit with higher material throughput.

The presented results showed that plasma gasification is a promising treatment technology for refuse-derived fuel. The flexibility of the system allows to control the characteristics of the produced syngas by the choice of gasifying agent(s).

Conclusions and Future Work

Conclusions

An elaborate study on the effects of approximating mixing rules for the calculation of thermodynamic and transport properties of a gas mixture on the simulated flow field was performed. This involved the development of a plasma jet model for the DC hybrid water/gas-stabilized torch, which boundary conditions were thoroughly evaluated. Three LES simulations with different models which employ mixing rules for thermophysical properties in different ways (or not al all) were successfully completed. The results showed substantial differences from the use of mixing rules, especially between two reacting gases (N_2 and H_2O). These can be primarily attributed to the poor accuracy of the mixing rules of Wilke, and Mason and Saxena which were used for dynamic viscosity and thermal conductivity, respectively. They are frequently used by researchers because of their simplicity and ease of implementation. Often, the large deviations of the calculated values from the exact values are ignored by stating that the contribution of the laminar transport properties with respect to their turbulent counterparts is negligible.
This assumption was proven not to be self-evident, since the different molecular transport properties were responsible for a different flow structure which led to a much faster onset of turbulence and entrainment of surrounding gas. The flow field of model 3 could be clearly distinguished form the two other models which used mixing models. With model 3, for the specific gas mixture studied in this work, the exact thermal conductivity values were much higher than the estimated ones in model 1 and model 2, which caused a higher conductive heat transfer in the radial direction. The resulting higher temperatures consequently increased the values of viscosity in the shear layer of the plasma jet. These higher viscosity values have a stabilizing effect on the flow in the shear layer, hence delaying the onset of turbulent mixing with the surrounding gas. This was observed by the higher temperature and velocity profiles and lower nitrogen concentration profiles at positions downstream of the torch exit.
The specific effects of the deviations from the exact values for the thermodynamic and transport properties of a gas mixture, introduced by approximating mixing

rules, can differ with each particular plasma problem and the corresponding boundary conditions in the simulation. Nevertheless, the results obtained with this work reveal that it is important to use correct thermophysical properties (especially transport properties) because the effects of erroneous approximations can be manifested in the laminar high-temperature region and in the shear layer of the plasma jet.

The successful conversion of solid materials to syngas with the plasma gasification system at the Institute of Plasma Physics (IPP) in Prague has been demonstrated and documented since 2005. Previous test campaigns on this system were mainly limited to homogeneous model substances with a very low inorganic content, such as biomass and plastics. To achieve the objective of demonstrating the effective treatment of a waste stream containing a high inorganic fraction, experiments with refuse-derived fuel (RDF) were performed. Over the course of the experimental run, different combinations of gasifying agents (CO_2, H_2O and O_2) were added to the reactor volume and different material feeding rates were set. Although the execution of these experiments gave rise to some complications (e.g. blocking of the feeding mechanism), caused by the inhomogeneous nature of the waste material, it was possible to analyse the performance of nine cases with different operational parameters. The fast response time and the constant composition and flow of syngas during steady-state operation the system are notable, given the invariability of the feed.

The syngas composition in all cases is in close agreement with the theoretical equilibrium composition, especially for the cases with water vapour as gasifying agent. Based on the clear trends in syngas composition between the different cases, it can be concluded that plasma gasification allows a good control of the syngas composition by adjusting the amount and type of gasifying agent. Based on the performance criteria (carbon conversion efficiency, CO yield and H_2 yield), it was clear that the optimal conditions of the oxy-steam plasma gasification case achieved the most performant conversion to syngas. The criteria and energy efficiencies of the other plasma gasification cases also showed reasonably good values, but it is believed that the performance of the process can be increased by adjusting the process parameter (and the corresponding amount of energy required for complete conversion of the waste) to the available energy in the system (net plasma energy).

The residual material in the reactor vessel after the experiments was mainly collected as particulates, which indicates that the inorganic fraction of the waste did

not reach its melting point. It can therefore be concluded that the single-stage in-flight plasma gasification system in the current configuration is not ideally suited for the immobilisation of the ash fraction to a valuable vitrified by-product. The analysis of the level of tar in the produced syngas was limited to three gas samples, but revealed a destruction efficiency of unwanted complex higher hydrocarbons which is higher than for conventional gasification.

From the production of high-quality syngas with low levels of tar at good process yield and the improved control of the syngas characteristics, it can be concluded that plasma gasification is rightfully labelled an advanced technology for waste treatment.

Future work

The future work related to CFD modelling of plasma (jets) will greatly benefit from the rapid advancement of computing capacities and computing power. Therefore, in the foreseeable future, it might be possible to incorporate the rigorous calculation of thermodynamic and transport properties of a multicomponent gas mixtures directly in the calculation routines of a CFD simulation. Until then, an approach for more accurate calculation of thermophysical properties in flow simulations could be developed which links the multicomponent model in the quasi-laminar high-temperature region of the plasma flow with a model relying on mixing rules in the lower-temperature, turbulent region where the gas can interact with a large number of additional gases (e.g. syngas in plasma gasification).

Future work in the field of plasma gasification will without a doubt entail numerous experimental studies. Learning from the challenges encountered during the analysis of the experimental results, it is strongly suggested to allow sufficiently long time periods for each set of operating conditions. This improves the quality of the statistically averaged process variables. Additionally, there is a scarcity of data about unwanted contaminants in the syngas besides tar, such as nitrous oxides (NOx), sulphur oxides (SOx), halogens, etc. Along with more quantitative tar measurements (e.g. for each set of process parameters), it is advised to monitor those components more intensively. Furthermore, while predictive equilibrium plasma gasification models might not attribute significantly to the understanding of the specific processes of the plasma gasification processes, they should be consulted a priory when establishing an experimental plan to choose appropriate operating conditions in relation to the capacity of the system.
Not only will future experiments be directed towards maximizing the gasification performance by optimal adjustment of the process parameters, they can simultaneously function as experimental validation of CFD modelling of the system. The CFD modelling of plasma gasification systems is only in the early-development

stage and provides huge opportunities for future research. The challenging task of combining the correct representation of the plasma flow, solving the flow equations while taking turbulent mixing and other physical phenomena into account, describing detailed mass and heat transfer mechanisms between the multicomponent gas flow and the solid particles, and including an extensive set of chemical reactions and their kinetics can benefit the development of the plasma gasification technology immensely. This is illustrated by the following example. The shortcoming of the single-stage in-flight plasma gasification system in converting the inorganic fraction of the treated material has been addressed by two-stage plasma gasification systems in which the melting of the ash and metals is separated from the gasification process. In some systems, this plasma conversion unit also incorporates the destruction of unwanted components in the syngas by passing it through the melter volume. By separating the plasma element from the gasification aspect, the process becomes autothermal and the quality and the energy content of the syngas decreases. Developing a system which allows the efficient production of a high quality syngas (in terms of composition and energy content) with low levels of polluting contaminants and the immobilization of the inorganic fraction into a valuable by-product simultaneously could be achieved by design optimization with a comprehensive CFD model.

Additionally, the development of plasma gasification for research purposes has advanced to the stage where the performance of the process should be evaluated on a larger scale. The design for up-scaling can also be optimized by a previous suggested comprehensive CFD model.

Appendices

APPENDIX A

Expression for the Diffusion Flux in a Three-Component Mixture in Terms of Binary Combined Diffusion Coefficients

A gas mixture of Ar (A), H_2O (B) and N_2 (C) is considered. The diffusion flux of gas A (consisting of species 1 to p) can be written as:

$$\bar{J_A} = \frac{N^2}{\rho} \sum_{i=1}^{p} k_i m_i \sum_{j=1}^{q} m_j D_{ij} \nabla x_j^{(3)} - \sum_{i=1}^{p} k_i D_i^T \nabla \ln T \tag{A.1}$$

in which $i = 1,...,q$ corresponds to the species making up gas B and C. N is the total number density and $x_j^{(3)}$ represents the mole fraction of species j in the three-component gas mixture. For further details on the derivation of this expression, see Murphy [132].

Because the mole fraction of species j ($x_j^{(3)}$) is function of temperature and composition, and because composition is determined by the mole fractions of two out of three gases, the gradient of the mole fraction becomes:

$$\nabla x_j^{(3)} = \left.\frac{\partial x_j^{(3)}}{\partial x_B}\right|_{x_C,T} \nabla x_B + \left.\frac{\partial x_j^{(3)}}{\partial x_C}\right|_{x_B,T} \nabla x_C + \left.\frac{\partial x_j^{(3)}}{\partial T}\right|_{x_B,x_C} \nabla T \tag{A.2}$$

in which x_B and x_C are respectively the mole fractions of gas B and gas C at temperature T. The species 1 to q are the collection of species originating from both gas B and gas C. Since no combination species are considered between species

from B and species from C, the species 1,...,q can be split up into 1,...,q_B (species from gas B) and q_{B+1},...,q_C (species from gas C).
The following relations are then being considered:

– For $j = 1, ..., q_B$: $$\left.\frac{\partial x_j^{(3)}}{\partial x_C}\right|_{x_B,T} \cong 0$$

– For $j = q_B + 1, ..., q_C$: $$\left.\frac{\partial x_j^{(3)}}{\partial x_B}\right|_{x_C,T} \cong 0 \tag{A.3}$$

– For $j = 1, ..., q_B$:

- $$\left.\frac{\partial x_j^{(3)}}{\partial T}\right|_{x_B,x_C} \cong \left.\frac{\partial x_j^{(2)}}{\partial T}\right|_{x_B} \tag{A.4}$$
- $$\left.\frac{\partial x_j^{(3)}}{\partial x_B}\right|_{x_C,T} \cong \left.\frac{\partial x_j^{(2)}}{\partial x_B}\right|_{T} \tag{A.5}$$

with $x_j^{(2)}$ the mole fraction of species j in the binary gas mixture of A and B with the same mole fraction of gas B, x_B as in the three-component gas mixture.

– For $j = q_B + 1, ..., q_C$:

- $$\left.\frac{\partial x_j^{(3)}}{\partial T}\right|_{x_B,x_C} \cong \left.\frac{\partial x_j^{(2)}}{\partial T}\right|_{x_C} \tag{A.6}$$
- $$\left.\frac{\partial x_j^{(3)}}{\partial x_C}\right|_{x_B,T} \cong \left.\frac{\partial x_j^{(2)}}{\partial x_C}\right|_{T} \tag{A.7}$$

with $x_j^{(2)}$ the mole fraction of species j in the binary gas mixture of A and C with the same mole fraction of gas C, x_C as in the three-component gas mixture.

With the definitions of combined diffusion coefficients:

$$\overline{D^x_{AB}} = \frac{1}{m_A m_B} \sum_{i=1}^{p} k_i m_i \sum_{j=1}^{q_B} m_j D_{ij} \left. \frac{\partial x_j^{(2)}}{\partial \bar{x}_B} \right|_T \tag{A.8}$$

$$\overline{D^x_{AC}} = \frac{1}{m_A m_C} \sum_{i=1}^{p} k_i m_i \sum_{j=p_B+1}^{q_C} m_j D_{ij} \left. \frac{\partial x_j^{(2)}}{\partial \bar{x}_C} \right|_T \tag{A.9}$$

$$\overline{D^T_{AB}} = -\frac{N^2}{\rho} \sum_{i=1}^{p} k_i m_i \sum_{j=1}^{q_B} m_j D_{ij} \left. \frac{\partial x_j^{(2)}}{\partial T} \right|_{x_B} + \sum_{i=1}^{p} k_i D_i^{T(AB)} \tag{A.10}$$

with $D_i^{T(AB)}$ the thermal diffusion coefficient of species i in the binary mixture of A and B

$$\overline{D^T_{AC}} = -\frac{N^2}{\rho} \sum_{i=1}^{p} k_i m_i \sum_{j=q_B+1}^{q_C} m_j D_{ij} \left. \frac{\partial x_j^{(2)}}{\partial T} \right|_{x_C} + \sum_{i=1}^{p} k_i D_i^{T(AC)} \tag{A.11}$$

with $D_i^{T(AC)}$ the thermal diffusion coefficient of species i in the binary mixture of A and C

(A.12)

The diffusion flux of gas A becomes:

$$\begin{aligned} \bar{J}_A = & \frac{N^2}{\rho} \left(m_A m_B \overline{D^x_{AB}}\,(x_B, T)\, \nabla x_B + m_A m_C \overline{D^x_{AC}}\,(x_C, T)\, \nabla x_C \right) \\ & - \overline{D^T_{AB}}\,(x_B, T)\, \nabla \ln T - \overline{D^T_{AC}}\,(x_C, T)\, \nabla \ln T + S \end{aligned} \tag{A.13}$$

with the extra term S:

$$S = \sum_{i=1}^{p} k_i D_i^{T(AB)} \nabla \ln T + \sum_{i=1}^{p} k_i D_i^{T(AC)} \nabla \ln T + \sum_{i}^{p} k_i D_i^{T(3)} \nabla \ln T \tag{A.14}$$

in which $D_i^{T(3)}$ is the thermal diffusion coefficient of species i in the three-component mixture.

The term S consists of the terms describing the Soret effect, which is considered small, therefore the term S is neglected in the expression for the diffusion flux of gas A in the three-component mixture of A, B and C.

APPENDIX

Comparison of the Position of the Dissociation Peaks Between Thermal Conductivity and Heat Capacity

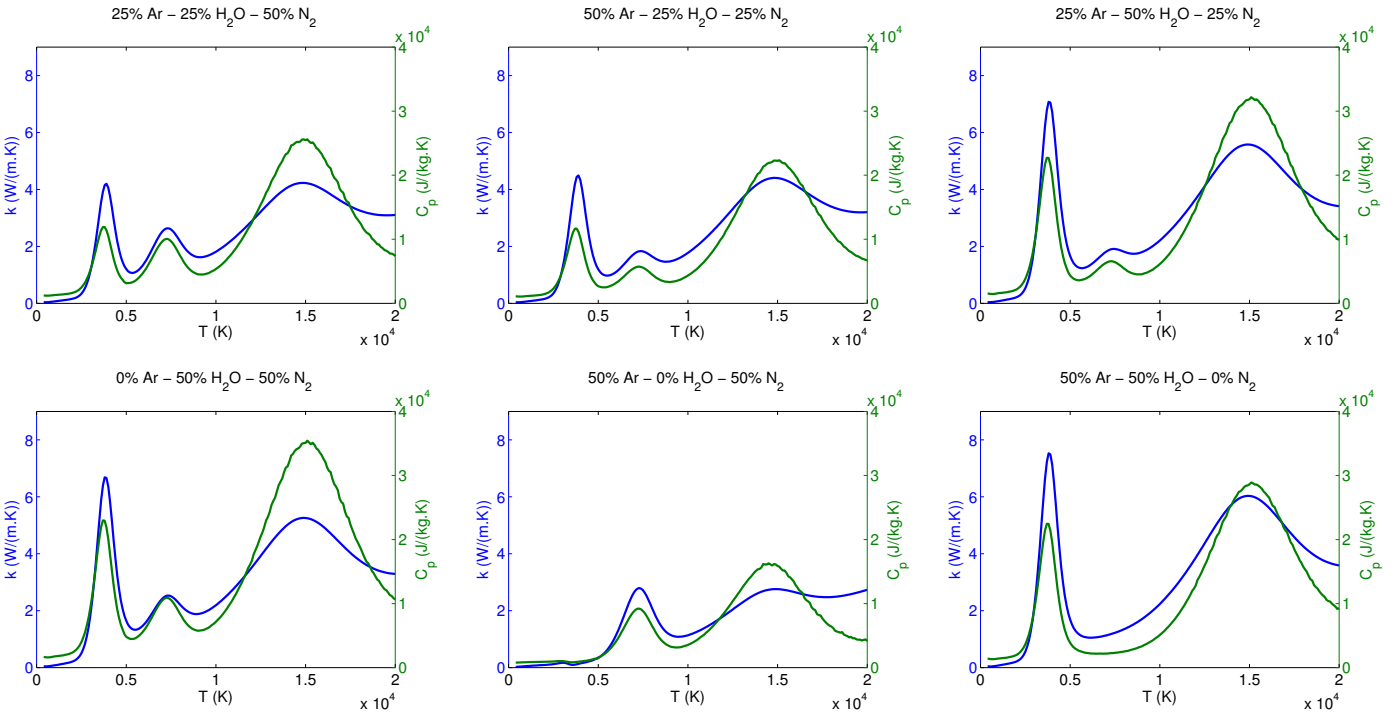

Figure B.1: Comparison of the location of the dissociation peaks for thermal conductivity (blue line) and heat capacity (green line) calculated with model 1 for six different gas mixture compositions.

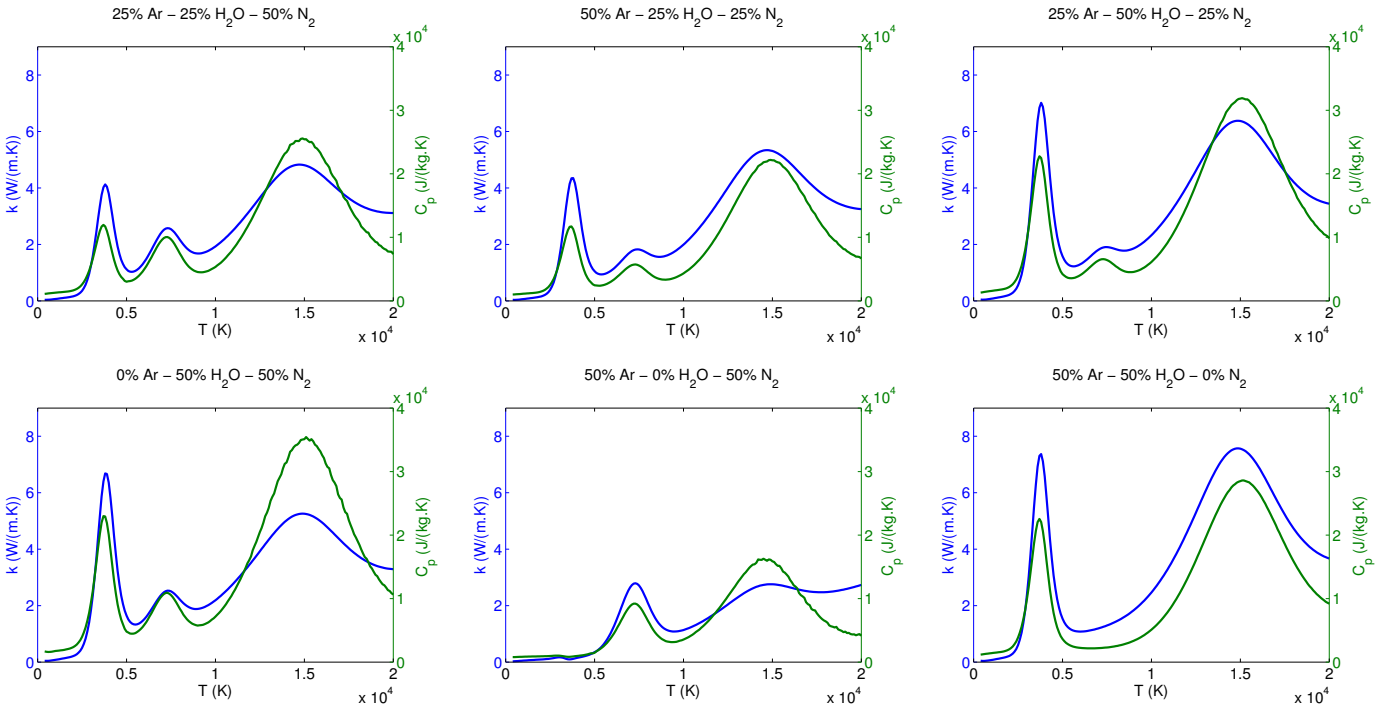

Figure B.2: Comparison of the location of the dissociation peaks for thermal conductivity (blue line) and heat capacity (green line) calculated with model 2 for six different gas mixture compositions.

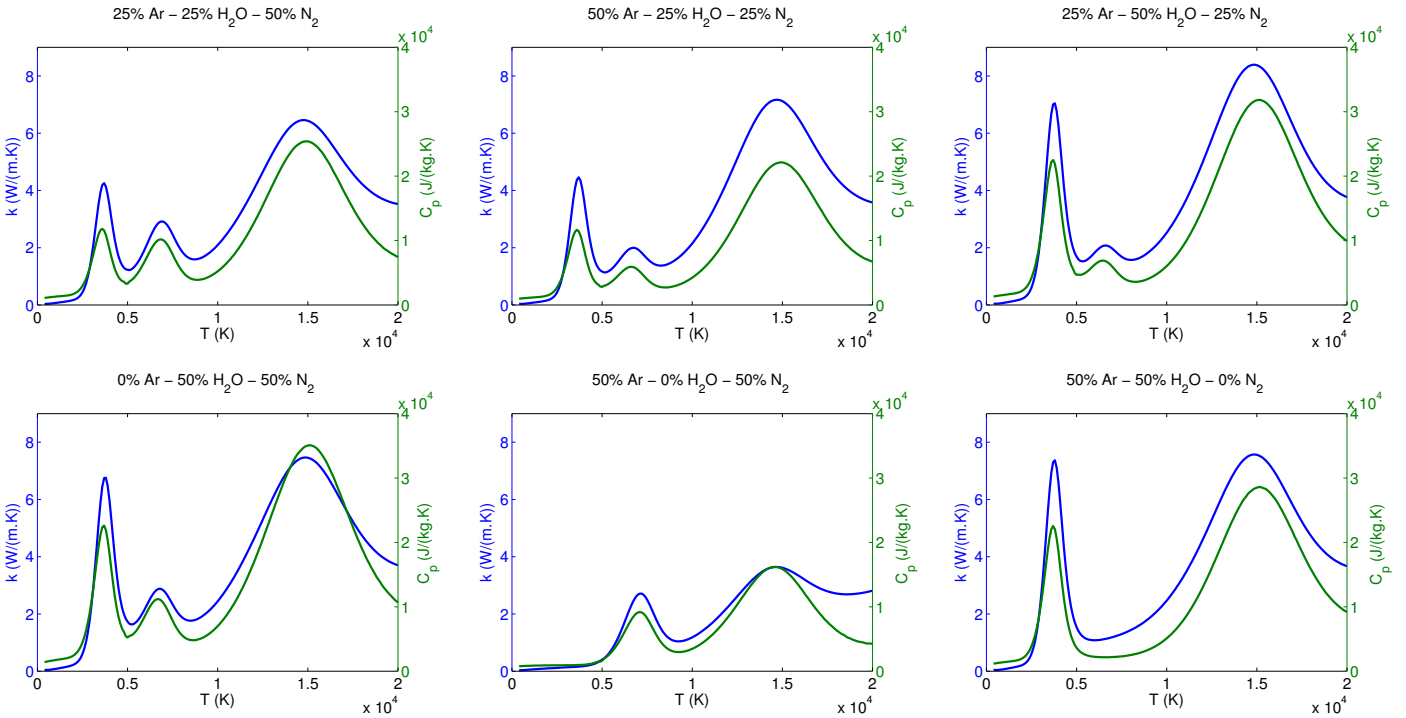

Figure B.3: Comparison of the location of the dissociation peaks for thermal conductivity (blue line) and heat capacity (green line) calculated with model 3 for six different gas mixture compositions.

List of Figures

List of Tables

List of Publications

Peer-reviewed papers

- N. Agon, J. Vierendeels, M. Hrabovský, A.B. Murphy and G. Van Oost. Interaction of a H_2O/Ar plasma jet with nitrogen atmosphere: Effect of method for calculating thermophysical properties of the gas mixture on the flow field. *Plasma Chemistry and Plasma Processing*, 35:365-389, 2015.
- N. Agon, M. Hrabovský, O. Chumak, M. Hlína, V. Kopecký, A. Mašláni, A. Bosmans, L. Helsen, S. Skoblja, G. Van Oost and J. Vierendeels. Plasma gasification of refuse derived fuel in a single-stage system using different gasifying agents. *Waste Management*, article in press, 2015.

Conference Proceedings

- N. Agon, J. Vierendeels, M. Hrabovský and G. Van Oost. *Modeling of thermal plasma jet in open atmosphere - investigation of the method for calculating thermodynamic and transport properties of the gas mixture.* XX^{th} Symposium on Physics of Switching Arc, September 2-6, Nové Město na Moravě (Czech Republic), 2013.
- N. Agon, T. Kavka, J. Vierendeels, M. Hrabovský and G. Van Oost. *LES simulation of a hybrid water/gas DC thermal plasma torch in open atmosphere - experimental comparison.* 9^{th} International Symposium on Applied Plasma Science, September 23-27, Istanbul (Turkey), 2013.
- N. Agon, A. Chumak, M. Hrabovský, M. Hlína, V. Kopecký, A. Mašláni, A. Bosmans, L. Helsen, G. Van Oost and J. Vierendeels. *Single-stage plasma gasification of RDF.* 22^{nd} International Symposium on Plasma Chemistry, July 5-10, Antwerp (Belgium), 2015.

Bibliography

[1] S. Achinas and E. Kapetanios. Basic design of an integrated plasma gasification combined cycle system for electricity generation from RDF. *International Journal of Engineering Research & Technology*, 1:1–8, 2012.

[2] S. Achinas and E. Kapetanios. Efficiency evaluation of RDF plasma gasification process. *Energy and Environment Research*, 3(1):150–157, 2013.

[3] adaptiveARC. adaptiveARC, 2015. `http://adaptivearc.com/` (accessed February 16, 2015).

[4] T. Alexakis, P. Tsantrizos, A. Kaldas, S. Pelletier, and P. Manoliadis. Compact plasma waste elimination system for ships. *International conference on ship design and operation for environmental sustainability*, London, United Kingdom, 2002.

[5] T. Alexakis, P. Tsantrizos, P. Manoliadis, D. Beverly, and S. Pelletier. A plasma-assisted thermal treatment system for shipboard waste. *Conference on Incineration and Thermal Treatment Technologies*, New Orleans, Louisiana, USA, 2002.

[6] B. Amigun, J. Gorgens, and H. Knoetze. Biomethanol production from gasification on non-woody plant in South-Africa: optimum scale and economic performance. *Energy Policy*, 38:312–322, 2010.

[7] U. Arena. Process and technological aspects of municipal solid waste gasification. A review. *Waste Management*, 32:625–639, 2012.

[8] V. Aubrecht, M. Bartlova, F. Urban, and J. Valenta. Partial characteristics of radiation for thermal plasmas in H_2O and argon. *15^{th} International Conference on Gas Discharges and their applications*, 141–144, Toulouse, France, 2004.

[9] B.V. Babu. Chemical kinetics and dynamics of plasma-assisted pyrolysis of assorted non-nuclear waste. `http://citeseerx.ist.psu.edu/viewdoc/download?doi=10.1.1.207.1778&rep=rep1&type=pdf` (Accessed February 2, 2015).

[10] M. Balat. Potential importance of hydrogen as a future solution to environmental and transportation problems. *International Journal of Hydrogen Energy*, 33:4013–4029, 2008.

[11] A. P. Ballantyne, C. B. Alden, J. B. Miller, P. P. Tans, and J. W. C. White. Increase in observed net carbon dioxide uptake by land and oceans during the past 50 years. *Nature*, 488(7409):70, 2012.

[12] G. Balmigere, E. Meillot, S. Vincent, and J-P. Caltagirone. Unstady 3D Large Eddy Simulation of an Ar-H_2 plasma jet: analysis of initial results. *Thermal Spray: Global Coating Solutions: Proceedings of the 2007 International Thermal Spray Conference*, 185–189, Bejing, China, 2007.

[13] C. Baudry, G. Mariaux, A. Vardelle, C. Delalondre, and E. Meillot. Modeling of arc formation in a DC plasma spray torch. *16^{th} International Symposium on Plasma Chemistry*, Taormina, Italy, 2003.

[14] P.J. Bhuyan and K.S. Goswami. Two-dimensional and three-dimensional simulation of DC plasma torches. *IEEE Transactions on Plasma Science*, 35:1781–1786, 2007.

[15] A. Bogaerts, E. Neyts, R. Gijbels, and J. van der Mullen. Gas discharge plasmas and their applications. *Spectrochimica Acta Part B-Atomic Spectroscopy*, 57(4):609–658, 2002.

[16] A. Bosmans, I. Vanderreydt, D. Geysen, and L. Helsen. The crucial role of waste-to-energy technologies in enhanced landfill mining: a technology review. *Journal of Cleaner Production*, 55:10–23, 2013.

[17] M. I. Boulos. Thermal plasma processing. *IEEE Transactions on Plasma Science*, 19(6):1078–1089, 1991.

[18] M. I. Boulos, P. Fauchais, and E. Pfender. *Thermal plasmas: fundamentals and applications.* Plenum Press, New York, USA, 1994.

[19] A. Boussagol, G. Mariaux, E. Legros, A. Vardelle, and P. Nylen. 3-D modeling of a DC plasma jet using different commercial CFD codes. *15^{th} International Symposium on Plasma Chemistry*, 1015–1020, Orléans, France, 2001. GREMI-CNRS.

[20] N. S. J. Braithwaite. Introduction to gas discharges. *Plasma Sources Science & Technology*, 9(4):517–527, 2000.

[21] A.N. Bratsev, I.I. Kumkova, V.A. Kuznetov, V.E. Popov, S.V. Shtengel, and A.A. Ufimtsev. Air plasma gasification of RDF as a prospective method for reduction of carbon dioxide emission. *IOP Conference Series: Materials Science and Engineering*, 19:1–6, 2011.

[22] V. Březina, Hrabovský M., M. Konrád, V. Kopecký, and V. Sember. New plasma spraying torch with combined gas-liquid stabilization of arc. *5^{th} International Symposium on Plasma Chemistry (ISPC 15)*, Orléans, France, 2001.

[23] J. Burgard. Coskata integrated bio-refinery technology - Update on commercialization progress. Report, Coskata, 2010.

[24] Y. Byun, M. Cho, S-M. Hwang, and J. Chung. Thermal plasma gasification of municipal solid waste (MSW), In Y. Yun, editor, *Gasification for practical applications*, book section 7. InTech, 2012.

[25] C. Cagliardi, A. Gorodetsky, B. Grichin, J. James, A. Newman, F. Petrocelli, and J. Santoianni. The value of pilot plant studies in advancing the understanding of plasma gasification of municipal solid waste. IChemE New Horizons in Gasification, editor, *12^{th} European Gasification Conference*, Rotterdam, The Netherlands, 2014.

[26] Cahill Energy. Cahill Energy to invest $240 million in Barbados clean energy plant. Press Release, 2014.

[27] M.W. Chase. *NIST-JANAF thermochemical tables.* Gaithersburg, Maryland, 1998.

[28] K. Cheng, X. Chen, and W. Pan. Comparison of laminar and turbulent thermal plasma jet characteristics - a modeling study. *Plasma Chemistry and Plasma Processing*, 26:211–235, 2006.

[29] J. Chianello and M. Pearson. Ottawa severs ties with Plasco as company files for creditor protection, 2015.

[30] C. Chronopoulos, P. Chevalier, I. Picard, A. Kaldas, P. Carabin, and G. Holcroft. The plasma arc waste destruction system - one year of maritime experience. *24^{th} International Conference on Incineration and Thermal Treatment Technologies*, Galveston, Texas, USA, 2005.

[31] O. Chumak, M. Hrabovský, and V. Kopecký. Interaction between anode attachment and plasma jet in DC arc plasma spraying torch. V. Zhovtyansky, editor, *International Conference on Physics of Low Temperature Plasma*, Kiev, Ukraine, 2003.

[32] Y-P. Chyou. R&D concepts and status of IGCC+POLYGEN+CCS technologies in Taiwan. *Taiwan Symposium on Carbon Dioxide Capture, Storage and Utilization*, Taipei, Taiwan, 2012.

[33] V. Colombo and E. Ghedini. Time dependent 3-D simulation of a DC nontransferred arc plasma torch: anode attachment and downstream region effects. *17th International Symposium on Plasma Chemistry*, 169, Toronto, Canada, 2005.

[34] V. Colombo, E. Ghedini, and P. Sanibondi. A three dimensional investigation of the effects of the excitation frequency and sheath gas mixing in an atmospheric pressure inductively coupled plasma system. *Journal of Physics D: Applied Physics*, 43:1–13, 2010.

[35] Committee on the effectiveness of international and national measures to prevent and reduce marine debris and its impacts. *Tackling marine debris in the 21th century.* The National Academies Press, Washington, D.C., USA, 2009.

[36] H. Conrads and M. Schmidt. Plasma generation and plasma sources. *Plasma Sources Science and Technology*, 9:441–454, 2000.

[37] O. Coufal. Composition and thermodynamic properties of thermal plasma up to 50kK. *Journal of Physics D: Applied Physics*, 40:3371–3385, 2007.

[38] O. Coufal, P. Sezemsky, and O. Živný. Database system of thermodynamic properties of individual substances at high temperatures. *Journal of Physics D: Applied Physics*, 38:1265–1274, 2005.

[39] O. Coufal and O. Živný. Composition and thermodynamic properties of thermal plasma with condensed phases. *European Physical Journal D*, 61(1):131–151, 2011.

[40] V. Cozzani, C. Nicolella, L. Petarca, M. Rovatti, and L. Tognotti. A fundamental study on conventional pyrolysis of a refuse-derived fuel. *Industrial & Engineering Chemistry Research*, 34(6):2006–2020, 1995.

[41] G. Crandell. The foundry of the future casting manufacturing as 'Green Energy Center'. *American Foundry Society's (AFS) 22nd Environmental, Health and Safety (EHS) Conference*, Nashville, Tennessee, USA, 2010.

[42] F. Creutzig, J. C. Goldschmidt, P. Lehmann, E. Schmid, F. von Blucher, C. Breyer, B. Fernandez, M. Jakob, B. Knopf, S. Lohrey, T. Susca, and K. Wiegandt. Catching two European birds with one renewable stone: mitigating climate change and Eurozone crisis by an energy transition. *Renewable & Sustainable Energy Reviews*, 38:1015–1028, 2014.

[43] G. D'Alessio. Gasificación de "pulper waste" mediante technología de plasma. *Congreso Nacional del Medio Ambiente*, Madrid, Spain, 2008.

[44] De Openbare Afvalstoffenmaatschappij voor het Vlaamse Gewest (OVAM). Uitvoeringsplan gescheiden inzameling bedrijfsafval van klein ondernemingen. Report, OVAM, 2000.

[45] D. Deegan, C. Chapman, S. Ismail, M. Wise, and H. Ly. The thermal treatment of hazardous waste materials using plasma arc technology. *IMechE Conference on Delivering Waste Solutions Balancing Targets, Incentives and Infrastructures*, London, UK, 2006.

[46] A. Demirbas. Biorefineries: current activities and future developments. *Energy Conversion and Management*, 50:2782–2801, 2009.

[47] S.V. Dighe. Plasma gasification: a proven technology. *16th Annual North American Waste-to-energy conference*, Philadelphia, Pennsylvania, USA, 2008.

[48] A.H. Dilawari, J. Szekeley, R. Westhoff, B.A. Detering, and Shaw Jr. C.B. A comparison of the experimentally measured and theoretically predicted temperature profiles for an argon jet discharging into a nitrogen environment. *MRS Spring Meeting & Exhibit*, San Fransisco, California, USA, 1990.

[49] P. Eichert, M. Imbert, and C. Coddet. Numerical study of an Ar-H_2 gas mixture flowing inside and outside a DC plasma torch. *Journal of Thermal Spray Technology*, 7:505–512, 1998.

[50] M.F. Elchinger, B. Pateyron, P. Fauchais, and A. Vardelle. Calculation of thermodynamic and transport properties of Ar-H_2-air plasma , comparison with simple mixing rules, 1997.

[51] D.C. Elliot. Relation of reaction time and temperature to chemical composition of pyrolysis oils, In E.J. Soltes and T.A. Milne, editors, *Pyrolysis oils from biomass*, book section 6. American Chemical Society, Denver, Colorado (USA), 1988.

[52] European Committee for Standardization. Draft report from CEN TF -118 on solid recovered fuels (part 1). Report, CEN, 2001.

[53] F. Fabry, C. Rehmet, V. Rohani, and L. Fulcheri. Waste gasification by thermal plasma: a review. *Waste and Biomass Valorization*, 4(3):421–439, 2013.

[54] K. Fang, D. Li, M. Lin, M. Xiang, W. Wei, and Y. Sun. A short review of heterogeneous catalytic process for mixed alcohols synthesis via syngas. *Catalysis Today*, 147:133–138, 2009.

[55] P. Fauchais and A. Vardelle. Plasma spraying - present and future. *Pure and Applied Chemistry*, 66:1247–1258, 1994.

[56] P. Fauchais and A. Vardelle. Thermal plasmas. *IEEE Transactions on Plasma Science*, 25:1258–1280, 1997.

[57] P. Fauchais and A. Vardelle. Pending problems in thermal plasmas and actual development. *Plasma Physics and Controlled Fusion*, 42:B365–B383, 2000.

[58] D. Flynn. Plasma ordnance demilitarization system (PODS) for the destruction of pyrotechnic ordnance. *Global Demilitarization Symposium & Exhibition*, Reno, Nevada, USA, 2007.

[59] A. Fridman and L.A. Kennedy. Elementary processes of charged species in plasma, In *Plasma Physics and Engineering*, book section 2, pages 15–72. CRC Press, 2004.

[60] FutureNrg. FutureNrg, 2014. `http://www.futurenrg.net/` (accessed April 22, 2015).

[61] G. Galeno, M. Minutillo, and A. Perna. From waste to electricity through integrated plasma gasification/fuel cell (IPGFC) system. *International Journal of Hydrogen Energy*, 36(2):1692–1701, 2011.

[62] P. Galindo-Cifre and O. Badr. Renewable hydrogen utilisation for the production of methanol. *Energy Conversion and Management*, 48:519–527, 2007.

[63] A. Gendebien, A. Leavens, K. Blackmore, A. Godley, K. Lewin, K.J. Whiting, R. Davis, J. Giegrich, H. Fehrenbach, U. Gromke, N. del Bufalo, and D. Hogg. Refuse derived fuel, current practice and perspectives (B4-3040/2000/306517/MAR/E3). Report, European Commission - Directorate General Environment, 2003.

[64] T.B. Gibbons and I.G. Wright. A review of materials for gas turbines firing syngas fuels. Report, Oak Ridge National Laboratory, 2009.

[65] S. Giddey, S. P. S. Badwal, A. Kulkarni, and C. Munnings. A comprehensive review of direct carbon fuel cell technology. *Progress in Energy and Combustion Science*, 38(3):360–399, 2012.

[66] A. Gleizes, Y. Cressault, and Ph. Teulet. Mixing rules for thermal plasma properties in mixtures of argon, air and metallic vapours. *Plasma Sources Science and Technology*, 19:1–13, 2010.

[67] A. Gleizes, J.J. Gonzalez, and P. Freton. Thermal plasma modelling. *Journal of Physics D: Applied Physics*, 38:R153–R183, 2005.

[68] E. Gomez, D. A. Rani, C. R. Cheeseman, D. Deegan, M. Wise, and A. R. Boccaccini. Thermal plasma technology for the treatment of wastes: a critical review. *Journal of Hazardous Materials*, 161(2-3):614–626, 2009.

[69] Government Liquidation. Plasma arc system at Norfolk, Virginia. Report, US Government, 2007.

[70] P. Grammelis. Report on RDF/SRF utilization applications and technical specifications. Report, CERTH/ISFTA, 2011.

[71] D. Guenadou, E. Meillot, and A. Saget. Particle treatment modeling in a time-dependent DC plasma flow. *International Thermal Spray Conference*, Basel, Switzerland, 2005.

[72] A.K. Gupta and W. Cichonski. Ultrahigh temperature steam gasification of biomass and solid wastes. *Environmental Engineering Science*, 24:1179–1189, 2007.

[73] J. Heberlein and A. B. Murphy. Thermal plasma waste treatment. *Journal of Physics D-Applied Physics*, 41(5), 2008.

[74] J.V.R. Heberlein. Generation of thermal and pseudo–thermal plasmas. *Pure Applied Chemistry*, 64(5):629–636, 1992.

[75] L. Helsen and A. Bosmans. Waste-to-energy through thermochemical processes: matching waste with process. *International Academic Symposium on Enhanced Landfill Mining*, Houthalen-Helchteren, Belgium, 2010.

[76] Hera Group. Sustainability Report. Report, Hera Group, 2010.

[77] G. Herdin. Gasmotorentechnologie für Holzgas. *'Syngas: l'enfant terrible'*, Montichiari, Italy, 2013.

[78] J.O. Hirschfelder. Heat transfer in chemically reacting mixtures. *Journal of Chemical Physics*, 26:271–285, 1957.

[79] M. Hlína, M. Hrabovský, V. Kopecký, M. Konrád, T. Kavka, and S. Skoblja. Plasma gasification of wood and production of gas with low content of tar. *Czechoslovak Journal of Physics*, 56:B1179–B1184, 2006.

[80] M. Hoel and S. Kverndokk. Depletion of fossil fuels and the impacts of global warming. *Resource and Energy Economics*, 18(2):115–136, 1996.

[81] M. Hrabovský. Generation of thermal plasmas in liquid-stabilized and hybrid DC-arc torches. *Pure Applied Chemistry*, 74(3):429–433, 2002.

[82] M. Hrabovský. Thermal plasma gasification of biomass, In S.S. Shaukat, editor, *Progress in biomass and bioenergy production*, book section 3. InTech, 2011.

[83] M. Hrabovský, M. Hlína, M. Konrád, V. Kopecký, O. Chumak, A. Mašláni, T. Kavka, O. Živný, and G. Pellet. Steam plasma-assisted gasification of organic waste by reactions with water, CO_2 and O_2. *21^{th} International Symposium on Plasma Chemistry (ISPC 21)*, 2013.

[84] M. Hrabovský, M. Hlína, M. Konrád, V. Kopecký, T. Kavka, O. Chumak, and A. Mašláni. Thermal plasma gasification of biomass for fuel gas production. *High Temperature Material Processes*, 13(3-4):299–313, 2009.

[85] M. Hrabovský, M. Konrád, V. Kopecký, M. Hlína, T. Kavka, O. Chumak, and A. Mašláni. Steam plasma gasification of pyrolytic oil from used tires. *20^{th} International Symposium on Plasma Chemistry*, 200–203, Drexel University, Philadelphia, U.S.A., 2011.

[86] M. Hrabovský, M. Konrád, V. Kopecký, M. Hlína, T. Kavka, O. Chumak, A. Mašláni, and G. Van Oost. Plasma aided gasification of biomass and plastics using CO_2 as oxidizer. *International Symposium on Non-Thermal/Thermal Plasma Pollution Control Technology & Sustainable Energy (ISNTP 7)*, 2010.

[87] M. Hrabovský, M. Konrád, V. Kopecký, M. Hlína, T. Kavka, O. Chumak, G. Van Oost, E. Beeckman, and B. Defoort. Pyrolysis of wood in arc plasma for syngas production. *High Temperature Material Processes*, 10(4):557–570, 2006.

[88] M. Hrabovský, M. Konrád, V. Kopecký, M. Hlína, T. Kavka, G. Van Oost, E. Beeckman, and B. Defoort. Gasification of biomass in water/gas-stabilized plasma for syngas production. *Czechoslovak Journal of Physics*, 56:B1199–B1206, 2006.

[89] M. Hrabovský, V. Kopecký, and P. Macura. Investigation of propagation of perturbations in thermal DC arc plasma jet. *Progress in Plasma Processing of Materials*, 223–228, Strasbourg, France, 2001.

[90] M. Hrabovský, V. Kopecký, V. Sember, T. Kavka, O. Chumak, and M. Konrád. Properties of hybrid water/gas DC arc plasma torch. *IEEE Transactions on Plasma Science*, 34(4):1566–1575, 2006.

[91] R. Huang, H. Fukunuma, Y. Uesugi, and Y. Tanaka. An improved local thermal equilibrium model of DC arc plasma torch. *IEEE Transactions on Plasma Science*, 39:1974–1982, 2011.

[92] I. H. Hwang, J. Kobayashi, and K. Kawamoto. Characterization of products obtained from pyrolysis and steam gasification of wood waste, RDF, and RPF. *Waste Management*, 34(2):402–410, 2014.

[93] Integrated Environmental Technologies. InEnTec Inc., 2015. `http://www.inentec.com/` (accessed April 22, 2015).

[94] Israel NewTech. Israeli cleantech companies catalog. Report, The Israel Export & International Cooperation Institute, 2011.

[95] S. Janssens. *Modeling of heat and mass transfer in a reactor for plasma gasification using a hybrid gas-water torch.* Thesis, Universiteit Gent, 2007.

[96] P.T. Jones, D. Geysen, Y. Tielemans, S. Van Passel, Y. Pontikes, B. Blanpain, M. Quaghebeur, and N. Hoekstra. Enhanced Landfill Mining in view of multiple resource recovery: a critical review. *Journal of Cleaner Production*, 55:45–55, 2013.

[97] Juniper Consultancy Services Limited. The Alter NRG / Westinghouse plasma gasification process. Report, Alter NRG, 2008.

[98] A. Kaldas and G. Alexander. Sixty day endurance testing of the plasma arc waste destruction system (PAWDS). *27th Conference on Incineration and Thermal Treatment Technologies*, Montreal, Quebec, Canada, 2008.

[99] T. Kavka, V. Kopecký, V. Sember, A. Mašláni, and O. Chumak. Analysis of plasma jets generated in gas and gas-water torches. *High Temperature Material Processes*, 11:59–70, 2007.

[100] O. Kitani and C.W. Hall. *Biomass Handbook*. Gordon and Breach Science Publishers, 1989.

[101] Y. Kong, J. Kim, D. Chun, S. Lee, Y. Rhim, J. Lim, H. Choi, S. Kim, and J. Yoo. Comparative studies on steam gasification of ash-free coals and their original raw coals. *International Journal of Hydrogen Energy*, 39(17):9212–9220, 2014.

[102] R. Krampitz, I. Horn, A. Quack, and U. Werner. Jetzt das Plasma - an der Schwelle zur Kreislaufwirtschaft für die Veredelung von Kohlenstoffträger. *51st Internationales Wissenschaftliches Kolloquium*, Ilmenau, Germany, 2006.

[103] T. Kraus. Hydrogen fuel - an economically viable future for the transportation industry? Culminating project for Economics 195S, 2007.

[104] P. Krenek. Thermophysical properties of H_2O-Ar plasmas at temperatures 400-50,000 K and pressure 0.1 MPa. *Plasma Chemistry and Plasma Processing*, 28:107–122, 2008.

[105] B. Kruyt, D. P. van Vuuren, H. J. M. de Vries, and H. Groenenberg. Indicators for energy security. *Energy Policy*, 37(6):2166–2181, 2009.

[106] A. Kumar, D. D. Jones, and M. A. Hanna. Thermochemical biomass gasification: a review of the current status of the technology. *Energies*, 2(3):556–581, 2009.

[107] F.S. Lau, D.A. Bowen, R. Dihu, S. Doong, E.E. Hughes, R. Remick, R. Slimane, S.Q. Turn, and R. Zabransky. Techno-economic analysis of hydrogen production by gasification of biomass. Report, Gas Technology Institute, December 2002. Final Technical Report for the Period September 15, 2001 to September 14, 2002.

[108] E. Leal-Quiros. Plasma processing of municipal solid waste. *Brazilian Journal of Physics*, 34(4B):1587–1593, 2004.

[109] B. Lemmens, H. Elslander, I. Vanderreydt, K. Peys, L. Diels, M. Oosterlinck, and M. Joos. Assessment of plasma gasification of high caloric waste streams. *Waste Management*, 27(11):1562–1569, 2007.

[110] H-P. Li and X. Chen. Three-dimensional modeling of a DC non-transferred arc plasma torch. *Journal of Physics D: Applied Physics*, 34:L99–L102, 2001.

[111] H-P. Li and E. Pfender. Three dimensional modeling of the plasma spray process. *Journal of Thermal Spray Technology*, 16:245–260, 2007.

[112] X. Li, D. Chen, M. Rong, and R. Dai. Study of the influence of Cu vapour on air arc characteristics. *53rd IEEE Holm conference on Electrical contacts*, Pittsburgh, Philadelphia, USA, 2007.

[113] Y. Li, Z. Huang, Y. Xu, and H. Sheng. Plasma-arc technology for the thermal treatment of chemical wastes. *Environmental Engineering Science*, 26:731–737, 2008.

[114] R.W. Liebermann and J.J. Lowke. Radiation emission coefficients for sulfur hexafluoride arc plasmas. *Journal of Quantitative Spectroscopy and Radiative Transfer*, 16:253–264, 1976.

[115] Ming Liu. *Biomass–powered solid oxide fuel cells.* Thesis, Delft University of Technology, 2013.

[116] H. Lorcet, M. Brothier, D. Guenadou, C. Latge, and A. Vardelle. Modeling bio-oil gasification by a plasma process. *High Temperature Material Processes*, 14:11–27, 2010.

[117] J.J. Lowke. Predictions of arc temperature profiles using approximate emission coefficients for radiation losses. *Journal of Quantitative Spectroscopy and Radiative Transfer*, 14:111–122, 1974.

[118] G. Mariaux and A. Vardelle. 3D time-dependent modeling of the plasma spray process; Part 1: flow modeling. *International Journal of Thermal Sciences*, 44:357–366, 2005.

[119] G. Marland, T.A. Boden, and R.J. Andres. Global, regional, and national fossil fuel CO_2 emissions. *In Trends: A Compendium of Data on Global Change*, Carbon Dioxide Information Analysis Center, Oak Ridge National Laboratory, U.S. Department of Energy, Oak Ridge, Tenn., U.S.A., 2008.

[120] E.A. Mason and S.C. Saxena. Approximate formula for the thermal conductivity of gas mixture. *Physics of Fluids*, 1:361–369, 1958.

[121] M. Materazzi, P. Lettieri, L. Mazzei, R. Taylor, and C. Chapman. Fate and behavior of inorganic constituents of RDF in a two stage fluid bed-plasma gasification plant. *Fuel*, 150(0):473–485, 2015.

[122] P. Mayne, S. Burns, and L. Circeo. Plasma magmavication of soils by non-transferred arc. *Journal of Geotechnical and Geoenvironmental Engineering*, 387:387–396, 2000.

[123] S. Mehmood, B. V. Reddy, and M. A. Rosen. Energy analysis of a biomass co-firing based pulverized coal power generation system. *Sustainability*, 4(4):462–490, 2012.

[124] E. Meillot, D. Guenadou, and C. Bourgois. Three dimension and transient DC plasma flow modeling. *Plasma Chemistry and Plasma Processing*, 28:69–84, 2008.

[125] E. Meillot, S. Vincent, C. Caruyer, J-P. Caltagirone, and D. Damiani. From DC time-dependent thermal plasma generation to suspension plasma spraying interactions. *Journal of Thermal Spray Technology*, 18:875–886, 2009.

[126] F. Menon. Hazardous waste treatment technology by plasma thermal destruction recovery. *The International Conference on Management, Policy, Treatment and Disposal Technology of Hazardous Waste*, Beijing, China, 2005.

[127] G. Mescavage. Development of a plasma ordnance demilitarization system for pyrotechnic ordnance. *17^{th} Global Demilitarization Symposium & Exhibition*, San Diego, California, USA, 2009.

[128] K. Miki, J. Schulz, and S. Menon. Large eddy simulation of a free-burning arc discharge in argon with a turbulent cross flow and external field. *Plasma Chemistry and Plasma Processing*, 33:959–978, 2013.

[129] M.F. Modest. *Radiative heat transfer*. Academic Press, New York, USA, 2*nd* edition, 2003.

[130] A. Mountouris, E. Voutsas, and D. Tassios. Solid waste plasma gasification: equilibrium model development and exergy analysis. *Energy Conversion and Management*, 47:1723–1737, 2006.

[131] A.B. Murphy. Diffusion in equilibrium mixtures of ionized gases. *Physical Review E*, 48:3594–3603, 1993.

[132] A.B. Murphy. Transport coefficients of air, argon-air, nitrogen-air, and oxygen-air plasmas. *Plasma Chemistry and Plasma Processing*, 15:279–307, 1995.

[133] A.B. Murphy. A comparison of treatments of diffusion in thermal plasmas. *Journal of Physics D: Applied Physics*, 29:1922–1932, 1996.

[134] A.B. Murphy. Transport coefficients of hydrogen and argon-hydrogen plasmas. *Plasma Chemistry and Plasma Processing*, 20:279–307, 2000.

[135] A.B. Murphy. Treatments of diffusion in thermal plasmas. *High Temperature Material Processes*, 4:1–20, 2000.

[136] A.B. Murphy. Thermal plasmas in gas mixtures. *Journal of Physics D: Applied Physics*, 34:R151–173, 2001.

[137] A.B. Murphy. Transport coefficients of plasmas in mixtures of nitrogen and hydrogen. *Chemical Physics*, 398:64–72, 2012.

[138] A.B. Murphy. Thermodynamic properties and transport coefficients of arc lamp plasmas: argon, krypton and xenon. *Journal of Physics D: Applied Physics*, 47:295202 (295210pp.), 2014.

[139] A.B. Murphy and C.J. Arundell. Transport coefficients of argon, nitrogen, oxygen, argon-nitrogen and argon-oxygen plasmas. *Plasma Chemistry and Plasma Processing*, 14:451–490, 1994.

[140] F. Nachtrodt. *Development of a method for plasma-induced combustion of intermediate to low-level radioactive waste.* Thesis, Universita di Bologna, 2013.

[141] NASA. Solid oxide fuel cells & electrolysis membranes, 2015. `http://www.grc.nasa.gov/WWW/StructuresMaterials/Ceramics/research_solid.html` (accessed April 15, 2015).

[142] National Research Council. *Plasma processing of materials: scientific opportunities and technological challenges.* The National Academies Press, Washington, DC, 1991.

[143] V. Nehra, A. Kumar, and H.K. Dwivedi. Atmospheric non-thermal plasma sources. *International Journal of Engineering*, 2:53–68, 2008.

[144] NETL. Integrated gasification fuel cell, 2015. `http://www.netl.doe.gov/research/coal/energy-systems/gasification/gasifipedia/integrated-gasification-fuel-cell` (accessed April 15, 2015).

[145] NETL. Power from integrated gasifciation combined cycle, 2015. http://www.netl.doe.gov/research/coal/energy-systems/gasification/gasifipedia/igcc-config (accessed April 25, 2015).

[146] M. Ni, M.K.H. Leung, K. Sumathy, and D.Y.C. Leung. Potential of renewable hydrogen production for energy supply in Hong Kong. *International Journal of Hydrogen Energy*, 31:1401–1412, 2006.

[147] M. Niehuser. *Analyst's* report of visit to Air *Products*Êź Tees Valley project, 2014.

[148] G.E. Palmer and M.J. Wright. Comparison of methods to compute high temperature gas viscosity. *Journal of Thermophysics and Heat Transfer*, 17:232–239, 2003.

[149] B. Pateyron, M.F. Elchinger, G. Delluc, and P. Fauchais. Thermodynamic and transport properties of Ar-H_2 and Ar-He plasmas gases used for spraying at atmospheric pressure: I: properties of the mixtures. *Plasma Chemistry and Plasma Processing*, 12:421–448, 1992.

[150] PEAT International. PEAT: waste-to-energy company, 2015. http://www.peat.com/ (accessed April 21, 2015).

[151] M.A. Polkanov, V.A. Gorbunov, I.I. Kadyrov, N.A. Spirin, A.P. Kobelev, F.A. Lifanov, and S.A. Dmitriev. Technology of plasma treating radioactive waste: the step forward in comparison with incineration, 2010.

[152] PyroGenesis. Government liquidation: Pyrogenesis plasma gasification and waste incineration system, 2013. http://www.govliquidation.com/auction/view?auctionId=6241220 (accessed April 18, 2015).

[153] PyroGenesis Canada Inc. PyroGenesis Canada Inc., 2015. http://www.pyrogenesis.com/ (accessed April 21, 2015).

[154] M. Quaghebeur, B. Laenen, D. Geysen, P. Nielsen, Y. Pontikes, T. Van Gerven, and J. Spooren. Characterization of landfilled materials: screening of the enhanced landfill mining potential. *Journal of Cleaner Production*, 55:72–83, 2013.

[155] J.D. Ramshaw and C.H. Chang. Computational fluid dynamics modeling of multicomponent thermal plasmas. *Plasma Chemistry and Plasma Processing*, 12:299–325, 1992.

[156] H.Z. Randrianandraina, Y. Cressault, and A. Gleizes. Improvements of radiative transfer calculation for SF_6 thermal plasmas. *Journal of Physics D: Applied Physics*, 44:1–11, 2011.

[157] L. Rao, P. Carabin, and G. Holcroft. Plasma waste gasification: decentralized approach to production of energy from waste. Pyrogenesis Inc., Unpublished, 2013.

[158] J. Rezaiyan and N.P. Cheremisinoff. *Gasification technologies - a primer for engineers and scientists*. CRC Press, Florida, USA, 2005.

[159] Risk Reduction Engineering Laboratory US Environmental Protection Agency (EPA). Superfund innovative technology evaluation: Retech, Inc. plasma centrifugal furnace - applications analysis. Report, EPA, 1992.

[160] J. Rizkiana, G. Q. Guan, W. B. Widayatno, X. G. Hao, X. M. Li, W. Huang, and A. Abudula. Promoting effect of various biomass ashes on the steam gasification of low-rank coal. *Applied Energy*, 133:282–288, 2014.

[161] D. Robau. Update on the Transportable plasma waste to energy system at Hurlburt Field. *NDIA Environment, Energy & Sustainability Symposium & Exhibition*, Denver, Colorado, USA, 2010.

[162] M. Rovatti, A. Converti, M. Bisi, and G. Ferraiolo. Pyrolysis of refuse-derived fuel - kinetic modeling from product composition. *Journal of Hazardous Materials*, 36(1):19–33, 1994.

[163] J. A. Ruiz, M. C. Juarez, M. P. Morales, P. Munoz, and M. A. Mendivil. Biomass gasification for electricity generation: review of current technology barriers. *Renewable & Sustainable Energy Reviews*, 18:174–183, 2013.

[164] B. Ruj and S. Ghosh. Technological aspects for thermal plasma treatment of municipal solid waste – A review. *Fuel Processing Technology*, 126:298–308, 2014.

[165] K. Sandeep and S. Dasappa. Oxy-steam gasification of biomass for hydrogen rich syngas production using downdraft reactor configuration. *International Journal of Energy Research*, 38(2):174–188, 2014.

[166] B. Sartwell. Plasma arc destruction of DOD hazardous waste. Report, Environmental Security Technology Certification Program (ESTCP) US Department of Defense, 2003.

[167] H. Schulz. Short history and present trends of Fischer-Tropsch synthesis. *Applied Catalysis A: General*, 186:3–12, 1999.

[168] B. Selvan and K. Ramachandran. Comparisons between two different three-dimensional arc plasma torch simulations. *Journal of Thermal Spray Technology*, 18:846–857, 2009.

[169] K.A. Senelwa. *The air gasification of woody biomass from short rotation forests – opportunities for small scale biomas-electricity systems.* Thesis, Massey University, 1997.

[170] A.E. Sheindlin, I. S. Belevich, and I.G. Kozhevnikov. Enthalpy and specific heat of graphite in temperature range 273-3650 degrees K. *High Temperature*, 10(5):897–900, 1973.

[171] N.S. Siefert and S. Litster. Exergy and economic analyses of advanced IGCC-CCS and IGFC-CCS power plants. *Applied Energy*, 107:315–328, 2013.

[172] K. Skrinak. Cool plasma gasification. *Sustainability Seminar*, Illinois Sustainable Technology Center - Prairie Research Institute, 2013.

[173] I.A. Sobolev, S.A. Dmitriev, F.A. Lifanov, A.P. Kobelev, V.N. Popkov, M.A. Polkanov, A.E. Savkin, A.P. Varlakov, S.V. Karlin, S.V. Stafanovsky, O.K. Karlina, and K.N. Semenov. High temperature treatment of intermediate-level radioactive wastes - Sia Radon experience. *Waste Management Symposium*, Tuscon, Arizona, USA, 2003.

[174] Solena Fuels. GreenSky London project taking off, 2014. `http://www.solenafuels.com/index.php/projects/greensky-london` (accessed April 22, 2015).

[175] C.T. Spaeth. *Performance Characteristiscs of a diesel fuel piloted syngas compression ignition engine.* Thesis, Queen's University, 2012.

[176] P.L. Spath and D.C. Dayton. Preliminary screening - tecnical and economic assessment of synthetic gas to fuels and chemicals with emphasis on the potential for biomass-derived fuel. Report, National Renewable Energy Laboratory, 2003.

[177] X. W. Sun, Z. J. Liu, Q. F. Chen, H. W. Lu, T. Song, and C. W. Wang. Heat capacity of ZnO with cubic structure at high temperatures. *Solid State Communications*, 140(5):219–224, 2006.

[178] J. Surma. Emerging technologies: plasma gasification. *12^t Annual LEA, Tire Enforcement, and CIWMB Training and Technical Course Series*, Sacramento, California, USA, 2009.

[179] J. Surma. Conversion of municipal solid waste into clean energy products using the Inentec plasma enhanced melter. InEnTec Inc., Pamphlet, 2010.

[180] R. Taylor, C. Chapman, and A. Faraz. Transformations of syngas derived from landfilled wastes using the Gasplasma process. *2nd International Symposium on Enhanced Landfill Mining*, Houthalen-Helchteren, Belgium, 2013.

[181] R. Taylor, R. Ray, and C. Chapman. Advanced thermal treatment of auto shredder residue and refuse derived fuel. *Fuel*, 106:401–409, 2013.

[182] Y. Tielemans and P. Laevers. Closing the circle, an enhanced landfill mining case study. *International Academic Symposium on Enhanced Landfill Mining*, Houthalen-Helchteren, Belgium, 2010.

[183] J.P. Trelles, C. Chazelas, A. Vardelle, and J.V.R. Heberlein. Arc plasma torch modeling. *Journal of Thermal Spray Technology*, 18:728–752, 2009.

[184] J.P. Trelles, E. Pfender, and J.V.R. Heberlein. Multiscale finite element modeling of arc dynamics in a DC plasma torch. *Plasma Chemistry and Plasma Processing*, 26:557–575, 2006.

[185] S.R. Turns. *An introduction to combustion: Concepts and Applications*. MA: McGraw-Hill, Boston, 2000.

[186] C-C. Tzeng, Y-Y. Kuo, T-F. Huan, D-L. Lin, and Y-J. Yu. Treatment of radioactive wastes by plasma incineration and vitrification for final disposal. *Journal of Hazardous Materials*, 58:207–220, 1998.

[187] United States Securities and Exchange Commission. Form 8-K Commission File Number 333-120908. Report, Global Technologies Group, Inc., 2010.

[188] C.M. van der Meijden, A. van der Drift, and B.J. Vreugdenhil. Benefits of allothermal biomass gasification for co-firing. *2nd Workshop on Cofiring Biomass with Coal*, Copenhagen, Denmark, 2012.

[189] P. van Nierop and P. Sharma. Plasma gasification - integrated facility solutions for multiple waste streams. Westinghouse, Unpublished, 2010.

[190] G. Van Oost. Plasma physics - part 1: high temperature plasma physics, 2009. Lecture notes for physics and engineering students.

[191] G. Van Oost, M. Hrabovský, V. Kopecký, M. Konrád, M. Hlína, and T. Kavka. Pyrolysis/gasification of biomass for synthetic fuel production using a hybrid gas-water stabilized plasma torch. *Vacuum*, 83(1):209–212, 2008.

[192] G. Van Oost, M. Hrabovský, V. Kopecký, M. Konrád, M. Hlína, T. Kavka, O. Chumak, E. Beeckman, and J. Verstraeten. Pyrolysis of waste using a hybrid argon-water stabilized torch. *Vacuum*, 80(11-12):1132–1137, 2006.

[193] G. Van Oost, M. Hrabovský, J. Pieters, M. Tendler, and J. Verstraeten. Novel Project on Total Plasma Based Treatment of Waste. *Problems of Atomic Science and Technology. Series: Plasma Physics*, 10(1):157–160, 2005.

[194] N. Venkatramani. Industrial plasma torches and applications. *Current Science*, 83(3):254–262, 2002.

[195] J. Vijgen and R. McDowall. In flight plasma arc waste treatment process (PLASCON) - annex to annex to POPs technology specification and data sheet. Report, United Nations Environment Programme (UNEP), 2008.

[196] S. Vincent, G. Balmigere, C. Caruyer, E. Meillot, and J-P. Caltagirone. Contribution to the modeling of the interaction between a plasma flow an a liquid jet. *Surface and Coatings Technology*, 203:2162–2171, 2009.

[197] K. Vrancken, R. Torfs, A. Van der Linden, P. Vercaemst, and P. Geuzens. Vergelijking van verwerkingscenario's voor restfractie van HHA en niet-specifiek categorie II bedrijfsafval. Report, Vito, 2001.

[198] G.Q. Wang, Y.J. Li, Y.X. Xu, and H.Z. Sheng. Equilibrium modeling for optimum design of operation parameters of MSW plasma gasification. *International Conference on Thermal Treatment Technologies and Hazardous Waste Combustors*, Jacksonville, Florida, USA, 2011.

[199] R. Warnecke. Gasification of biomass: comparison of fixed bed and fluidized bed gasifier. *Biomass & Bioenergy*, 18(6):489–497, 2000.

[200] L. G. Wei, S. P. Xu, L. Zhang, C. H. Liu, H. Zhu, and S. Q. Liu. Steam gasification of biomass for hydrogen-rich gas in a free-fall reactor. *International Journal of Hydrogen Energy*, 32(1):24–31, 2007.

[201] R. Westhoff and J. Szekeley. A model of fluid, heat flow, and electromagnetic phenomena in a nontransferred arc plasma torch. *Journal of Applied Physics*, 70:3455–3466, 1991.

[202] Westinghouse Plasma Corporation. Westinghouse plasma coal gasification & vitrification technology. *Power Generation Conference*, Hershey, Pennsylvania, USA, 2002.

[203] Westinghouse Plasma Corporation. Energy evolved - clean, sustainable energy recovery through plasma gasification. Westinghouse, Pamphlet, 2012.

[204] Westinghouse Plasma Corporation. Transformation of waste into syngas using plasma gasification for the production of energy or biofuels. Westinghouse, Unpublished, 2012.

[205] Westinghouse Plasma Corporation. Westinghouse plasma gasification is the next generation of energy-from-waste technology. *Energy from Waste*, Manchester, United Kingdom, 2012.

[206] Westinghouse Plasma Corporation. Westinghouse plasma gasification technology - summary of qualifications. Westinghouse, Unpublished, 2013.

[207] C.R. Wilke. A viscosity equation for a gas mixture. *Journal of Chemical Physics*, 18:517–519, 1950.

[208] J. Wilkinson and D. Watt. Review of demilitarisation and disposal techniques for munitions and related materials. Report, NATO, 2006.

[209] R.L. Williamson, J.R. Fincke, D.M. Crawford, S.C. Snyder, W.D. Swank, and D.C. Haggard. Entrainment in high velocity, high temperature plasma jets; Part II: computational results and comparison to experiment. *International Journal of Heat and Mass Transfer*, 46:4215–4228, 2003.

[210] K.P. Willis, S. Osada, and K.L. Willerton. Plasma gasification: lessons learned at Eco-Valley WtE facility. *18th North American Waste to Energy Conference (NAWTEC)*, Orlando, Florida, USA, 2010.

[211] D. C. Wilson. Development drivers for waste management. *Waste Management & Research*, 25(3):198–207, 2007.

[212] J. Xiao, L. Shen, Y. Zhang, and J. Gu. Integrated analysis of energy, economic, and environmental performance of biomethanol from rice straw in China. *Industrial and Engineering Chemistry Research*, 48:9999–10007, 2009.

[213] D-Y. Xu, X. Chen, and K. Cheng. Three-dimensional modelling of the characteristics of long laminar plasma jets with lateral injection of carrier gas and particulate matter. *Journal of Physics D: Applied Physics*, 36:1583–1594, 2003.

[214] K-S. Yun, S. Weissman, and E.A. Mason. High-temperature transport properties of dissociating nitrogen and dissociating oxygen. *Physics of Fluids*, 5:672, 1962.

[215] Q. Zhang, L. Dor, D. Fenigshtein, W. Yang, and W. Blasiak. Gasification of municipal solid waste in the plasma gasification melting process. *Applied Energy*, 90:106–112, 2012.

[216] Q. Zhang, Y. Wu, L. Dor, W. Yang, and W. Blasiak. A thermodynamic analysis of solid waste gasification in the Plasma Gasification Melting process. *Applied Energy*, 112:405–413, 2013.

[217] M.F. Zhukov, I.M. Zasypkin, A.N. Timoshevskii, B.I. Mikhailov, and G.A. Desyatkov. *Thermal Plasma Torches: Design, Characteristics, Applications*. Cambridge International Science Publishing Ltd, Cambridge, United Kingdom, 2007.